Structure Shielding

Against Fallout Radiation

From Nuclear Weapons

U.S. DEPARTMENT OF COMMERCE

NATIONAL BUREAU OF STANDARDS

THE NATIONAL BUREAU OF STANDARDS

Functions and Activities

The functions of the National Bureau of Standards are set forth in the Act of Congress, March 3, 1901, as amended by Congress in Public Law 619, 1950. These include the development and maintenance of the national standards of measurement and the provision of means and methods for making measurements consistent with these standards; the determination of physical constants and properties of materials; the development of methods and instruments for testing materials, devices, and structures: advisory services to government agencies on scientific and technical problems; invention and development of devices to serve special needs of the Government; and the development of standard practices, codes, and specifications. The work includes basic and applied research, development, engineering, instrumentation, testing, evaluation, calibration services, and various consultation and information services. Research projects are also performed for other government agencies when the work relates to and supplements the basic program of the Bureau or when the Bureau's unique competence is required. The scope of activities is suggested by the listing of divisions and sections on the inside of the back cover.

Publications

The results of the Bureau's research are published either in the Bureau's own series of publications or in the journals of professional and scientific societies. The Bureau itself publishes three periodicals available from the Government Printing Office: The Journal of Research, published in four separate sections, presents complete scientific and technical papers; the Technical News Bulletin presents summary and preliminary reports on work in progress; and Basic Radio Propagation Predictions provides data for determining the best frequencies to use for radio communications throughout the world. There are also five series of non-periodical publications: Monographs, Applied Mathematics Series, Handbooks, Miscellaneous Publications, and Technical Notes.

A complete listing of the Bureau's publications can be found in National Bureau of Standards Circular 460, Publications of the National Bureau of Standards, 1901 to June 1947 ($1.25), and the Supplement to National Bureau of Standards Circular 460, July 1947 to June 1957 ($1.50), and Miscellaneous Publication 240, July 1957 to June 1960 (Includes Titles of Papers Published in Outside Journals 1950 to 1959) ($2.25); available from the Superintendent of Documents, Government Printing Office, Washington 25, D.C.

Structure Shielding

Against Fallout Radiation

From Nuclear Weapons

L. V. Spencer

Foreword

The problem of providing protection against the radiations generated by nuclear weapons is of much concern to the Federal Government and to the people of the United States. A great deal of effort and money is being spent currently on attempts to analyze existing structures for shielding properties, and plans are being carried forward to design and build special shelters of many kinds.

The National Bureau of Standards has maintained a continuing research program directed to the development of engineering data and methods basic to the solution of these radiation shielding problems. Most of the work of the past few years on this project has been concerned with gamma rays from radioactive fallout. This Monograph summarizes both the methods and the data which have been generated as a result of research on the penetration of fallout radiations.

Financial support for this project has come primarily from the Office of Civil and Defense Mobilization and from the Defense Atomic Support Agency of the Department of Defense.

A. V. Astin, *Director.*

Contents

Structure Shielding Against Fallout Radiation From Nuclear Weapons

L. V. Spencer

The theory of structure shielding from fallout gamma radiation is developed to the point of applications to elementary structure types. Examples discussed in the text include the density interface, foxhole, shielded foxhole or basement, light superstructure, vertical wall, blockhouse, vents, compartmentalization effects, and mazes. A large number of engineering charts and graphs are presented for engineering calculations, including many obtained from angular distributions of the exposure dose. Results are given for a fission spectrum, and for Co^{60} and Cs^{137} sources. This information has been obtained almost completely by machine calculations utilizing basic cross section data. A number of sources of experimental data are mentioned, but detailed comparisons with experiment are not included.

I. Introduction

1. Purpose

This Monograph is to assist scientists and engineers in the solution of problems of protection from ionizing radiation, particularly radiation from fallout. Important activities in which such problems arise include (a) the design of new protective structures, (b) analysis of existing structures to determine the nature of their shielding capabilities, and (c) assessing the possibilities for improvising shelter.

2. Comments about Radiation Shielding Problems and Publications

The analysis of structures for their protection against ionizing radiation represents a new field of engineering which has many similarities to illuminating engineering. Estimating radiation levels at different locations in a complex structure is comparable to the problem of determining the illumination levels in a similar structure on a cloudy day, but with all partitions and walls having varying degrees of transparency or translucence rather than being opaque. The complexity of the problems is such that, despite intensive research, significant gaps in our knowledge still remain.

Reactor shielding problems are rather different from the problems of shielding against nuclear weapons. The former involve a localized source and shield whose various aspects are readily available for study and possible modification. Further, both source and shield differ in many ways from the sources and the barrier configurations encountered in weapons shielding problems. For these and other reasons the different reactor shielding handbooks are not an adequate basis for the study of weapons shielding problems, though they do contain a great deal of useful information [1–5].*

The joint AEC, DOD, and OCDM publication, "The Effects of Nuclear Weapons," gives a general description of all aspects of nuclear explosions, together with many tables and graphs relevant to radiation shielding [6]. However, the material included in the book on the subject of protection against fallout constitutes an introduction to the problems rather than a detailed methodology for their solution.

A number of reports have been published in the past three years on shielding against fallout radiation [7–11]. The problems and the different approaches to their solution contained in these reports tend to have close similarities to each other and to the material in this monograph. Nevertheless, there are differences worth noting. The approach taken here is less empirical, relying on basic data derived from first principles rather than on field test experiments. This has the advantage of providing more different types of data, as well as a basis for different kinds of estimates. Enough experimental confirmations of the basic data exist to give confidence in its overall accuracy [12]; but further research can be expected to complement and modify this information in various ways.[1]

3. Choice and Presentation of Material

The contents and organization of this Monograph have been influenced by the fact that the analysis of structure shielding may properly be considered a branch of either nuclear or civil engineering. It is, however, a subject with which few people are familiar; hence it has seemed worth while to include general information about fallout radiation and its characteristic properties. Thus, Part II describes fallout in an elementary way and Part III gives properties of gamma radiation.

Part IV introduces the formal approach to structure shielding analysis adopted in this manuscript together with the basic parameters of

---

*Figures in brackets indicate the literature references at the end of this Monograph.

[1] Recently, OCDM has published a series of manuals, prepared by L. N. FitzSimons of that agency, and based on the methods and data presented in this monograph. See, e.g., "Fallout Shelter Surveys: Guide for Architects and Engineers," Report No. NP-10-2 (May 1960), and "OCDM Engineering Manual," (Dec. 1, 1960).

1

description and measurement. Part V is a discussion of graphical data for use in applications. Part VI gives an analysis of elementary structures. Finally, Part VII presents a methodology for generalizing the calculations to a wide group of barrier shapes.

It was originally intended to incorporate into this Monograph analyses of a number of complex structures in terms of the data presented here. However, this has been omitted for a number of reasons. Instead, we include an appendix which gives two additional sets of graphical data, one for Co^{60} and the other for Cs^{137}, for use in analyzing experiments. The data contained in the body of the manuscript are for radiation from fission products.

II. Description of Fallout

4. Fallout vs Initial Effects

Whenever a nuclear bomb is exploded, a tremendous pressure wave, large quantities of heat and light, and a vast amount of radiation and radioactive material are produced concurrently [6, Chapters II and III]. Where these three effects are all important, their interrelations complicate nearly all protection problems. For example, completely protective structures must be blast resistant as well as radiation resistant, and they must be built with due consideration for the possibility of a fire storm. Furthermore, the nature of blast and heat phenomena affect the radiation problem, e.g., through vertical drafts which alter the spatial distribution of radioactive material.

Exposure to the initial radiations ceases about a minute after the explosion, by which time the radioactive material from the explosion is carried out of range by the upward drafts. Large amounts of earth and debris are also drawn upward, and the resulting mushroom-shaped cloud may rise 80,000 feet or more. This cloud contains particles ranging in size from submicroscopic specks to grains as large as coarse sand. Radioactive residue from the bomb and its surroundings adheres to these particles. The general term for this particulate matter, as it is brought to earth again, is "fallout."

5. Regional Variations in Fallout

Some of the fallout particles rise higher than others; and some are more buoyant than others, thus falling to earth less rapidly [6, Sections 10.1–10.24]. Close to the explosion there occurs the "throwout"—rocks blown out by the blast; while at the other extreme are particles so small and raised so high above the earth that they are in the stratosphere above the weather and are little influenced by gravitational forces. It takes years for these tiniest particles to settle to earth again, and they may come down anywhere on the earth. We shall not discuss this long-duration "worldwide" fallout, nor shall we be concerned with the "throwout" [6].

A large fraction of the fallout material is big enough to come to earth within hours or days, yet small enough to be easily blown about by winds. Correspondingly, the distribution of particle
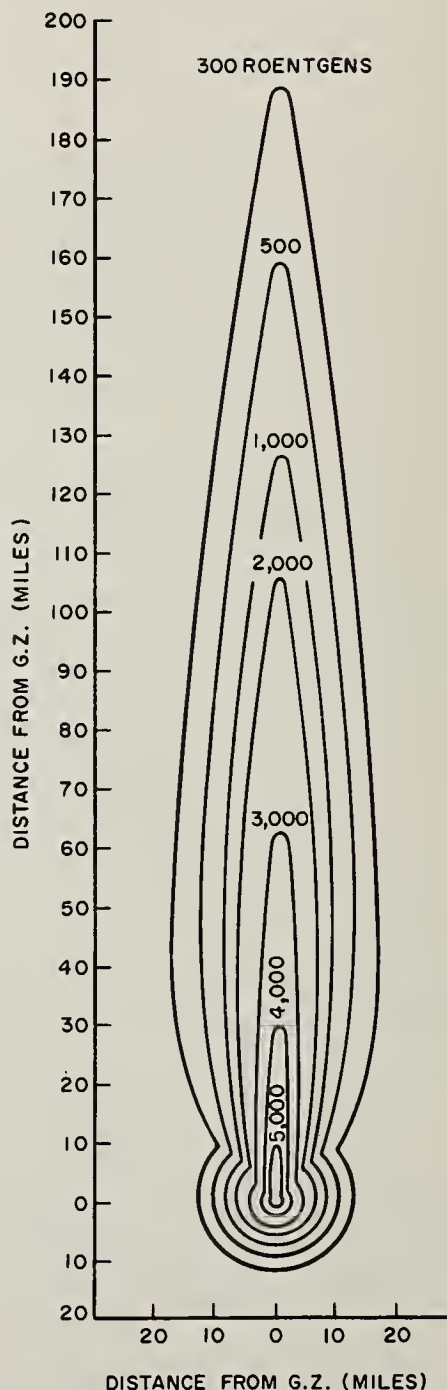

FIGURE 5.1. *Idealized total (accumulated) dose contours from fallout in the first 36 hours after the high yield explosion at Bikini Atoll on March 1, 1954. (Ref. 6.)*

2

sizes and the regional wind structure determine the spatial distribution of the deposit. Sustained strong winds may carry fallout in lethal amounts for hundreds of miles, whereas light winds may leave most of it much closer to the explosion.

Figure 5.1 gives idealized contours of total fallout exposure from a large (multi-megaton) explosion, indicating how the fallout was carried by winds away from the point of explosion. Attempts to calculate such gross variations have had some success, at least to the point of being useful in estimations for broad planning purposes [6, Sections 9.55–9.138].

It is clear from figure 5.1 that intense fallout can occur in wide areas far beyond blast and heat effects. This makes it reasonable to consider the fallout as a problem separate from blast and heat complications. In this Monograph, problems of protection from fallout radiation are discussed without reference to the effects of blast and heat; it should be remembered, however, that intense fallout also occurs in the proximity of the explosion.

6. Local Variations in Fallout

Just as the gross features of fallout spatial distributions are affected by the general wind pattern over a large area, so the fine features depend on the local winds. For example, fallout may collect more on one side of a building than on another, or blow down one set of streets more than another, more or less in the manner that the drifting of snow is determined by local variations in the surface winds. We do not have explicit data on the effects of such variations, and a thorough analysis of the problem is needed before a reliable estimation of the magnitude of these "micro-meteorological" effects can be established [13]. *In the absence of specific information we assume for the present that fallout will be uniformly distributed horizontally over exposed surfaces.*

A question of particular importance relates to the amount of fallout material which may remain suspended above the earth in trees and shrubbery. This has not been accurately determined. There is evidence that not more than a few percent of the material descending, e.g., upon a tree will remain on the limbs and leaves of the tree if the surfaces are dry [14–15]. But the possibility of weather conditions which will cause fallout to adhere even to vertical wall surfaces, and the sensitivity of basement protection to the amount of suspended source material, make this a major problem for future research.

7. Types of Fallout Radiation

Two types of radiation are emitted by radioactive fallout materials,[2] namely, (a) gamma rays and (b) fast charged particles (alpha and beta rays). Both types are biologically destructive; however, the charged particle radiations are not

---

[2] Neutrons are not emitted by fallout particles.

very penetrating. The fast beta-rays (electrons) can produce burns on unprotected skin, especially when fallout material is in contact with the skin; but very little shielding, such as is provided by average to heavy clothing, is capable of providing almost complete protection. The alpha rays are not even able to penetrate through the external layer of skin. In problems of ingestion of contaminated food, water, and air, however, both alpha and beta rays must be considered, because when taken internally their full energy is effective in causing damage to the internal tissues [16].

The gamma rays present the primary shielding problem because they are extremely penetrating as well as biologically destructive. They may be described as high energy X-rays, but for historical reasons the term "γ-rays" is frequently used when the radiation is produced by nuclear processes and "X-rays" when it is produced by electron bombardment of an anode.

8. Characteristics of Fallout Gamma Rays

Both the *quality* and the *quantity* of fallout gamma rays have been investigated in many research studies [17–23].

Gamma radiation may be visualized as a stream of individual "energy packets," called "photons." The energy content of each packet may be referred to as the "photon energy." Quantitative descriptions of fallout gamma rays may utilize directly the total photon energy crossing unit area of a surface per second; alternately they may involve a standard detector whose response is in some way descriptive of the strength of the beam, as discussed in Sections 9 and 15.

Qualitative descriptions are nearly always in terms of the "spectrum," which gives the relative importance of the different gamma ray photon energies present. A typical spectrum will be a list of numbers or a graph giving, e.g., the fraction of the total beam energy in the form of photon energies between 1 and 2 Mev, between 2 and 3 Mev, etc.

Radioactive material is a mixture of many types of atoms, each emitting characteristic photon energies. These radioactive atoms originated in one of two ways: (1) Some were originally part of an atom which fissioned in the nuclear explosion (mixed fission products); (2) others were part of the bomb or were nearby and were made radioactive through capture of a neutron (neutron induced activities). The mixed fission products have usually been considered the most important radiation source, to the extent that the neutron-induced activities have often been neglected in calculations pertaining to fallout. From both sources a variety of photon energies is generated over a range extending up to perhaps 3 Mev.

9. Exposure to Gamma Rays

Biological effects depend upon the energy absorbed from the gamma rays per unit mass of

3

biological material [24]. This absorbed energy is usually measured in "rads" (1 rad = 100 ergs/gram).

The energy absorbed in biological material depends in turn on the strength of the radiation field and the duration of exposure. For protection purposes, this is measured in terms of the cumulative effect of the field on a standard material, namely air, in units of roentgens (r) or milliroentgens (mr).[3]

Though the roentgen is a measure of exposure to a radiation field, whereas the rad is a measure of the result of this exposure, it has long been common practice to blur this distinction by speaking of the biological effect of a "dose" of y roentgens, meaning the effect resulting from energy absorbed during an exposure totalling y roentgens. The International Commission on Radiological Units has recommended that the term "exposure dose" be used in this context to prevent confusion with the energy absorbed in the biological (or other) material.[4]

The strength of a gamma ray field at a given time is frequently measured in terms of the "dose-rate," in units of roentgens per hour (r/hr) or, in weak fields, in units of milliroentgens per hour (mr/hr).

Perhaps the best way to gain a feel for the magnitude of different exposure dose rates and total doses is by noting the effects upon human beings, insofar as this is known or surmised. Specific effects depend upon the health of the individual the time-duration of exposure, etc., but some generalized statements about the effects caused by short-duration exposures can be made, as in Table 9.1 below.

TABLE 9.1. *Probable Effects of Fallout Gamma Radiation on Humans* [a]

Short Term Whole-Body Exposure (roentgens)	Probable Effect
0 to 100	No obvious effects
100 to 200	Some sickness
200 to 300	Sickness and some deaths
300 to 600	Severe sickness and many deaths
Over 600	Few, if any, survivors

[a] Note that the effects given all refer to the extent of general incapacitation following exposure. Effects on the gonads, the eyes, etc., which may be extremely important but not immediately obvious, have not been included.

10. Decrease of Fallout Radioactivity With Time

When fallout material has stopped falling upon a given location gamma ray intensities produced by the fallout can be observed to decrease with time. If the fallout is not being spatially displaced by winds, this decrease is described roughly by the following formula:

$$D(t_2) = (t_2/t_1)^{-1.2} D(t_1), \qquad (10.1)$$

where t_1, t_2 represent different elapsed times following the explosion and $D(t)$ is the dose-rate at time t [6, Sections 9.4–9.17]. Equation (10.1) can be roughly described in another way: For every sevenfold increase in time there is a tenfold decrease in radiation intensity. For example, if the radiation dose-rate in a given location is 1,000 r/hr four hours after the explosion, the dose-rate twenty-eight hours after the explosion would be about 100 r/hr.

Another convenient rule-of-thumb relates radiation dose-rate (r/hr) to total exposure (r): The total exposure dose (r) over a very long time interval beginning one hour after the explosion is numerically about five times the dose-rate (r/hr) at one hour in the same place, assuming that no displacement or arrival of the fallout material has taken place after one hour. Thus, if the dose-rate one hour after the explosion were measured to be 30 r/hr, the total exposure at the same location over a very long time interval following this measurement would be about 150 r. A more general expression is

$$E(t_1,t_2) = 5t_1 D(t_1)[1 - (t_2/t_1)^{-.2}], \qquad (10.2)$$

where $E(t_1,t_2)$ is the total exposure *dose accumulated* between times t_1 and t_2 following an explosion. Note that if $t_1 = 1$ and $t_2 = \infty$, $E(1,\infty) = 5D(1)$, in agreement with the special rule-of-thumb mentioned. These rules do not apply if the shielding conditions are changed during the time interval.

The functions of the ratio (t_2/t_1) appearing in eqs (10.1) and (10.2) are given in figure 10.1. *It should be remembered that the time variation expressed by the foregoing expressions is only approximate, that it depends upon the predominance of fission product radiation over induced radiation, and that it becomes a very poor approximation when times after the explosion stretch out into many months or years* [25].[5]

EXAMPLE. The dose-rate of radiation in a given place 4 hours after an explosion is measured to be 32 r/hr. (a) What will the dose-rate be 48 hours after the burst; and (b) what will be the total accumulated exposure dose during the time interval from 4 to 48 hours?

(a) Taking $t_1 = 4$ hours, $t_2 = 48$ hours, one obtains $t_2/t_1 = 12$. According to figure 10.1, $(t_2/t_1)^{-1.2} = (12)^{-1.2} = 0.053$. Multiplying this by $D(t_1) = 32$ r/hr, one obtains $D(t_2) = 1.7$ r/hr at 48 hours. *ANSWER.*

[3] Exposure dose of X- or gamma radiation at a certain place is a measure of the radiation that is based upon its ability to produce ionization. The unit of exposure dose of X- or gamma radiation is the roentgen (r). One roentgen is an exposure dose of (X or) gamma radiation such that the associated corpuscular emission per 0.001293 g (ram) of air produces, in air, ions carrying 1 electrostatic unit of quantity of electricity of either sign [24].

[4] See footnote 3, above.

[5] For a recent investigation of this time variation see the report USNRDL-TR-425, by Carl Miller (U.S. Naval Radiological Defense Laboratory, May 27, 1960).
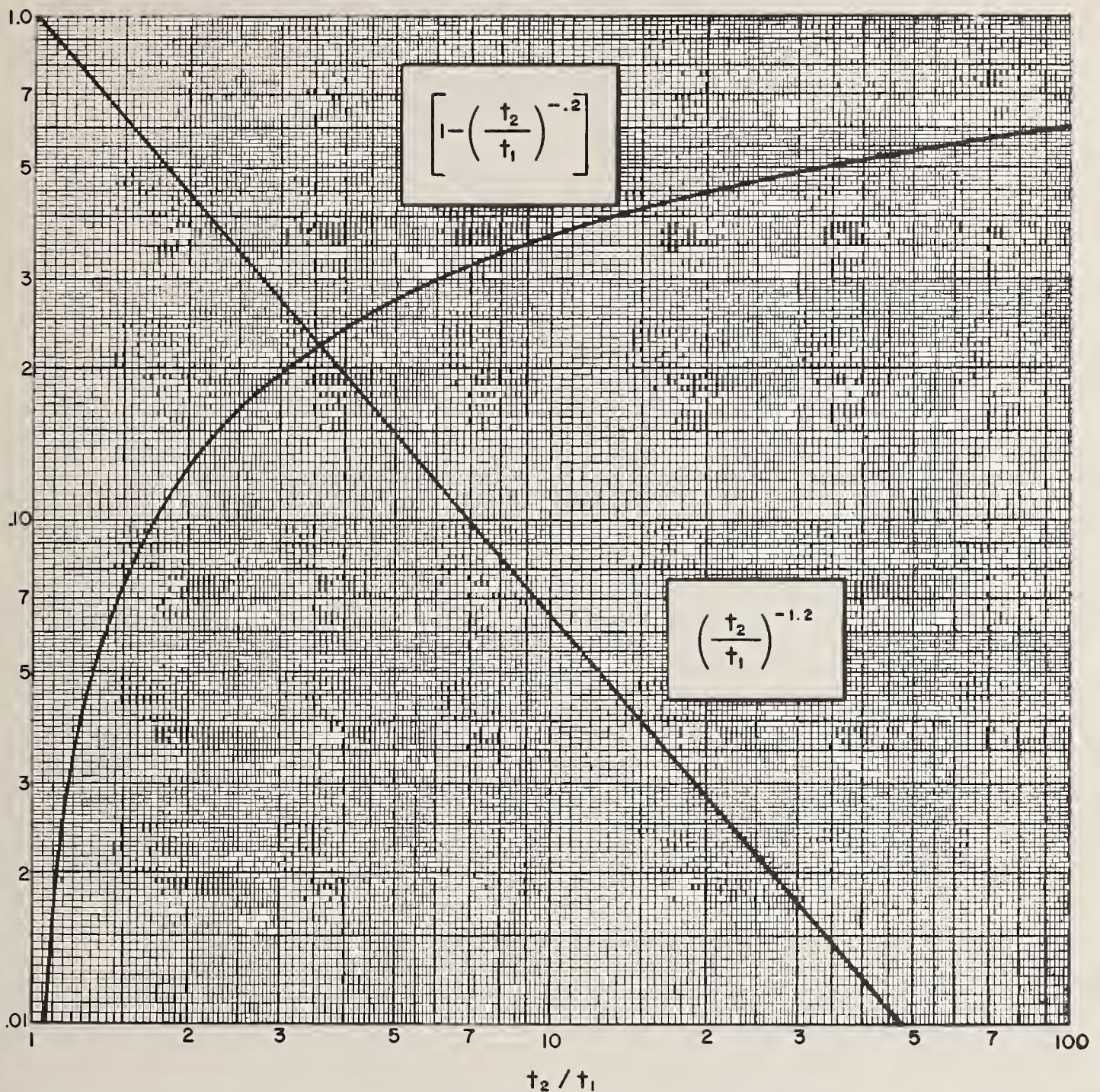
FIGURE 10.1. *Functions for obtaining the radiation dose rates and cumulative dose at different times after fission.*

(b) To obtain the accumulated exposure dose, one determines from figure 10.1 that $[1-(t_2/t_1)^{-.2}]=$ $1-(12)^{-.2}=0.39$. The product $(5)\times(4\ hr)\times(32\ r/hr)\times(0.39)$ then yields the value 250 r. *ANSWER.*

11. Time Variation of the Fallout Spectrum

The fallout gamma ray spectrum changes with time [17–23, 25–27]. This important feature comes about because many varieties of fission fragments are contained in the fallout mateiral, and each goes through a succession of transformations. Thus the very nature of the radiating material

changes with time, and this affects the spectrum emitted.

An example of these spectral changes is given in figure 11.1. At one hour after fission (top figure) the total energy is fairly evenly distributed among gamma rays with photon energies from about 0.5 Mev to 2.5 Mev. At the end of a day, however, most of the radiation is made up of photons below 1 Mev. With further increase in elapsed time following the fission process, higher energies again become very important. Finally, although not shown, the lower portions of the spectrum increase in importance.

The intense, high energy component which dominates the spectrum about a week following the
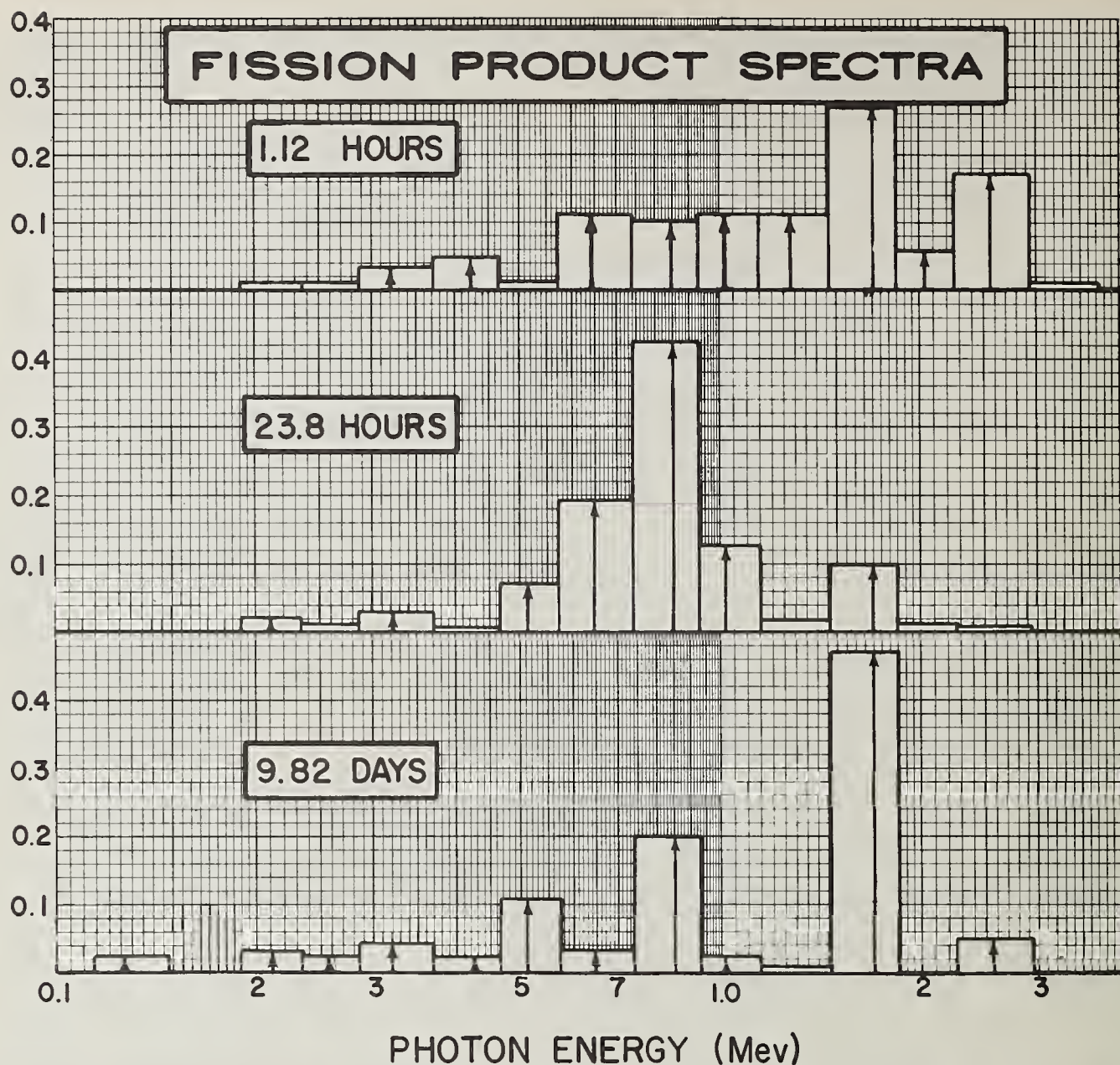
5

FIGURE 11.1. *The relative intensities of different spectral components at several times after fission. The height of each box is proportional to the (energy content) of gamma rays in the energy interval, and the central line indicates an energy assumed for all photons in the interval for purposes of calculation. The lines do not correspond to spectral energies actually present. The total intensity is unity for each spectrum. (Ref. 18, Table 11. Volatile components have been removed from the fission products.)*

fission is due to an isotope of Lanthanum, which is the fourth member of a radioactive family which begins with Xenon fission fragment. The spectral energy of these gamma rays is 1.6 Mev, and they are important over a time interval of more than two weeks.[6]

Because of the time variations of the gamma ray spectrum, it is necessary to make some decision regarding choice of a spectrum to be used as the basis for shielding calculations. It turns out that penetration properties of fallout gamma rays are less sensitive to spectral changes than might be supposed, except for very large penetrations—this will be discussed in the next Sections. The data in

this monograph correspond to the spectrum existing 1.12 hours after the fission process. This spectrum is the one given in figure 11.1 (top curve), with no additions for neutron capture components. This choice results from two considerations: (1) A large part of the exposure to radiation is apt to occur during the first few hours; and (2) the spectrum one hour after the explosion is representative of other early times in the sense of having about the same penetrability.

12. Magnitude of Fallout Gamma Ray Intensities and Exposures

Precise information about *likely* fallout dose-rates is not available; but there is some information about *possible* dose-rates produced by large (megaton) explosions. These vary up to thousands of

---

[6] Note that Xenon is a rare gas, so that when this type of fission fragment is initially formed, it will not enter into chemical combination. The Xenon quickly (in a few seconds) disintegrates to produce Cesium, which is very active chemically and which should become attached to fallout material. Thus Lanthanum and other daughter products of this chain should contribute to the fallout spectrum.

r/hr at early times after the explosion, and could result in accumulated exposures up to tens of thousands of roentgens for unprotected people, even outside blast areas (see fig. 5.1). Furthermore, there exists strong likelihood of overlapping fallout fields, increasing total intensities additively. Since a human exposure to a few hundred roentgens is considered very severe, one attempts to provide shielding sufficient to reduce radiation intensities by "protection" factors of the order of 1000 to insure in practically all cases reduction of exposures to an order of magnitude below the danger levels. In different types of structures, different "protection factors" turn out to be feasible. For example, in an underground shelter it may be relatively easy to incorporate a protection factor of 5000, whereas in an above-ground shelter, it may be difficult to incorporate more than a factor of, say, 100. Figure 5.1 illustrates the value of protection factors still lower than 100.

III. Description and Measurement of the Radiation

13. Introductory Remarks

This part contains a brief outline of terms and ideas used in the latter parts of this Monograph. Also included is a description of some of the characteristic physical properties of gamma radiation. References are given to other publications containing a more complete discussion of some of the topics.

14. Physical Properties

Gamma ray photons act in many ways as if they were tiny "bullets." They travel in a straight line until they "collide" with an atom. When a "collision" takes place the photon may vanish altogether, or it may "ricochet" and continue traveling in a new direction with lower energy. The "collisions" are usually referred to as interactions. Those in which the photon disappears altogether are called *absorptive* interactions. The others in which the photon "ricochets," are called *scattering* interactions [12, Part A].

As a photon moves along its trajectory, there is always a possibility that in the next segment of the path an interaction of some type may take place. Although the nature and location of an interaction is a matter of chance, the probability of occurrence for each interaction type per unit path length traveled depends upon the photon energy and the type of material being traversed. At very low photon energies an absorptive interaction has such a large probability that a long path unimpeded by such an interaction is extremely unlikely.

The average distance between interactions in a given type of material is called the "mean free path." The mean free path is proportional to the density of the material traversed, and this is the main reason why the gamma rays travel about 700 times farther between interactions in air than in water. Mean free paths in air for fallout gamma rays are of the order of several hundred feet, i.e., large compared with the dimensions of most buildings. This has the consequence that most gamma ray interactions within buildings do not take place in the air, but in the walls, floors, and objects of furniture.

When gamma rays "scatter" they continue with lower energy in a new direction, so that they may undergo one or more additional interactions.

There is a correlation between the angle of deflection and the energy loss which accompanies a scattering interaction. On the basis of this correlation the following statements can be made: Gamma rays deflected through 90° by a scattering interaction cannot have a residual photon energy above 0.511 Mev. Similarly, gamma rays which have been deflected through 180° by a scattering interaction cannot retain an energy above 0.256 Mev. Thus, gamma rays which have undergone large changes in direction are apt to be much lower in energy than unscattered gamma rays. This is the case even when the direction change is the cumulative result of several interactions.

15. Radiation Detectors

An object which is affected by radiation to a measurable extent can be used as a radiation detector [28]. Since the effect of radiation on human beings is of primary interest, one might wish to discuss all shielding problems in terms of tissue damage to the exposed human body. This is impractical because the body does not make a very suitable detector for experimental or theoretical investigations. Instead, detectors are used whose response has similarities to the response of a human body, while being more easily measured and interpreted. These detectors tell us about the radiation field. The tissue damage caused by exposure to a known radiation field is treated as a separate problem, and we do not concern ourselves with it further.

Every detector is characterized by its "response function," which is the "efficiency" of gamma rays of photon energy E, incident on the detector from various directions, in producing the measured effect. It is frequently advantageous to have an "isotropic" detector, i.e., one equally efficient regardless of the direction of incidence of the photons.[7]

The most commonly used radiation detector consists of an enclosed air space containing a pair of oppositely charged electrodes. When exposed to radiation, the gamma rays interact with the material surrounding the air space, producing high-velocity recoil electrons, some of

---

[7] Note that the response function depends, in general, on both direction and photon energy and might be denoted by $\epsilon(E,\theta,\phi)$. An isotropic detector would correspondingly have a response function $\epsilon(E)$, i.e., independent of θ,ϕ.

which traverse the cavity and ionize the air within. A measurable electron current is produced as the ions travel to the electrodes and deposit their charge. It is this current, divided by the volume of the air space, which constitutes the response of the instrument.

These so-called "cavity ionization chambers" are usually constructed in such a way that their response is nearly isotropic. But the current per cm³ measured by the instruments is not proportional to the total energy *incident* upon the detector. Instead it is nearly proportional to the energy *deposited* per gram of detector material, as a result of gamma ray interactions occurring within the detector. When such detectors have cavity walls of a material similar to air in its reaction to irradiation, the response can be measured in roentgens and referred to as "dose," or more precisely as the "exposure dose," as explained in Section 9.

Reference to the "detector response" in this monograph will always imply an isotropic detector of this type, i.e., of air-equivalent material, whose response in roentgens is called the "exposure dose."

16. Measurement of the Radiation Flux From Particular Directions

To determine the flux of radiation traversing a given region one needs to introduce a suitable detector as a probe. For this purpose one of the isotropic detectors just described can be used, with a response calibrated in roentgens. The detector should be small enough so that all parts of it are exposed to the same radiation flux, and also so that its presence does not appreciably disturb the flux distribution.

The response measured is due to photons which traverse the detector material. These photons are characterized by the direction of their trajectory at the time they enter the detector. We identify direction by means of polar coordinates θ, ϕ which are measured with respect to an arbitrary polar axis through the center of the detector and a reference half-plane terminating along the polar axis. Both "obliquity," θ, and "azimuth," ϕ, are determined from a line extending out from the center of the detector parallel to the trajectory but *opposite* the direction of travel of the photon.[8] The angle which this line forms with the polar axis is θ, while ϕ is the angle between the reference plane and the plane terminating along the polar axis which contains the line. (See fig. 16.1.) Any direction of incidence is uniquely specified by values for these two direction coordinates.

Note that the coordinate pairs (θ, ϕ) are in one-to-one correspondence with points on a sphere

of unit radius centered at the detector. We can refer to (θ, ϕ) either as a direction or as a point on such a unit sphere.

The total detector response D is made up of contributions from all (θ, ϕ): If $D(\theta, \phi) \sin\theta d\theta d\phi$ is the contribution to the detector response due to gamma rays with incident trajectories between θ and $\theta + d\theta$, and between ϕ and $\phi + d\phi$, the total response from all directions is expressed by the integral

$$D = \int_0^\pi \sin\theta d\theta \int_0^{2\pi} d\phi D(\theta, \phi)$$

$$= \int_{-1}^1 d(\cos\theta) \int_0^{2\pi} d\phi D(\theta, \phi). \quad (16.1)$$

We refer to $D(\theta, \phi)$ as the detector *dose angular* (or *directional*) *distribution*.

One reason for introducing $D(\theta, \phi)$ is simply that the radiation affecting a detector may be analyzed into components coming, say, from a wall or a ceiling. If there is negligible air scattering, the photon trajectories of importance all intercept both detector and wall or ceiling surface of interest. We designate this surface by S, and define a function $g_S(\theta, \phi)$ which is to be unity if a direction (θ, ϕ) can intercept both surface and detector, but zero otherwise. Then if D_S is the detector response to radiation from S,

$$D_S = \int_{-1}^1 d(\cos\theta) \int_0^{2\pi} d\phi D(\theta, \phi) g_S(\theta, \phi). \quad (16.2)$$

This expression reduces to (16.1) if contributions from all (θ, ϕ) are included. If $D(\theta, \phi)$ does not depend upon ϕ, we write $D(\theta, \phi) = (2\pi)^{-1} D(\theta)$, and

$$g_S(\theta) = 1/2\pi \int_0^{2\pi} d\phi g_S(\theta, \phi)$$

to obtain

$$D_S = \int_{-1}^1 d(\cos\theta) D(\theta) g_S(\theta) \quad (16.3)$$

Note that $g_S(\theta)$ is the fraction of the azimuth contributing, at obliquity θ [29, 30].

The directions (θ, ϕ) which intercept both a given surface (S) and a point at the center of a sphere of unit radius form a kind of cone with apex at the point. (See fig. 16.2.) The aperture of this cone is measured by the size of the area intercepted on the unit sphere; if unit area is intercepted, the surface is said to "subtend a solid angle of one steradian at the point." Since the area of the unit sphere is 4π, the solid angle subtended at any point cannot exceed 4π steradians. *We shall find it convenient to use a different measure of the solid angle in this Monograph: Our unit will equal 2π steradians.* We shall designate the solid angle in these units by ω, and to avoid confusion will refer to ω as the "solid angle fraction."

The solid angle fraction ω_S subtended by a surface S can be obtained from eq (16.2) by replacing

---

[8] It would seem more natural, perhaps, to identify (θ, ϕ) with the direction of photon travel rather than its inverse. We would do this if the current of radiation were to be our focus of attention. But we will be more directly concerned with radiation *sources* than with radiation *fields*. It is therefore natural to refer directions to a polar axis extending from the detector outwards towards the radiation source, since this is the reference system which is easy to use in solid angle calculations of radiation sources.
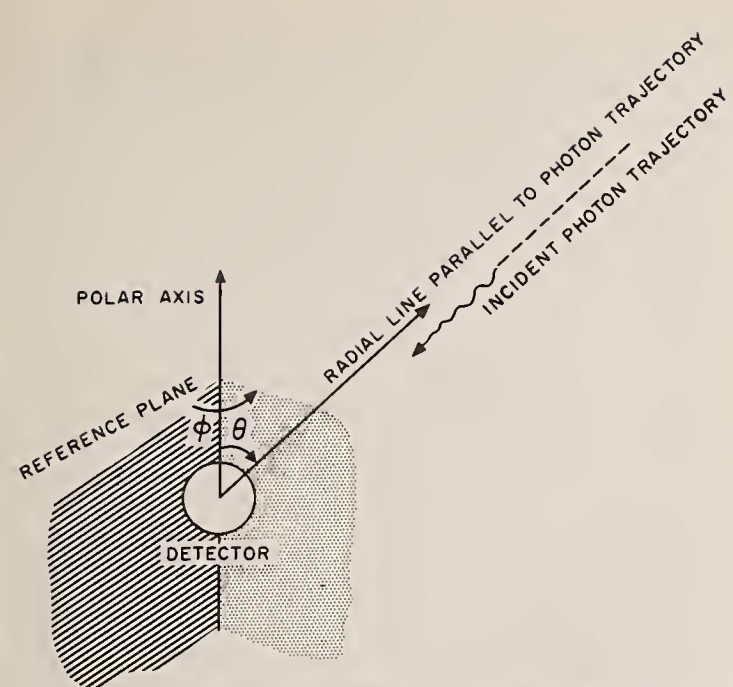
FIGURE 16.1. *A detector about to be traversed by a photon. The photon path passes through the edge of the detector. The polar angles* (θ, ϕ) *correspond to the line parallel to the photon trajectory which passes through the reference point at the center of the detector.*
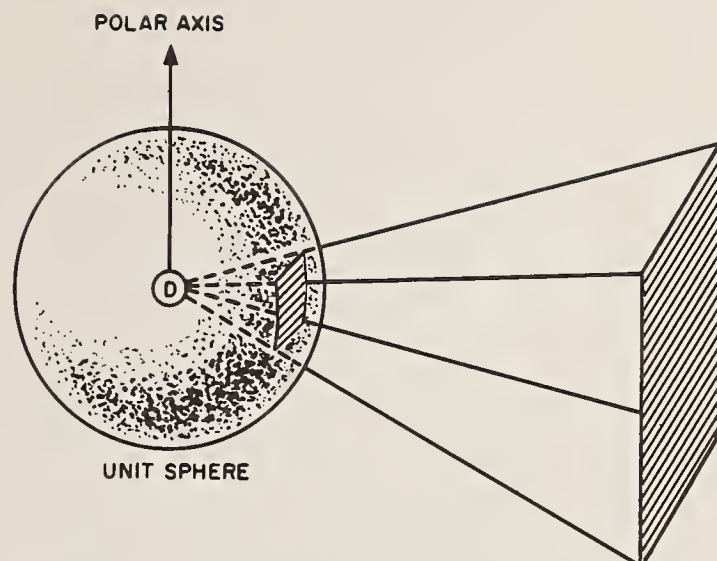

FIGURE 16.2. *A surface subtending at the center of a detector a solid angle whose magnitude in steradians is equal to the shaded area on the unit sphere.*
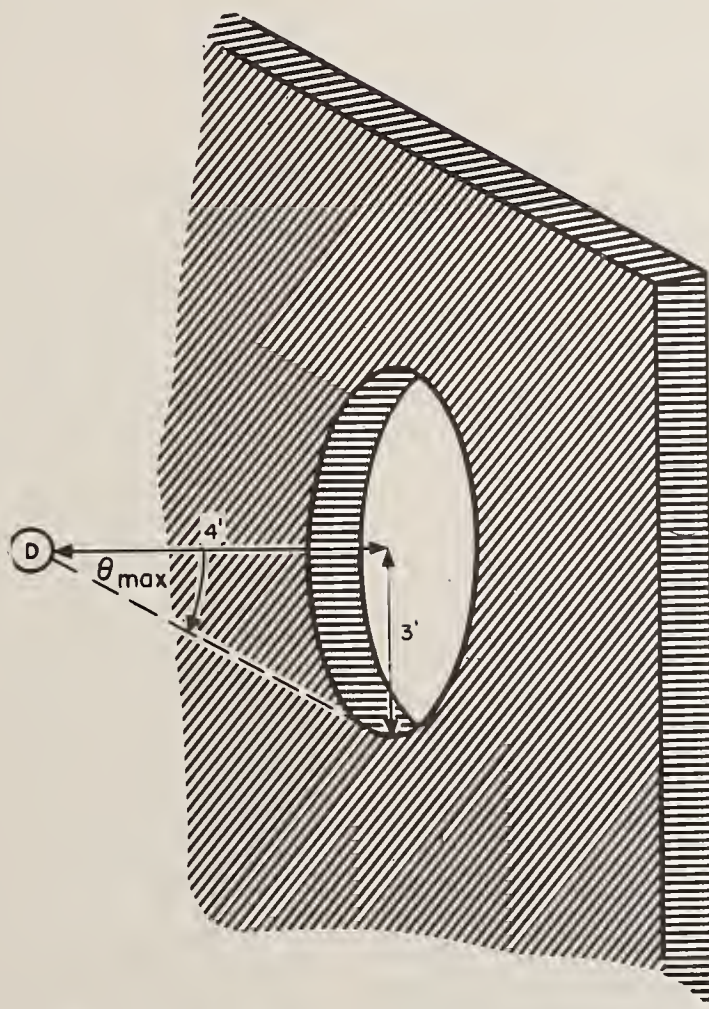

FIGURE 16.3. *A circular aperture of radius 3 feet, through which radiation passes towards a detector placed 4 feet from the aperture and on the perpendicular line through its center.*

9

$D(\theta,\phi)$ by the constant $(2\pi)^{-1}$, or from eq (16.3) by replacing $D(\theta)$ with 1.

$$\omega_S = \int_{-1}^{1} d(\cos\theta) \int_{0}^{2\pi} d\phi (1/2\pi) g_S(\theta,\phi)$$

$$= \int_{-1}^{1} d(\cos\theta) g_S(\theta). \quad (16.4)$$

For a plane surface extending in all directions to infinity, with polar axis taken along the perpendicular to this surface, $g_S=1$ for $0 \leq \cos\theta \leq 1$, so that both expressions in eq (16.4) give $\omega_S=1$ for this case. Any single plane surface of finite extent will subtend an ω smaller than 1.

EXAMPLE. Calculate the detector response D at a position opposite the center of a circular aperture of radius 3 ft through which radiation is entering a building, and distant 4 ft from the aperture. Assume that the dose angular distribution from all points of the aperture has the constant value D_A, that only radiation entering through the aperture contributes to the detector response (see fig. 16.3), and neglect air scattering.

We choose as polar axis the direction from the detector through the center of the aperture. Then the angular distribution of the dose becomes D_A for $\theta < \theta_{max} = \tan^{-1} 3/4$ and zero for $\theta > \theta_{max} = \tan^{-1} 3/4$. Since $\tan^{-1} 3/4 = \cos^{-1}(4/5)$, we write

$$g_S(\theta,\phi) = \begin{matrix} 1, \cos\theta \geq 4/5 \\ 0, \cos\theta < 4/5 \end{matrix}.$$

Since both g_S and D are independent of ϕ, eq (16.2) reduces to eq (16.3), and

$$D_S = \int_{4/5}^{1} d(\cos\theta) D_A = 1/5 \ D_A. \quad ANSWER$$

Note that for constant D_A, as in this case, D_S is always given by $D_A \omega_S$, i.e., that $\omega_S = 1/5$ for the aperture of this example.

17. Radiation Sources

Fallout material has already been referred to as the "source" of the fallout gamma rays. We often refer to the gamma ray generating material as the *primary source*, because it is a convenience at times to treat any interface through which radiation emerges as a "source." If the radiation is not actually produced at such an interface, it is termed a *secondary source*. Note that the aperture of the preceding example acts as a secondary source.

Fallout material can be spatially distributed into almost any geometric configuration conceivable; but two configurations are of special importance because they occur frequently and also because many others of real importance can be obtained from these two. One of these is called a *point source* and is approximated by a local concentration of fallout material into a volume of negligible dimensions. The other is called a *plane*

source and corresponds to a uniform spread of fallout material in a plane. If the source is assumed to cover the whole plane, one speaks of the source as an *infinite plane source;* but if the source has finite area it is called a *finite plane source.*

The strength of a radiation source can be described in various ways. It is customary in physics to measure the source strength in terms of the number of nuclear disintegrations occurring every second. A source is said to have a strength of one curie if 3.7×10^{10} nuclear disintegrations occur per second. On the other hand, in radiology one speaks of a source which produces an exposure dose of one roentgen per hour at a location one meter from the source [see, e.g., 31]. Since protection is a relative matter, we discuss source strengths in this Monograph in terms of the exposure dose they produce at fixed positions; and we do not attempt to specify source strengths in curies even though this is possible. Our practice here is thus akin to that just attributed to radiologists. More specifically, the real problem in radiation protection is to determine how much safer one location is than another. We therefore define a standard "unprotected" position and measure the protection according to reduction of the exposure dose below that experienced in the standard position.

18. Protection and Reduction Factors

We wish to introduce a quantitative measure of the protection afforded by structures, by one structure relative to another, or one location in a structure relative to another. Also, in order to gauge the overall effectiveness of protective construction, a standard "unprotected" position is needed for comparison.

Fallout is assumed to cover uniformly all surfaces according to their horizontal projection, as already mentioned. From this primary source the radiation travels to the detector, wherever it may be. A fairly obvious choice for a completely unprotected detector location would be above ground in a large, open field. This choice has been made frequently; but it has two difficulties: One is that the detector response depends upon the "roughness" of the ground surface; and the other is that location of the source at the ground-air interface makes it very difficult to calculate the detector response accurately even if the spectrum and strength of the primary source are completely known. The first difficulty makes it hard to "standardize the standard," so to speak, while the second makes it hard to evaluate the standard.

For these reasons we have chosen as a "standard unprotected position" a detector location three feet above a hypothetical source of the same character as the fallout on the ground, but at a hypothetical smooth, infinite plane "interface" with the ground replaced by compressed air of

the same density.[9] By making the source plane ideally smooth we avoid the ground roughness difficulty; and by replacing the ground by "compressed air" we make an accurate theoretical analysis possible in a fairly realistic case and thus avoid the second difficulty. To complete the description of the "standard unprotected position" it is necessary to add that the 3 ft separation is in dry air at 76 cm Hg pressure and a temperature of 20° centigrade.

There are at least three additional reasons for this choice of reference detector location: (1) It gives an extreme, but not unrealistic estimate of the dose to which the centroid of the body is exposed in an open contaminated field. (2) Given the spectrum and strength of the gamma rays emitted per unit area of the primary source, the reference dose rate can be calculated to about 2–3 percent accuracy, which is an order of magnitude more accurate than necessary for most shielding estimates. (3) It appears easier and more natural to consider ground roughness as an additional "bonus" shielding from fallout on the ground, because the same "bonus" protection does not exist against the fallout on top of the protective structure.

We define the "protection factor," P, as the ratio of the detector response D_0 in the standard unprotected position to the detector response D in a protected position, i.e.,

$$P = D_0/D. \qquad (18.1)$$

The reciprocal quantity is what is actually determined in structure analysis, and for easy reference it will be termed the "reduction factor" and usually referred to simply as D/D_0. In this monograph D_0 always refers to detector response at the "standard unprotected position."

Note that the protection factor is not defined in terms of a "standard" spectrum, so that it is a quantity which will vary, e.g., with time after fission, weapon type, etc. This reflects accurately the situation because the protection which a structure gives will itself vary with circumstances; and in all likelihood, the actual variation will cover a wider range than given by a variety of different estimates. All fission data in this monograph correspond to a spectrum calculated for 1.12 hour old mixed fission products, as already indicated.

19. Attenuation of Gamma Rays

Before proceeding to the discussion of structure analysis, we wish to examine briefly what happens to gamma rays emitted by a point source embedded in some material, in order to form a picture of their "history" and an appreciation of the different factors leading to their attenuation (reduction in strength). [See also 12, Section 5.]

Very near to the source most of the gamma rays are diverging radially away from their point of origin. As they diverge from the common source, they also tend to spread apart from each other. The effect can be visualized by thinking of concentric spheres surrounding the radiation source, with radii designated by r. As gamma rays from the source travel outwards they will intercept spheres of increasing radii which have an ever greater surface area. Even if all the gamma rays pass unhindered through the spheres, they will be spread ever more thinly the farther out they travel, simply because they will be distributed over a larger area. This has the consequence that the exposure dose measured by a small detector of cross sectional area a will decrease with distance r from the source in proportion to r^{-2}, because the detector can only respond to a fraction $a/4\pi r^2$ of the total flux emerging from the sources. This is the *inverse square law of attenuation* with distance from a source.

Each gamma ray photon from the source penetrates unhindered through the surrounding material until an interaction occurs, but the interactions are chance occurrences. There is a fixed probability determined by the photon energy and type of material traversed that in a given segment of the path an interaction will occur. This means that in each succeeding layer of material a fraction of the photons undergo their first interaction, and the number of photons penetrating the layer without interaction is correspondingly reduced. We say that the "unscattered beam" undergoes *exponential attenuation*. Successive layers of material equally thick reduce the number of unscattered photons by the same fraction, assuming the layers to be homogeneous and equally dense. Tables of attenuation coefficients are given in [32].

If the first interaction is a scattering, the gamma ray photon may travel further, though with reduced photon energy and changed direction. Other interactions follow, separated by path segments which tend to become shorter as the photon energy becomes smaller. Eventually an absorptive interaction terminates each photon "history."

Many of the gamma ray photons continue to increase their distance from the source even after a number of scattering interactions. Thus, at any fixed distance there will be gamma rays which have been scattered once, twice, many times, in addition to some which have not been scattered at all. Because all "orders of scattering" must be considered as giving a contribution to the detector response, the exponential attenuation of the unscattered gamma rays does not describe accurately the law of attenuation due to the combined effect of all interactions. It is customary to modify the exponential law (accurate for unscattered photons) by a factor called the *build-up factor* to take into account the presence of scattered gamma rays. (Tables of build-up factors are given in [33].)

If the primary source is located in the air, gamma rays from the source may strike a wall. Because gamma rays can have scattering interactions which completely reverse their direction,

---

[9] Note that the density of the "compressed air" is immaterial except for purposes of visualization, so that the reference configuration is actually an infinite plane source in an infinite homogeneous medium. (See Section 25.)

11

some of the radiation will be "backscattered" from the wall, re-emerging again into the air. A great deal of interest attaches to the fraction of the gamma ray energy entering the wall which comes back out again in this way, i.e., the "energy albedo." If the different spectral components are weighted according to the efficiency of detection by an air-equivalent detector, an analogous "dose albedo" may be determined. We view this latter ratio as a type of reduction factor for purpose of comparison with the other factors, and refer to it simply as the *albedo* [34].[10]

Other definitions might be useful, but for the most part these four—the inverse square law, the exponential factor, the build-up factor, and the albedo—are sufficient for discussion purposes. Figure 19.1 illustrates the first three factors in a particular case.

IV. Introduction to Structure Shielding Analysis

20. Basic Approach

The analysis of structure shielding can best be described in connection with a typical, but elementary example. Figure 20.1 shows a "blockhouse," i.e., a building with four walls and a roof. Fallout rests on the roof and on the ground around the structure. We are primarily interested in the dose measured at detector position A.

Radiation contributing to the detector response comes from all directions. Because of the low density of air, most of the detected radiation moves in straight lines to the detector from points of emergence at the walls. Thus it is natural to speak of detector response due to radiation "from the walls," "from the roof," "from the window," etc. We expect that radiation "from the walls" will have little resemblance to radiation "from the roof" in intensity or directional distribution. Radiation "from the roof" originates from the fallout resting on top of the roof, while radiation "from the walls" originates from fallout on the ground, possibly a long distance from the structure. These marked differences make it reasonable to differentiate between detector response "components" from the different wall surfaces.

Radiation from a wall ordinarily has entered the wall from the outside. Thus when one speaks of radiation "from a wall," the reference may be either to the radiation passing from wall to detector or to radiation initially incident upon the exterior surface of the wall in question. In other words, one can classify the detector response components according to interior *or* exterior surface crossed. For our purposes the latter is usually preferable and can be expressed as follows: If that part of the detector response due to radiation entering the "*i*"-th distinct wall section from the outside is designated D_i, the total detector response will be

$$D = \sum_i D_i, \qquad (20.1)$$

where the sum extends over all distinct exterior wall surfaces. Such a classification is useful for many reasons. In addition to differences in incident radiation characteristics, the attenuation is apt to differ widely from one wall section to another. This has the consequence that the dominant source of radiation can be a particular wall or wall section. Further, it is usually a straightforward

matter to treat backscattering from interior surfaces by a simple corrective factor.[11]

We next select a particular wall surface, namely that adjacent to detector positions B and C in figure 20.1; only radiation entering and leaving this wall surface is to be considered for the moment. To contribute to the detector response, radiation must first pass through the wall and then "locate" the detector. The detector response at B divided by the response at position C is approximately the reduction factor due to interactions within the wall material. If the detector is moved away from B towards A, the detector response will decrease further. This additional "attenuation" is due to the "inverse square" effect described in the preceding Section.

We distinguish between these two types of attenuation and refer to them separately. The first, attenuation by interactions with wall material, we shall call *barrier reduction* due to *barrier shielding*. The second, accompanying a displacement of the detector farther from the wall, we shall call *geometry reduction* and speak of it as due to *geometry shielding*. The following subsections describe these quantities in greater detail and give reasoning which leads to their introduction. Here it will suffice to say that geometry reduction can often be considered as mainly a limited-source effect. The wall acts as a secondary source; and if this source were constant on a plane extending laterally to infinity, there would be no appreciable difference in intensity between detector positions A and B. The geometry reduction comes about primarily because the wall, being finite, subtends a smaller solid angle at A than at B.

If a reduction B_1 of the detector response occurs between C and B, and a further reduction G_1 occurs when the detector is moved from B to A, the detector response D_1 at A may be written

$$D_1 = G_1 B_1 D_C \qquad (20.2)$$

where D_C is the detector response at a reference

---

[10] Still other types of albedo factor have been defined, using number of photons in place of energy or dose. Only the "dose albedo" appears in this manual, so that the use of "albedo" to refer to dose albedo should not be confusing.

[11] By classifying according to exterior surfaces one estimates that a certain fraction of the radiation entering the room from one wall will affect the detector after backscattering from other walls. An estimate of this corrective factor is then made with little concern about the detailed history of the radiation or about effects due to radiation entering through the other walls.
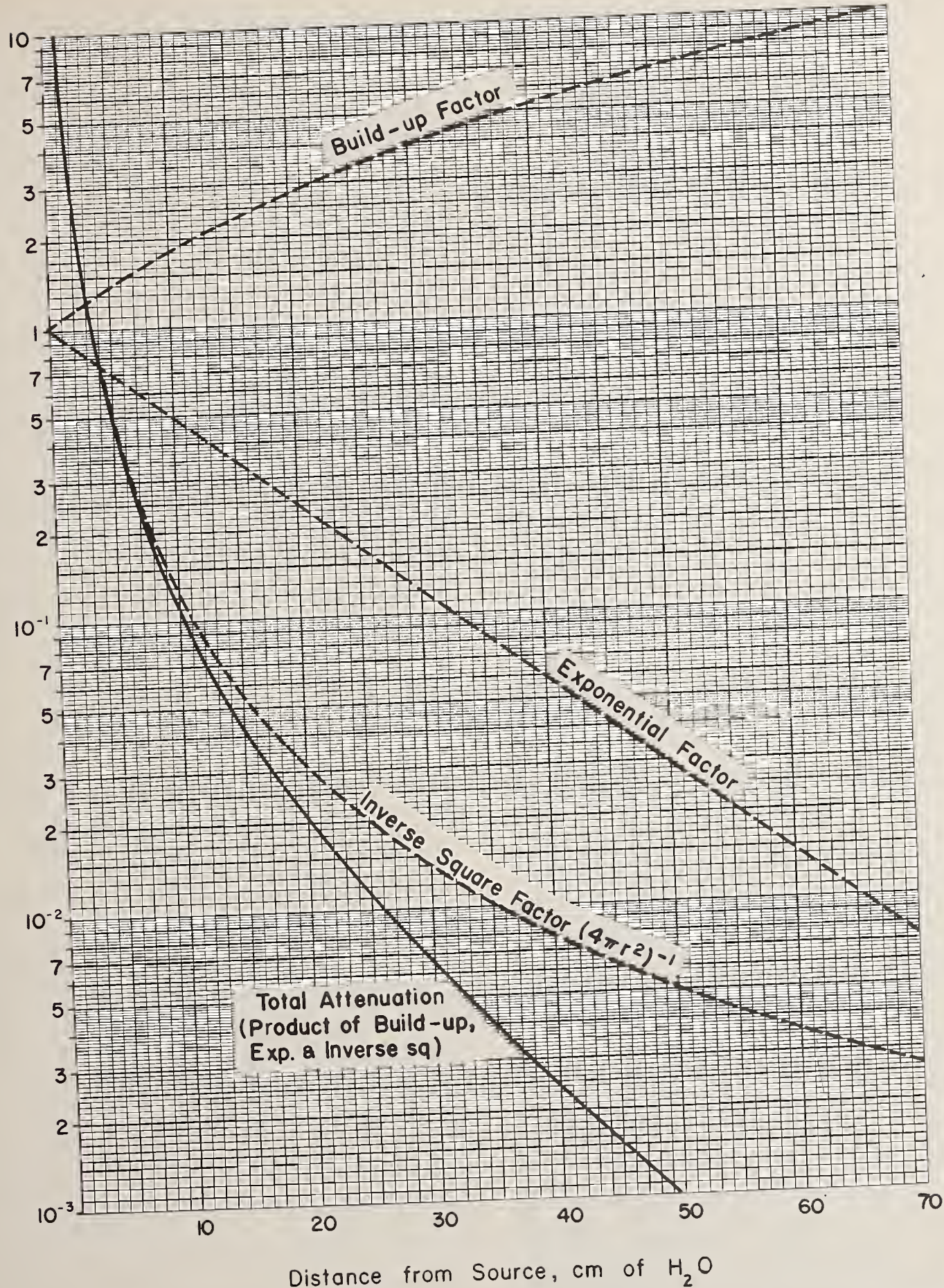
12

FIGURE 19.1. *Factors describing radiation attenuation. The solid curve gives the gamma ray dose at various distances from a 1 Mev point source in H_2O. The dashed curves give inverse square, exponential, and build-up factors which combine to give the solid curve.*
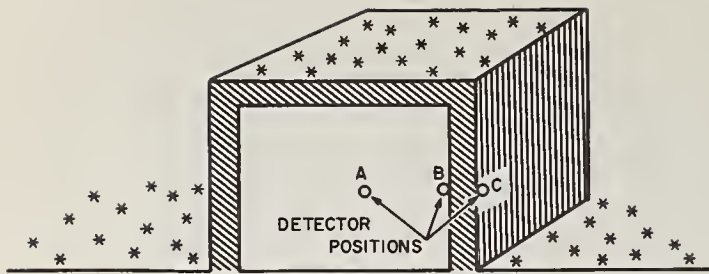
13

FIGURE 20.1. *A blockhouse, with fallout on roof and ground.*

position C, which is here shown as just outside the wall.

The dose from a wall section nearly always will be written in the form eq (20.2), so that calculation of the D_i involves determination of appropriate barrier and geometry reduction factors for each type of wall surface.

Though D_C in this example is the dose just outside the exterior wall, the comparison with the standard value D_0 is of most fundamental interest. This change requires definition of a modified barrier factor $B'_1 = B_1 D_C / D_0$, which expresses the combined reduction due to attenuation in the wall and exterior air. Henceforth barrier factors will be of this type, i.e., ratios of the detector response at position adjacent to a barrier to the standard response D_0.

The approach described here depends for its success on the fact that only ~15 percent of the radiation energy incident on a surface is backscattered. This relatively low albedo insures that most of the detector response is due to radiation which has had contact with only one wall.

21. Discussion of Barrier and Geometry Reduction Factors

In the preceding Section a distinction was made between two types of reduction in the detector response. The reasoning which leads to this distinction is essentially as follows:

Most theoretical data derives from the study of an especially simple case in which the medium has no irregularities (infinite homogeneous medium). The source may be concentrated on a plane in the medium or localized at a point. Calculations of the detector response as a function of distance from the source in such an elementary case can be done to within a precision of a few percent. Because these calculations have internal consistency and reliability, and also because they usually represent a good approximation to the reduction in intensity due to actual slab barriers, we nearly always find it convenient to consider ratios between actual detector response due to radiation from a particular wall, say, and detector response as estimated by such infinite medium calculations. The resulting ratios express nearly all the special characteristics of the configuration, but they vary slowly as the position or the configuration is changed. It is possible to *estimate* these ratios with calculations for an infinite

medium, since they express effects such as source "finiteness." [12]

Thus, the detector response is expressed as the product of two factors: One gives the attenuation in the wall material which would occur if the source were of a particularly simple type and the medium everywhere uniform in density; and the other is a ratio which expresses all the other features of the actual configuration. For convenience we give these two factors names. The name "barrier factor" for the first is a fairly obvious choice. The name "geometry factor" is chosen for lack of a more accurate term of reasonable length. (Note that the term "configuration factor" would be more appropriate but is not used here because of its length.)

One more aspect of this development deserves comment. In practice, structure shielding analysis requires a great variety of standardized functions expressible in the form of tables, graphs, and possibly empirical formulas. Many of these functions are rather naturally classified as geometry or barrier factors. We make the attempt to carry this classification as far as possible, with the consequence that standard functions may be referred to as "geometry factors" which are not obviously related to other functions also referred to as geometry factors. The next two sections describe some of the independent variables which determine these factors both as to type and as to numerical value.

22. Barrier Shielding and Effective Mass Thickness (X)

The shielding provided by a barrier depends upon many variables, among which are
  (1) the weight per unit area of the barrier,
  (2) the type of barrier material,
  (3) the gamma ray spectrum, and
  (4) the directional distribution of the radiation striking the barrier.

We discuss items (3) and (4) first: Data will be given only for a single fixed spectrum, namely that of figure 11.1, (top); variations of the fallout gamma spectrum with time after the burst are not taken into account. The directional distributions of incident gamma rays vary widely, so that results for each of the most important cases will be identified with a special symbol.

Items (1) and (2), the type and thickness of the barrier, can be treated together because of a fortunate circumstance: Nearly all important construction materials have atomic numbers low enough so that the attenuation is due primarily to scattering interactions, which are independent of the energy states occupied by the electrons. Thus, the attenuation produced by a barrier depends almost completely on how many electrons it puts in the path of the gamma rays, and this is

[12] Basically, reduction due to attenuation in barriers is exponential, while reduction due to configuration is a power function. We are in fact using the same ideas that lead to the introduction of the Build-up Factor concept. Estimation of these new ratios requires a knowledge of dose angular distributions.

simply the product of the number of electrons per unit volume with the thickness of the barrier.

Therefore, to measure the effectiveness of barrier shielding a parameter X is used which is proportional to Δ (barrier thickness), and to $\rho<Z/A>$ where ρ is the density and $<Z/A>$ is the ratio of atomic charge to atomic mass number, averaged over the constituent elements of the barrier.[13] (Note that $\rho<Z/A>$ is proportional to electrons per unit volume, the proportionality constant being Avogadro's number.) In particular, we define X by the expression

$$X = 2<Z/A>\rho\Delta. \qquad (22.1)$$

The factor of two is introduced because $<Z/A>$ is nearly 0.5 for such important construction materials as brick and concrete, so that $2<Z/A> = 1$ for those materials. If the factor $2<Z/A> \approx 1$ is treated as a dimensionless proportionality constant, X can be measured in units lb/ft^2 (psf), since the unit weight is usually given in lbs/ft^3, thickness in feet, and $lb/ft^3 \times ft = lb/ft^2$. Because X is nearly always close to the weight per unit area, or mass thickness, we call this quantity the *effective mass thickness*.[14] Table 22.1 gives $2<Z/A>$ for a number of common materials, together with the density of the solid material.

TABLE 22.1. *Values of $2<Z/A>$ and ρ*

Material	$2<Z/A>$	ρ, Density in pcf
Water	1.11	62.4
Wood	1.06	34.0 (average)
Air	1.0	0.076
Brick	1.0	115
Concrete	1.0	144
Soil (depending on water content)	1.00–1.02	100 (average)
Steel	0.931	480
Lead [a]	0.791	710

[a] Lead is included strictly for comparison. It should be remembered that the data in this monograph do not apply to lead because it absorbs rather than scatters the radiation. See the last paragraph of this section.

TABLE 22.2. *Mass thickness of common building materials used in various building components.*

INDIVIDUAL BUILDING MATERIALS			
Item	Thickness	Weight Psf	Component
	Inches		
Adobe	12	116	Wall
Asbestos board	$3/16$	1.7	Do.
Asbestos, corrugated	--------	4	Roof, wall
Asbestos shingles	$5/32$	1.8	Do.
Asphalt roofing, 3-ply ready.	--------	1	Roof
Asphalt roofing, 4-ply & gravel.	--------	5.5	Do.

[13] In particular, $<Z/A> = \sum_i \left(\frac{Z_i}{A_i}\right) f_i$, where f_i is the fraction of the mass due to the ith constituent.

[14] "Effective mass thickness" and "equivalent thickness of concrete," a term used in the ODM report [7] are different names for essentially the same quantity.

INDIVIDUAL BUILDING MATERIALS			
Item	Thickness	Weight Psf	Component
	Inches		
Asphalt roofing, 5-ply & gravel.	--------	6.2	Do.
Asphalt shingles	--------	2.3	Do.
Brick	4	39±1	Wall
Do	8	79±10	Do.
Do	12½	115±15	Do.
Do	17	154±20	Do.
Clay tile shingles	--------	15±5	Roof
Clay tile, structural	4	18	Wall
Concrete block, hollow.	4	30±4	Do.
Do	8	55±5	Do.
Do	12	85±10	Do.
Concrete, reinforced	1	12½	
Do	12	144	
Fiber board	½	0.8	Wall
Fiber sheathing	½	0.9	Do.
Gypsum block	2	9.5±1.5	Do.
Do	4	12.5±2.5	Do.
Gypsum board	½	2.1	Wall, ceiling
Gypsum, sheathing	½	2.0	Wall
Marble facing	2	26	Do.
Plaster, directly applied.	¾	5	Wall, ceiling
Plaster on fiber lath	½	5.0	Do.
Plaster on gypsum lath.	½	6.0	Do.
Plaster on metal lath	¾	6.0	Do.
Plaster on wood lath	¾	5.0	Do.
Plaster, solid	2	20	Wall
Do	4	30	Do.
Plywood, finish	$5/16$	1.0	Do.
Do	½	1.5	Ceiling
Plywood, sheathing	$3/8$	1.1	Wall, roof
Slate	$3/16$	7.3	Roof
Steel, corrugated, 20 ga.	--------	2	Roof, wall
Steel panel, 18 ga	--------	3.26	Wall, roof
Stone	12	130	Wall
Stone, cast, facing	2	24	Do.
Stucco, metal lath	¾	9.0	Do.
Stucco, wood lath	¾	8.0	Do.
Terra cotta facing	1	5.4	Do.
Wood block, flooring	3	10	Floor
Wood finish flooring	$25/32$	2.5	Do.
Wood sheathing	¾	2.5	Floor, roof
Wood shingles	--------	2.5	Roof
Wood shingles 6½ in. to weather.	--------	1.1	Wall
Wood siding, 8 in. bevel.	--------	1.5	Do.
Wood siding, 6 in. drop.	--------	2.5	Do.

COMPOSITE MATERIALS			
Brick	4		
and structural clay tile.	4	60	Wall
Ceramic tile	$5/16$		
on mortar bed	¾	11	Do.
Do	$5/16$		Floor
	2	23	Do.
Concrete, reinforced ribbed slabs (see section on components).	--------	--------	
Marble or terrazzo on concrete fill.	4	50	Do.
Plaster, hollow wall with steel studs.	4	22	Wall
Plaster on suspended metal lath.	--------	10	Ceiling
Wood finish floor on wood sleepers	¾		
	4	--------	
Lightweight concrete fill.	4	23	Floor

TABLE 22.2 *Mass thickness of common building materials used in various building components*—Continued

DOORS AND GLASS			
Item	Thickness	Weight Psf	Component
	Inches		
Door, wood exterior, standard 3 ft–0 in. x 6 ft–8 in. solid core flush panel.	1¾	4.5	Small buildings
Door, wood interior, standard 2 ft–6 in. x 6 ft–8 in. hollow core.	1⅜	1.9	
solid core	1⅜	4.0	Do.
Door, glass, exterior, aluminum edge, standard 3 ft–0 in. x 7 ft–0 in.	ª¼	5.1	Large buildings
Door, glass, exterior standard, 3 ft–0 in. x 7 ft–0 in.	¾	11.0	Do.
Glass, double strength.	⅛	1.6	Small buildings
Glass, plate	¼	3.5	Large buildings

ª Glass.

Barrier shielding factors are considered functions of the effective mass thickness, i.e., $B=B(X)$. Use of the concept of effective mass thickness makes it possible to perform calculations even when barriers are composed of several layers of different materials. One merely sums the effective mass thickness (X_i) of the different layers to obtain the total effective mass thickness $X=\sum_i X_i$.

It should be remembered that the effective mass thickness is *not* $\rho\Delta$, the weight per unit area, though the two can be numerically equal. Table 22.2 summarizes effective mass thickness data for a variety of common construction materials and combinations. This data is taken from the compilation of [35]. It is important to realize also that the mass thickness of a wall, floor, etc., can ordinarily be obtained by use of the usual dead load tables in engineering handbooks, though for very thick walls (several hundred psf), one may have to adjust for hollow spaces within the construction (see Section 36).

EXAMPLE: A barrier is composed of wood and concrete layers having weights per unit area 5 lb/ft² and 50 lb/ft², respectively. Find the effective mass thickness for the barrier.

$$X=(5 \text{ lb/ft}^2)\times1.06+(50 \text{ lb/ft}^2)\times1.00=55.3 \text{ psf.}$$
ANSWER.

Figure 22.1 illustrates the dependence of barrier attenuation on the mass thickness and atomic number. Notice that even steel (atomic number 26) gives only slightly more protection than concrete of the same effective mass thickness. If desired, the ratio between the curves in figure 22.1 can be applied as a correction to take into account the minor differences between low atomic number material; but with composite barriers this must be done with care.

Materials with high atomic numbers, such as Pb, give additional protection; but the difference is not so great as is commonly supposed. To reduce the intensity of 1 Mev radiation by a factor of 1,000 requires a concrete barrier having $X=305$ psf as compared with a Pb barrier having $X=190$ psf. But the weight per unit area is $X(2<Z/A>)^{-1}$, which for Pb is $190/.791=240$ lb/ft² while for concrete it is $305/1.0=305$ lb/ft². Thus nearly ⅘ as much Pb (by weight) is required as concrete.

23. Geometry Reduction and Solid Angle Fraction

To identify other important variables on which the detector response depends, we consider again the blockhouse illustration and in particular the detector response at position A due to the wall on the right (fig. 20.1).

(1) Solid angle fraction: It is clear that the detector response will depend on the "apparent" size of the wall, as seen from the detector.[15] Since "apparent size" is conveniently measured in terms of solid angle or solid angle fraction, we say that the detector response will depend upon the solid angle fraction ω subtended at the detector by the radiation source.

(2) Barrier thickness: The thickness of the wall (X) will have an effect upon the detector response over and above the attenuation which we describe by a barrier factor. This is because the directional distribution of radiation emerging from the wall affects the detector response but is in turn affected by the wall thickness. In most cases and up to a limit, thicker walls tend to produce directional distributions more and more concentrated along the perpendicular to the wall surface.

(3) Wall shape and detector position: The dependence on detector position is easy to demonstrate in the blockhouse illustration by the fact that one can find detector positions at the ceiling and floor in which the wall subtends the same ω, but in which the detector response is expected to differ considerably. Shape effects can also be easily demonstrated: A detector 10 ft out from the center of the wall will have one response if the wall is long and narrow and another if the wall is square, though subtending the same solid angle.

(4) Type of source: The type of primary source, as in the case of barrier factors, varies widely enough so that we identify each with a special symbol.

(5) Type of wall material: We treat for the present only the case of materials of atomic number ~30 or below, this range including the most important materials commonly employed in construction. As indicated in the preceding Section, these low-Z materials have a certain equivalence which we utilize.

In line with the discussion of Sections 20 and 21, we consider all effects other than that due to

[15] The detector response could equally well be said to be a sum of contributions from each element of the source. Following this idea, the detector response could be written in terms of the radiation current flowing through the differential area elements of the wall. This point of view is equivalent to one we adopt, in which the emphasis is on flux directional distributions at the detector, provided the radiation current emerging from the wall is independent of position on the wall. We make this assumption throughout this manuscript.
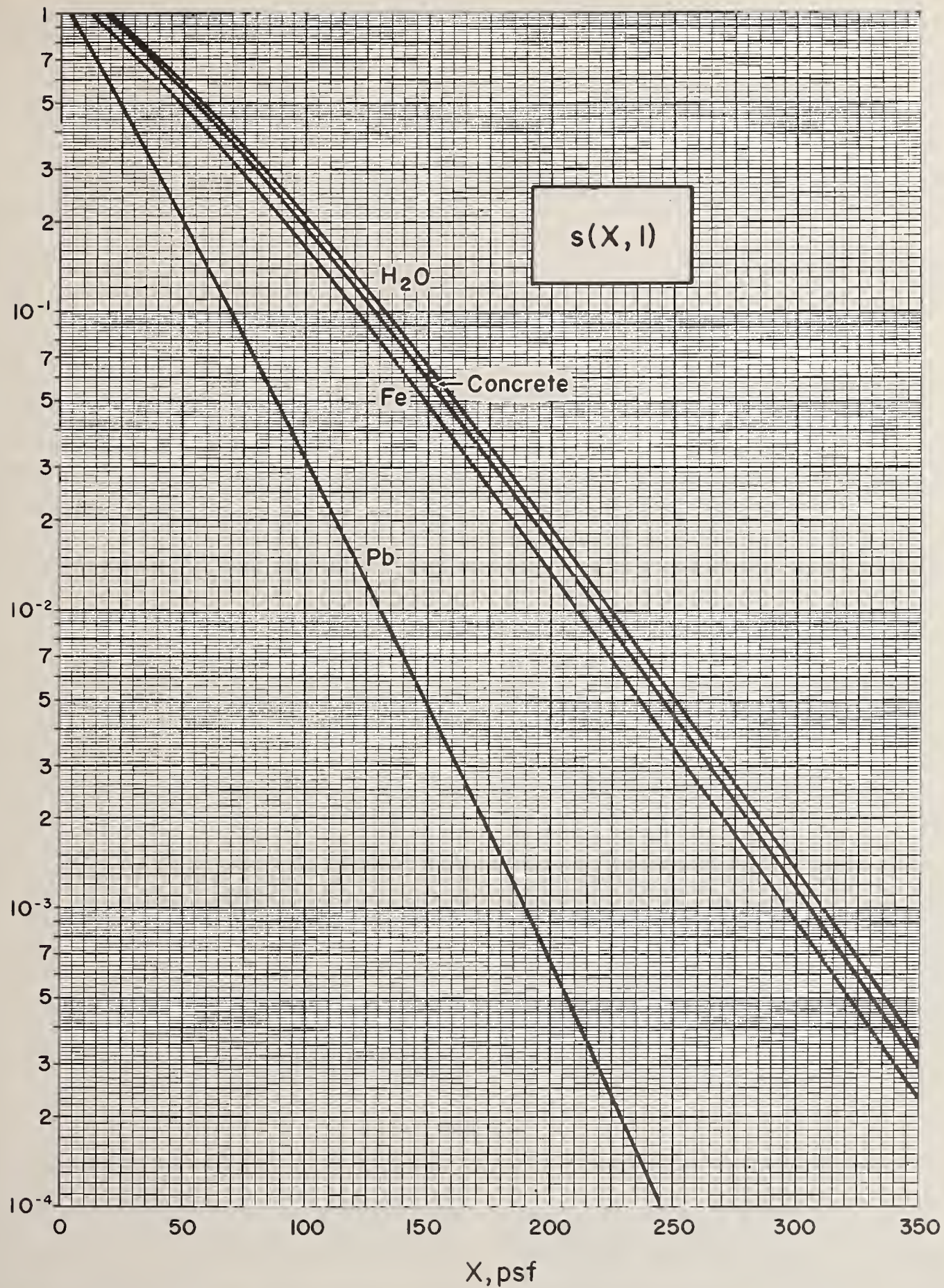
FIGURE 22.1. *Attenuation of 1 Mev gamma rays in different materials (plane perpendicular source).   Notice that Fe, concrete, and H_2O are separated by small, nearly constant factors.*

simple attenuation in the wall as expressed by a single "geometry" factor G. Variations due to X and ω are taken into account by writing

$$G=G(X,\omega). \qquad (23.1)$$

To take shape dependence into account we represent actual source shapes as superpositions of simpler, and different, source shapes. This makes it possible to estimate geometry reduction factors for a set of "standard shapes" which can be combined to approximate most of the important shapes encountered in practice (see Part VII). Formally, this means that we write

$$G(X,\omega)=\sum_i G(X,\omega_i), \qquad (23.2)$$

where $G(X,\omega_i)$ is the geometry factor for one of the "standard shapes." Note that to insure the correct solid angle fraction, the condition $\omega=\sum_i \omega_i$ must be imposed.[16]

Although the blockhouse illustration is useful for purposes of identifying variables, it does not show how one might refer to quite different quantities as "geometry factors." For this purpose we use a different example: Consider a heavy multistory building with fallout on the (flat) roof and detector in the basement. Radiation can reach the detector only after passing through several heavy floor slabs. To account for barrier attenuation and remove it from consideration, we may divide the detector response by the expected response if the material between source and detector were uniformly distributed, and if the radiation source extended unchanged in the plane of the roof to infinity in all directions (infinite plane source). The resulting ratio, which we consider a type of geometry factor, would depend upon the following things: (1) The extent of the roof, which can be expressed in terms of the solid angle fraction subtended by the roof at the detector; (2) the thickness (X) of the barrier between roof and detector; and (3) the shape and position of the roof relative to the detector. Equations (23.1) and (23.2) are as applicable to this case as to the blockhouse wall. The chief difference is that ω is determined for the fallout on the roof, a *primary* radiation source, in contrast to the blockhouse wall example in which ω is subtended by a *secondary* radiation source.

The preceding illustration also makes it clear that the estimation of actual barrier and geometry factors consists mainly in finding a simpler configuration, resembling the actual one in important respects, which is amenable to a detailed theoretical or experimental analysis. This point is elaborated in Parts V and VI.

24. Brief Summary of the Analysis Procedure

The preceding discussion may be summarized by stating that the dose D measured in a structure (such as a blockhouse) will be represented as the sum of contributions D_i entering through different wall sections and ceiling. Each of the D_i will be the product of a barrier factor $B(X_i)$ and a geometry factor $G(X_i,\omega_i)$. Each geometry factor consists of one or more terms corresponding to "partial surfaces" chosen to represent approximately the actual source surface whether primary or secondary. If the reference detector response for the barrier factors is taken to be the standard value D_0 three feet above an infinite, smooth, air-air interface having uniform contamination equal to that on and around the structure, the complete expression for the detector response takes the form

$$D=D_0\sum_i B(X_i)\left\{\sum_j G(X_i,\omega_{ij})\right\} \qquad (24.1)$$

Structure configurations exist which call for more complicated expressions than this. For example, in maze-type geometries the radiation may have to turn corners to reach the detector. In basements below grade the detector response may consist largely of contributions due to gamma rays which have scattered downwards from the exposed superstructure through intervening floor slabs. Such "higher order" contributions give terms involving additional factors, but otherwise of the same type as the terms in eq (24.1).

To differentiate between different types of data, we will replace "B" and "G" by a variety of other symbols, each referring to a single type of data, as indicated in the preceding Sections. We discuss next the theoretical methods for estimating B's and G's, i.e., the derivation of data for applications.

V. Data

25. Introductory Comments

In Part IV a formal approach to shielding calculations has been described. This approach developed out of a study of simple configurations to be described in Part VI; but it has also been designed to emphasize the use of quantities which can be estimated theoretically.

In Part V we turn to the presentation and discussion of data for applications. First we give a description of the "basic" data used to obtain the functions for applications, so that an appreciation of the limitations of the graphs of barrier and geometry factors is possible and also so that one can get an idea how additional information might be obtained. This discussion can probably be skipped or skimmed by readers interested in a particular application, though the

---

[16] For an alternative procedure, see Section 49 and references 29, 30, and 41.

18

"basic" data have some fairly direct applications to shielding problems.

Not all the factors which one might desire can be easily obtained theoretically, or even experimentally. In applications, the graphs of the various factors will no doubt be used in cases beyond their range of applicability. This makes it especially important to give a clear statement of their origin and interpretation. Because this type of background information is least ambiguous when stated mathematically, no attempt is made to avoid mathematical terminology.

26. Basic Data

To produce varied types of basic data, digital computers have proved essential. They are used to generate solutions of the integral equations describing the transport, diffusion, and energy loss of gamma radiation. These "transport equations" have been solved by "moment methods" and by "Monte Carlo methods." The former yield solutions for a source in a medium without boundaries, while the latter permit calculation of boundary effects [12, Section 7].

All tables and graphs presented here have been obtained from four types of basic data: (1) Plane isotropic source case; (2) point isotropic source case; (3) plane oblique source case; and (4) albedo results. The first three were obtained using moment methods; while the last required Monte Carlo calculations. We discuss each type briefly here. Appendix A contains an outline of the actual moment calculations of the first three data types.

(1) Plane isotropic source case: Consider an infinite, plane source of fallout radiation imbedded in an infinite, homogeneous medium. Distance of the detector from the source plane is represented by d. Alternately, distances may be referred to in terms of X, lb/ft² effective mass thickness between source and detector. If the medium is air (at 20°, 76 cm Hg), the relation between the two is

$$d/X = 13.3 \text{ ft of air/psf.} \quad (26.1)$$

At a distance d from the source plane, the radiation produces a dose angular distribution which we refer to as $l(d, \cos\theta)$, where θ is the obliquity measured from the perpendicular from the detector to the source plane.[17] We fix the scale of $l(d, \cos\theta)$ so that an isotropic detector which registers D_0 roentgens three feet above the source will register $dD = D_0 l(d, \cos\theta)\sin\theta d\theta$ roentgens due to gamma rays striking the detector between obliquities θ and $\theta + d\theta$. This implies that[18]

$$\int_{-1}^{1} d(\cos\theta) l(3 \text{ ft}, \cos\theta) = 1. \quad (26.2)$$

Computations of these angular distributions have usually involved their representation as a sum of Legendre polynomials,

$$l(d, \cos\theta) = \sum_{n=0}^{\infty} (n+1/2) l_n(d) P_n(\cos\theta). \quad (26.3)$$

In one type of calculation the first seven or eight functions $l_n(d)$ were determined. An extrapolation $n \to \infty$ was then performed using the fact that $l(d, \cos\theta)$ resembles $(\cos\theta)^{-1} \exp(-a/\cos\theta)$ for $\cos\theta > 0$ when the unscattered component is important. In another type of calculation the unscattered component was calculated exactly and the scattered component determined by summing a series of the type eq (26.3) up to seven or eight terms. (See Appendix A.)

Figure 26.1 illustrates the appearance and behavior of $l(d, \cos\theta)$.[19] The various features of these curves have fairly simple interpretations: Near the source plane (small d), $l(d, \cos\theta)$ is proportional to $(\cos\theta)^{-1}$ for angles approaching but less than $\pi/2$ (i.e., $\cos\theta \to 0^+$). This results in large values for directions nearly parallel to the source plane, an important feature of the radiation from this type of source. With increasing penetration the directional distributions become nearly isotropic in the forward direction (for $d \approx 150$ ft, corresponding to about 0.3 mean free paths for a photon of average energy). For still greater penetrations the distributions become increasingly peaked at $\cos\theta = 1$, as the initially dominant oblique components are preferentially removed.

(2) Point isotropic source case: A source concentrated in a region of negligible dimensions generates gamma rays which penetrate outwards into an infinite, homogeneous medium. At a penetration distance d from the source, the dose angular distribution is identified by $p(d, \cos\theta)$, where θ is measured relative to the axis from detector to source.[20] The scale of $p(d, \cos\theta)$ can be fixed conveniently relative to $l(d, \cos\theta)$ by considering a small contaminated area A of a plane surface located a radial distance r from an isotropic detector, with $A/r^2 \ll 1$. We identify $D_0 p(r, \cos\theta) \times A/4\pi r^2$ with the dose angular distribution at the detector due to this source; but if the whole plane surface were similarly contaminated, we would want the total detector response to be D_0 at a distance of 3 ft from the plane. To write this condition in the form of an integral we take A to be an annular sector of width $d\rho$ and length $\rho d\phi$, as shown in figure 26.2. The detector response D_0 at height 3 ft is then given by the integral over
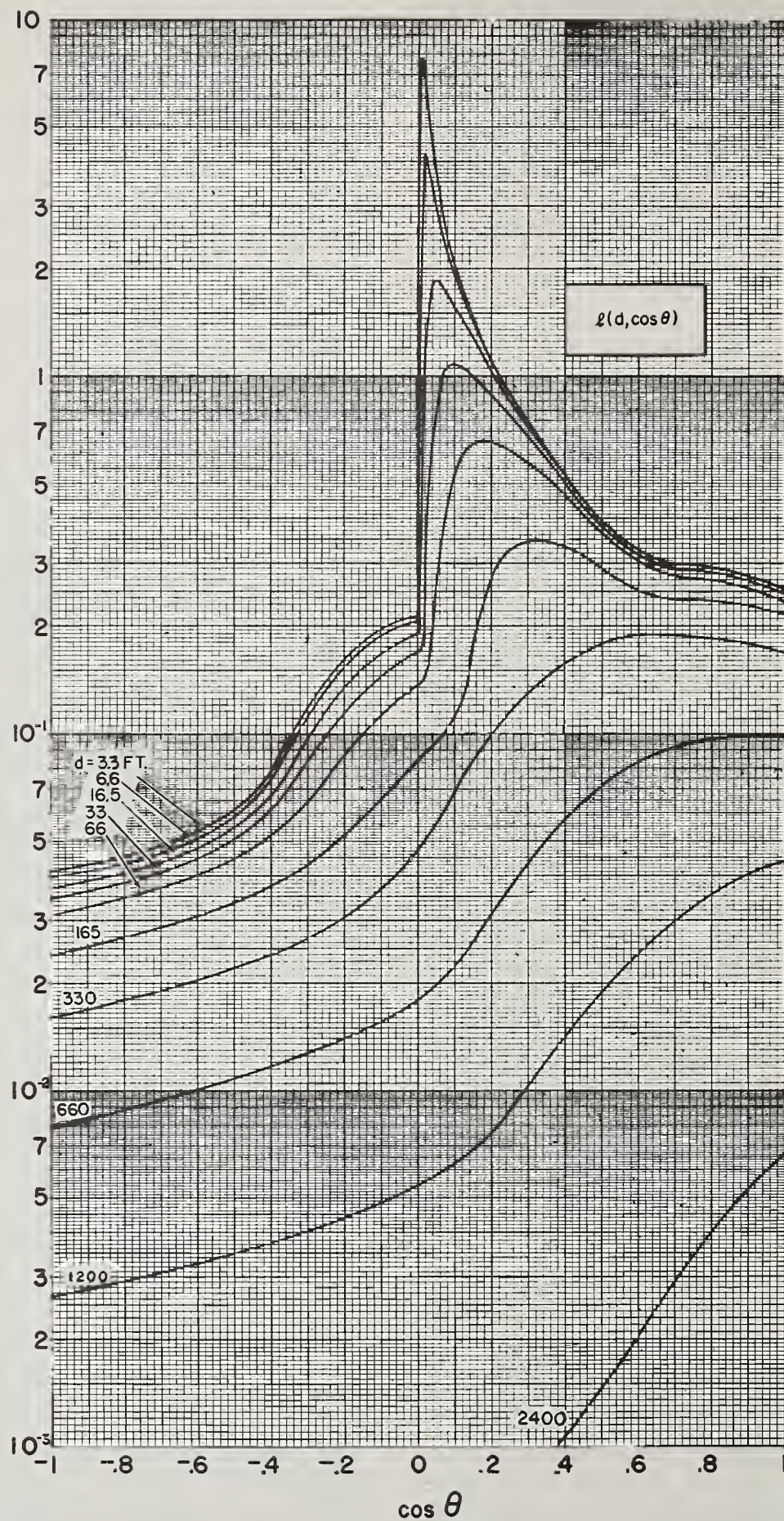
FIGURE 26.1. *Dose angular distributions l(d,cosθ) for an idealized plane fallout source, at different heights in air (d) above the source. (H₂O, 1.12 hr fission. See also figs. B1 and B2.)*
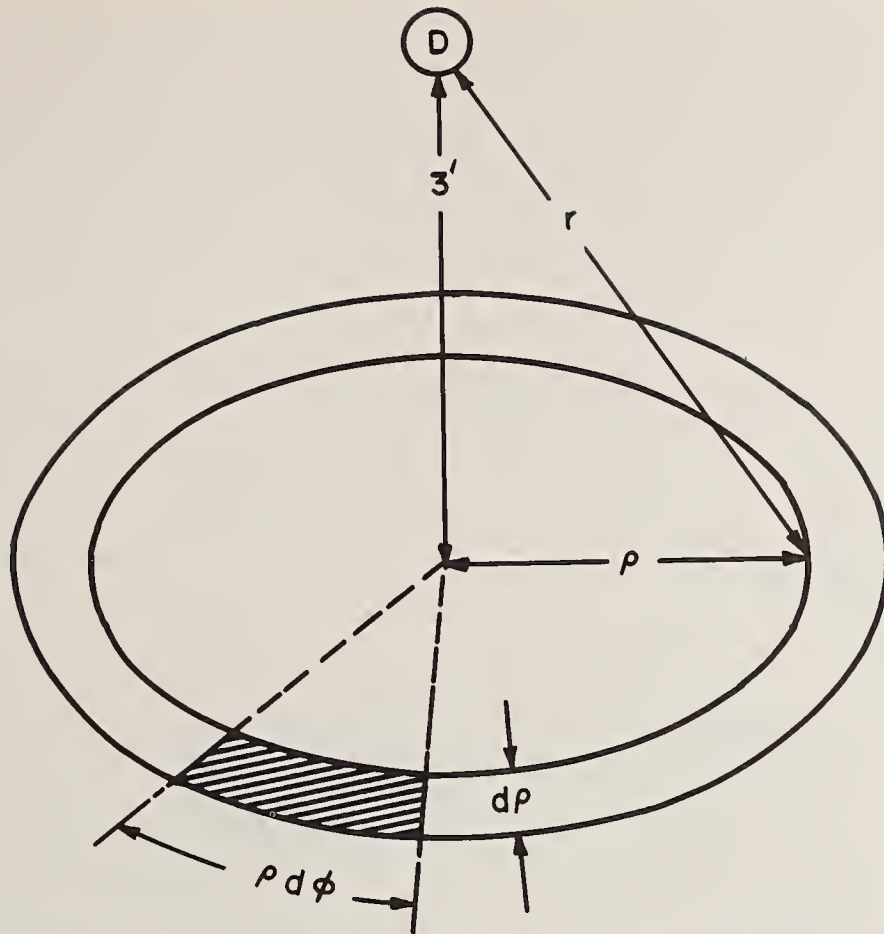
20

FIGURE 26.2. *A small annular sector of a source plane located a distance* $r=\sqrt{3^2+\rho^2}$ *ft from a detector 3 ft above the plane.*

obliquities θ and the total contribution from all area elements:

$$D_0=\int_{3'}^{\infty}\frac{\rho d\rho}{4\pi r^2}\int_0^{2\pi}d\varphi\int_{-1}^{1}d\left(\cos\theta\right)D_0p(r,\cos\theta)$$

$$=D_0\left\{\frac{1}{2}\int_{3'}^{\infty}\frac{dr}{r}P(r)\right\},\quad(26.4)$$

where $P(r)=\int_{-1}^{1}d\left(\cos\theta\right)p(r,\cos\theta)$. Cancelling D_0 from eq (26.4) we obtain the normalizing condition on $p(r,\cos\theta)$ in terms of its integral over all obliquities.[21]

The scattered and unscattered components of $p(r,\cos\theta)$ have quite different characteristic features. The unscattered component, $p^{(0)}(r,\cos\theta)$ is concentrated at the angle $\theta=0$, while the scattered component, designated $p^{(s)}(r,\cos\theta)$, is distributed over all obliquities. As in the case of the plane isotropic source, $p(r,\cos\theta)$ has been calculated by using its Legendre polynomial representation.[22] The calculation proceeds more or less as follows: A digital computer determines the total strength of the unscattered component and also the first seven or eight functions $p_n^{(s)}(r)$ by standard techniques [12, Part C]. An extrapolation in n is then performed, which uses a resemblance of

$p^{(s)}(r,\cos\theta)$ to the function $(a+\cos\theta)^{-3/2}$. (See Appendix A.)

Figure 26.3 shows curves of $p(r,\cos\theta)$ for several values of r, but rescaled so that the integral of $p^{(s)}(r,\cos\theta)$ over all obliquities is unity. All the distributions are strongly peaked at $\cos\theta=1$; but the truly remarkable feature is the similarity of trends. About the only change worth noting from one value of r to the next is in the relative strengths of scattered and unscattered components, which is indicated by the separation of the curves vertically and (qualitatively) by the lengths of the arrows at $\cos\theta=1$. With increasing penetration the unscattered copmonent steadily decreases in importance.

(3) Plane oblique source case: Radiation from a plane source goes in all directions; but for some purposes it is advantageous to consider only those gamma rays which go initially at an obliquity θ_0 relative to the normal to the source plane. The detector response at different distances from a plane source originating gamma rays with the fixed obliquity θ_0 will be designated $s(X,\cos\theta_0)$, with X measuring distance from the source in terms of the effective mass thickness (psf). For our purpose it is convenient to fix the scale of this function so that $\cos\theta_0 s^{(0)}(X,\cos\theta_0)$ is unity at $X=0$, where $s^{(0)}(X,\cos\theta_0)$ is the detector response to the unscattered component.[23]

---

[21] As in the case of $l(d,\cos\theta)$, other functions, corresponding to penetration in other materials than air (or water), will be called $p(X,\cos\theta)$ if the *source strength* is the same as that implied by eq (26.4).
[22] Do not confuse the Legendre polynomial $P_n(\cos\theta)$ with $P(r)$ of eq (26.4). Note that $P(r)=p_0(r)$.

[23] Note that $\underset{X\to0}{\text{Lim}}\cos\theta_0 s^{(0)}(X,\cos\theta_0)$ is independent of $\cos\theta_0$, for $\cos\theta_0>0$.
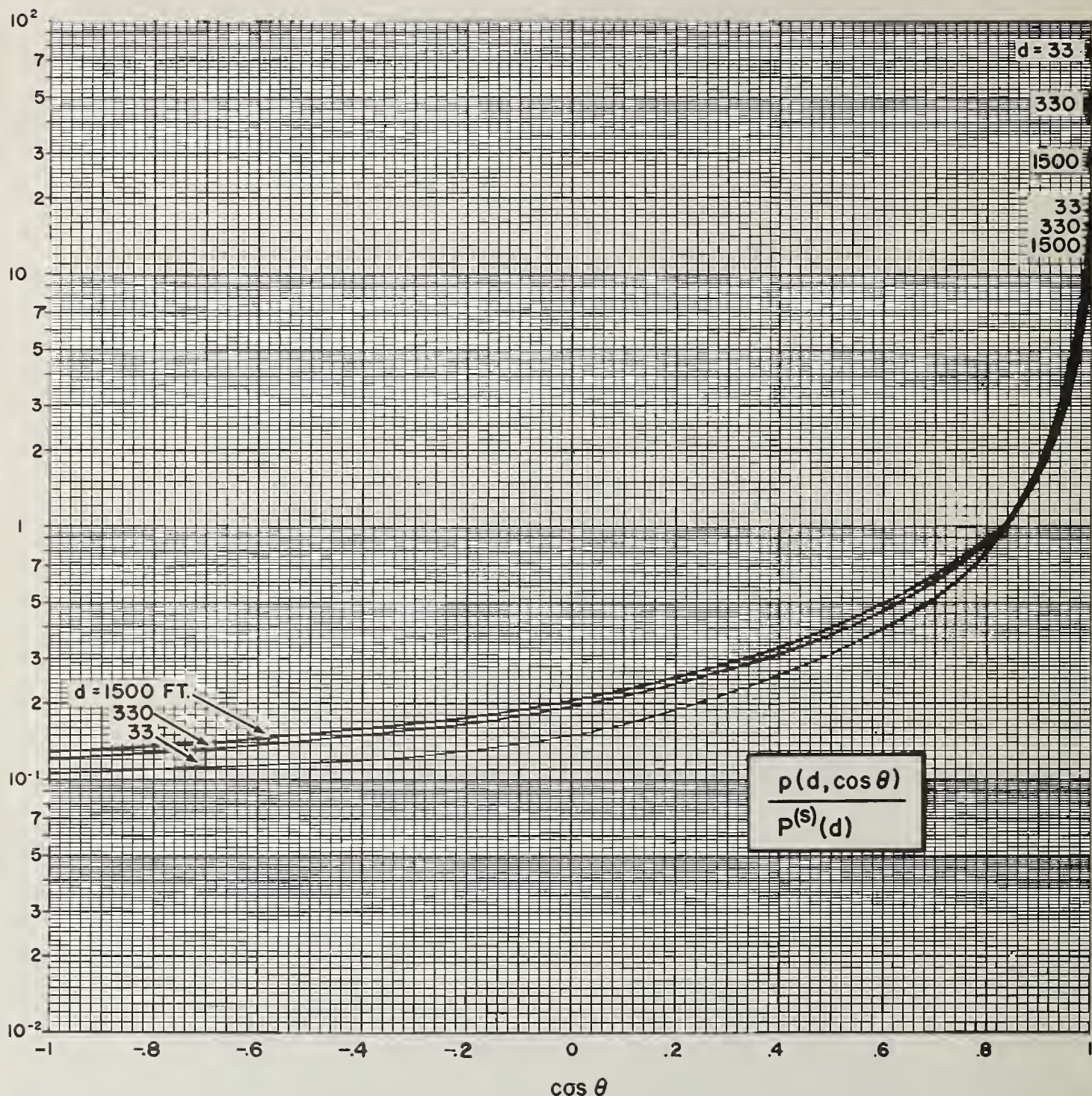
FIGURE 26.3 *Dose angular distributions* $p(r,\cos\theta)$ *for a point fallout source, normalized by dividing by the total intensity of scattered gamma rays. The arrows at $\cos\theta = 1$ indicate the unscattered component. The arrow lengths have no quantitative significance. (H_2O, 1.12 hr fission. See also figs. B3 and B4.)*

Figure 26.4 gives this function for different values of $\cos\theta_0$, corresponding to penetration by a 1.12 hr spectrum of fission gamma rays in H_2O (or air). Special features exhibited by these curves have interpretations as follows: The curves correspounding to $\cos\theta_0 \approx 1$ describe gamma rays initially traveling directly away from the source plane. These curves lie above the others for large X because a large part of the "path length" traversed by each gamma ray contributes to distance from the source plane. Conversely, when gamma rays initially move almost parallel to the source plane ($\cos\theta_0 \ll 1$), the initial layers of

barrier material greatly reduce the radiation intensity.

It is possible for radiation from a plane oblique source to be scattered back into the region behind the source plane. The characteristics of this back-penetrating radiation are of considerable interest and have applications to shielding problems. It is possible to view such cases either as corresponding to obliquity angles greater than $\pi/2$ ($\cos\theta < 0$) or as corresponding to negative values of X, with $\cos\theta_0 > 0$. The terminology is a little easier to manage in the former case and so we adopt that point of view. Figure 26.5 gives

22
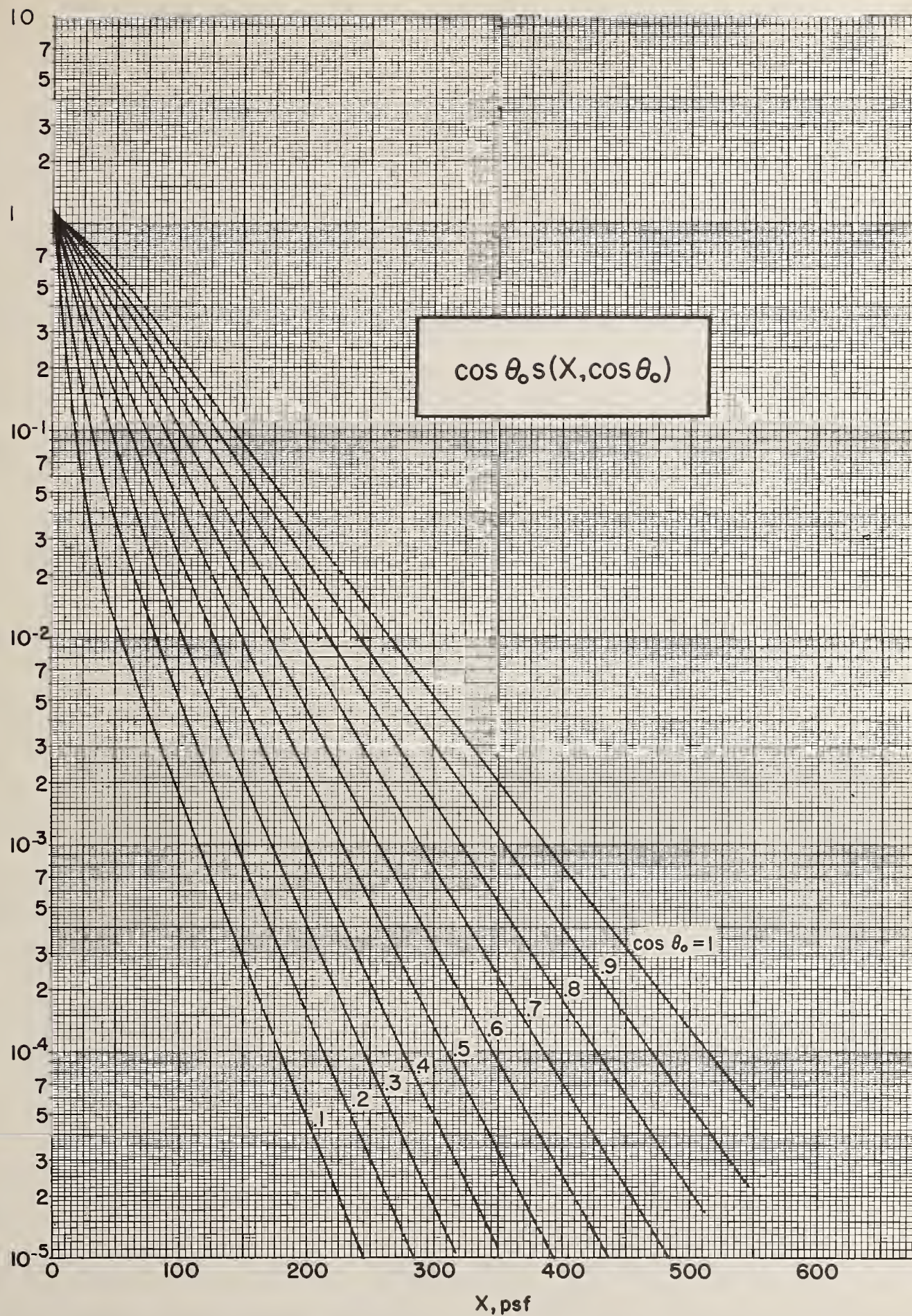
FIGURE 26.4. *Gamma ray attenuation curves for monodirectional gamma rays from a plane source, for incident obliquities $\theta_0 < 90°$ relative to the normal to the source plane.* (H_2O, *1.12 hr fission. See also figs. B5 and B6.*)

23

curves of $s(X, \cos\theta_0)$ for negative $\cos\theta_0$. Only scattered radiation contributes to the detector response. The curves are continued to $X=0$, although strictly speaking the detector response changes discontinuously at this point because the contribution due to unscattered gamma rays begins here. Data for grazing incidence $(\cos\theta_0)=0$ is included. The various curves are seen to be rather rough. High accuracy is difficult to obtain in this type of calculation because a differencing of large numbers is involved, and the irregularities reflect the inaccuracy of the calculation.

It is by means of the plane oblique data that we most easily make comparisons of the penetrability and scattering properties of fallout gamma rays at different times after fission, together with similar comparisons involving Co^{60} and other radioactive materials. Figures 26.6 and 26.7 give curves proportional to $s(X,1)$ and $s(X,0)$ for different fission sources, with data also for Co^{60}. In figure 26.6, marked differences appear only for rather large penetrations $(X>144$ psf). Differences in scattering properties are indicated in figure 26.7. The calculations are less reliable, and these differences may be exaggerated by the inaccuracy of the data for X near 0. All curves correspond to penetration in water-equivalent materials.

(4) Albedo or backscattering data [34]. The gamma ray albedo has been mentioned in Section 19. If a plane gamma ray source is incident on a thick slab, a detector at the interface will observe a dose angular distribution $D(\cos\theta)$. The albedo (α) to which we refer is defined by

$$\alpha = \frac{\int_{-1}^{0} d(\cos\theta)\cos\theta\, D(\cos\theta)}{\int_{0}^{1} d(\cos\theta)\cos\theta\, D(\cos\theta)}. \qquad (26.6)$$

This ratio depends on the incident source, and for monodirectional sources is a function of the angle of incidence (θ_0) relative to the normal to the slab face.

Berger and Raso have made machine Monte Carlo calculations, for monoenergetic sources, of this function [34]. Figure 26.8 gives data for a 1.12 hr fission spectrum incident on a concrete slab, as calculated from their data.

27. Catalogue of Functions

The detector response to radiation from an arbitrary source is represented by an expression like eqs (16.2) or (16.3), which sums contributions from different parts of the source. Source shapes can vary enormously, and to cut down the number of variables, we do calculations for *circular* sources, illustrated by figure 16.3, with the detector directly opposite the center of the circle. Applying eqs (16.2) and (16.3) to this simple case, we find that

$$D_S(\omega) = \int_{1-\omega}^{1} d(\cos\theta) \int_{0}^{2\pi} d\varphi D_S(\theta,\varphi),$$

or

$$D_S(\omega) = \int_{1-\omega}^{1} d(\cos\theta)\, D_S(\theta), \qquad (27.1)$$

where $\omega = 1 - \cos\theta_{max}$ as discussed in Section 40. We approximate both barrier and geometry factors by use of integrals of this type with the integrand taken as one or another of the functions described in Section 26. Interpretation of these integrals is given mostly in the next section; here we simply list them for intercomparison and reference.

(1) Barrier Factors: The following expressions define functions which we use to approximate different types of barrier factors: [24]

$$L(d) = \int_{-1}^{1} d(\cos\theta)\, l(d, \cos\theta), \qquad (27.2)$$

$$S(d) = \int_{-1}^{0} d(\cos\theta)\, l(d, \cos\theta), \qquad (27.3)$$

$$S'(X) = \frac{\int_{-1}^{0} d(\cos\theta_0)\, s(X, \cos\theta_0)}{\int_{-1}^{0} d(\cos\theta_0)\, s(0, \cos\theta_0)}, \qquad (27.4)$$

$$P(d) = \int_{-1}^{1} d(\cos\theta)\, p(d, \cos\theta), \qquad (27.5)$$

$$P^{(s)}(d) = \int_{-1}^{1} d(\cos\theta)\, p^{(s)}(d, \cos\theta), \qquad (27.6)$$

$$W(X,d) = \int_{0}^{1} d(\cos\theta)\cos\theta\, s(X, \cos\theta)$$
$$\times (1/2\pi) \int_{0}^{2\pi} d\varphi\, l(d, \sin\theta\cos\varphi). \qquad (27.7)$$

Most of these quantities have fairly obvious designations and interpretations. "L" stands for "layer," "S" stands for "skyshine," "P" stands for "point," and "W" stands for "wall." $P^{(s)}$ and $p^{(s)}$ refer to the scattered component only from a point source.

(2) Geometry Factors: The ratios to be used in estimating geometry factors are listed below: [25]

$$L_c(X,\omega) = \frac{1}{L(X)}\left[L(X) - L\left(\frac{X}{1-\omega}\right) \right], \qquad (27.8)$$

$$L_a(X,\omega) = \frac{1}{L(X)} \int_{1-\omega}^{1} d(\cos\theta)\, l(X, \cos\theta), \qquad (27.9)$$

[24] Notes: $P^{(s)}(d)$ is the same as $p_o^{(s)}(d)$ in eq (26.5). P and $P^{(s)}$ should not be confused with the Legendre polynomials P_n. We consider these definitions to hold even when the l, p, and s data corresponds to materials other than air (or H_2O).

[25] It is assumed that both denominator and numerator in these ratios correspond to penetration in the same material, by gamma rays from the same source.

Note that in the alternative approach mentioned in Section 49 and described in references 29, 30, and 41, it would be logical to use Legendre coefficient ratios in a manner closely analogous to the use of the ratios defined here.
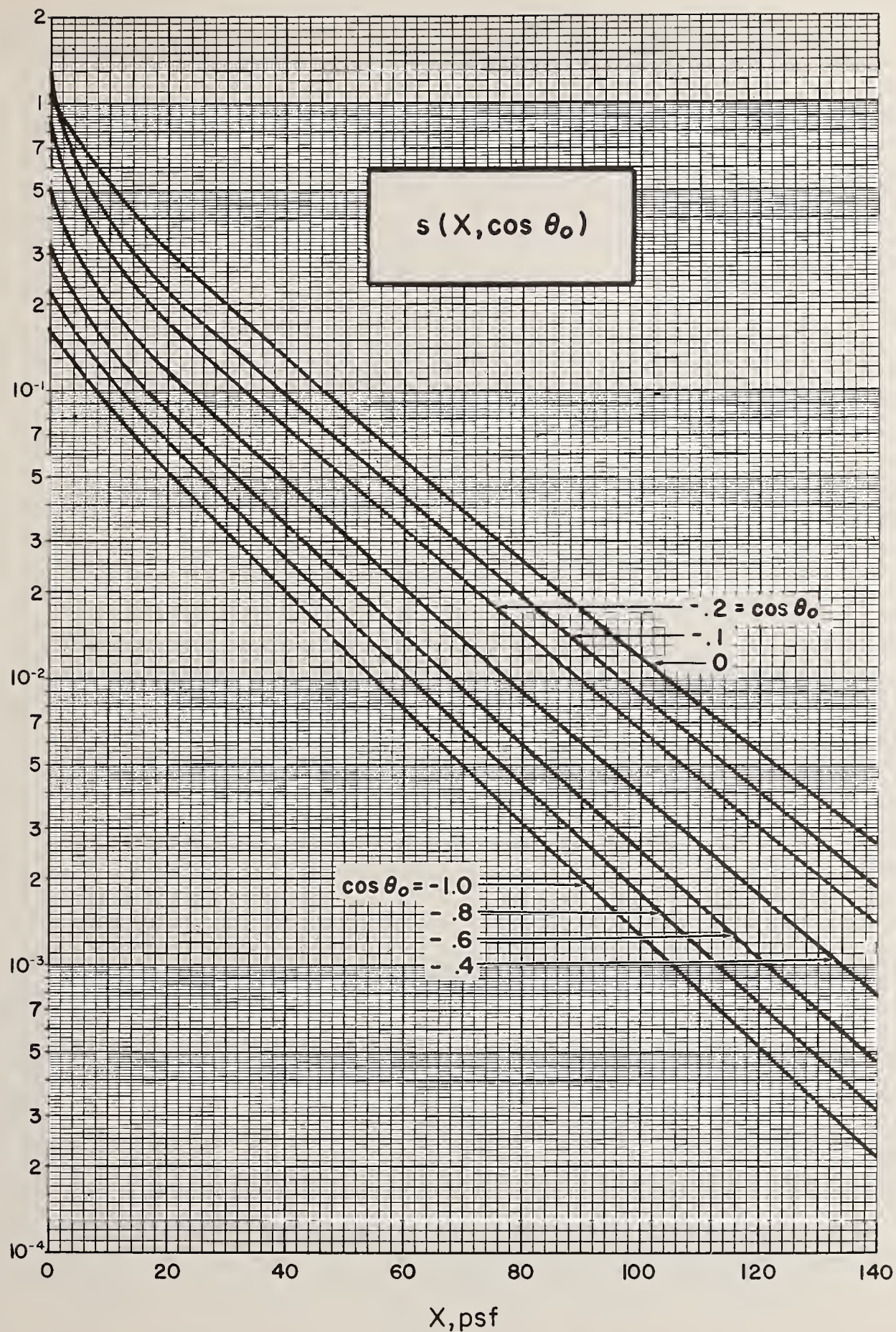
FIGURE 26.5. *Gamma ray attenuation curves for monodirectional gamma rays from a plane source, for incident obliquities* $\theta_0 > 90°$ *relative to the normal to the source plane.* (H_2O, 1.12 hr fission. *See also figs. B7 and B8.*)
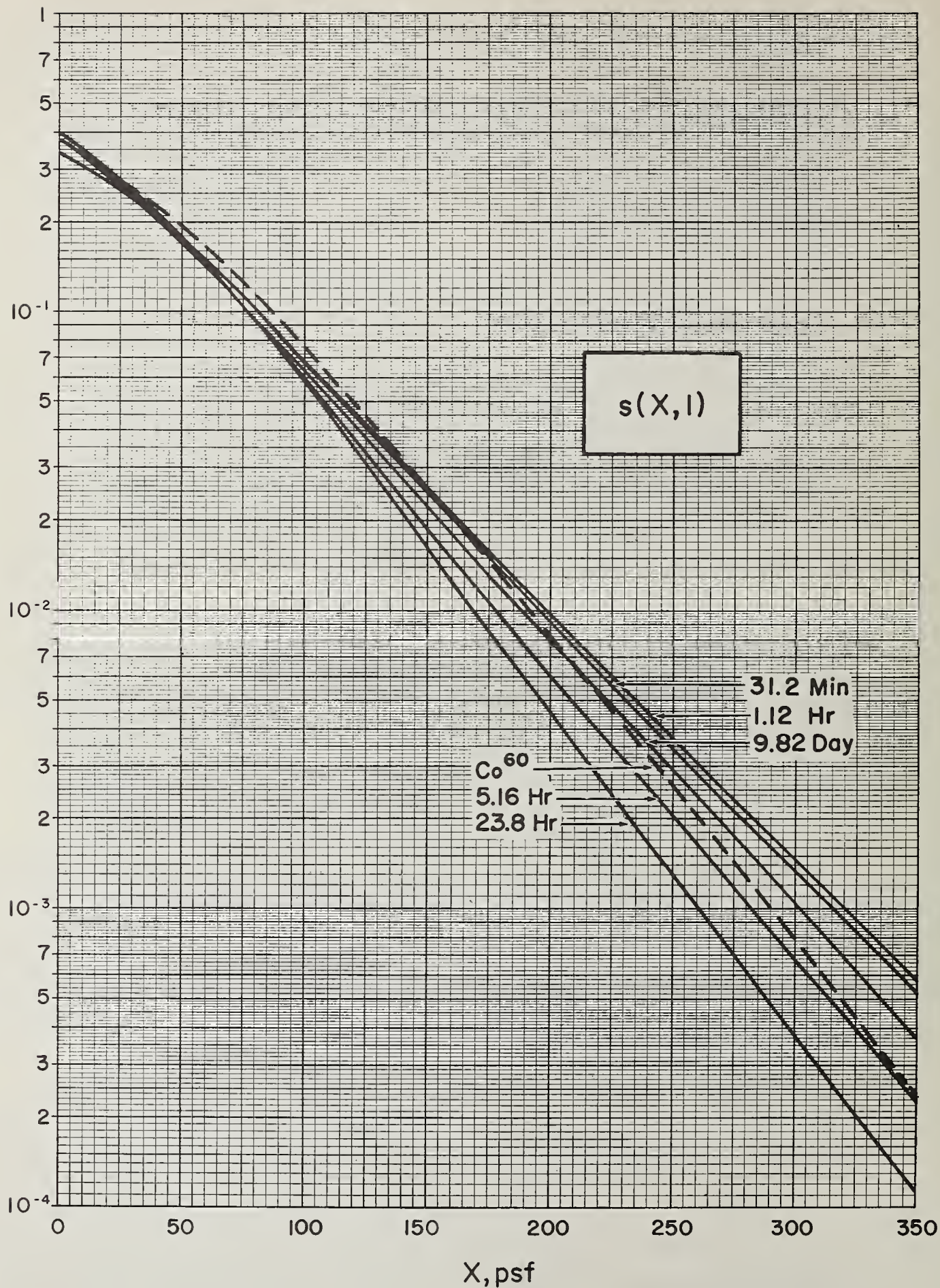
FIGURE 26.6. *Penetration of fallout gamma rays at different times after fission. Also included for comparison is a curve for* Co^{60}. *The curves are normalized to equal total energy dissipation, integrated over all penetrations.* (H_2O, *plane perpendicular source.*)
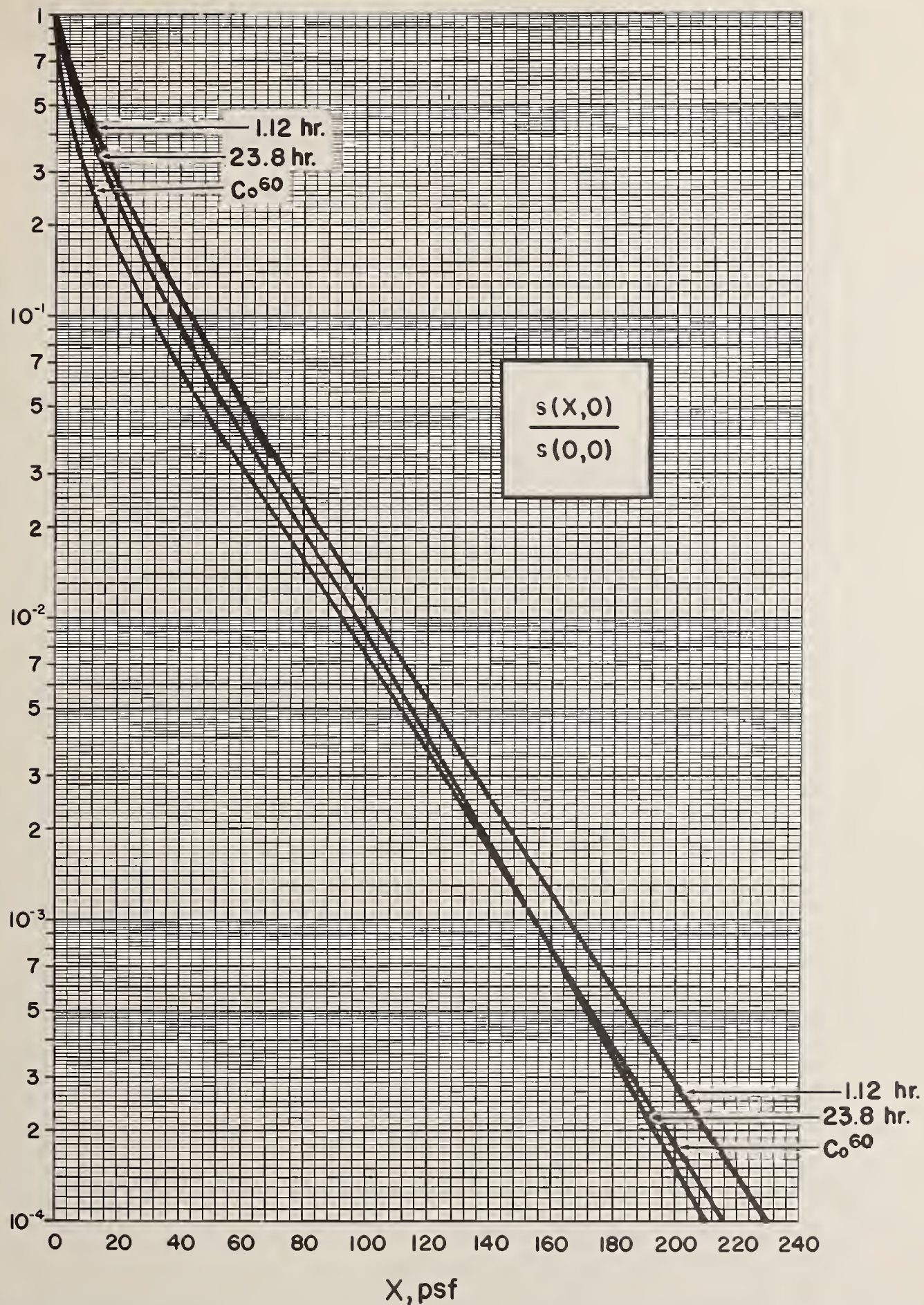
FIGURE 26.7. *Penetration of gamma rays from a plane, monodirectional source generating gamma rays only in directions along the source plane.* *Substantial penetrations away from the source plane presuppose large scattering angles.* (H_2O.)

27
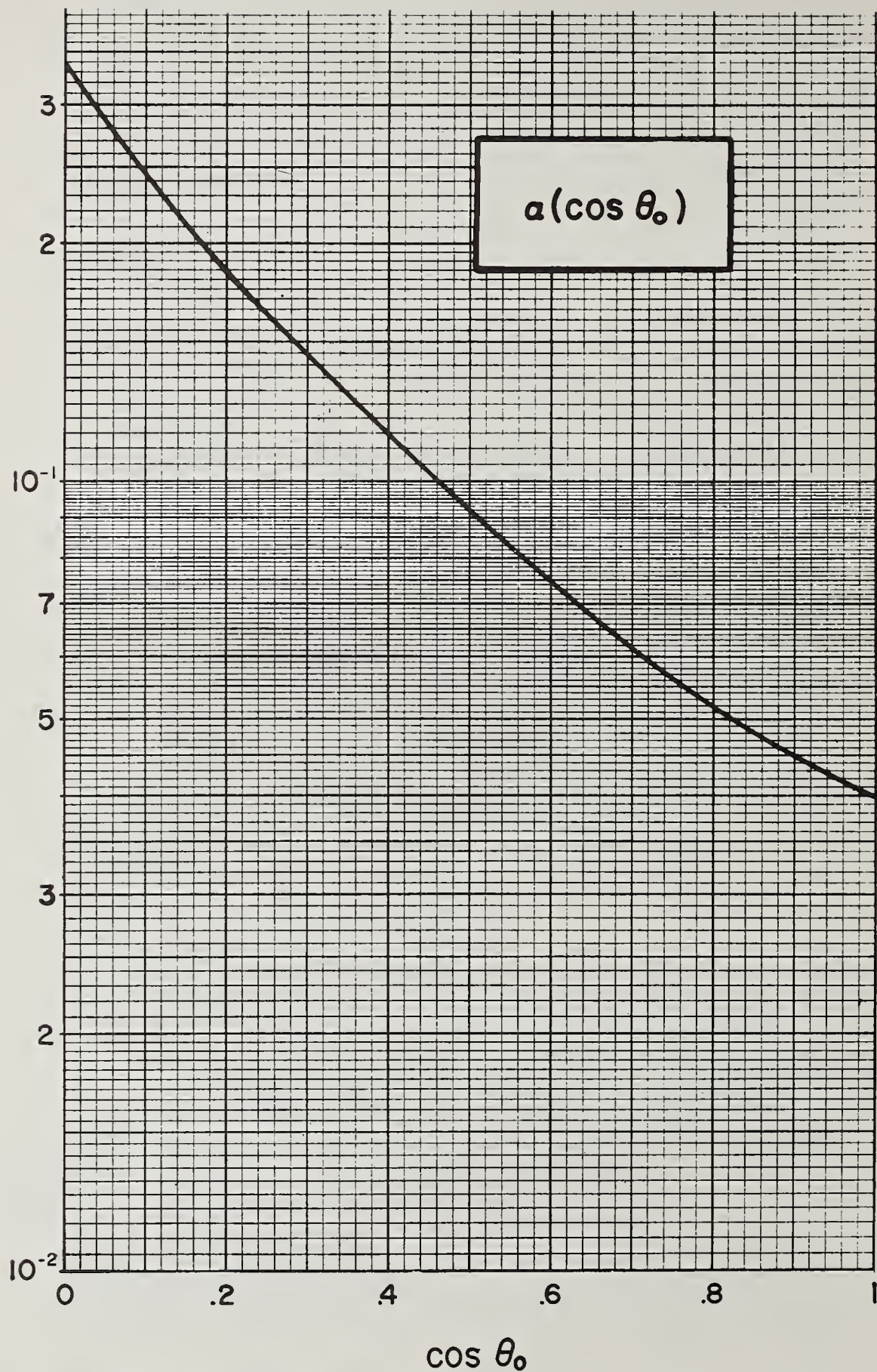
FIGURE 26.8. *Dose albedo for monodirectional gamma rays incident on concrete, as a function of the cosine of the incident obliquity.* (*1.12 hr fission. See also figs. B9 and B10.*)

28

$$L_b(X,\omega) = \frac{\nu}{L(X)} \int_{1-\omega}^{1} d(\cos\theta)\, s(X,\cos\theta),$$
(27.10)

$$W_a(d,\omega) = \frac{1}{W(d,0)} \int_{1-\omega}^{1} d(\cos\theta)\,(1/2\pi)$$

$$\times \int_{0}^{2\pi} d\varphi\, l(d,\sin\theta\cos\varphi), \quad (27.11)$$

$$W_b(d,\omega) = \frac{2}{S(d)} \int_{1-\omega}^{1} d(\cos\theta)\,(1/2\pi)$$

$$\times \int_{\pi}^{2\pi} d\varphi\, l(d,\sin\theta\cos\varphi), \quad (27.12)$$

$$S_a(d,\omega) = \frac{1}{S(d)} \int_{-1}^{-1+\omega} d(\cos\theta)\, l(d,\cos\theta),$$
(27.13)

$$P_a(d,\omega) = \frac{1}{P(d)} \int_{1-\omega}^{1} d(\cos\theta)\, p(d,\cos\theta),$$
(27.14)

$$P_a^{(s)}(d,\omega) = \frac{1}{P^{(s)}(d)} \int_{1-\omega}^{1} d(\cos\theta)\, p^{(s)}(d,\cos\theta),$$
(27.15)

$$P_b^{(s)}(d,\omega) = \frac{2}{P^{(s)}(d)} \int_{1-\omega}^{1} d(\cos\theta)\,(1/2\pi)$$

$$\times \int_{0}^{2\pi} d\varphi\, p(d,\sin\theta\cos\varphi). \quad (27.16)$$

All these definitions are complete except for eq (27.10). The factor ν multiplying the right side of eq (27.10) is chosen so that $L_b(X,2)=1$, i.e., so that the integral over all directions gives the plane isotropic source result, $L(X)$. Since $L(X)$, $P(X)$, and $s(X,\cos\theta)$ are connected by the relations

$$L(X) = 1/2 \int_{x}^{\infty} \frac{dX'}{X'} P(X') = \nu \int_{-1}^{1} d(\cos\theta)\, s(X,\cos\theta),$$
(27.17)

it turns out that $\nu = (1/2)P(0)$.[26]

The names assigned to the ratios eqs (27.8) to (27.16) are less obvious than in the case of barrier factors. In general the letter used, "L", "P", etc., is determined by the type of barrier factor appearing in the denominator. A more detailed description of these quantities is reserved for the next Section.

[26] This is easily seen for monoenergetic sources, for which

$$P^{(0)}(X) = P(0)e^{-\mu X}; \quad s^{(0)}(X,\cos\theta) = (\cos\theta)^{-1}e^{-\mu X/\cos\theta}, \quad \cos\theta > 0.$$

Inserting these functions into eq (27.17), and remembering that the unscattered component is completely dominant in the limit $X\to 0$, the value for ν is immediately obtained. But eq (27.17) holds for all X and for scattered as well as unscattered radiation, since both integrals represent the plane isotropic dose rigorously. Extension of the argument to include polychromatic sources is therefore straightforward.

Notice that in some cases d and in some cases X is the penetration variable. The two are interchangeable, provided the proper conversion is used (eq (26.1)).

28. Description of Graphical Data

We next take each of the functions given in the preceding Section, describe the physical situation for which it applies most accurately, present one or more graphs, and discuss important features exhibited by these graphs.

(1) $L(d)$, $L(X)$: In eq (27.2), $L(d)$ is defined as the integral over all obliquities of the quantity $l(d,\cos\theta)$. Therefore $L(d)$ is simply the total detector response at a distance d (in air) from an infinite, plane, isotropic source, divided by the total detector response at 3 ft in air from the same source. $L(X)$ is the same function except that "distance from the source" is expressed in terms of the effective mass thickness. Figure 28.1a is a sketch of the simple configuration for which this quantity is directly applicable. The absorbing medium is homogeneous, and the detector response is isotropic. Figures 28.2a and 28.2b give typical curves of this quantity. Both figures show that near the source plane the radiation intensity falls rapidly with increasing distance from the source. This is characteristic of gamma rays having initial directions nearly parallel to the source plane (see fig. 26.1). After considerable penetration, the trend of the curves is nearly that for gamma rays which leave the source plane perpendicularly (see fig. 26.3).

(2) $S(d)$: The definition of this quantity given in eq (27.3) differs from the definition of $L(d)$ in regards to the limits of integration. Only obliquity angles greater than 90° are included. Since gamma rays with these obliquities are traveling towards the source plane, they have been backscattered. Thus this function gives the total detector response to skyshine radiation at a distance d in air from an infinite, plane, isotropic source in a homogeneous medium. Figure 28.1b sketches the physical situation. Figure 28.3 gives a curve of $S(d)$, obtained from the data of figure 26.1. The intensity of the backscattered radiation can be seen to change rather slowly with distance from the source out to perhaps a mean free path of the source radiation. As indicated on the graph, $S(0)=0.098$.

(3) $S'(X)$: This quantity (eq 27.4) is a ratio of integrals and is unity for $X=0$. Both integrals sum over negative $\cos\theta$, i.e., over gamma ray slant sources of radiation which travels initially away from the detector. The configuration is sketched in figure 28.1c, which shows a plane source emitting gamma rays isotropically in an upward direction into an infinite homogeneous medium. The detector is *below* the source plane, separated from it by an effective mass thickness X. Radiation can be backscattered to the detector, giving a response measured by the function $S'(X)$. The normalization to unity at $X=0$ is for convenient use as

29

a reduction factor in the applications. Data are given in figure 28.4. The curve bears a considerable similarity to $s(X,0)$ as given in figure 26.5; but this is not surprising, since the grazing incidence component of the source contributes strongly to this function.

(4) $P(d)$, $P(X)$: The integral in eq (27.5) includes all obliquities, so that $P(d)$ relates to the total detector response at a distance d from a point isotropic source in an infinite homogeneous medium (see fig. 28.1d). Results obtained from the data of figure 26.2 are given in figures 28.5a and 28.5b. The scale has been chosen to simplify the use of the curve in determining detector response due to a small plane area (A) of contamination, as discussed in Section 26:

$$D/D_0 \approx P(d) A/4\pi d^2. \qquad (28.1)$$

(5) The only difference between $P^{(s)}(X)$ and $P(X)$ is omission of unscattered gamma ray contributions to the integrand. Thus $P^{(s)}(X)$ relates to the total detector response due to scattered gamma rays. Graphs of this function and also of $P^{(0)}(X) = P(X) - P^{(s)}(X)$ are given in figure 28.6, as obtained from the data which also yielded figure 26.2.

(6) $W(X,d)$: This is a more complicated quantity than those preceding. Figure 28.1e is a sketch of the relevant physical situation. The angular distribution of radiation incident on a vertical wall is assumed to be the same as if the wall were not present. This distribution, $l(d,\sin\theta\cos\varphi)$, corresponds to a distance d in air from an infinite plane source in a homogeneous medium, but with directions referred to a polar axis perpendicular to the vertical wall (i.e., parallel to the source plane).[27] Assuming the spectrum incident on the wall to be that generated by the primary source on the ground, an integral over all oblique angles of incidence is made, each weighted according to our information about oblique penetration (fig. 26.4). The result approximates the total detector response at a height d above the source plane and with a thickness X of barrier material between detector and external barrier surface. Errors in this calculation arise from inaccuracies in the angular distribution, changes in the incident spectrum as the scattered radiation component becomes more important, and incorrect correlation of spectrum with direction. In general, this function is expected to represent the vertical wall barrier factor accurately for d small compared with a mean free path of the source radiation, i.e., $d \ll 1000$ ft. Data are given in figure 28.7. The curves have a maximum value of $W(0,d) \approx (1/2)L(d)$, corresponding to radiation from half an infinite plane, namely the half beyond the wall. Notice that the bottom curves are not expected to be reliable.

(7) $L_c(d,\omega), L_c(X,\omega)$: The significance of $L_c(X,\omega)$ is illustrated in figure 28.8a: A circular area of fallout has its center directly opposite a detector and separated by a layer of air of thickness d and equivalent mass thickness X. Noting eq (26.4), together with the relation $\cos\theta_{max} = 1 - \omega$, we represent the detector response due to the circular area in the form

$$D/D_0 = 1/2 \int_X^{X/(1-\omega)} \frac{dX'}{X'} P(X') = L(X) - L\left(\frac{X}{1-\omega}\right).$$

$$(28.2)$$

Equation (27.8) is the ratio of the response due to the circular area to the response due to fallout on the whole plane. Data corresponding to penetration in water-equivalent materials are given in figure 28.9. While this quantity is easily obtained from figures 28.2a and 28.2b by differencing, and is included in the data of figure 28.18, the curves of figure 28.9 are convenient for comparison purposes.

(8) $L_a(d,\omega), L_a(X,\omega)$: The integral in eq (27.9) is over a cone of obliquities of incidence on the detector. Thus, this ratio expresses the reduction in detector response which occurs if an isotropic detector (separated from an infinite plane source of fallout gamma rays by a distance d in air, or a corresponding barrier thickness X) is replaced by a detector responding only to gamma rays incident within a particular cone of directions, as indicated in figure 28.8b. The response cone has aperture θ_{max} and subtends solid angle fraction ω at the detector, with $\omega = 1 - \cos\theta_{max}$. Curves of this ratio are given in figure 28.10, as obtained from the data of figure 26.1. Notice that these curves go to unity only for $\omega \to 2$, i.e., including backscattered contributions for which $1 < \omega \leq 2$, and amounting to ~ 15 percent.

(9) $L_b(d,\omega), L_b(X,\omega)$: The integral of eq (27.10) is over a cone of initial source obliquities. The function $L_b(d,\omega)$ therefore expresses the fractional reduction in detector response occurring if an (infinite plane) isotropic source is suddenly allowed to emit radiation only into a limited cone of directions about the perpendicular toward the detector (see fig. 28.8c). The cone of emission has an aperture θ_{max} defined by $\cos\theta_{max} = 1 - \omega$, where ω is the solid angle fraction of the cone of emission, subtended at the detector. Graphs of L_b, obtained from the data of figure 26.4, are given in figure 28.11. These bear a noteworthy resemblance to the curves for L_c and L_a. As in the case of figure 28.10, the curves go to unity only as $\omega \to 2$, although figure 28.9 doesn't give data for the region of emission in directions away from the detector (i.e., $\omega > 1$).

(10) Equation (27.11) defines $W_a(d,\omega)$ as a ratio whose numerator is an integral over a cone of obliquities of incidence on the detector. The cone axis is parallel to the source plane and the cone angle (θ_{max}) is related to the solid angle fraction

---

[27] Notice that $l(d,\cos\Theta)$ becomes $l(d,\cos\theta\cos\alpha+\sin\theta\sin\alpha\cos\phi)$ relative to a second polar axis inclined at an angle α to the original axis, with ϕ measured relative to the plane of the two reference axes. When $\alpha = \pi/2$, this reduces to $l(d,\sin\theta\cos\phi)$.

subtended by the aperture by the usual relation $\cos\theta_{max}=(1-\omega)$, as in figure 28.8d. The denominator of eq (27.11) has the same interpretation but with cone angle $\theta_{max}=\pi/2$, so that all radiation incident on one side of the detector is included in the response. Curves of $W_a(d,\omega)$ are presented in figure 28.12, as obtained from the data of figure 26.1 for penetration in water-equivalent materials.

(11) In some cases one wants to know the amount of skyshine radiation passing through a vertical aperture. The function $W_b(d,\omega)$, defined by eq (27.12), is presented here because of possible applications of this type. The definition of W_b is like the definition of W_a except for integration limits which include only skyshine contributions. Thus W_b refers to a half-cone of skyshine radiation of aperture θ_{max} about an axis parallel to the source plane, with $\cos\theta_{max}=1-\omega$, where ω is the solid angle fraction subtended by the *whole* cone (see fig. 28.13a). The denominator is the total
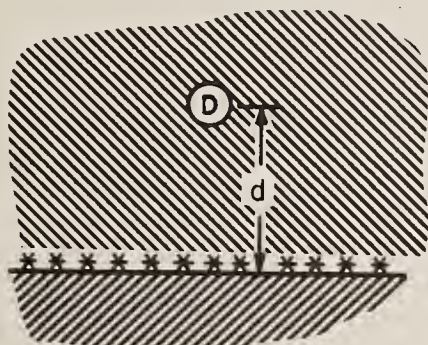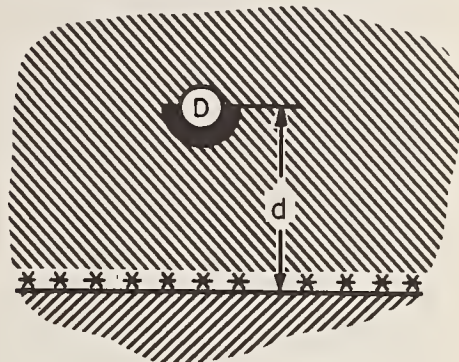
(a)　　　　　　　　　　　　　　　　　(b)

(c)
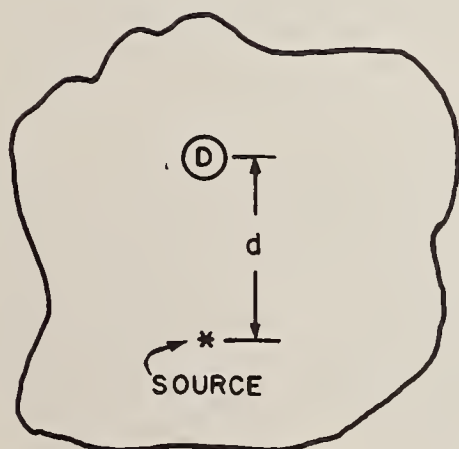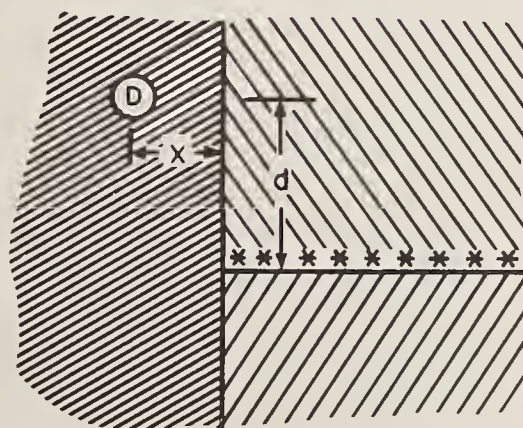
(d)　　　　　　　　　　　　　　　　　(e)

FIGURE 28.1. *Simple detector-source-medium arrangements:*

(o) *Isotropic detector, plone isotropic source; (b) isotropic detector shielded on the side toward the source, plone isotropic source; (c) isotropic detector, source "isotropic" only in directions pointing oway from detector; (d) isotropic detector, point isotropic source; (e) isotropic detector ond ptone isotropic source: The rodiotion field at height d above the primory source is token os a new source at o penetration distance X to the right of the detector. In all cases the calculations ore for infinite homogeneous medio, and alt cases but (d) olso correspond to medio with ptane density variations.*
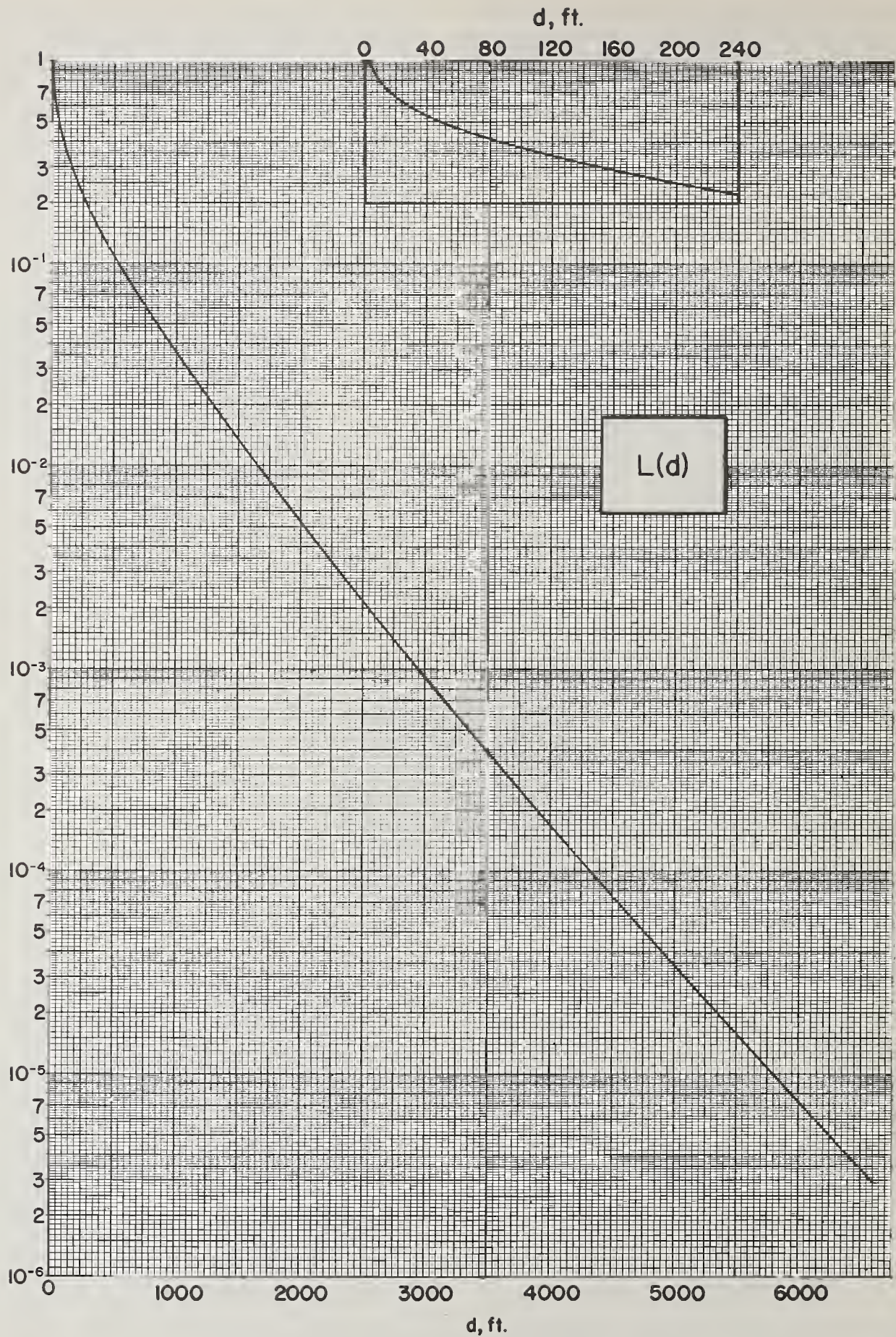
FIGURE 28.2a. *Plane source of fallout radiation: The (isotropic) detector response ratio D/D_0 as a function of height d in air above the source plane.* (H_2O, 1.12 hr fission. *See also figs. B11 and B12.*)
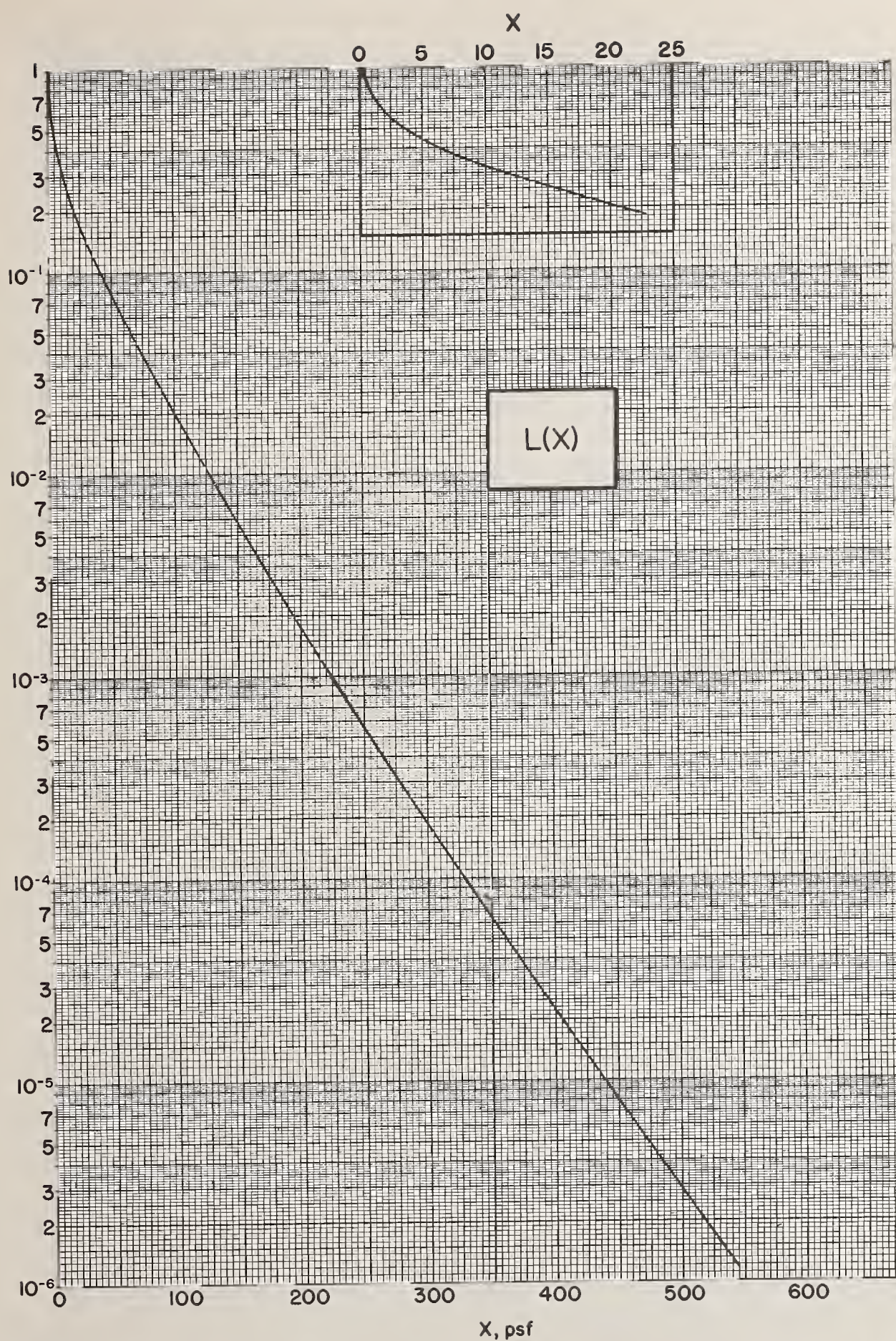
FIGURE 28.2b. *Plane source of fallout radiation: The (isotropic) detector response ratio D/D_0 as a function of effective mass thickness separating the detector and the source plane. (H_2O, 1.12 hr fission. See also figs. B13 and B14.)*
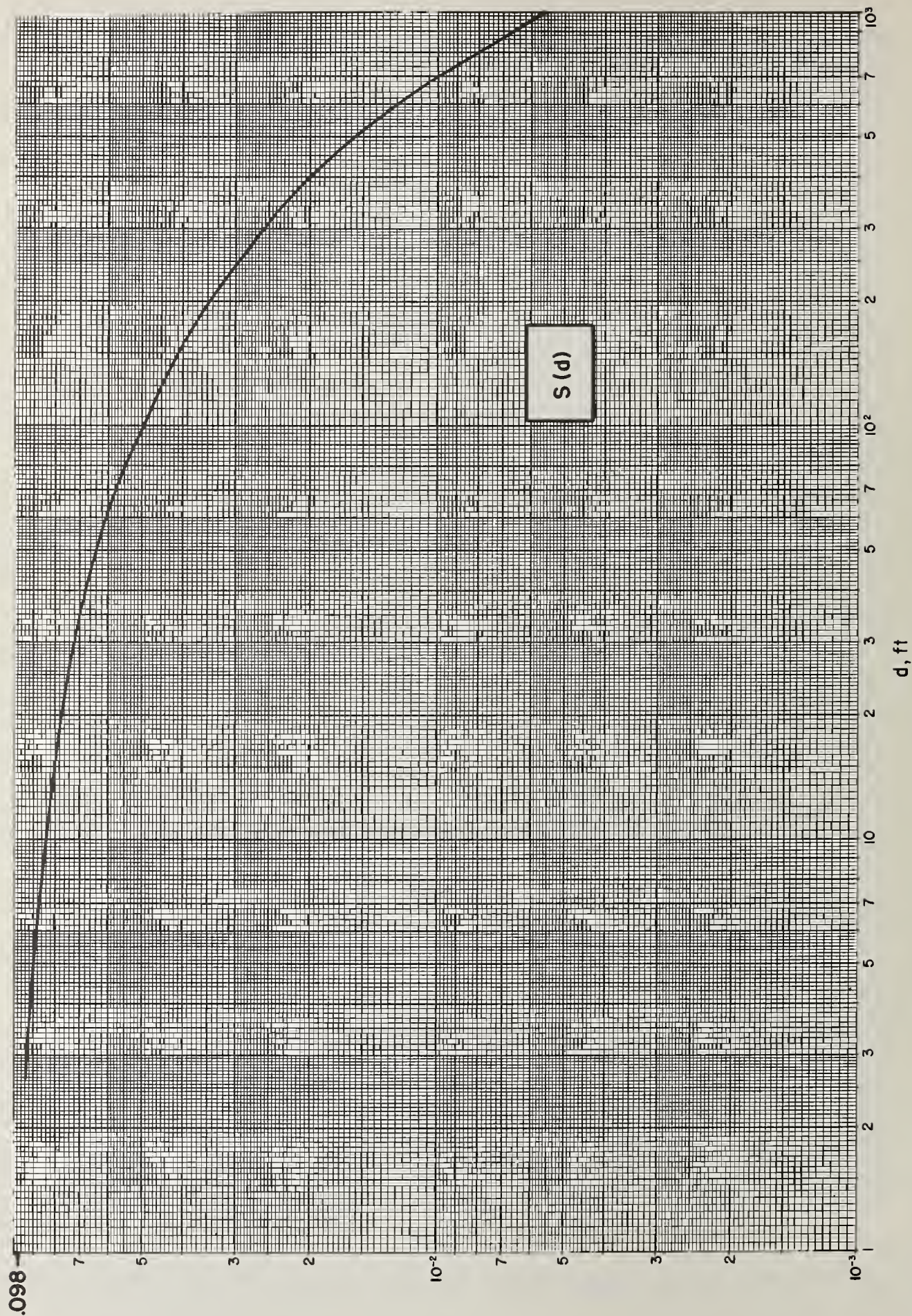
FIGURE 28.3. *The detector response ratio D/D_0 due to skyshine, as a function of height above a plane source of fallout radiation.* (H_2O, 1.12 hr fission. *See also figs. B15 and B16.*)

34
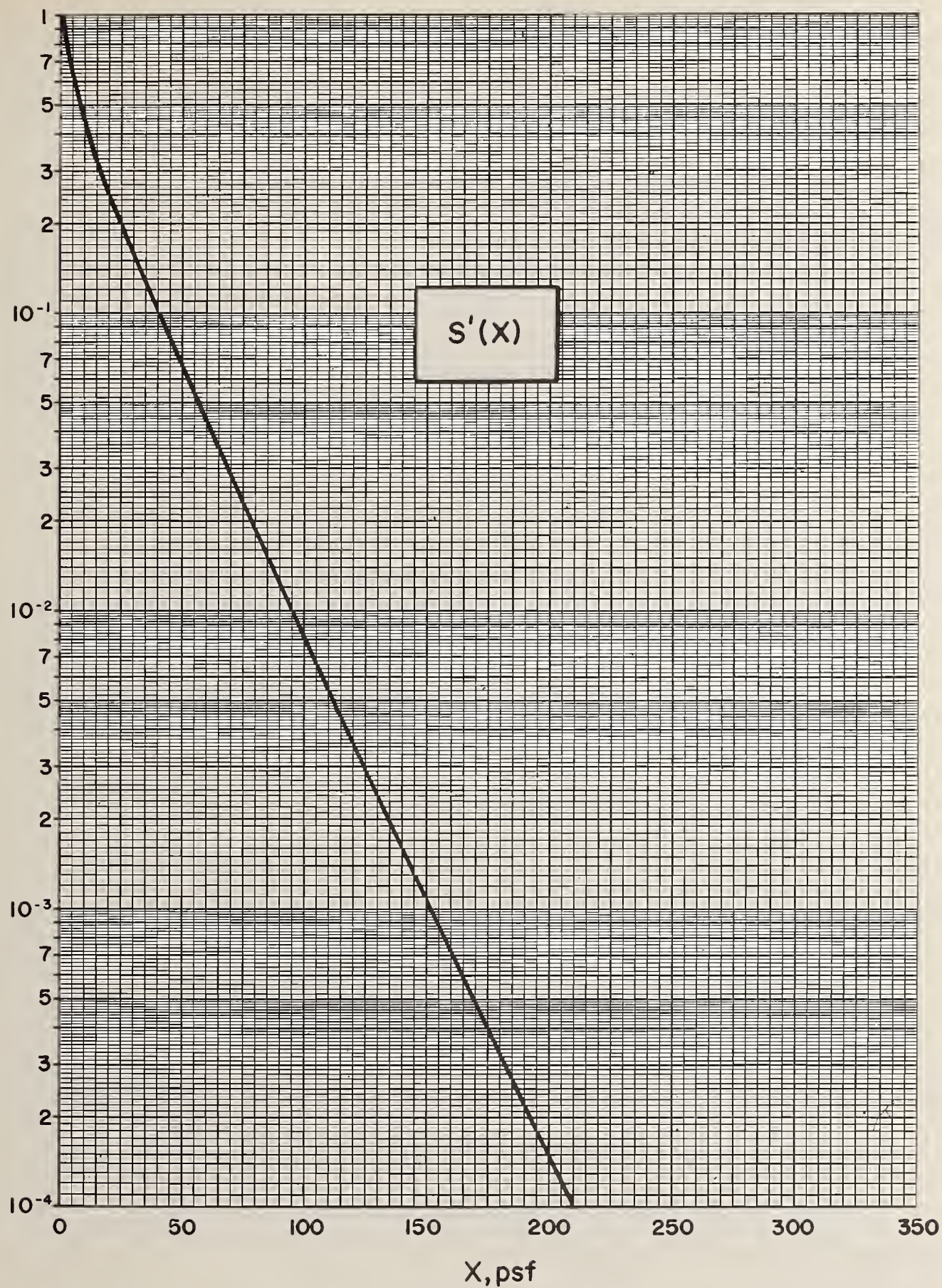
FIGURE 28.4. *Attenuation curve for radiation* backscattered *from a plane source isotropic over one hemisphere only, corresponding to skyshine radiation incident on the ground.* (H_2O, *1.12 hr fission. See also figs. B17 and B18.*)

35
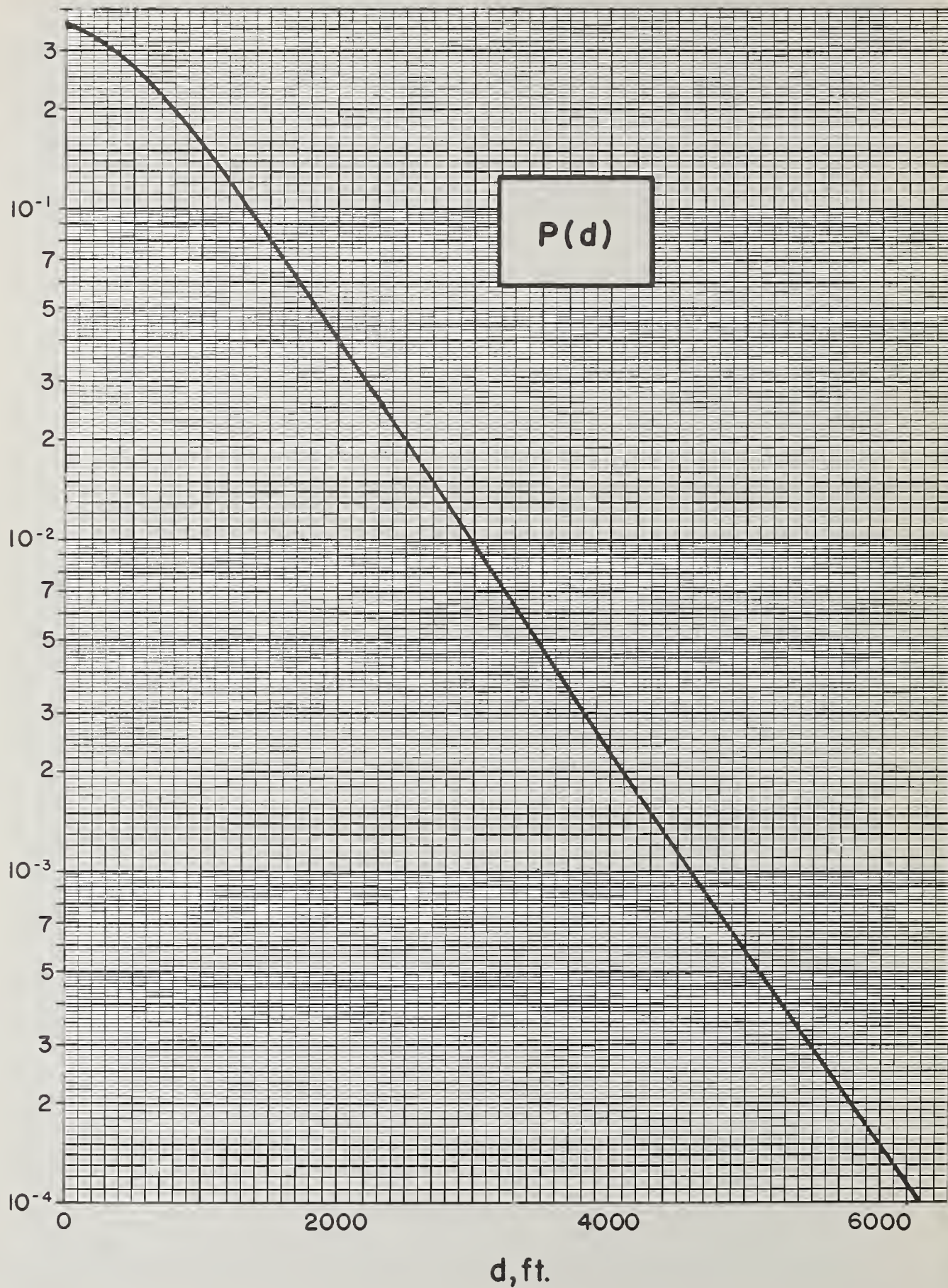
FIGURE 28.5a. *Point source of fallout radiation: P*(d) *as a function of distance* d *in air between detector and source.* (H₂O, *1.12 hr fission. See also figs. B19 and B20.*)
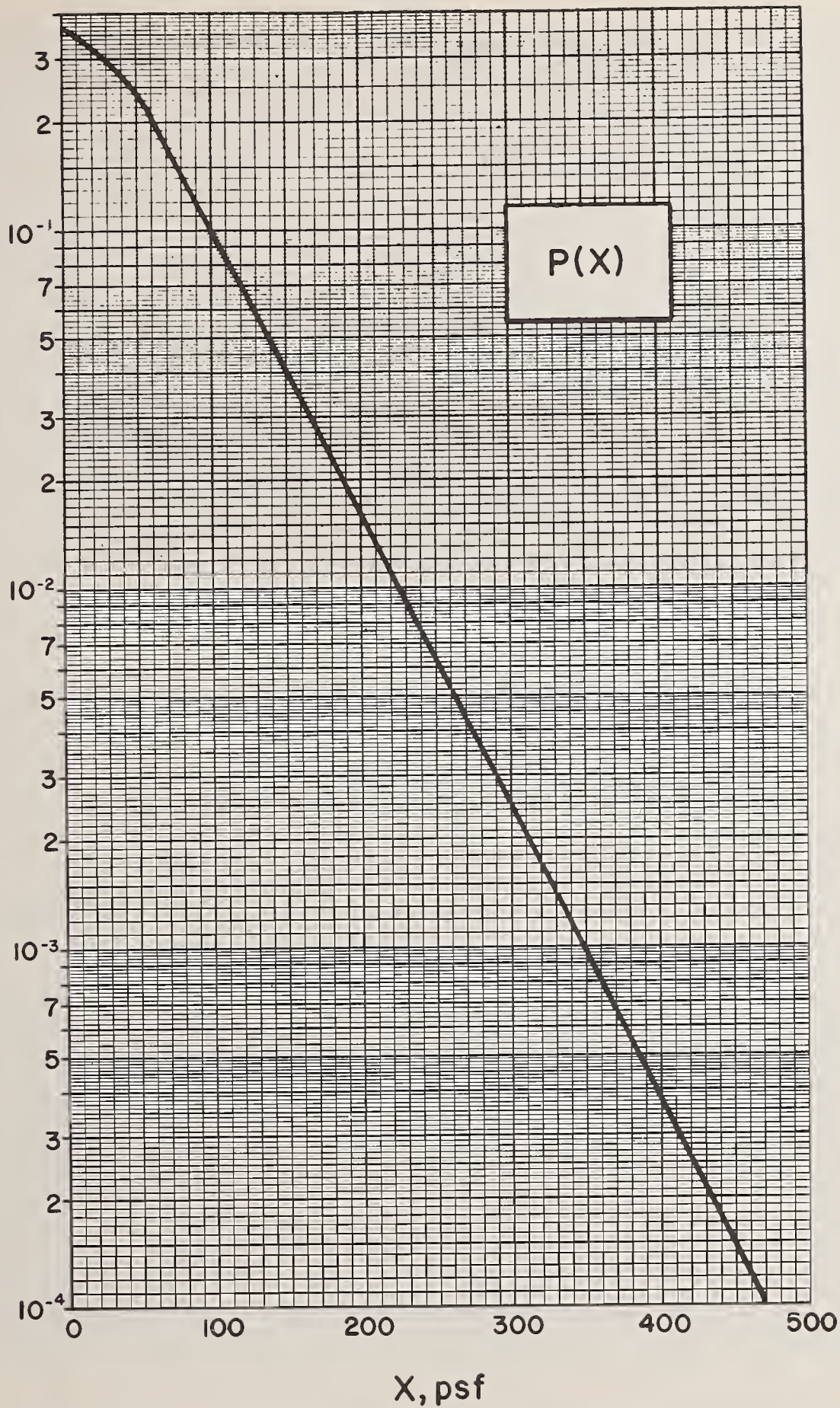
FIGURE 28.5b. *Point source of fallout radiation: $P(X)$ as a function of effective mass thickness between source and detector.* *(H_2O, 1.12 hr fission. See also figs. B21 and B22.)*
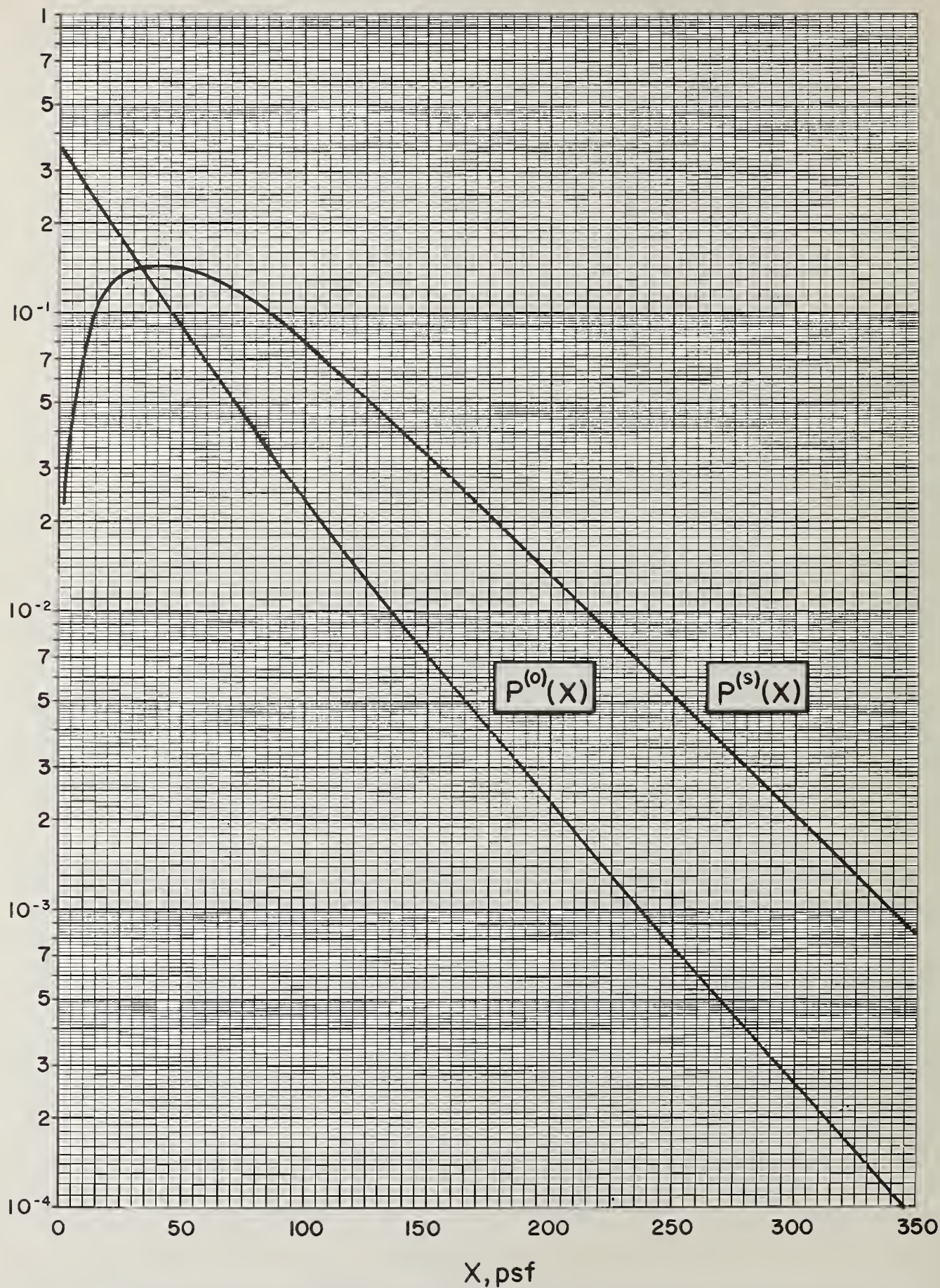
FIGURE 28.6. *Unscattered and scattered components of* $P(X)$. (H_2O, *1.12 hr fission. See also figs. B23 and B24.*)

38
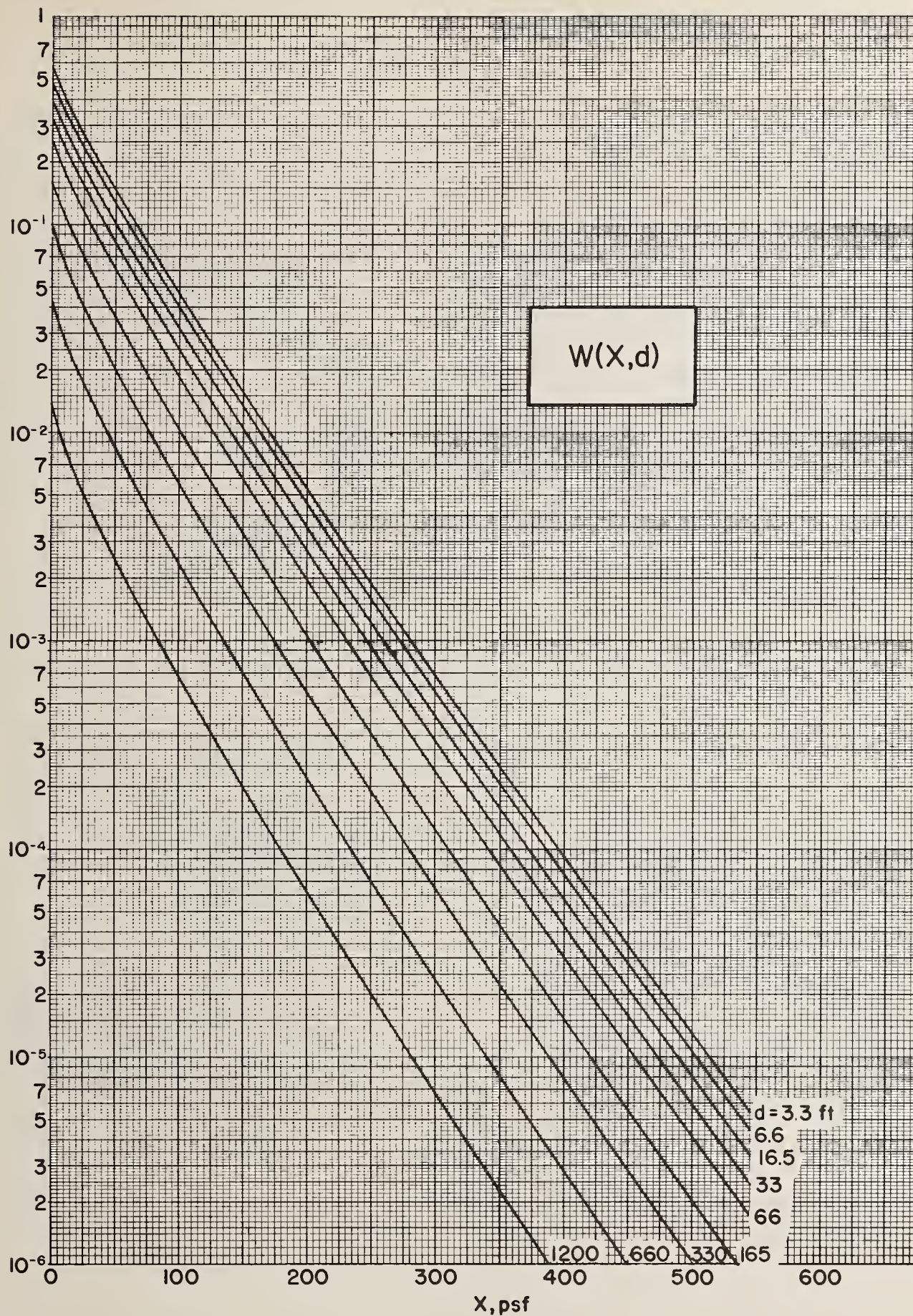
FIGURE 28.7. *Detector response ratio for effective mass thickness X separating the detector from a plane fallout source of angular distribution* $\frac{1}{2\pi}\int_0^{2\pi} d\phi l(d,sin\theta cos\phi)$. *($H_2O$, 1.12 hr fission. See also figs. B25 and B26.)*

39
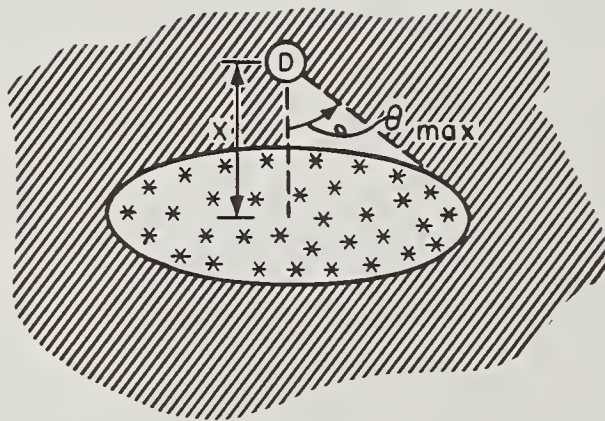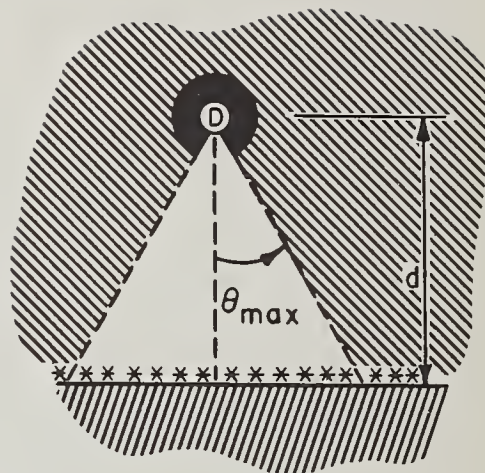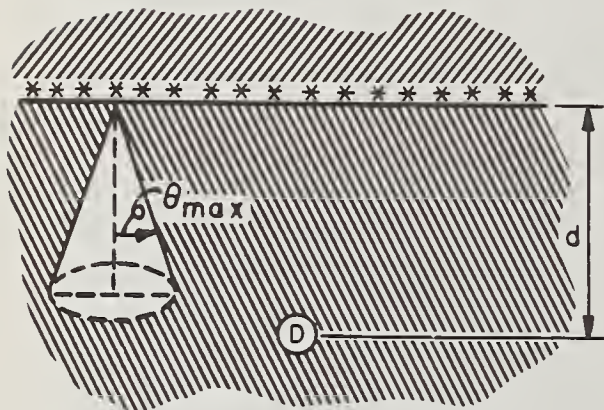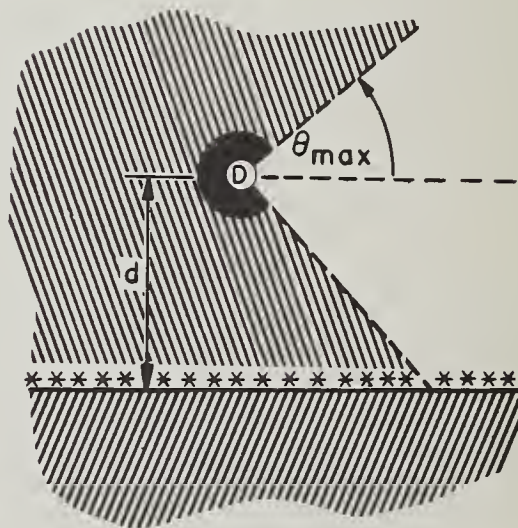
FIGURE 28.8. *Simple detector-source-medium arrangements:*

(a) *Isotropic detector, isotropic circular source;* (b) *conical detector pointed towards the source plane, plane isotropic source;* (c) *isotropic detector, conical source pointed towards the detector;* (d) *conical detector pointed parallel to the source plane, plane isotropic source.* *All configurations correspond to an infinite homogeneous medium and the latter three to an infinite medium with plane density variations.*
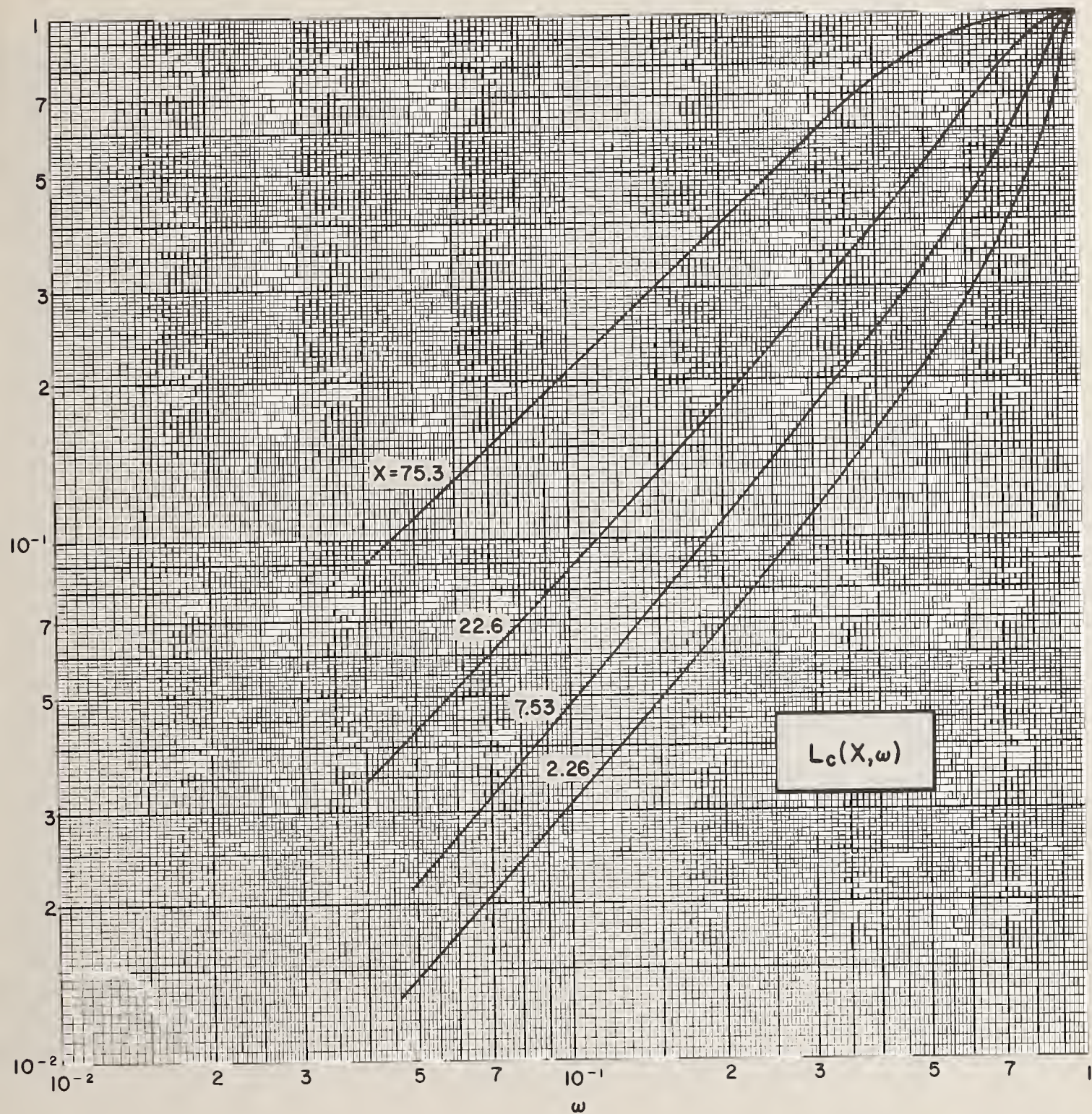
FIGURE 28.9. *Geometry factor describing detector response due to circular plane sources of fallout radiation, as shown in figure 28.8a. (H_2O, 1.12 hr fission. See also figs. B27 and B28.)*
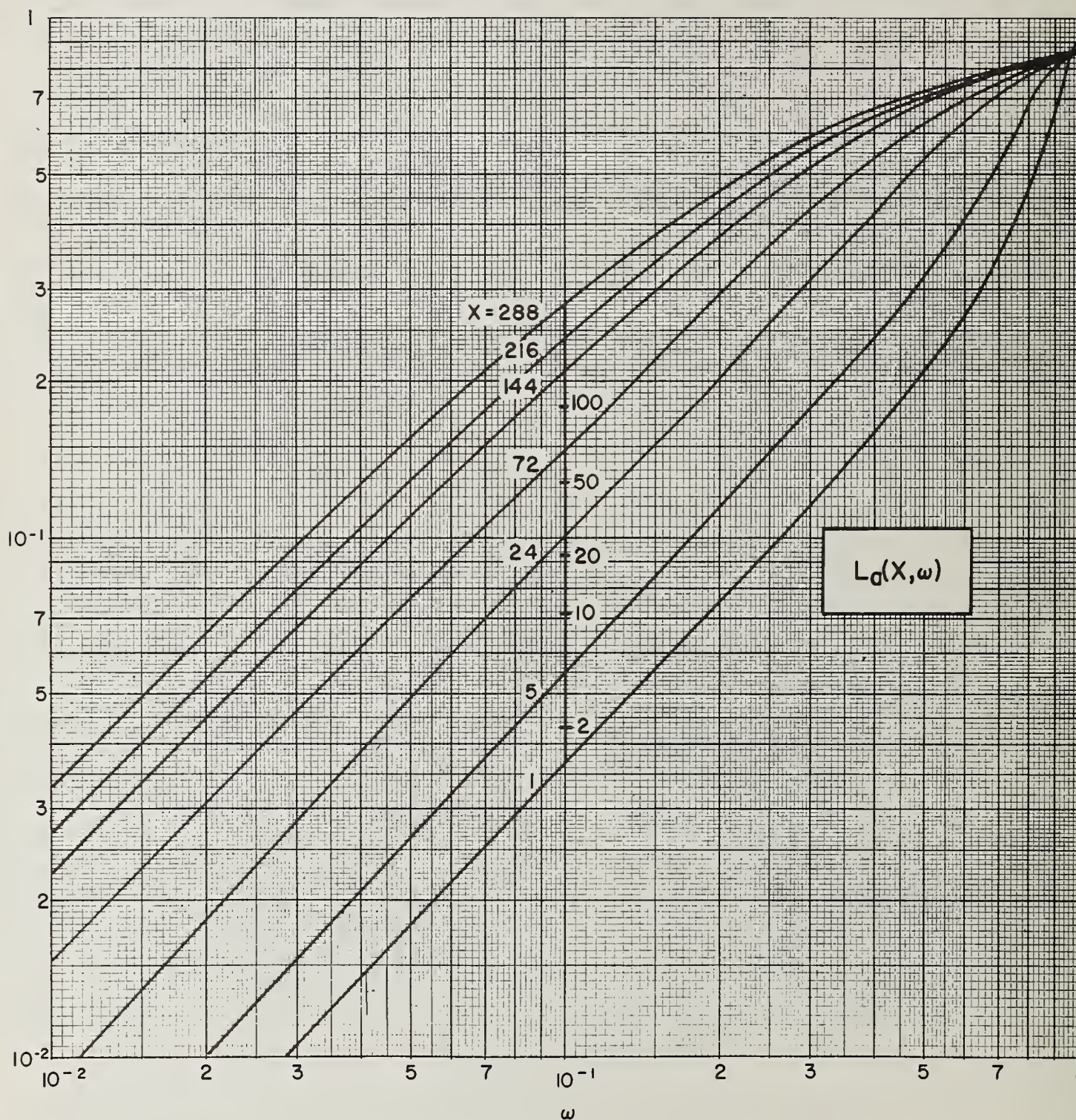
FIGURE 28.10. *Geometry factor for detector response to radiation striking the detector from a limited cone of directions, as shown in figure 28.8b.* (H₂O, 1.12 hr fission. See also figs. B29 and B30.)
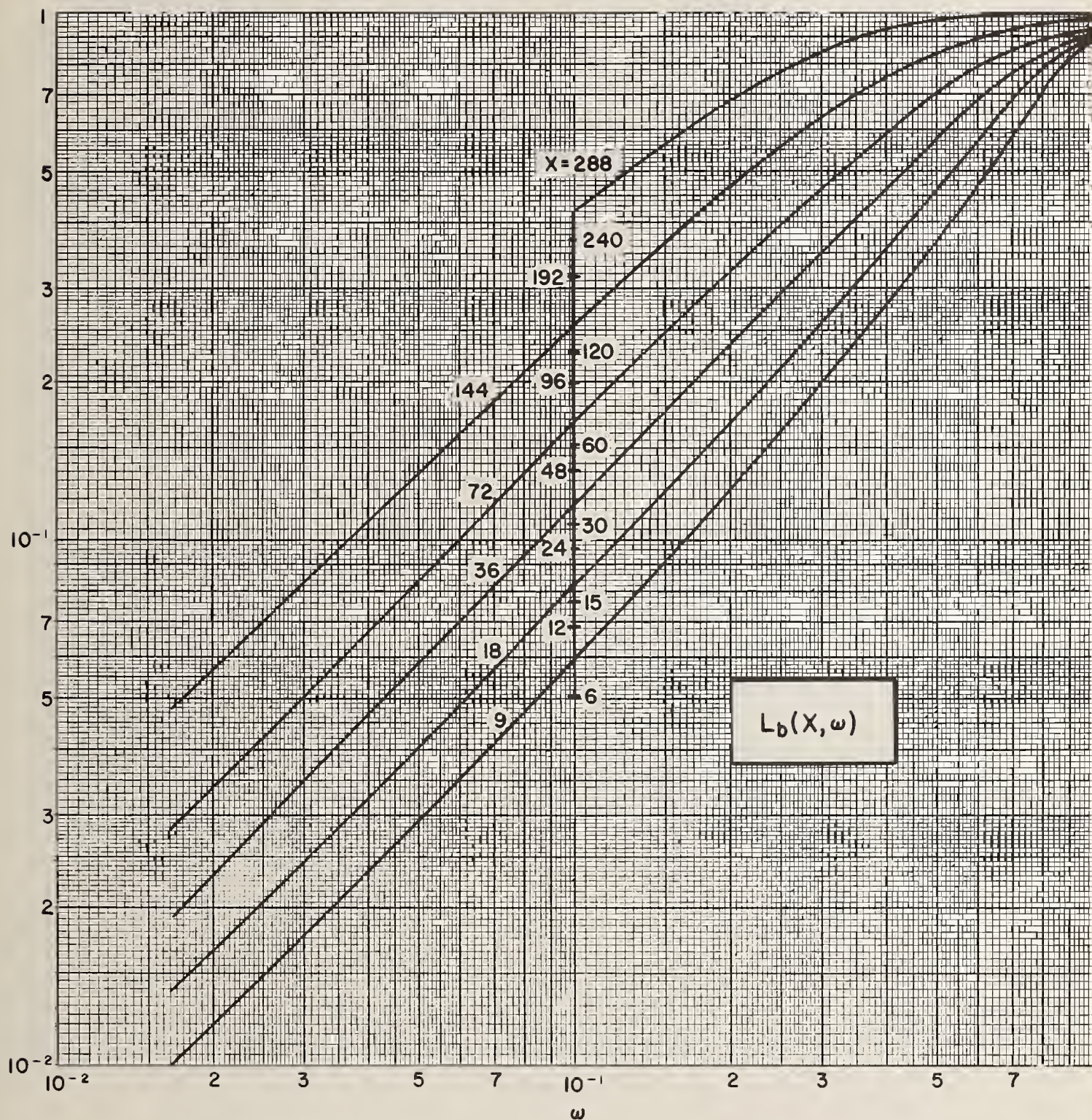
FIGURE 28.11. *Geometry factor for response of an isotropic detector adjacent to a plane source emitting radiation in a limited cone of directions, as sketched in figure 28.8c.* (H_2O, 1.12 hr fission. *See also figs. B31 and B32.*)
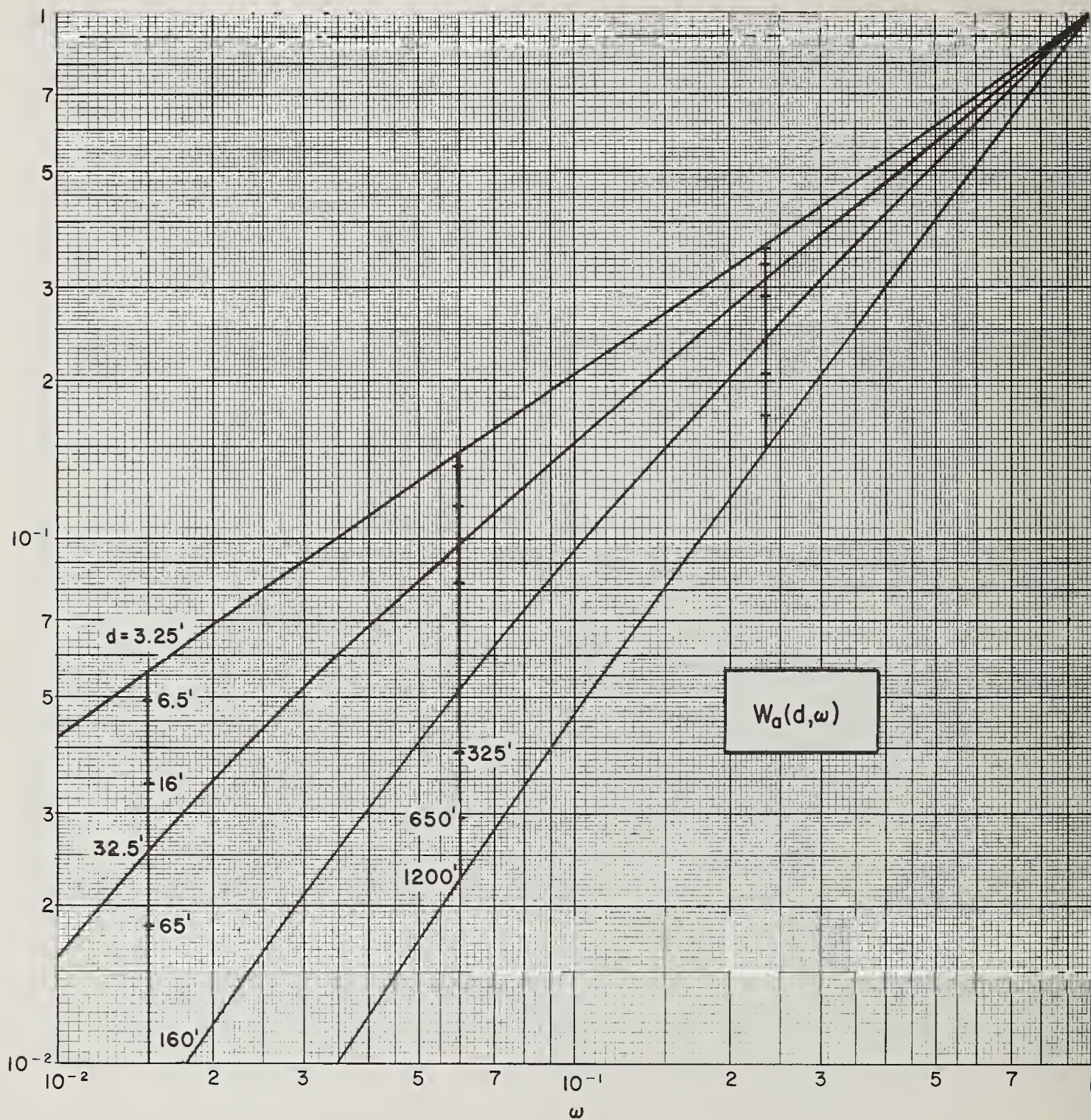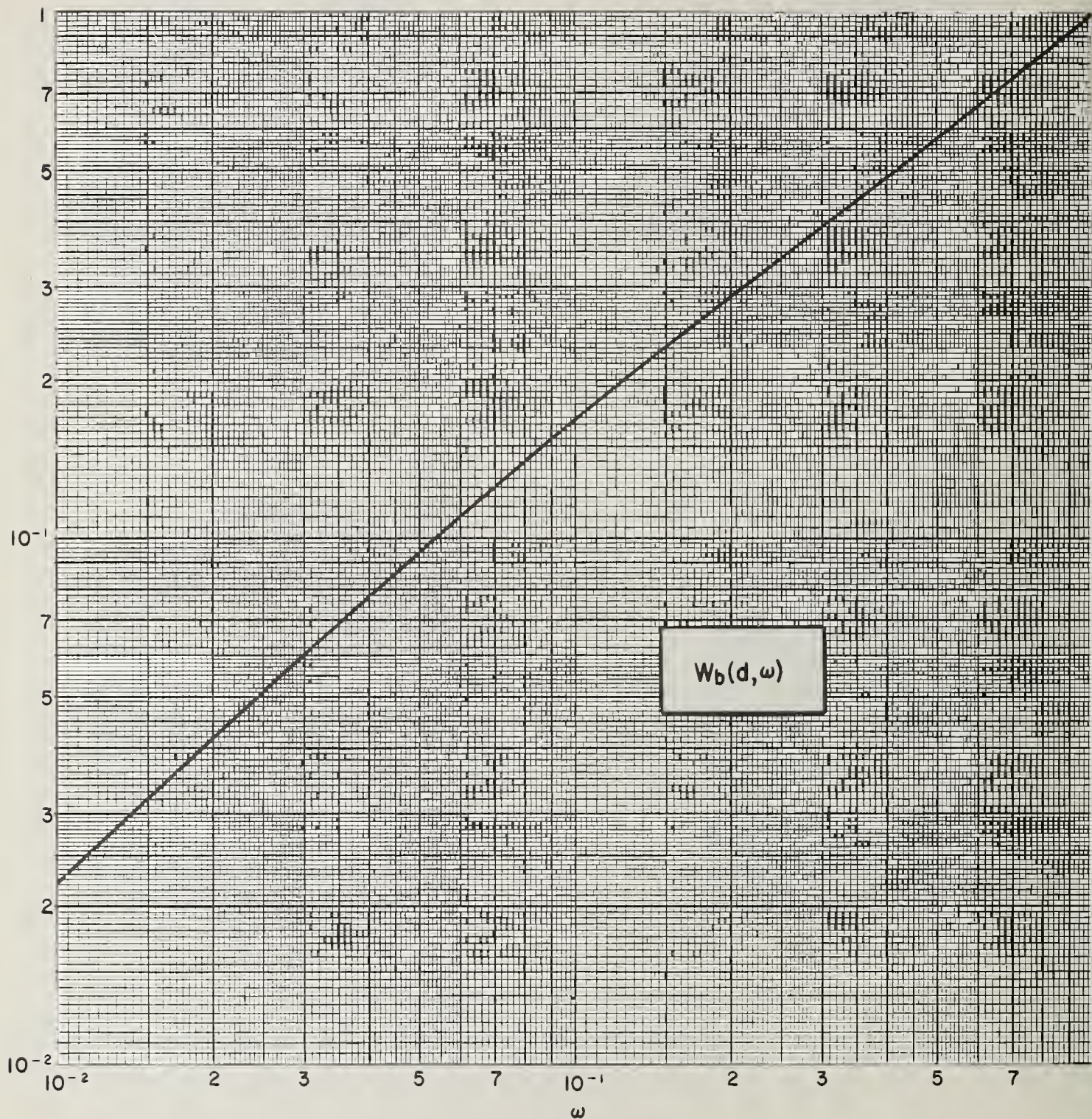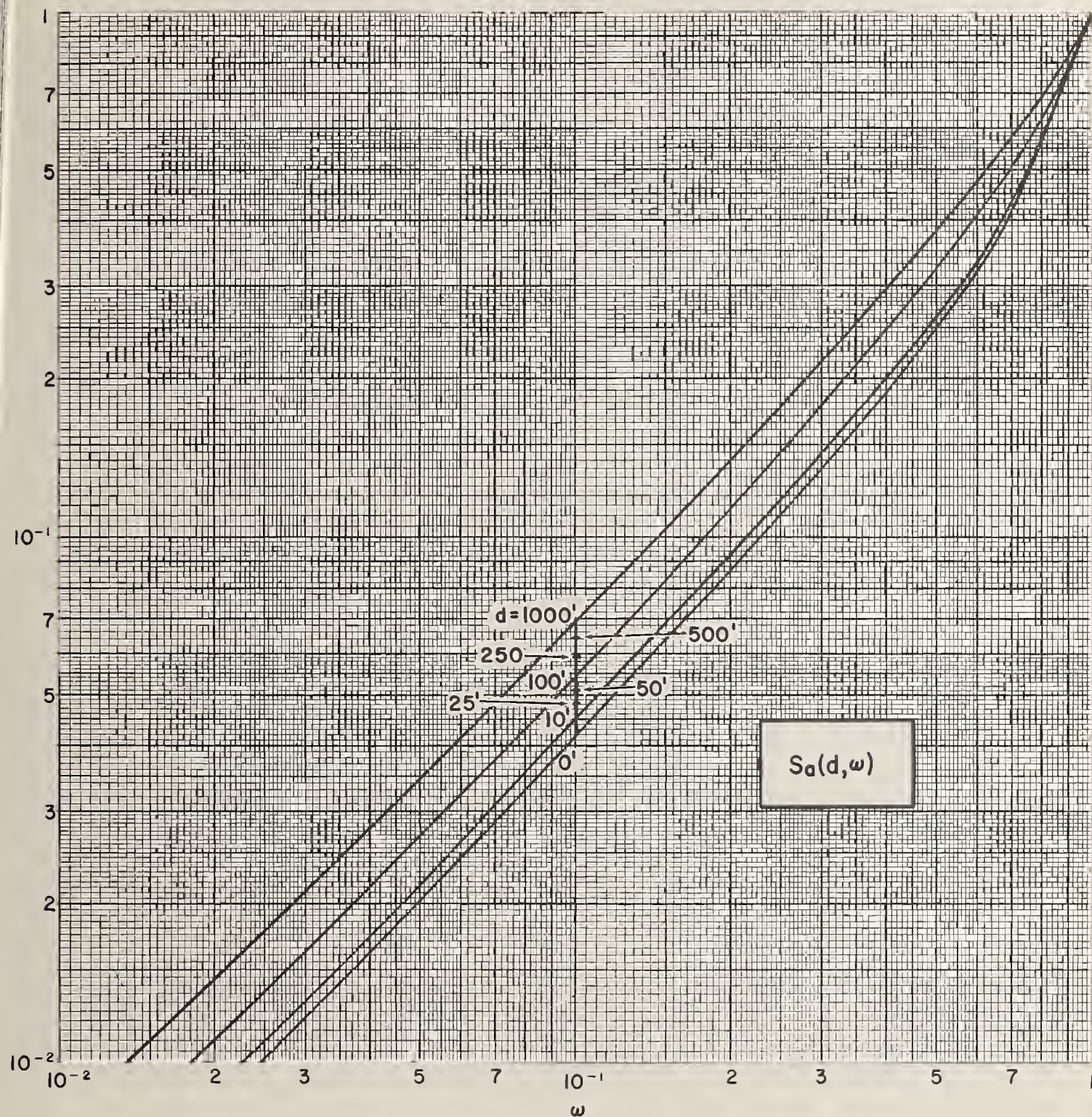
FIGURE 28.12. *Geometry factor describing detector response to radiation incident in a limited cone of directions about an axis parallel to the primary source plane, at height* d, *as shown in figure 28.8d.* (H_2O, *1.12 hr fission. See also figs. B33 and B34.*)
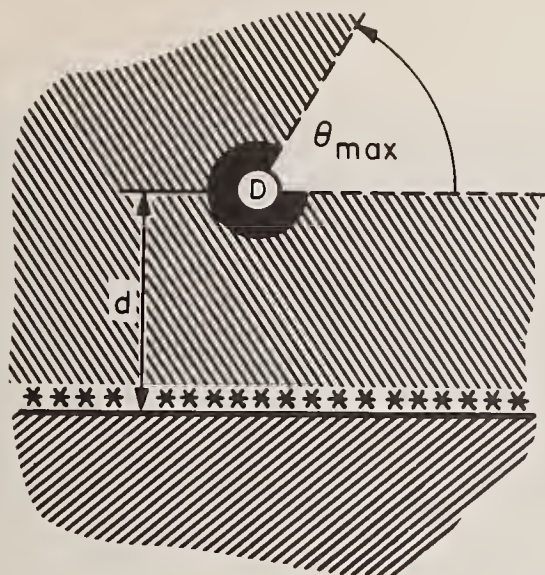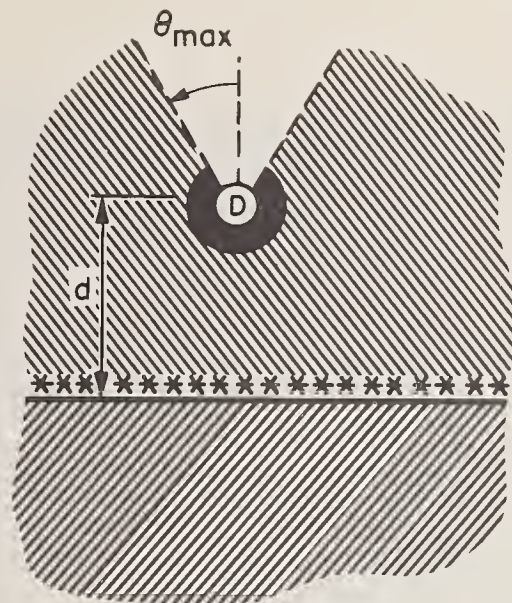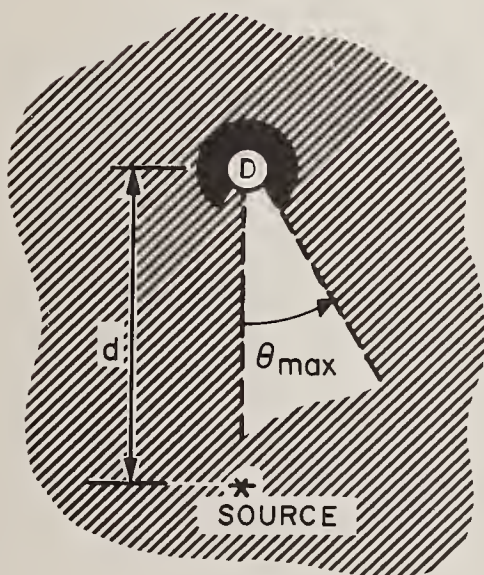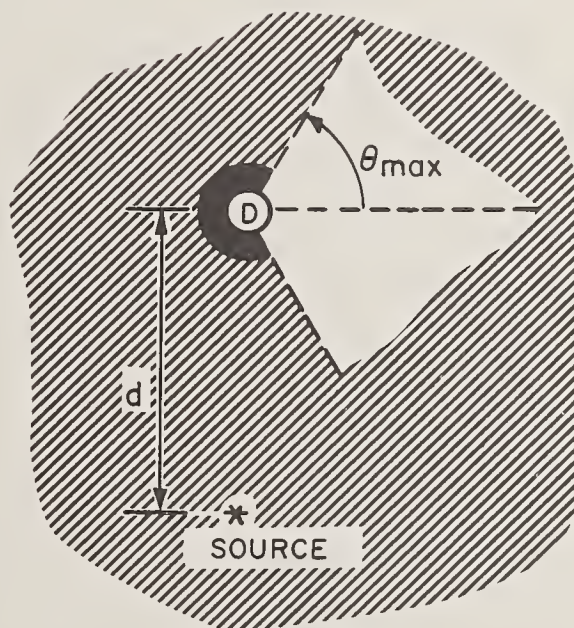
FIGURE 28.13. *Simple detector-source-medium arrangements:*

(a) *Detector which responds to the upper half of a cone of directions with axis parallel to a plane isotropic source;* (b) *conical detector pointed away from a plane isotropic source;* (c) *conical detector pointed towards a point isotropic source;* (d) *conical source pointed 90° away from the source-detector line, point isotropic source.* *All media may be considered infinite and homogeneous; and the first two may be considered infinite with plane density variations.*

FIGURE 28.14. *Geometry factor describing detector response to skyshine radiation incident in a limited cone of directions about an axis parallel to the primary source plane, as sketched in figure 28.13a. This graph is accurate for* $d \lesssim 200$ *ft of air.* (H_2O, *1.12 hr fission. See also figs. B35 and B36.*)

FIGURE 28.15. *Geometry factor describing detector response to skyshine radiation incident in a limited cone of directions about an axis perpendicular to the primary plane, at height d above ground, as sketched in figure 28.13b.* (H_2O, *1.12 hr fission.* *See also figs. B37 and B38.*)
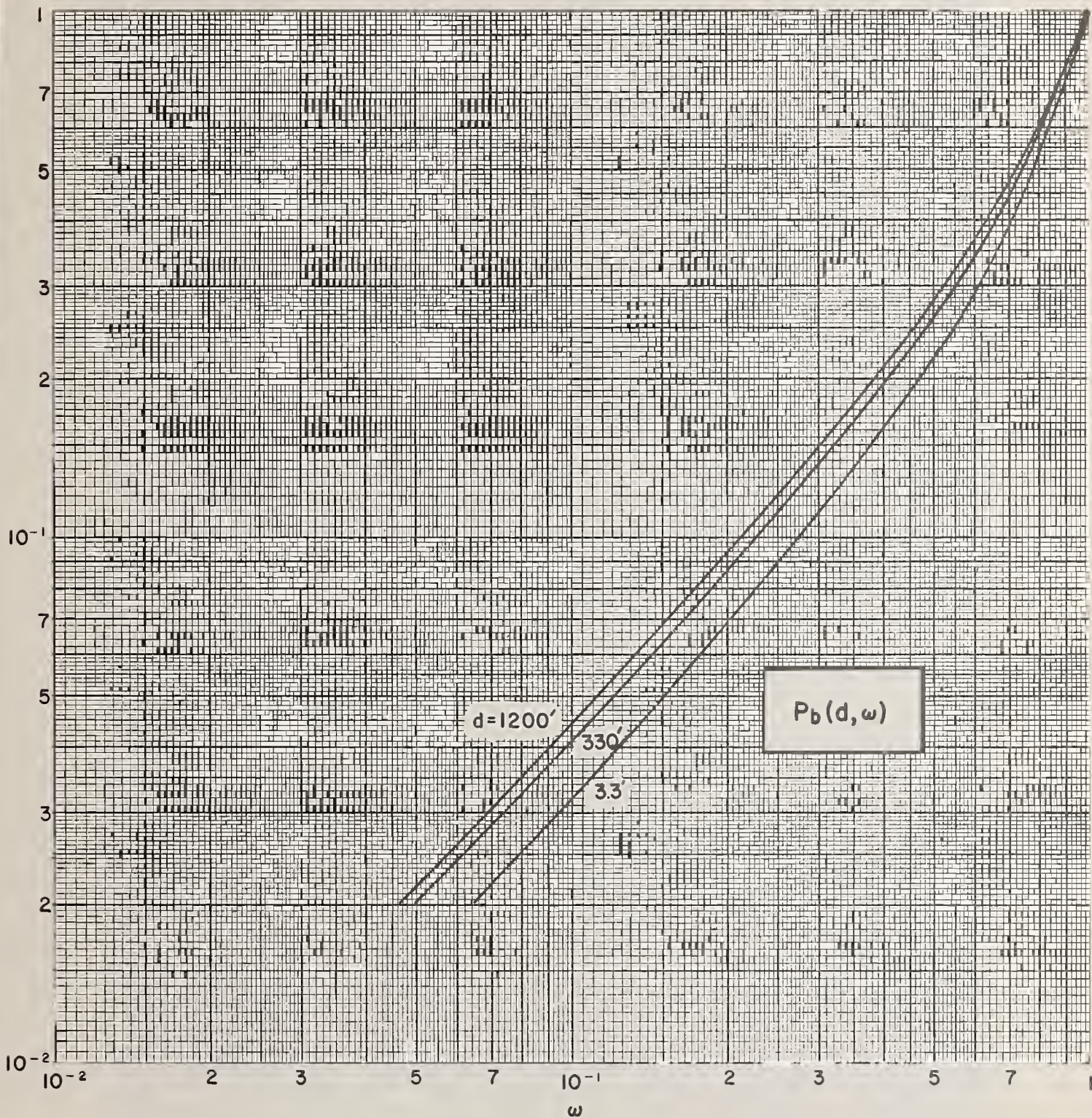
47
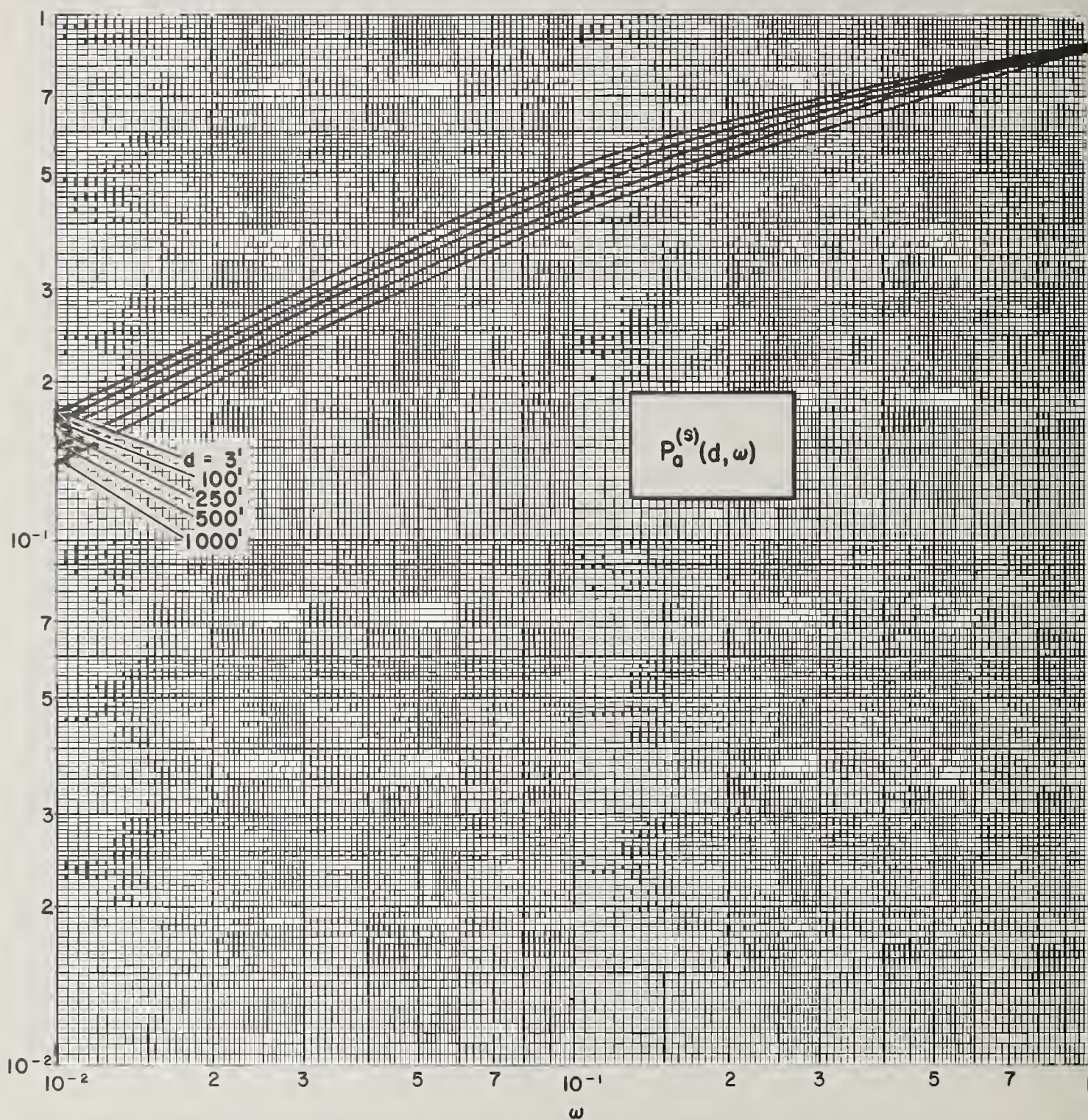
FIGURE 28.16. *Geometry factor describing detector response to scattered gamma rays from a point source of radiation, striking the detector in a limited cone of directions about the line from source to detector, as sketched in figure 28.13c.* (H_2O, 1.12 hr fission. *See also figs. B39 and B40.*)
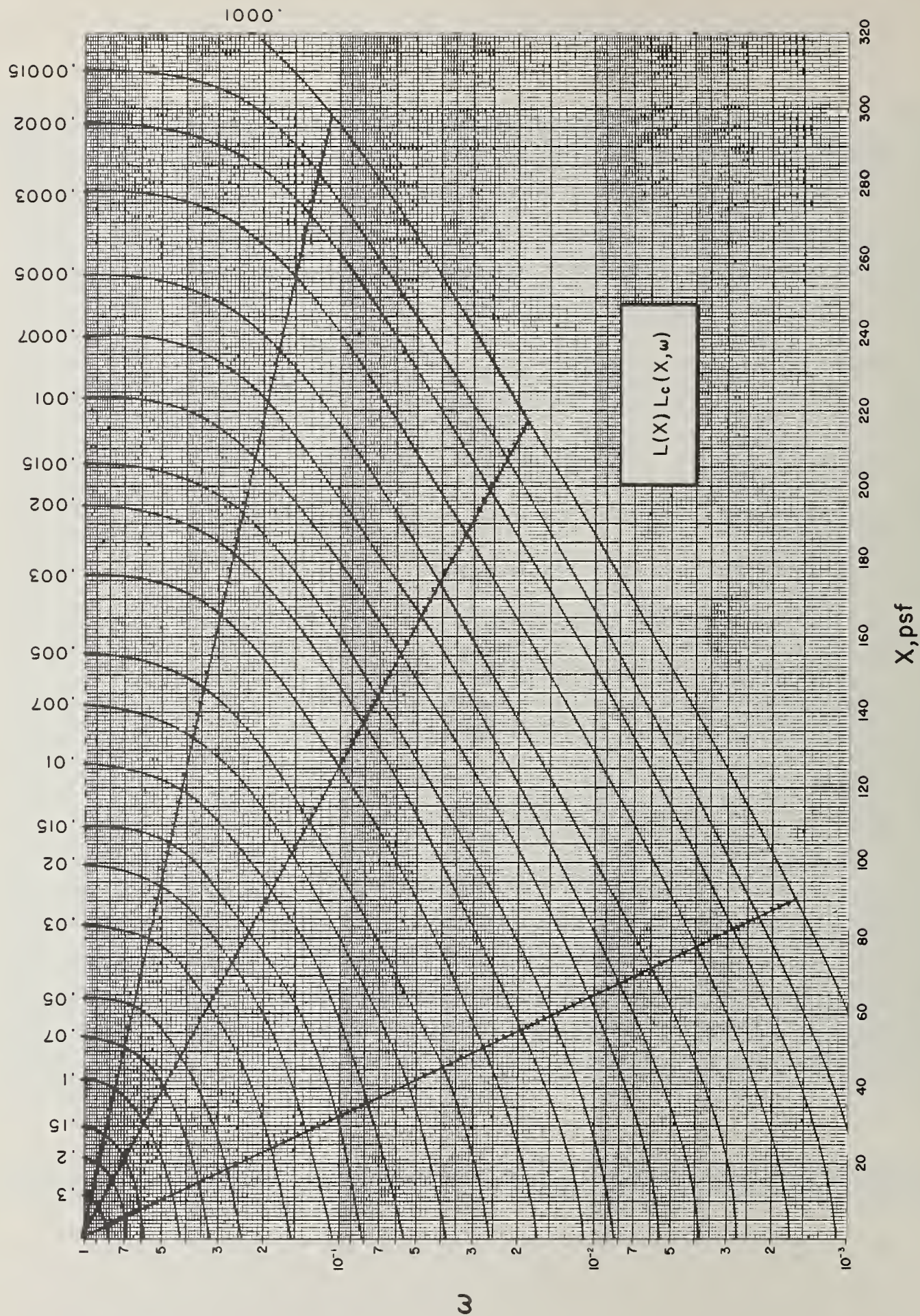
FIGURE 28.17. *Geometry factor describing detector response to fallout gamma rays from a point source, striking the detector in a limited cone of directions about an axis perpendicular to the line from source to detector, as sketched in figure 28.13d. (H_2O, 1.12 hr fission. See also figs. B41 and B42.)*

49

FIGURE 28.18. *Contours of constant* $L(X)L_c(X,\omega)$. *(H_2O, 1.12 hr fission. See also figs. B43 and B44.)*
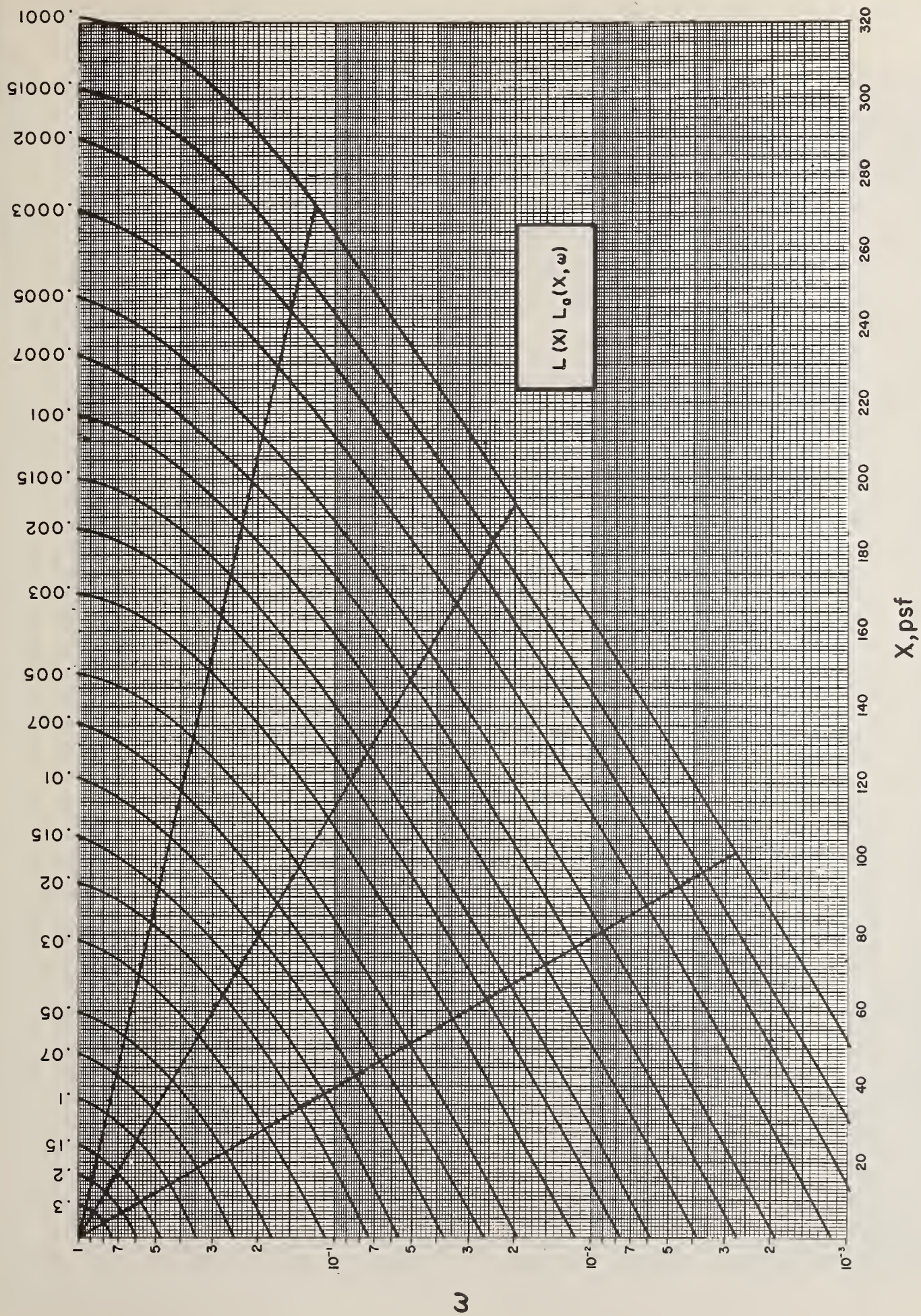
50

FIGURE 28.19. *Contours of constant* $L(X) L_a(X,\omega)$. *(H$_2$O, 1.12 hr fission. See also figs. B45 and B46.)*
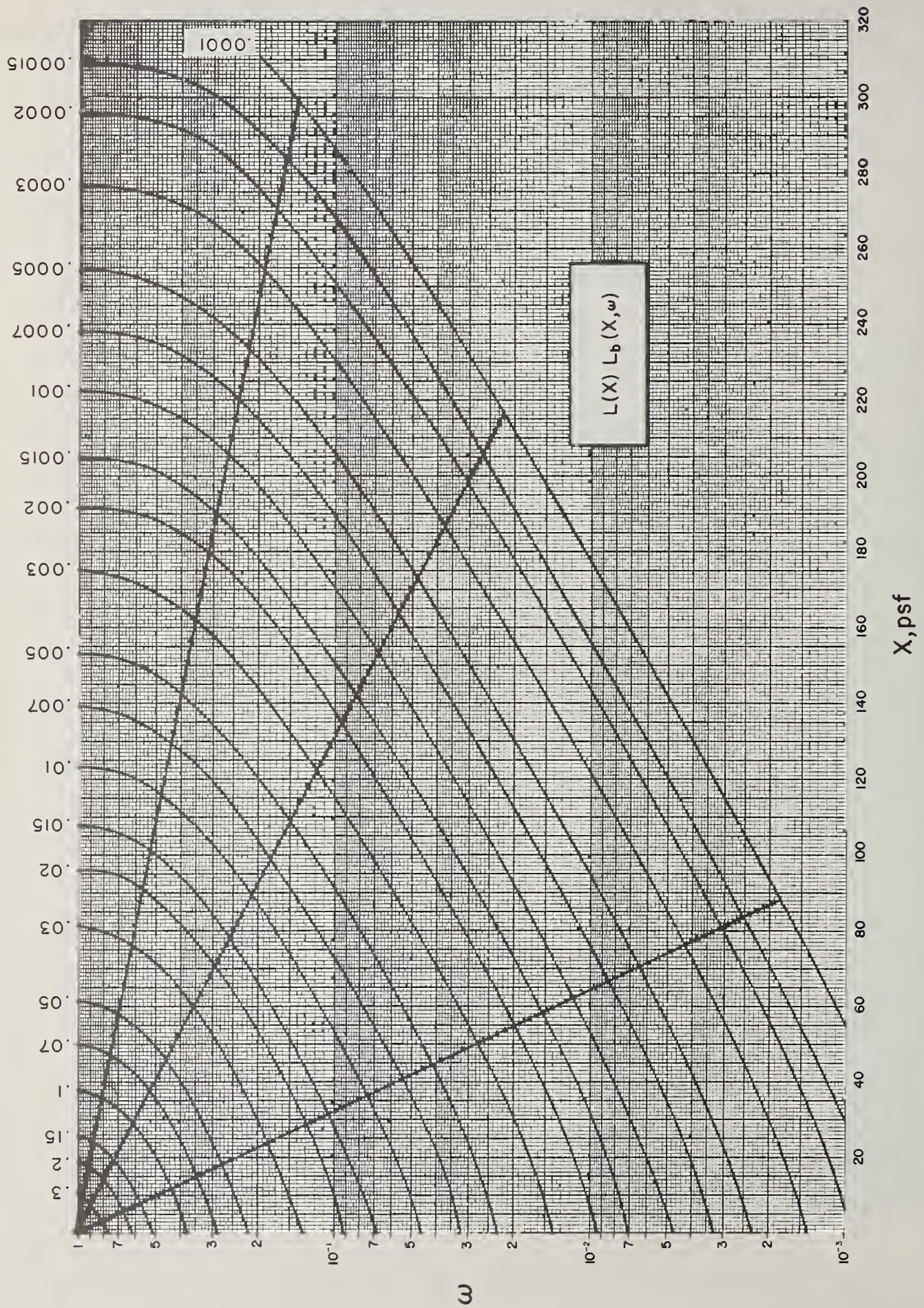
51

FIGURE 28.20. *Contours of constant* $L(X)L_b(X,\omega)$. (H_2O, 1.12 hr fission. See also figs. B47 and B48.)

52

skyshine intensity. Data for this function obtained from the data of figure 26.1 are given in figure 28.14. Notice that $\omega=1$ corresponds to an aperture passing skyshine from one side only, i.e., only *half* the total skyshine; this is reason for the factor 2 in eq (27.12). The variations with d were too small to warrant separate curves for different d values.

(12) $S_a(d,\omega)$: This function is defined by an integral over a cone of obliquities of incidence pointed *away* from the source plane (see eq (27.13)). Thus only skyshine contributes to the detector response. The relevant configuration is sketched in figure 28.13b. The allowed cone has aperture angle θ_{max} and subtends solid angle fraction $\omega=1-\cos\theta_{max}$. The denominator is the response to all backscattered gamma rays incident on the detector. Data, given in figure 28.15, have been obtained from the data of figure 26.1. Note the steepness of the curves near $\omega=1$, expressing the strong component of the gamma ray directional distribution in directions parallel to the source plane.

(13) $P_a(d,\omega)$ and $P_a^{(s)}(d,\omega)$: All preceding ratios are for plane sources. The P_a ratios defined by eqs (27.14) and (27.15) are like the L_a ratios, but with reference to a point source. The numerator is the response of a detector to scattered radiation incident within a cone of directions about the radial axis from detector to source (see fig. 28.13c). The denominator is the total response of an isotropic detector to the scattered radiation. Data obtained from figure 26.3 is given in figure 28.16. Note that the curves go to unity only for $\omega\to2$, so that the backscattered contributions

are not included in figure 28.16. The following expression relates P_a and $P_a^{(s)}$:

$$P_a(X,\omega)=\frac{1}{P(X)}\,[P^{(0)}(X)+P^{(s)}(X)P_a^{(s)}(X,\omega)].$$

$$(28.4)$$

This merely expresses total detector response as the sum of responses due to scattered gamma rays and to unscattered gamma rays. The latter are always concentrated along the radial line connecting source and detector.

(14) $P_b^{(s)}(X,\omega)$: For completeness we include the point source analogue to the W_a (plane source) function. The function is defined by eq (27.16) and illustrated by figure 28.13d. It has in the numerator the response of a detector to scattered gamma radiation incident within a cone of directions perpendicular to the radial line from detector to source. The aperture angle θ_{max} is related to the solid angle fraction ω by $\cos\theta_{max}=1-\omega$. The denominator represents the *total* response of an isotropic detector to scattered radiation, while the numerator never represents more than half, hence the factor of 2. Data is presented in figure 28.17, as calculated from the basic data of figure 26.3.

(15) $L(X)L_c(X,\omega)$, $L(X)L_a(X,\omega)$, $L(X)L_b(X,\omega)$: These combinations of barrier and geometry factors come up so frequently in applications that contour diagrams have been prepared to permit direct determination of the product. Figures 28.18, 28.19, and 28.20 present the diagrams. Radial lines have been superimposed and calibrated to permit accurate interpolation. Use of French curves facilitates this interpolation.

VI. Elementary Structure Types

29. Comments

A number of elementary barrier arrangements have been the subject of special studies. Because of their simplicity they permit a fairly complete analysis, both experimentally and theoretically; and they appear over and over again in various combinations in nearly all structures. One might say that complicated structures are a composite of these simpler types. As an example, the blockhouse described already in Section 20 combines vertical walls (Section 33) with a fallout-covered shelter (Section 32).

In this part we discuss these configurations with the help of the data and approach already presented. Our intention is to describe them schematically in a manner which leads to numerical values for the detector response. At the same time we hope to give an appreciation for the nature for the approximations involved, so that a feeling for size of possible errors can be achieved.

Because this Part is intended to be illustrative rather than exhaustive, we limit the examples to

circular source and barrier shapes. The generalization to arbitrary detector position relative to arbitrary rectangular shapes is given in Part VII.

30. Density Interface

The simplest configurations of real importance comprise a radiation source at a density interface, with the detector placed some distance above in air (see fig. 30.1a). One may visualize a vast, smooth, level field supporting the radiating material.

(1) Air-air, infinite plane source case: In the simplest of these cases, the interface is smooth and separates two semi-infinite regions, one of air at standard pressure and the other of compressed air of the same density as earth. We have already commented that reference to "compressed" air has importance only as aid to visualization, if the source covers the plane uniformly. This is because of a scaling principle which guarantees that compression of the material into plane layers of different density does not alter
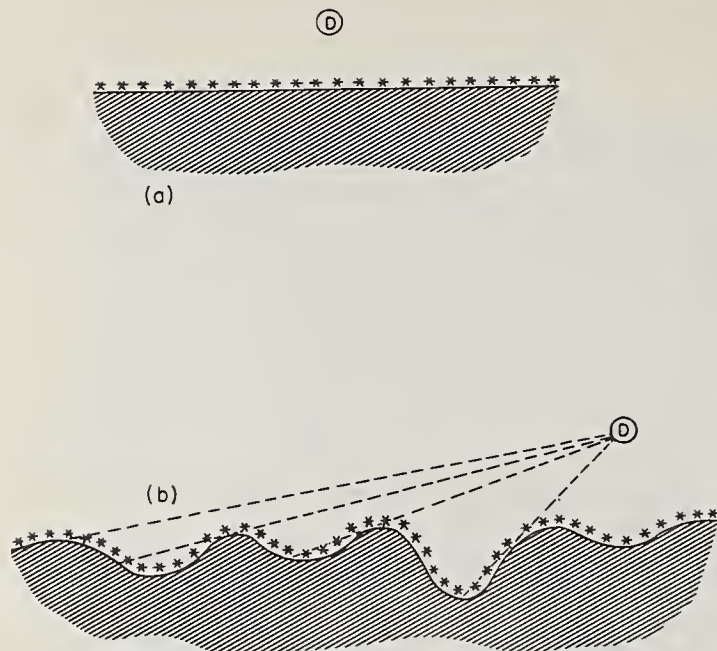
53

(a)

(b)

FIGURE 30.1. (a) Plane, isotropic fallout source at a simple density interface; (b) fallout source on rough ground.
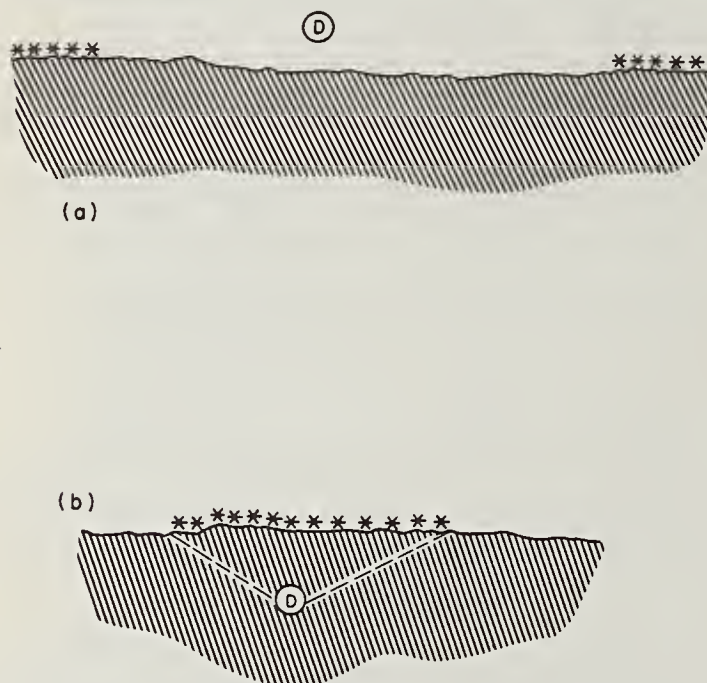

(a)

(b)

FIGURE 30.2. (a) Detector above an area cleared of fallout; (b) detector below a finite source on the ground.

the radiation flux anywhere, in intensity, spectrum, or angular distribution, if "distance from the source" is measured in mean free paths, lbs/ft², gm/cm², effective mass thickness, or other indicators of the amount of material between source and detector.[28]   Thus, this case is just the one to which calculations of $L(X)$ and $L(d)$ apply precisely, and the detector response as a function of distance from the source is simply

$$D/D_0 = L(d). \qquad (30.1)$$

---

[28] Note that this scaling principle does not hold for non-uniform or finite source spatial distributions.
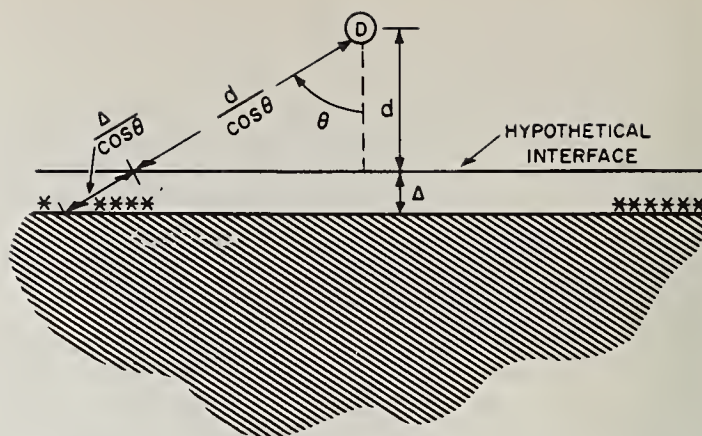

FIGURE 30.3. Geometry of a detector above a circular fallout-free area, when the fallout elsewhere is considered to be buried beneath a hypothetical layer of thickness Δ.

(2) Air-earth or air-concrete case, infinite plane source: If instead of the location at an interface between air and compressed air the source is at an interface between air and earth, or air and concrete, a modification of the detector response is expected. This is because the interaction probabilities for gamma rays in earth and concrete differ from those of air, for low energy gamma rays. This has the consequence that near an air-earth interface the flux of low energy photons falls a little below the flux near the source in an air-air case. The effect is small, a few percent, and is due to photons which in earth or concrete undergo absorptive interactions at higher energies than in air.

This same effect is expected for the flux penetrating downward into earth or concrete. By and large, earth and concrete can be treated as if they were equivalent to water in penetration properties, because the differences in interaction probabilities give differences in detector response which are significant only for very large penetrations, or for very low energy photons. For our purposes it is sufficient to write

$$D/D_0 \approx 0.9L(X), \qquad (30.2)$$

within or at the surface of the semi-infinite earth or concrete region, if the $L(X)$ data is for penetration in H_2O, as in figure 28.2b. The factor 0.9 allows for the lower flux of low energy photons in concrete, and should be omitted if the data is for penetration in concrete. For an experiment of this type see [36].

(3) Ground roughness: If the interface between earth and air is rough, rather than smooth, a reduction in intensity is to be expected. The reason for this can be appreciated with the aid of figure 30.1b. That part of the radiation source which falls into "pockets" cannot contribute as much to the radiation component nearly parallel to the source plane. The gamma rays emitted nearly parallel to the source plane must penetrate a substantial amount of dense material before emerging into the air, and are correspondingly reduced in intensity.

54

One expects all earth surfaces to be rough to some extent; but this effect will be larger in the case of a ploughed field than a carefully smoothed baseball diamond. Investigation of ground roughness effects is still in a fairly rudimentary state. We note, however, that raising the detector height above a smooth interface has a similar effect of reducing the contribution of the unscattered "grazing" component through attenuation along the elongated path from the point of generation. Because of the importance of some type of rule for obtaining intensities and angular distributions corrected somehow for ground roughness, we tentatively adopt the simple procedure, suggested by Ksanda, Moshkin, Shapiro, and others, of writing

$$D/D_0 = L(d+\tau), \qquad (30.3)$$

where τ is a constant which is characteristic of the local terrain [37]. Values of τ are not available for widely different terrains. At least one case has been investigated experimentally, however, and for this case it has been calculated that $\tau \approx 40$ ft.[29] The experiments were performed in an open Nevada field without special treatment either to increase or decrease roughness. Equation (30.3) has no real justification beyond the comment that introduction of the parameter τ affects both intensity and angular distributions the way ground roughness affects them. The argument can be made to sound slightly more convincing by describing the fallout as effectively buried beneath a thin layer of earth.

(4) Finite plane sources: The preceding discussions assume that the source covers the plane of the interface uniformly. If the region of contamination does not cover the source plane, new and complicating aspects to the problem appear. Consider, for example, a circular clearing in a fallout field, with the detector above the center of the field (fig. 30.2a). Due to ground roughness, the detector response will be far from the value expected for a smooth source plane. Hardly any unscattered radiation will reach the detector because it will be blocked on its path along the ground by irregularities.

Another complicating feature of this type of problem involves the scattered component of the radiation. Gamma rays which travel long distances on a path which is always not far above ground have a large probability of being deflected into the ground. When this happens, distances between successive interactions shrink from hundreds of feet to inches. If the photon is to travel any significant distance farther, it must re-emerge into the air. This effect reduces the detector response in just the sort of configuration illustrated in figure 30.2a by an amount which is not well known but which depends on the radius of the clearing. Studies of this "path foreshortening" effect have been made, both theoretically and experimentally; but results for clearings are not available.

[29] C. M. Eisenhauer, private communication.

In spite of these difficulties it is possible to obtain estimates of a sort of the detector response to radiation above a clearing, taking ground roughness into account. To accomplish this we follow consistently the schematization in which the effect of ground roughness is approximated by performing a calculation at an increased height above ground. This implies that ground roughness has effects similar to those due to "burying" the source under a thin layer of earth, as already mentioned. In figure 30.3 a detector is pictured at a height d above ground. The source is buried under a layer of earth which has effective mass thickness Δ, equivalent to a layer of air of thickness τ. The clearing is circular, with the edge of the source at a radius $d/\tan\theta$ out from the point below the detector. The distance in air from the detector to the edge of the contamination is $d/\cos\theta$, and the additional penetration through the covering layer is $\Delta/\cos\theta$, which is equivalent to a distance in air of $\tau/\cos\theta$. The penetration from the edge of the source to the detector is thus equivalent to $\dfrac{d+\tau}{\cos\theta}$ feet of air. If we use this penetration distance in the expression for the detector response above a cleared area, we obtain the desired approximation:

$$D/D_0 \approx L\left(\frac{d+\tau}{1-\omega}\right), \qquad (30.4)$$

where $\omega = 1-\cos\theta$. No allowance is made in this expression for path foreshortening.

One advantage of this simple approximation is the possibility of using it to calculate anisotropic detector responses above clearings; but we don't pursue this here.

The accuracy of our predictions of detector response above a clearing is limited by lack of knowledge of ground roughness and path foreshortening; but in a related problem which is perhaps of greater practical importance these complicating effects are not operative. This problem is the calculation of the detector response in earth (or concrete) *below* the source plane, when the source is of limited extent. Figure 30.2b illustrates this case. Radiation from the source traveling initially upward goes such long distances through the air that it doesn't come back to the same locality. Thus the detector response will be lower than in cases which are similar but without the density interface. But this is a small effect even when the barrier thickness between source and detector is not very great. It is possible to determine the detector response fairly accurately from the expression

$$D/D_0 = 0.9L(X)L_c(X,\omega), \qquad (30.5)$$

where ω is the solid angle fraction of the source as seen from the detector. (The factor .9 is a rough correction when $L(X)$ and $L_c(X,\omega)$ represent H_2O penetration data.) This expression can be seen to

include a contribution due to radiation just mentioned as being, in fact, absent. Thus it will be an overestimate, particularly for $X \approx 0$.

EXAMPLE 1: Calculate the reduction factor due to ground roughness, for a detector 3 ft above a contaminated area, if the "roughness" parameter τ has a value of 40 ft for this type of surface.

From eq (30.3) and figure 28.2a we obtain $L(3+40)=0.52$. ANSWER.

EXAMPLE 2: How high above the ground must a detector be raised to reduce its response by a factor of 1000?

Applying eq (30.2), but omitting the factor 0.9 because of the height above the interface, we see from figure 28.2a that $L(d)=0.001$ for $d=2950$ ft. ANSWER.

EXAMPLE 3: Assuming a ground surface such that $\tau=40$ ft, calculate the radius of a clearing sufficient to reduce the detector response to $D_0/1000$, at a height of 3 ft above ground.

Applying eq (30.4), using figure 28.2a, we find that $L\left(\dfrac{43}{1-\omega}\right)=0.001$ for $\dfrac{43}{1-\omega}=2940$ ft. From this we see that $1-\omega \approx 3/\rho = 43/2940$, giving $\rho = 3(2940)/43 \approx 200$ ft. ANSWER.

This last should be considered only the crudest sort of estimate, in view of the state of knowledge of ground roughness effects.

31. Foxhole Problems

A typical foxhole configuration is shown in figure 31.1. Radiation generated at the ground-air interface can enter the aperture even though it faces away from the primary source, by backscattering from the air. This backscattered component of the radiation is also called the "skyshine". Normally the aperture will permit skyshine radiation to strike the detector only if it travels in an allowed cone of directions as indicated in figure 31.1 by the dashed line on the right.

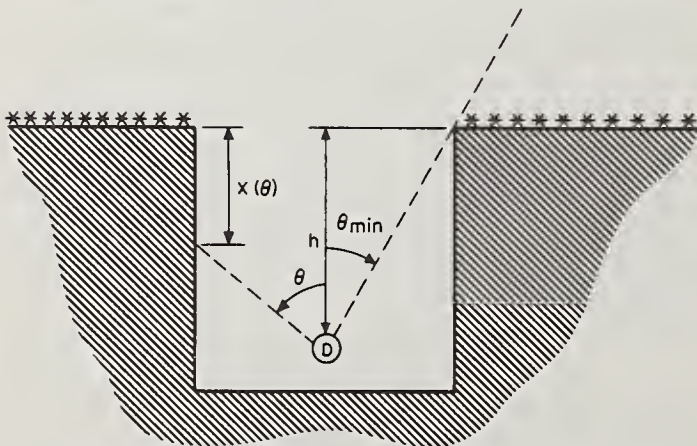The configuration bears a close correspondence to that of figure 28.13b, in which the detector is

FIGURE 31.1. *Detector on the centerline of a cylindrical foxhole.*

in an infinite medium but is sensitive only to radiation incident within an allowed cone. We therefore make estimates of detector response in foxholes by means of the functions $S(d)$ and $S_a(d,\omega)$, which represent infinite medium data relevant to the case sketched in figure 28.13b.

It should be noted that in the foxhole configuration there will be contributions to the detector response due to radiation backscattered from the bottom and sides of the foxhole. This introduces a correction factor of magnitude ~ 1.2. Taking this into account, our expression for the skyshine detector response becomes

$$D/D_0 = 1.2 S(d+\tau) S_a(d+\tau,\omega), \quad (31.1)$$

where d refers to height above ground, τ is the ground roughness coefficient and ω is the solid angle fraction of the aperture as seen from the detector.

Note that foxhole-type problems can occur at great heights as, for example in the case of a skylight in the roof of a tall building. (See Section 35.)

One complicating feature of the foxhole geometry is the possibility that radiation may go directly from fallout near the "lip" of the hole to the detector. Strictly speaking, eq (31.1) applies only if the radiation source has been removed to such a distance from the edge that it cannot penetrate through the earth to the detector.

Attempts have been made to ascertain whether direct radiation from fallout near the lip is significant in comparison with the skyshine radiation. This will certainly depend upon the size of the foxhole. The contribution "through the lip" should increase as foxhole size decreases, with the ratio of lip contribution to total response approaching unity as the foxhole size approaches zero. There should also be effects due to foxhole shape: An elongated foxhole, or one with the edges of the lip rounded off should differ from a cylindrical foxhole, or one with a sharply defined lip. It appears that for the ideal case of a foxhole large enough to hold a man, with vertical walls and a sharp lip, the direct radiation penetrating through the lip is comparable in importance with the skyshine.[30]

Calculations of the lip contribution involve integrals of the type (see fig. 31.1)

$$D/D_0 \approx \int_{-1}^{\cos \theta_{min}} d(\cos \theta) l[X(\theta), \cos \theta], \quad (31.2)$$

which sums the contributions from radiation emerging into the foxhole at various depths (X) below the ground surface, assuming that the directional distribution as a function of depth is not affected by the interface at the foxhole wall. Eq (31.2) applies only to a detector on the centerline of a cylindrical foxhole; but the generalization to other cases is fairly obvious and, in fact, great variations are not expected (a) if the detector is

[30] C. M. Eisenhauer, private communication.

moved off-center or (b) if the foxhole is not cylindrical, so long as the solid angle subtended at the detector by the aperture is held constant.

For most purposes the integral of eq (31.2) can be approximated by writing $d(\cos\theta) = \dfrac{d(\cos\theta)}{dX} dX$

and assigning $\dfrac{d(\cos\theta)}{dX}$ a constant value corresponding to the edge of the lip. This leads to an expression for D_c, dose through the lip:

$$D_c/D_0 \approx \frac{\omega(1-\omega)(2-\omega)}{\rho d} \int_0^\infty dX\, l(X, 1-\omega), \quad (31.3)$$

in which ρ is the density of the ground, $\omega = 1 - \cos\theta_{min}$ is the solid angle fraction of the aperture and d is the depth below the ground surface. Values of the integral in eq (31.3) can be obtained from figure 32.2. Clifford, Carruthers, and Cunningham have very recently reported foxhole experiments [38].

EXAMPLE: Calculate the protection factor provided by a cylindrical foxhole 3 ft in diameter and 4 ft deep at a point on the centerline and 1 ft above the bottom of the foxhole.

The solid angle fraction $\omega = 1 - 3/(3^2 + (3/2)^2)^{\frac{1}{2}} = 0.106$. We obtain the skyshine contribution using this value and $X = 0$ in eq (31.1). From figure 28.3 we obtain $S(0) = 0.098$, and from figure 28.15 we obtain $S_a(0, 0.106) \approx 0.044$. Thus $D/D_0 = 1.2 S(0) S_a(0, 0.106) = 0.0052$.

We calculate the lip contribution assuming that the density of earth is $\rho = 100$ pcf. From figure 32.2 we obtain using $\cos\theta = 1 - 0.106 = 0.894$ the value 13.1 for the integral in eq (31.3). Thus

$$D_c/D_0 = \frac{(0.106)(0.894)(1.894)}{(100)3}(13.1) \approx 0.008.$$

Thus the two contributions are of the same order of magnitude and the total response is given by $D/D_0 \approx 0.013$. *ANSWER.*

32. Shelter Covered with Fallout

Figure 32.1 is a sketch of a typical shelter covered with fallout. A different example of a similar configuration is the blockhouse illustration in figure 20.1, which has fallout on the roof. In both cases the radiation penetrates through the roof slab almost as if the source were imbedded in an infinite medium. The emerging flux and directional distribution both can be well represented by infinite medium calculation, and we make use of the analogy between figure 32.1 and the directional detector illustrated in figure 28.8b. Data for the latter case are employed.

The detector in figure 32.1 is exposed to backscattered radiation and to a total spectrum determined for concrete rather than for air. As in the foxhole configuration one should presumably in-
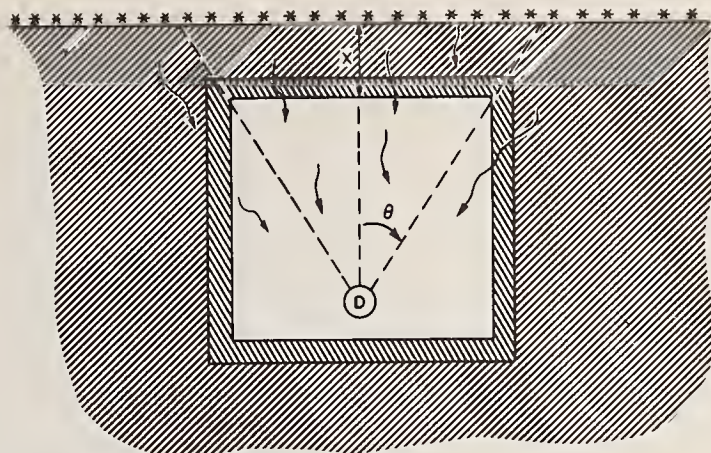

FIGURE 32.1. *Detector on the centerline of a cylindrical fallout shelter.*

clude a backscattering correction (1.15) and a correction (0.9) which takes into account the lack of low energy photons in concrete. These two corrections almost neutralize one another; and since our schematization is not expected to be accurate to 5 percent, we omit them both and write

$$D/D_0 = L(X) L_a(X, \omega), \quad (32.1)$$

where X is the effective mass thickness of the roof slab and ω is the solid angle fraction of the roof as subtended at the detector.

It can be seen in figure 32.1 that radiation can contribute to the detector response by entering through the basement walls rather than through the ceiling. To take account of this one should include a correction very similar to the "foxhole lip" correction discussed in the preceding Section. In fact, almost identically the same argument can be made, and it leads to an expression more general than eq (31.3), namely

$$D_c/D_0 = \frac{\omega(1-\omega)(2-\omega)}{\rho d} \int_X^\infty dX'\, l(X', 1-\omega), \quad (32.2)$$

where $\omega = 1 - \cos\theta$ and d is distance below the roof slab. Values for this integral are to be found in figure 32.2. Fortunately, this correction tends to be relatively small if the slab is moderately thick.

Experiments on structures equivalent to source-covered fallout shelters have been performed by Clarke, Batter, and Kaplan [39].

EXAMPLE 1: Calculate the reduction factor in a cylindrical basement 10 ft in diameter, covered by a roof slab of concrete 1 ft thick, and with the detector positioned on the centerline 9 ft below the roof slab.

For this case, $\omega = 1 - 9/(9^2 + 5^2)^{\frac{1}{2}} = 0.126$. This value of ω, and a value $X = 144$ psf can be inserted into eq (32.1). From figures 28.2b and 28.10, we then obtain $L(144) = 0.0067$ and $L_a(144, 0.126) = 0.257$, so that $D/D_0 = (0.0067)(0.257) = 0.00172$. *ANSWER.*

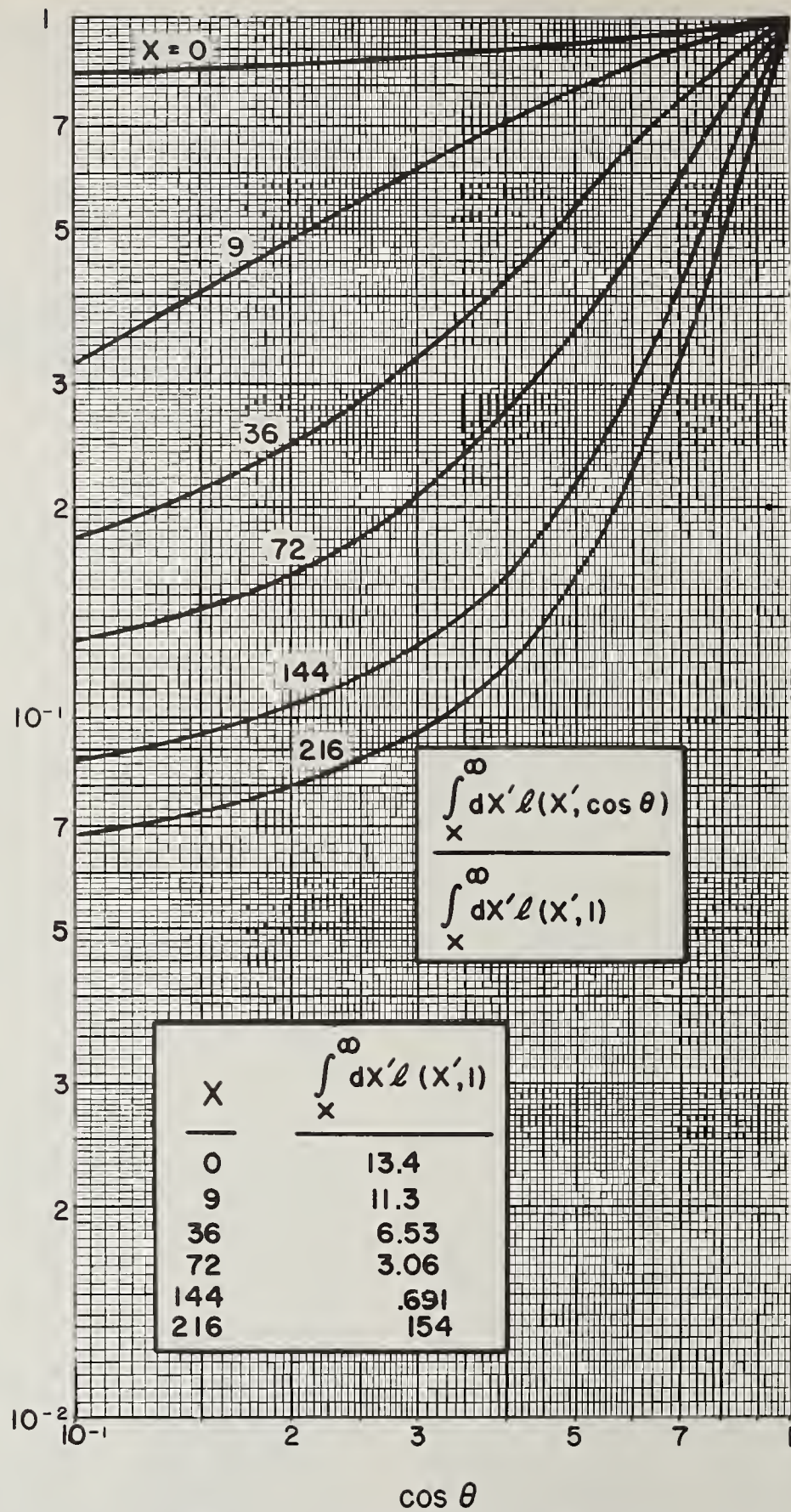It is of interest to calculate the correction due to radiation entering the compartment through

FIGURE 32.2. *Data for calculating "lip penetration" in foxholes and the wall contribution in shelters.* (H_2O, *1.12 hr fission.* *See also figs. B49 and B50.*)

the walls instead of the ceiling. From figure 32.2 we obtain, using $\cos\theta = 1 - 0.126 = 0.874$, the value $(0.69)(0.73) \approx .5$ for the integral in eq (32.2). Thus,

$$D_c/D_0 \approx \frac{(0.874)(0.126)(1.874)}{(144)(9)}(0.5) \approx 0.00008.$$

The correction is about 5 percent.

33. Vertical Walls

The case of a vertical barrier between a detector and a fallout source on the ground is well illustrated by the vertical wall in figure 20.1. Radiation from the source on the ground penetrates upward into the air, so that at different heights about the ground there are directional distributions similar to those given in figure 26.1 for an infinite homogeneous medium. The actual distributions are only "similar" because of modifications due to ground roughness and the perturbing effect of air-wall and air-ground interfaces.

Radiation from fallout penetrates vertical walls with surprising ease. This is because penetration into the wall depends on incident obliquity, i.e., the angle of incidence relative to an axis perpendicular to the wall (and therefore parallel to the source plane). The main feature of the radiation incident on the wall can be appreciated by making a simple approximation. Referring to figure 26.1, note a high concentration of radiation with $\cos\theta \approx 0$, thus travelling nearly parallel to the source plane. Suppose *all* radiation should travel parallel to the source plane, with directions uniformly distributed otherwise. If obliquity angles θ' are measured relative to an axis which is itself parallel to the source plane, the corresponding distribution, $l(d, \cos\theta')$, would be uniform in θ'. In other words,

$$l(d, \cos\theta')d(\cos\theta') \propto d\theta',$$

so that

$$l(d, \cos\theta') \propto \frac{1}{\sin\theta'} \qquad (33.1)$$

This illustrates that near the ground (small d) the actual function $l(d, \cos\theta')$ should have a peak value for θ' near zero. Since decreasing θ' corresponds to increasing penetrability, the consequence is that fallout radiation from the ground and incident upon vertical walls is very penetrating.

For our purposes it seems reasonable to neglect the perturbation in the radiation field due to air-wall and air-ground interfaces, and to take ground roughness into account in the manner indicated by eq (30.3). Thus we apply to this problem the data represented by the function $W(X,d)$; and we write for the detector response at height d above ground and behind a thickness X of wall,

$$D/D_0 = 0.9 W(X, d+\tau). \qquad (33.2)$$

The factor 0.9 corrects for the deficiency of low energy photons when the material adjacent to the detector is concrete rather than air, water, or wood. It should be omitted if the calculated $W(X, d+\tau)$ already assumes a concrete wall. If backscattered photons should make no contribution, the factor should probably be closer to 0.85; but in general backscattering will occur, even for a configuration like the blockhouse of figure 20.1, in which there is no material immediately behind the detector (Position B). Thus the corrective factor 0.9 is to be preferred.

Equation (33.2) does not apply to the detector response some distance behind a wall of limited size. For example, the detector response at B in figure 20.1 due to radiation from the adjacent wall is given by eq (33.2) but the detector response at A due to radiation from the same wall contains a further reduction, as discussed in Section 20. At present we do not have directional distributions for radiation emerging from such a vertical wall, so that at best we can only prescribe rough guesses for this reduction factor.

Various methods can be used to construct functions for estimating the detector response behind a vertical wall. We can, for example, interpolate between $W_a(d, \omega)$, which is reasonably accurate in the limit of zero wall thickness, and $P_a^{(s)}(\infty, \omega)$, which represents an upper limit to the geometry factor in the limit of very thick walls. To accomplish this we assume that radiation not scattered in the walls contributes according to the thin-wall function, while radiation scattered in the walls contributes according to the thick-wall function. Assuming the proportion of unscattered gamma rays to be given roughly by the ratio $P^{(o)}(X)/P(X)$, which we designate $b(X)$, we arrive at a function W_{a1} defined by

$$W_{a1}(X, d, \omega) = b(X) W_a(d, \omega) \\ + 1.15[1 - b(X)]P_a^{(s)}(\infty, \omega). \qquad (33.3)$$

The factor (1.15) in this expression is to normalize $P_a^{(s)}$ to unity at $\omega = 1$, to make it comparable with W_a.

According to figure 28.16, the function $P_a^{(s)}(d, \omega)$ varies slowly with d (or X); and we use the bottom curve (for $d = 1000$ ft) to represent $P_a^{(s)}(\infty, \omega)$ in calculations of W_{a1} without expecting to introduce errors more serious than those inherent in eq (33.3). In general, eq (33.3) is expected to give conservative estimates of the geometry reduction factor because $P_a^{(s)}$ overestimates the factors expected for thick walls.

Using eq (33.3) in lieu of a better estimate of the wall geometry factors, we represent the detector response in the form

$$D/D_0 = 0.9 W(X, d+\tau) W_{a1}(X, d+\tau, \omega), \qquad (33.4)$$

where d and X are height above the ground and wall thickness, respectively, and ω is the solid angle fraction subtended at the detector by the wall, and the factor 0.9 estimates the correction

of H_2O wall data to concrete wall data. Equation (33.4) is intended to apply only to walls nearly circular (or square), with the detector opposite the center of such a wall. It may certainly be greatly in error if applied indiscriminately to eccentric wall shapes and to off-center detector locations. (Note that a correction for backscattering has been included implicitly.)

EXAMPLE 1: How thick must a vertical wall be to reduce the detector response immediately behind the wall to $0.001D_0$, if the front of the wall faces a fallout field 6 ft below the detector and having a ground roughness coefficient $\tau = 40$ ft?

Making use of eq (33.2), we examine figure 28.7 to find that value of X for which $W(X,46 \text{ ft}) = 0.001/0.9$. This value turns out to be approximately $X = 238$ psf, which is just under 20 in. of concrete. *ANSWER.*

EXAMPLE 2: If the wall of the preceding example is square, 12 ft on a side, and if the detector is 12 ft behind the wall, opposite its center, what wall thickness would be required to reduce the detector response to $0.001D_0$?

This calculation is considerably more complicated. To begin with, it is necessary to calculate the solid angle fraction subtended by the wall at the detector. This can be most easily done by the method to be outlined in Section 41; but it could also be done by replacing the square with a circle having the same area. Using the method of Section 41, we note that for squares, $\epsilon = 1$, and for a distance from the square equal to the length of a side, $\eta = 2$. From figure 41.2 we then read off the value $\omega = .13$. Inserting this value, together with the value $(d+\tau) = 46$ into eq (33.4), we select several values of X which we expect to bracket the desired value, namely $X = 144$, 192, and 240. For these values we obtain from figures 28.6, 28.7, 28.12, and 28.16 the following information:

X	$b(X)$	$W_a(46',.13)$	$P_a{}^{(s)}(\infty,.13)$	$W_{a1}(X,46',.13)$	$W(X,46')$	D/D_0
144	0.182	0.18	0.46	0.47	0.0085	0.0040
192	.152	.18	.46	.48	.003	.0014
240	.127	.18	.46	.49	.00105	.00051

Plotting these values for D/D_0 on double-log paper we find by interpolation that $D/D_0 = 0.001$ for $X \approx 207$ psf, corresponding to about 17 in. of concrete. *ANSWER*

34. Light Superstructure with Shielded Basement

Figure 34.1 is a sketch of a structure which is similar to the blockhouse of figure 20.1 except that walls and roof are thin and the configuration includes a shielded basement. Our primary interest is in the detector response in the basement; and radiation penetrating into the basement may have originated either at the roof or on the surrounding contaminated ground.

Because the roof is thin it is no obstacle to radiation. Therefore the floor slab protecting the basement is subjected to a beam of gamma rays from the roof; and this radiation is incident on the floor slab along lines intercepting some part of the roof. Penetration through the floor slab proceeds as if there were a source located at the slab which could emit gamma rays only in directions corresponding to the directions of travel of radiation from the roof. Moreover, the cone of incident directions doesn't change significantly within a few feet of any point on the floor slab. For these reasons we consider the actual configuration to be in close correspondence with the infinite medium arrangement of figure 28.8c, and we estimate the detector response by means of data from figure 28.11. If we include a factor 0.9 to account for suppression of low energy components in concrete as compared with water or air when the $L(X)$ data is for penetration in water, the detector response (roof contribution only) is obtained from

$$D/D_0 = 0.9 L(X) L_b(X,\omega). \qquad (34.1)$$

Here ω is the solid angle fraction of the roof as seen from the opposite point on the other side of the barrier from the detector, as shown in figure 34.1.

In figure 34.1 it is clear that lowering the detector from its position adjacent to the slab will not change much the response to radiation from the roof because the floor slab will still subtend a large solid angle fraction. But it is easy to visualize configurations of this general type in which the detector response is sensitive to the distance from the barrier. (As a simple example one need only reduce the length and width of the structure pictured in figure 34.1 while keeping the height constant.) One may wish to include another factor in the expressions for D/D_0 to account for this variation:

$$D/D_0 = L(X) L_b(X,\omega) L_a(X,\omega'), \text{ or } \quad (34.2a)$$

$$= L(X) L_b(X,\omega) P_a(X,\omega'), \qquad (34.2b)$$

depending on whether ω is nearly unity eq (34.2a) or much smaller eq (34.2b). Here, ω' is the solid angle fraction of the protecting floor slab as subtended at the detector. The factor 0.9, which corrects the data to concrete, has been omitted from expressions eq (34.2) because backscattered radiation has been omitted altogether through the special normalization used for L_a and P_a; this backscattered radiation gives an increase of about a factor 1.15, thus slightly more than canceling the 0.9 factor. If data for concrete is used, a backscattering factor is appropriate.

The second part of this problem has to do with radiation which originates at the ground and penetrates "in and down." This is much more difficult to analyze. We proceed by trying to account for major factors one by one: If the heavy protecting floor slab were absent the problem would reduce
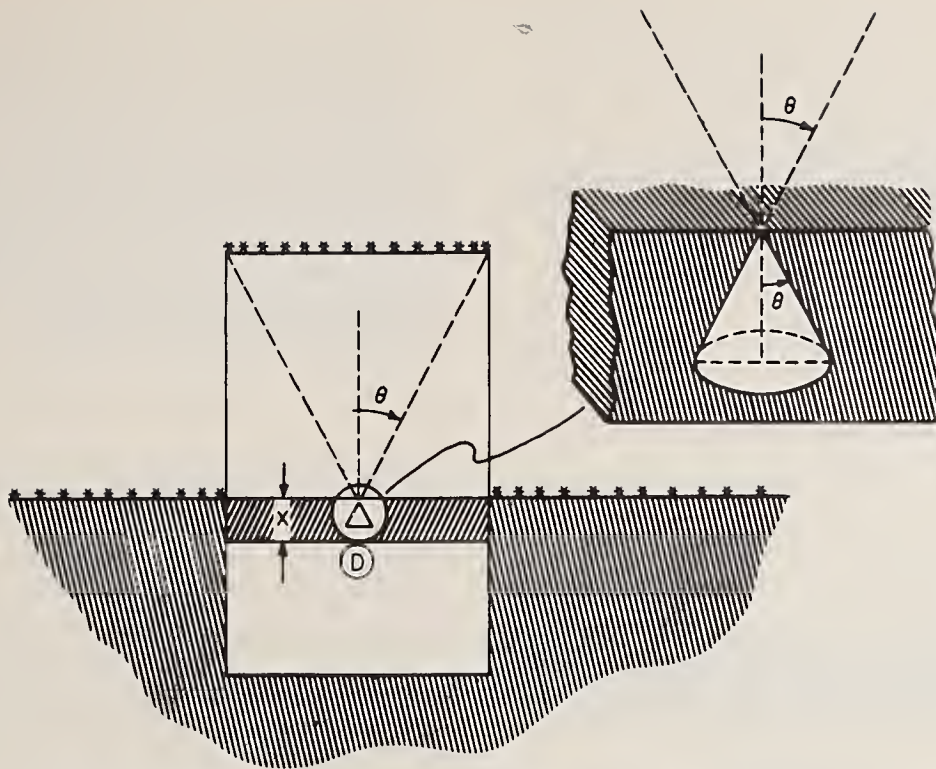
FIGURE 34.1. *Fallout on and around a light cylindrical superstructure covering a shelter. The radiation incident on the barrier slab is largely confined to a cone of aperture θ.*

to a fox-hole problem and the detector response would be given by an expression like eq (31.1). The floor slab introduces an extra attenuation, and the real problem is to estimate this attenuation as a function of slab thickness X. To this end we note that radiation from ground contamination must be scattered downwards to be incident on the floor slab, and that such incident radiation is not greatly affected by the clear area covered by the superstructure, for structures of average size. Therefore, we expect this radiation to resemble the skyshine both in intensity and directional distribution. This suggests use of the function $S'(X)$ to estimate the reduction of the detector response below that expected for a foxhole geometry with no floor slab (see Section 28, paragraph (3), and fig. 28.1c):

$$D/D_0 = S(d+\tau)S_a(d+\tau,\omega)S'(X), \qquad (34.3)$$

where d, τ, and ω all have the interpretations of the foxhole configuration.

Use of the function S_a in eq (34.3) is justifiable if the floor slab does not greatly modify the skyshine directional distribution, i.e., if the floor slab is thin. If X is substantial and ω isn't small, it would be better to omit this factor.

EXAMPLE 1: Consider a light, cylindrical superstructure rising 25 ft above ground level, and having a diameter of 35 ft. Underneath this superstructure there is a basement of depth 10 ft, as shown in figure 34.2. Calculate the protection factor at the center of the basement floor with and without a 6 in. first-floor slab ($X=72$ psf). Assume a ground roughness coefficient $\tau=40$ ft.
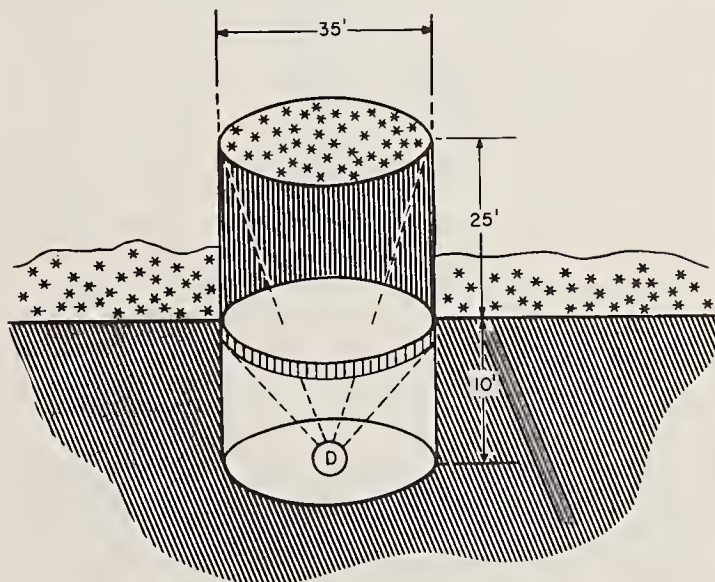
FIGURE 34.2. *Light superstructure geometry of Example 1.*

First we calculate the roof contribution for the two cases, using $\omega=1-25/\sqrt{(25)^2+(17.5)^2}=0.181$ and $\omega'=1-10/\sqrt{(10)^2+(17.5)^2}=0.504$, together with $X=72$ for the case with floor slab, and using $\omega=1-35/\sqrt{(35)^2+(17.5)^2}=0.106$, $\omega'=1$, and $X=0$ for the case without a floor slab. From figure 28.20 we obtain $L(0)L_b(0,0.106)=0.023$ and $L(72)L_b(72,0.181)=0.0125$. Using eq (34.2b) for both cases we must next determine appropriate values of $P_a(X,\omega)$: We note that $P_a(0,1)=1$, and that according to eq (28.4), $P_a(72,0.504)=(0.166)^{-1}[0.049+0.118(0.71)]=.8$. Therefore, the roof contribution turns out to be

61

No floor slab: $D/D_0 = (0.023)1 = 0.023,$

6 in. floor slab: $D/D_0 = (0.0125)(0.8) = 0.010.$

Next we perform the "foxhole" type calculation of eq (34.3). The values $S(40 \text{ ft}) = 0.068$, $S_a(40 \text{ ft}, 0.504) = 0.29$, and $S'(72) = 0.027$ give

No floor slab: $D/D_0 = (0.068)(0.29) = 0.020,$

6 in. floor slab: $D/D_0 = (0.068)$
$$(0.29)(0.027) = 0.00054.$$

Combining the two contributions, we obtain

No floor slab: $P = D_0/D = (0.023 + 0.020)^{-1} = 23,$

6 in. floor slab: $P = D_0/D = (0.010 + 0.00054)^{-1}$
$$= 95. \quad ANSWER.$$

Note (a) that the floor slab is most effective against radiation from the ground, and (b) that in the absence of the floor slab approximately half the detector response is from the ground component.

35. Apertures

The analogy between gamma rays and visible light may be used to clarify the effect of openings upon the detector response within a structure. Just as doors and windows permit light to enter a room from outside, according to their size and location, so also do doors and windows permit radiation to enter when fallout covers the surrounding ground. In one respect this analogy breaks down, however: Radiation from fallout can penetrate through opaque walls, so that if thin they may be almost as transparent to radiation as windows. In this case the size and location of windows makes very little difference.

This illustrates that there is a connection between effective mass thickness of a barrier and the permissible design of openings in the barrier from the point of view of radiation protection. When radiation enters a structure mostly through windows, the advantages of heavy walls are negated; and conversely, if the walls are very thin the window design matters little.

Openings of many different types occur normally in construction, and there doesn't exist much information, either experimental or theoretical, about aperture effects. Nevertheless, some general rules can be given for estimating their contribution to the detector response. In this section we discuss briefly openings in walls and roof; and we distinguish between two different cases: Apertures between source and detector, and apertures not between source and detector.

Figure 35.1 is a sketch of circular windows in a blockhouse wall and ceiling, with the detector placed opposite the center of each. In both cases the window represents a type of surface which differs from the main wall or ceiling in that the

effective mass thickness is nearly zero and the solid angle fraction subtended at the detector is apt to be small.

In the skylight case the detector will receive a contribution due to skyshine in addition to a contribution from fallout on the skylight. The relative sizes of these two contributions is of some interest. For purposes of determining the skyshine contribution the skylight can be viewed as a special type of foxhole, so that the detector response is given essentially by eq (31.1):

$$D/D_0 = S(d)S_a(d, \omega), \quad (35.1)$$

where d is the height above the surrounding ground and ω is the solid angle fraction of the skylight subtended at the detector. Equation (35.1) applies only for very small or zero effective mass thickness of window. If there is a covering of fallout on the skylight, its contribution *plus* the skyshine contribution can be estimated by viewing the configuration as an example of a fallout-covered shelter and applying the arguments leading to eq (32.1):

$$D/D_0 = L(X)L_a(X, \omega). \quad (35.2)$$

Here ω is again the solid angle fraction subtended by the skylight at the detector, and X, the effective mass thickness of the window, is very small.[31]

The case of a window in a vertical wall bears a close relation to the directionally dependent detector pictured in figure 28.8d. Radiation at the window entrance (fig. 35.1) should have a directional distribution much like that above an infinite plane source in an infinite medium, if we consider only gamma rays traveling towards the window. The detector behind the window in figure 35.1 "sees" only that part of the radiation field at the opening which travels in an "allowed" cone of directions, very much in the manner of the detector in figure 28.8d. We therefore apply the data obtained using eq (27.11) to obtain the detector response to radiation passing through the window, just as in the case of a thin vertical wall (eq (33.4)):

$$D/D_0 \approx 0.9 W(X, d)W_a(d, \omega) \quad (35.3)$$

where d is the height of the window above ground, ω is the solid angle fraction of the window subtended at the detector, and X is the window thickness, which is presumed to be small or zero. Note that it may be desirable to take account of ground roughness by increasing the value of d, and that the factor 0.9 is to be omitted if the $W(X,d)$ data is for a concrete wall.

Figure 35.2 shows openings in partitions which lie *between* the source and the detector. Radiation entering through these openings can reach the

---

[31] Backscattering has been omitted in both eqs 35.1 and 35.2. Strictly speaking a factor 1.15 should be incorporated in eq 35.2 and a factor perhaps as big as 1.3 in eq 35.1. The latter is larger because the radiation is lower in energy. Note, however, that if H_2O data is used a factor of 0.9 or so is also needed.
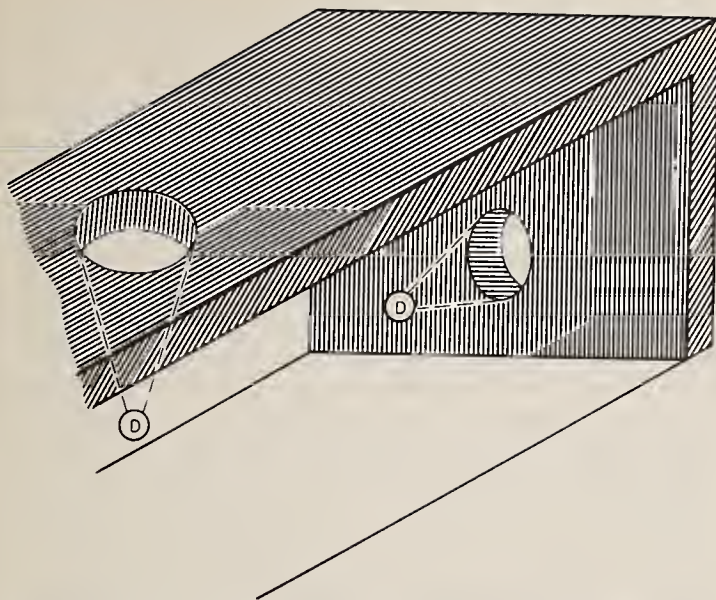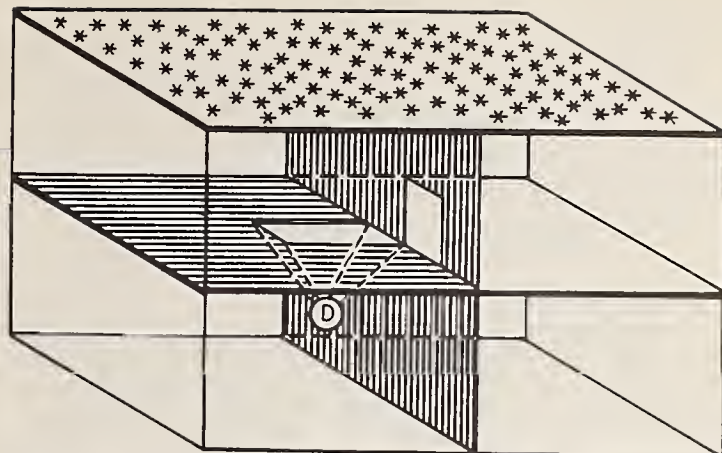
FIGURE 35.1. *Apertures in a blockhouse wall and roof.*

FIGURE 35.2. *Apertures directly between source and detector.*

FIGURE 35.3. *Apertures not directly between source and detector.*

detector without penetrating as much material as radiation which passes through the partitions to the detector. If the partitions are very light, one can probably take the openings into account by assigning an average value to the effective mass thickness between source and detector. On the other hand, the partitions may be thick, so that radiation penetrating through the partitions is significantly reduced in comparison with that passing through an opening. In this case the opening can be considered as giving a separate term (D_t) in eq (20.1), in which term the effective mass thickness between source and detector is given a value equal to the combined thickness of partitions between source and detector along lines through the opening, and the solid angle fraction is that subtended at the detector by the opening. If more than one opening lies between source and detector, additional terms may be required, each involving effective mass thickness and solid angle fraction determined by overlapping or non-overlapping parts of these openings.[32]

Figure 35.3 shows an example of openings which are not between source and detector. If the partitions are heavy, the presence of these openings can be expected to modify the detector response significantly. For example, the floor opening permits a substantial increase in the strength of the radiation field directly below, while the wall opening gives ready access laterally to the detector.

Notice that the radiation must turn the corner in order to take advantage of these openings, so that a scattering must occur at some position which is favored in the sense of being below the floor openings and (or) in front of the wall opening. This is actually a "maze" problem, and is quite different from the case of openings which permit radiation to travel directly from source to detector.

Methods for treating this case are essentially those used in maze problems, which are discussed in Section 38.

EXAMPLE: A radiation detector is at the center of a cubical blockhouse of side length 10 ft, and with very heavy walls. Small, circular windows of equal radius are placed in the center of the roof and one wall. Compare the contributions to the detector response from skyshine and direct radiation through the roof window and from radiation through the window in the wall.

For definiteness assume $X \approx 0$ and $\omega = 0.05$. We then obtain the following:

Figures

Roof, skyshine: $D/D_0 = S(10\text{ft})S_a(10\text{ft}, 0.05)$
$= (0.084)(0.021) = 0.0018$ *28.3, 28.15*

Roof, direct: $D/D_0 = \lim_{X \to 0} L(X)L_a(X, 0.05)$
$= 0.014$ *28.19*

Wall: $D/D_0 = W(0, 5\text{ft})W_a(5\text{ft}, 0.05)$
$= (0.45)(0.125) = 0.056$.   *28.7, 28.12*

---

[32] We say here that the openings "overlap" when a straight line from source to detector can pass through more than one opening.

From this we see that $0.056/(0.056+0.014+0.002)$ $=0.78$ of the detector response is from the window in the wall, and that of the remainder only about 11 percent is due to skyshine. *ANSWER.*

Note that backscattering corrections would change these figures somewhat.

36. Compartmentalization

From the point of view of radiation shielding, the single most prominent characteristic of ordinary buildings might be termed compartmentalization. Most of the mass of the building which may be expected to act as a radiation shield is concentrated in the floors and walls, which divide the building into compartments.

Consider a multi-story building, as schematized in figure 36.1, with fallout on the roof and on the surrounding ground. Radiation from the roof fallout penetrates the building traveling downwards. As this radiation penetrates deeper into the building, it *must* pass through successive layers of material, namely the floors. On the other hand, depending on the trajectory, the radiation *may or may not* pass through the walls. Thus the floors represent a sort of divided shield, while the walls act as a collimator which favors some trajectories over others.

Notice that the same effects are present also in the case of radiation originating on the ground around the building. As this radiation penetrates into the building it *must* pass through a set of walls. But the floors and the other set of walls
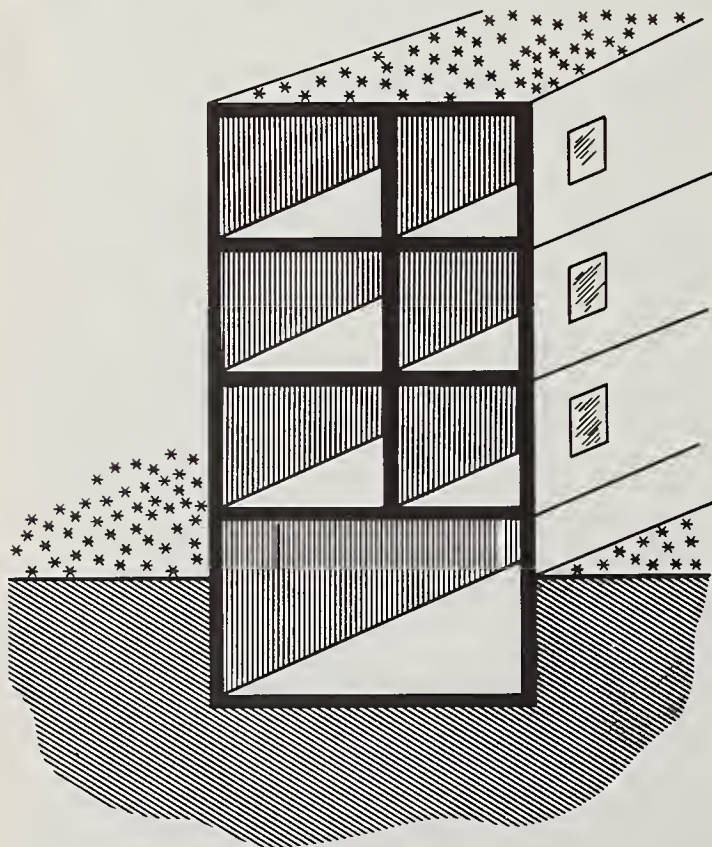
are so oriented that the radiation may miss them altogether if it follows an appropriate trajectory. Thus one set of walls forms a divided barrier while the other partitions lie more or less parallel to the direction of penetration and give advantage to radiation traveling directly inwards.

In addition to the compartmentalization of buildings into rooms and corridors, many or even most types of wall and floor construction involve compartmentalization on a smaller scale, because of voids introduced to reduce weight. The most obvious examples are hollow concrete blocks, hollow tile, and hollow bricks. Another example of slightly different type is that of floor joists, which have the effect of collimation on the downward-penetrating radiation. Such compartmentalization can cause overestimation of the protection afforded by a wall.

The simplest way to take account of compartmentalization in building materials is that of using approximations based on a more uniform distribution of material. For example, in the case of compartmentalized walls one might estimate the effective mass thickness by using weight/volume ratios, thus assuming the material in the wall to be spread uniformly through its volume. Experiments tend to confirm that such estimates are accurate enough for most purposes, largely because the barriers so constructed are usually rather light-weight. The effective mass thicknesses given in Table 22.2 were obtained from weight-volume ratios.

Approximations in which the material is assumed to be uniformly distributed can also be used in large, multi-room structures, depending on partition thicknesses. The method is essentially the same as for a single compartmentalized wall: One calculates the total mass of material between detector and roof, say, and assumes it to be distributed uniformly between. The accuracy of such a simple approximation depends primarily on the partition thicknesses. In general, one expects it to be accurate when the partitions do not individually reduce the radiation intensity by as much as a factor of $e \approx 2.7$. From figure 28.2b we find that this means partitions of less than about 40 psf effective mass thickness. It should be remembered, however, that such a limit is, for the present, more of a guess than an accurately known figure; and that it depends very much on the configuration, as will be indicated more clearly in the next Section in the discussion of other simple types of approximate calculations for compartmentalized structures.

37. Collimation and Divided Barrier Effects in Compartmentalized Structures

In a more detailed analysis of compartmentalization, it is advantageous to consider collimation and divided barrier effects separately, since they are quite different, even though they depend on the existence of particular directions of interest, such as "downward" and "inward." In this

FIGURE 36.1. *Multistory, compartmentalized structure with fallout on roof and ground.*

Section we make the distinction by giving separate consideration to partitions placed "parallel" and "perpendicular" to the direction of interest. (We include floors when we speak of "partitions.")

(1) Partitions perpendicular to the direction of penetration: When a barrier is divided into layers through which radiation must penetrate successively, the mass distribution can usually be expected to affect the detector response. But there is one case in which this is not so. When layers of material and a plane source do not terminate, but extend unchanged over the whole plane, as indicated in Section 30, the dose measured by a detector is independent of the particular manner in which the division into layers takes place, or even the existence of a layered structure, so long as the total effective mass thickness between source and detector remains fixed.

When the radiation source is finite in extent, or non-uniformly distributed, the nature of the layering must be taken into account. We consider three extreme cases, namely (a) the total barrier mass confined to a layer adjacent to the source; (b) the total barrier mass confined to a layer adjacent to the detector, and (c) the barrier material spread uniformly between source and detector. Other situations can arise which are combinations, or which can be expected to lie somewhere between the extremes just indicated. For example, the mass may be concentrated in a layer half-way between source and detector, or it may be divided into two layers, one adjacent to the source and one adjacent to the detector.

When the total barrier mass is confined to a layer adjacent to the source, one has essentially the fallout-covered shelter discussed in Section 32; and the analysis utilizes data for $L_a(X,\omega)$.

Cases in which the total barrier mass is confined to a layer adjacent to the detector have already been discussed in Section 34. They correspond to a radiation source emitting only within a restricted cone of directions, so that calculations for this configuration utilize data for $L_b(X,\omega)$.

Distributed barriers have been discussed in Section 30. The finite source cases of interest utilize data for the $L_c(X,\omega)$.

Very general arguments indicate that the detector readings in these three cases shouldn't differ greatly, a factor of two usually being sufficient to encompass the spread of values. This is essentially because the barrier and geometry reduction factors account for the large part of the barrier effectiveness, and these do not change significantly from one mass distribution to another. Therefore, these three extreme cases can be used in representing the different cases of layering in practical problems. We do not expect a slight mismatch of schematization and configuration to result in significant errors.

Notice that if the barrier is finite, as in figure 37.1, radiation can escape out the sides, lowering the observed dose and giving a slight increase to the barrier effectiveness.

(2) Partitions parallel to the direction of pene-
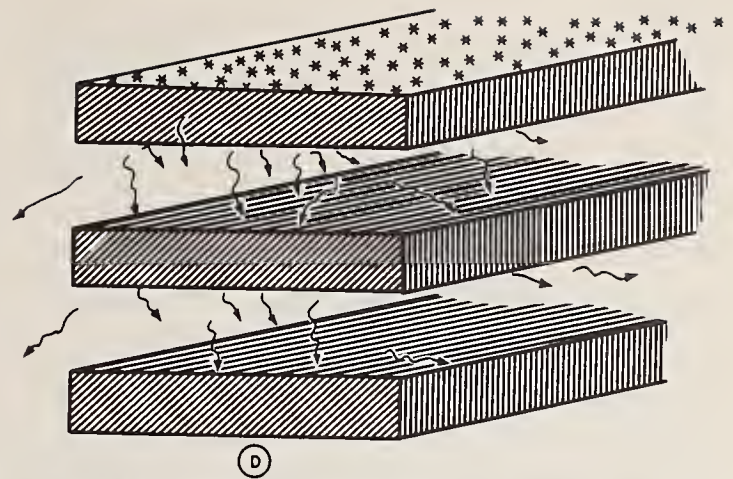
FIGURE 37.1. *Fallout on a finite divided barrier.*
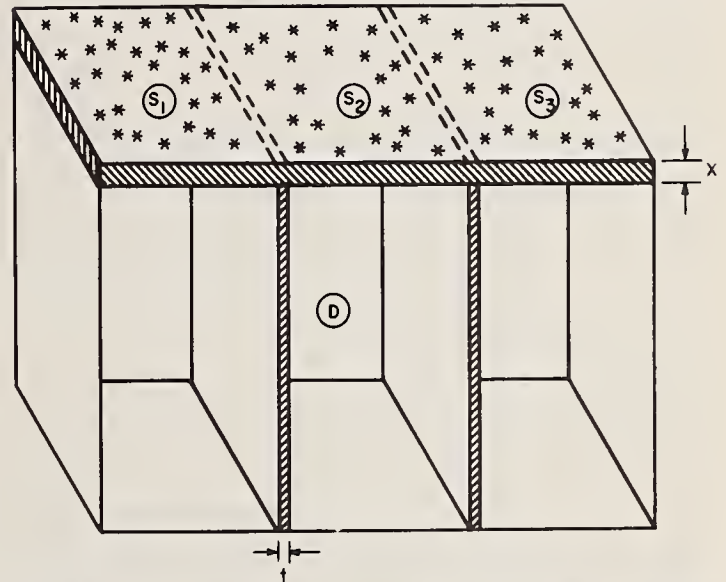
FIGURE 37.2. *Fallout on a simple structure with parallel partitions.*

tration: Collimation effects are more difficult to estimate than divided barrier effects. At present neither experimental nor theoretical studies are available. The discussion given here is mainly confined to limiting cases and is therefore incomplete even though indicating the nature of some of the main effects.

In the compartmentalized structure of figure 36.1, consider penetration by radiation from fallout on the roof. It is clear that collimation effects will depend on wall thickness, floor thickness, wall spacing and the distance of the detector from the source in terms of the number of compartments. Various limiting cases can be considered:

(1) The walls may be very thick, so that radiation can hardly penetrate into adjacent compartments. In this case the detector sees mainly radiation which has not penetrated through the walls, and the problem reduces to one of the divided barrier problems with a finite source.

(2) The floors may be very thick: In this case the radiation only penetrates through the floors if it travels always in a nearly vertical direction. This is because radiation traveling at a substantial obliquity has slight chance of getting through the

65

barrier, except when the oblique portion of the trajectory occurs near the exit surface of the barrier. The very thickness of the floors provides a sort of collimation in this way. It is possible, though very unlikely, for this type of collimation to be stronger than that provided by the walls, so that it doesn't matter when the walls are present.

(3) The walls may be thin, so that radiation readily travels from one "channel" to the next. In this case the collimation effect is slight unless the radiation can penetrate to distances large compared with the "channel width."

The most difficult cases concern walls and floors which are neither thick nor thin. It may be possible in such cases to justify the approximation in which all material between source and detector is distributed uniformly throughout the intervening space. But this approximation can lead to an overestimate of the shielding provided by the compartment partitions. A safer estimate can be obtained as follows: If the radiation cannot travel from source to detector without passing through parallel partitions, the total effective mass thickness of these parallel partitions is added to that of the perpendicular partitions; and the detector response is determined with this augmented barrier thickness.

To apply this rule the primary radiation source is divided into components according to the number and type of parallel partitions which must be penetrated, as shown in figure 37.2. Radiation from that part of the source directly above the detector is not shielded by parallel partitions; whereas radiation originating far to one side of the detector may have to go through several partitions to contribute to the detector response. The detector response for the simple case pictured in figure 37.2 would thus be estimated by

$$D = L(X+t)L_a(X+t,\omega_1) + L(X)L_a(X,\omega_2) \\ + L(X+t)L_a(X+t,\omega_3), \quad (37.1)$$

where ω_1, ω_2, ω_3 are the solid angle fractions subtended by S_1, S_2, S_3 at the detector.

Notice that even when the radiation might be expected to penetrate parallel partitions at a slant angle we do not use the slant penetration thickness, but rather the normal thickness of these partitions in equation (37.1). There are several reasons for this, but the weightiest is our desire not to over-estimate the protection factor seriously. We are treating parallel portions as if they were part of the divided barrier, and this procedure under-estimates their effect somewhat.

This approach to the parallel partition shielding increases the amount of calculation necessary because each component requires a separate calculation.

38. Mazes

Figure 38.1 shows an elementary maze. To pass from source to detector the radiation must follow openings, because the barrier is much too
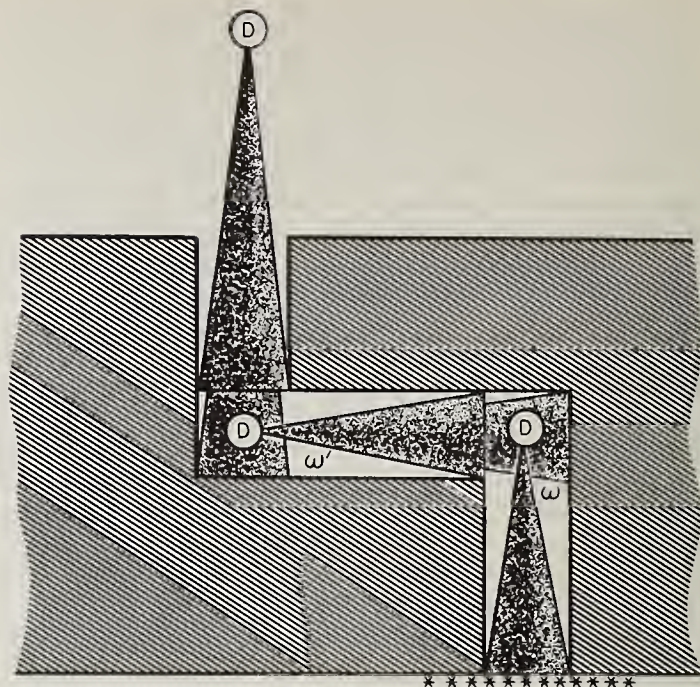
FIGURE 38.1. *A simple maze with two 90° bends. The solid angle fractions ω' and ω are subtended at the detector by the near and far sides of the bend.*

thick to permit "shortcuts." At least two changes of direction are necessary for the gamma rays contributing to the detector response in this example.

Radiation readily passes down the initial passageway leading from the source. The intensity of the radiation diminishes steadily with distance from the source, maintaining a rough proportionality with the solid angle fraction which the source subtends at the detector.[33] At the end of the first passageway, as at positions all along, the detector response is partially due to scattered gamma rays, though mostly to gamma rays coming directly from the source. Once the corner has been turned, direct radiation can no longer reach the detector in significant amounts, and the detector response is due to scattered radiation almost entirely.

It is possible to examine this scattered radiation to determine where it "turned the corner." This leads to the conclusion that the wall surface at the corner which can "see" both source and detector contributes a substantial fraction of the scattered gamma rays which go down the second corridor. It follows that maze shielding can be enhanced somewhat by removing or recessing these scattering areas so that they no longer have access to both source and detector, or by covering the walls at the corner with a layer of tin or lead sufficiently thick to reduce the albedo considerably.

Experiments now in progress are leading to a further analysis of radiation "turning the corner" into contributions from individual wall surfaces, and a report on this subject by J. C. Le Doux

---

[33] This dependence upon solid angle would not hold for an anisotropic source. In an extreme case, for a plane-parallel source, the detector response is independent of the length of the first corridor.

and A. Chilton is to be published.[34] The results are by no means simple. Apparently three different components are distinguishable: (1) Radiation scattering from ceiling, floor, and the end wall of the first corridor; (2) radiation scattering from the end wall of the second corridor, i.e. the side wall of the first corridor; and (3) radiation "cutting the corner." Wall positions contributing to each component can be seen using figure 38.1. As the detector is moved down the second corridor, each component is expected to be reduced in strength according to the solid angle fraction subtended by the scattering surface at the detector. This means that components (1) and (3) vary inversely with the *cube* of the distance and component (2) with the *square* of the distance of the detector from the corner. On the other hand, components (1) and (2) do not depend on the absolute dimensions of the maze, while component (3) decreases in inverse proportion to the magnitude of an increase of scale. That is, if the maze size is doubled without change in shape, and with the detector in the same relative position, the third component will contribute only half as much to the detector response at the corresponding position in the larger maze, but the other two components are unaffected. The third component is very important for small mazes and ducts, but relatively unimportant for large mazes.

This type of analysis suggests a simple expression for representing the detector response in mazes, namely

TABLE 38.1. *Albedo coefficients A_1, B_1 for mazes with a long first corridor and large, square cross section. ω_0' is the solid angle of the entrance as subtended at the first bend.*

ω_0'	A_1	B_1
0.007	0.056	0.08
.063	.04	.19
.165	.054	.27

$$\frac{D}{D_0}=\frac{D_1}{D_0}\prod_{i=1}^{N}[(A_i\omega_i+B_i(\omega'_i-\omega_i)] \qquad (38.1)$$

in a maze with N bends, where ω_i,ω'_i are the solid angle fractions subtended by the far and near ends, respectively, of the i'th corner at the $(i+1)$'st corner on the detector; and D_1 is the detector response at the midpoint of the first corner. (See fig. 38.1. Note that ω_0 is taken to be 0.) The two terms represent the r^{-2} and r^{-3} components mentioned in the preceding paragraph, and A_i, B_i can be considered effective albedos for these two components. Experiments with single bend mazes, using Co–60 and a long first corridor, give estimates of A_1, B_1 as listed in Table 38.1.[35] Corresponding estimates for later bends are not available, but for a safe overestimate the values $A_i=1$, $B_i=0$, $i>1$, can be used. A closer estimate for $i>1$ might be $A_i=\dfrac{A_1}{A_1+B_1}$, $B_i=\dfrac{B_1}{A_1+B_1}$, which relies on the assumption that $(A_i/B_i)=(A_1/B_1)$.

VII. Rectangular Source Shapes

39. Introduction

Most of the surfaces of interest in radiation shielding are rectangular or representable by rectangles. On the other hand, it is much easier to generate data for circular surface shapes, with the detector opposite the center of the circle; and many, even most, calculations can be carried out with acceptable accuracy by applying circular-shape-data to rectangular-shape-walls. Therefore, in this and the following sections we discuss methods for doing this. In the last section we consider the problem of rectangular-source-data more generally.

The use of circular-source-data to obtain the detector response to a rectangular-shape-source involves several steps and a number of simple types of calculations, which we list below:

(1) Calculation of the solid angle fraction of circular sectors;

(2) determination of the solid angle fraction subtended by any rectangle at a point on the central axis of symmetry ("centered rectangle" case;)

(3) determination of the solid angle fraction subtended by any rectangle at *any* point, in terms of a linear combination of the simpler "centered rectangle" cases;

(4) approximation of a "centered rectangle" by circles or circular sectors, so that the approximation has the same solid angle fraction and perhaps the same "elongation" as the rectangle;

(5) determination of geometry factors for circular sectors. It is not difficult to see how these different types of calculations can be combined into a fairly accurate procedure for utilizing the circular data: We represent the general rectangle case first as a combination of "centered rectangles" and then, by representing each "centered rectangle" as a combination of circular sectors, we obtain the general case as a combination of circular sectors. Then we calculate the geometry factor for each circular sector independently and combine these results to obtain a value for the rectangle.

40. Solid Angle Calculations for Circles and Annular Sectors

The solid angle fraction ω subtended by a circular or annular sector is easy to calculate if the

[34] Private communications from J. C. Le Doux to C. M. Eisenhauer. Added Note: Very recent publications on this subject are: C. M. Eisenhauer, Scattering of Co–60 Gamma Radiation in Air Ducts, NBS Tech. Note 74 (PB161575), Oct. 1960 (Office of Technical Services, U.S. Dept. of Commerce), C. W. Terrell, A. J. Jeris, R. O. Lyday, D. Sperber, Radiation Streaming in Shelter Entranceways, ARF–1188-12, Oct. 1960 (Armour Research Foundation, Chicago, Ill.).

[35] Private communication from C. M. Eisenhauer, based on analysis of the data of Terrell, et al., of the preceding footnote and as yet unpublished data due to F. X. Rizzo and A. Quadrado, Brookhaven National Laboratory.
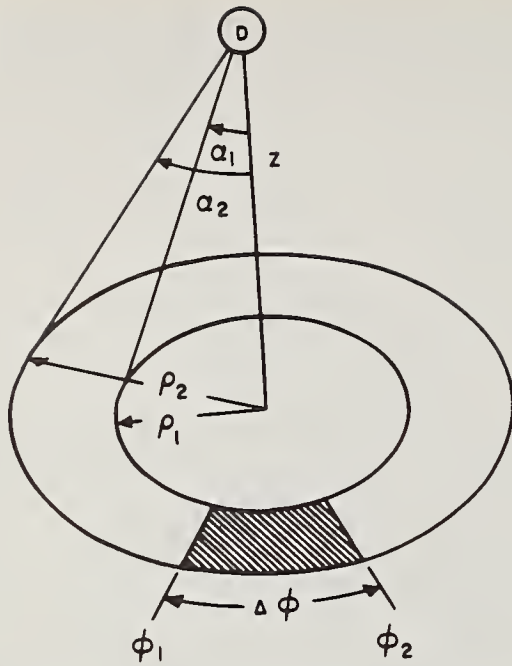
FIGURE 40.1. *Coordinates describing circles and circular sectors for calculations of the solid angle fraction subtended at detector D.*

reference point is on the axis (see fig. 40.1). This is the only case we consider here.

If ρ is the radius of a *circular* area, z the distance of the reference point from the sufrace plane, and $\cos \alpha = z/\sqrt{z^2+\rho^2}$, then

$$\omega = 1 - \cos \alpha. \qquad (40.1)$$

If two concentric circles have radii ρ_1 and ρ_2 and subtend solid angle fractions ω_1 and ω_2, then the solid angle fraction of the *annulus* between the circles is (for $\omega_2 > \omega_1$)

$$\omega = \omega_2 - \omega_1 = \cos \alpha_1 - \cos \alpha_2. \qquad (40.2)$$

Similarly, the solid angle fraction of the *annular sector* between circles of radii ρ_1 and ρ_2, and between azimuths φ_1 and φ_2, is $(\rho_2 > \rho_1)$

$$\omega = m(\omega_2 - \omega_1), \qquad (40.3)$$

where m is the fraction of the azimuth occupied by the sector, i.e.,

$$m = \frac{1}{2\pi} (\varphi_2 - \varphi_1). \qquad (40.4)$$

EXAMPLE: Calculate the solid angle fraction subtended by a 30° sector of the annulus between two concentric disks of radii 5 ft and 7 ft, as subtended at a point on the axis 10 ft from the plane of the disks.

Since $\cos \alpha_2 = 10/\sqrt{7^2+10^2} = 0.820$, and $\cos \alpha_1 = 10/\sqrt{125} = 0.894$, while $\varphi_2 - \varphi_1 = 30° = \pi/6$, we have $m = \frac{\pi/6}{2\pi}$ and $\omega = 0.08333 \times (0.894 - 0.820) = 0.0062$. *ANSWER.*

41. Solid Angle Fractions for Rectangular Surfaces [36]

It is particularly fortunate that the solid angle fraction for a rectangular surface can always be calculated analytically. The calculation is simplified if the conventions of Cartesian geometry are observed. The notation in the following paragraphs is that of figure 41.1, with the origin of coordinates in the plane of the rectangle and opposite the reference point (usually the detector location). The perpendicular distance from the plane of the rectangle to the reference point is z; and x_i, y_i ($i=1, 2, 3, 4$) are the coordinates of the four corners of the rectangle. The coordinate system is chosen so that the x and y axes are parallel to the sides of the rectangle; and the corners are numbered in counter-clockwise succession.

Having specified a coordinate system, we next list several important parameters, namely,

$$\epsilon_i = |y_i/x_i|,$$
$$\eta_i = |z/x_i|, \qquad (41.1)$$
$$q_i = y_i/\epsilon_i x_i.$$

The first two of these are referred to as "eccentricity ratios," while the last is ± 1, depending on the quadrant in which the corner is located. Finally, we define the function

$$\tau(\epsilon,\eta) = \frac{2}{\pi} \tan^{-1} \frac{\epsilon}{\eta\sqrt{\epsilon^2+\eta^2+1}}, \qquad (41.2)$$

which has the symmetry property

$$\tau(\epsilon,\eta) = \tau\left(\frac{1}{\epsilon}, \frac{\eta}{\epsilon}\right). \qquad (41.3)$$

In terms of these quantities, the following general rules hold precisely:

(1) Reference point opposite the center of the rectangle: For this case $\epsilon_i = \epsilon_1$ and $\eta_i = \eta_1$. The solid angle fraction ω subtended by the rectangle is given by

$$\omega = \tau(\epsilon_1,\eta_1). \qquad (41.4)$$

Extensive tabulations of $\tau(\epsilon,\eta)$ have been made and are presented in figures 41.2a and 41.2b.

(2) Reference point opposite one corner: The solid angle fraction ω is given by

$$\omega = \frac{1}{4} \tau(\epsilon_1,\eta_1). \qquad (41.5)$$

This result is easily obtained from symmetry by combining the rectangle of interest with three

---

[36] For a discussion of comparable problems in illumination see reference 40. Note, however, that in illumination the integrals are somewhat modified because the detectors are usually plane surfaces, having a response function which is not isotropic but is proportional to the cosine of the angle of incidence relative to the normal to the detector surface.
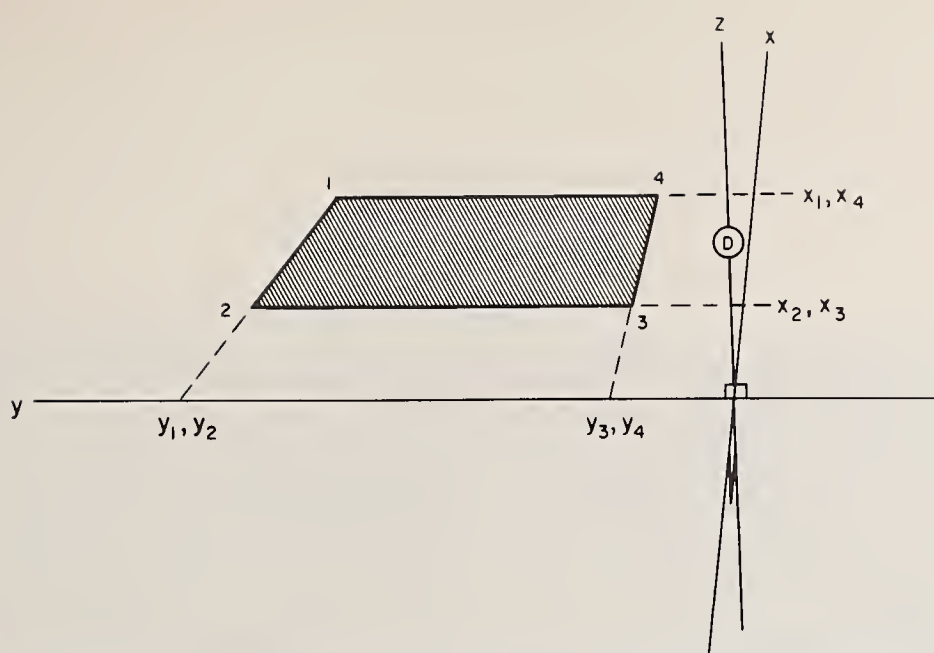
FIGURE 41.1. *Cartesian coordinate system used to describe a rectangle and a reference point (or detector), for calculations of the solid angle fraction.*

other identically shaped rectangles in the other quadrants (see fig. 41.3). The value of τ in eq (41.5) pertains to the larger rectangle comprising the four parts together.

(3) Reference point opposite the center of one edge: This arrangement is shown in figure 41.4. The detector can be considered opposite the corner of two similar, adjoining rectangles, each with eccentricity ratios ϵ_1, η_1, so that

$$\omega = \frac{1}{2}\,\tau(\epsilon_1, \eta_1). \qquad (41.6)$$

(4) Reference point on a plane of symmetry: An example of this case is pictured in figure 41.5. The detector can be considered at the corner of two similar, adjoining pairs of overlapping rectangles. The combination yields the result

$$\omega = \frac{1}{2}\,|q_1\tau(\epsilon_1, \eta_1) + q_3\tau(\epsilon_3, \eta_3)|. \qquad (41.7)$$

Notice that the terms add when the origin of coordinates is inside the rectangle and subtract when it is outside.

(5) General case: Figure 41.6 illustrates the important fact that a symmetric combination of rectangles can always be constructed which permits determination of the solid angle fraction subtended by any rectangular surface at any reference point whatsoever. One obtains therefrom the general expression

$$\omega = \tfrac{1}{4}|q_1\tau(\epsilon_1, \eta_1) - q_2\tau(\epsilon_2, \eta_2) + q_3\tau(\epsilon_3, \eta_3) - q_4\tau(\epsilon_4, \eta_4)|. \qquad (41.8)$$

Each term on the right corresponds to the solid angle fraction for one of the rectangles with a corner at the point opposite the detector. The terms all add if the origin of coordinates falls

inside the rectangle; while two terms add and two subtract if the origin is outside the rectangle.

Since the $\tau(\epsilon_i, \eta_i)$ correspond to solid angle fractions for "centered" rectangles, they are referred to frequently. We shall therefore make use of the shorter notation

$$\tau_i = \tau(\epsilon_i, \eta_i) \qquad (41.9)$$

for these "partial solid angle fractions."

EXAMPLE. Find the solid angle fraction subtended by a rectangular roof with dimensions 25 ft by 35 ft at points (a) 24 ft below the center, (b) 24 ft below one corner, (c) 24 ft below the middle of one of the short sides, (d) 24 ft below the roof and 10 ft out from one of the short sides, on the plane of symmetry, and (e) 24 ft below the roof and half-way between the center and one corner. All five positions are shown in figure 41.7.

Calculation of the solid angle fractions can proceed in two, sometimes three ways. For many, or most, cases it is sufficient to determine the parameters ϵ_i, η_i and then refer to figure 41.2. Thus, for the point designated (a) one has $\epsilon_1 = (25/2)/(35/2) = 0.7143$, $\eta_1 = (24)/(35/2) = 1.371$. One then locates the point having these coordinates on figure 41.2, places alongside this point a French curve which approximately matches the neighboring contours, and reads from a nearby radial line the value 0.173. *ANSWER.*

By comparison, for point (b) one first can determine the values $\epsilon_1 = |25/(-35)| = 0.7143$, $\eta_1 = |(24)/(-35)| = 0.6857$, and then calculate numerically the result $\omega = 0.25(2/\pi)\tan^{-1}(0.7402) = 0.1014$. *ANSWER.*

Notice that in all these calculations the coordinate system is oriented in the same way. For point (c), using $\epsilon_1 = 12.5/35 = 0.357$, $\eta_1 = 24/35 = 0.686$, one obtains from figure 41.2 the value $\omega = 0.124$. *ANSWER.*
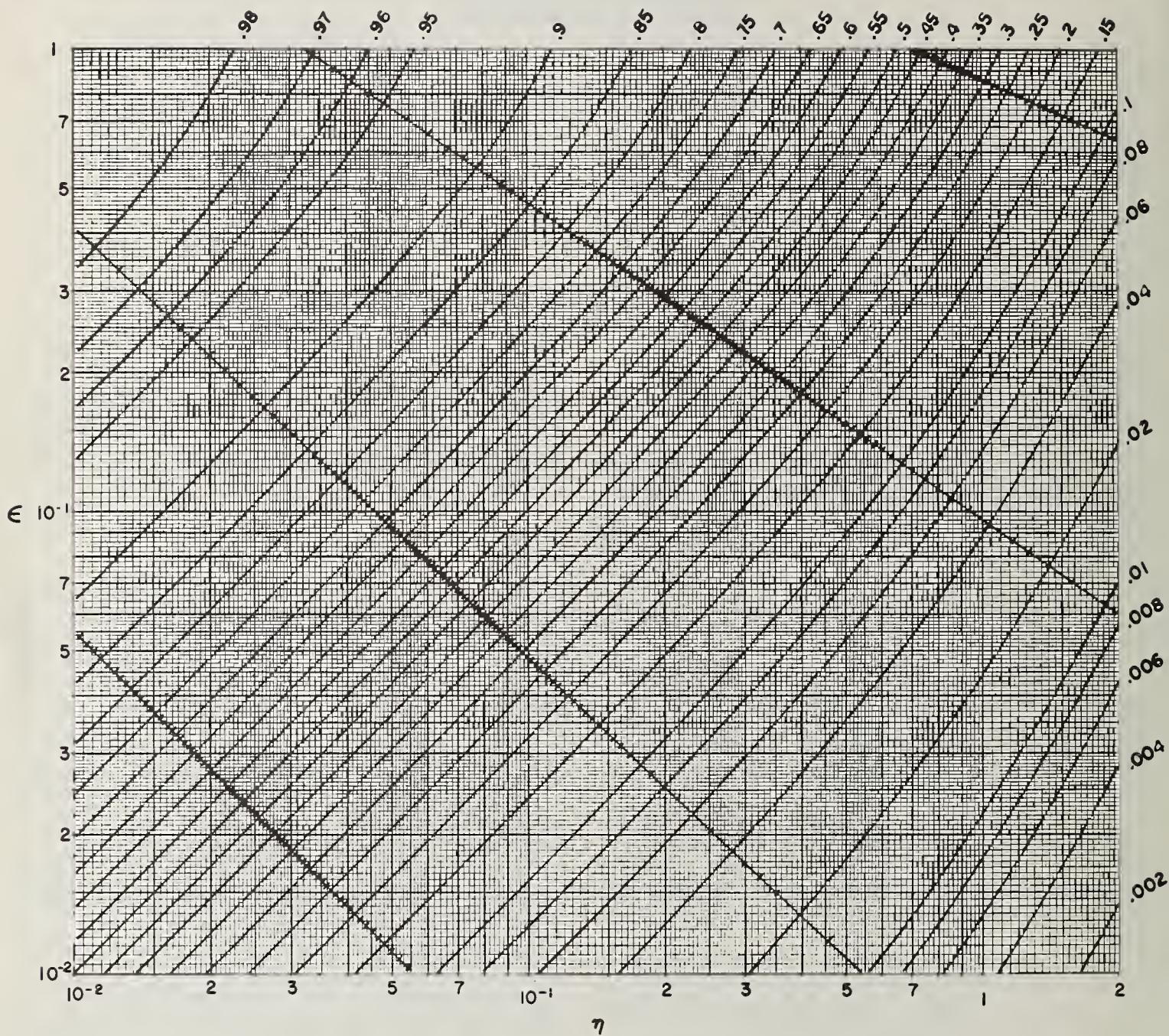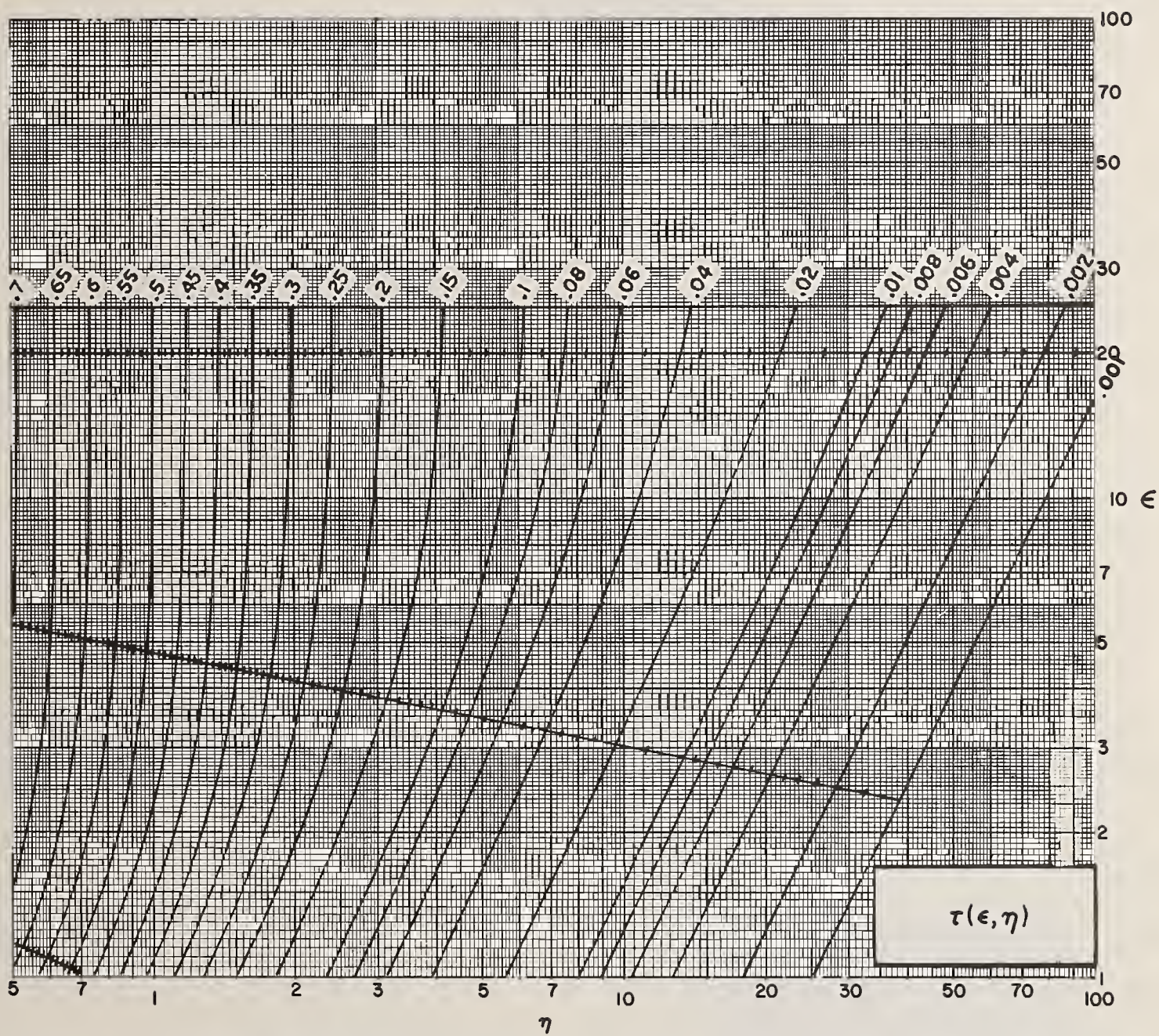
FIGURE 41.2a. *Contours of constant* $\tau(\epsilon, \eta), \epsilon \leq 1$. *This function is the solid angle fraction subtended by "centered rectangles."*
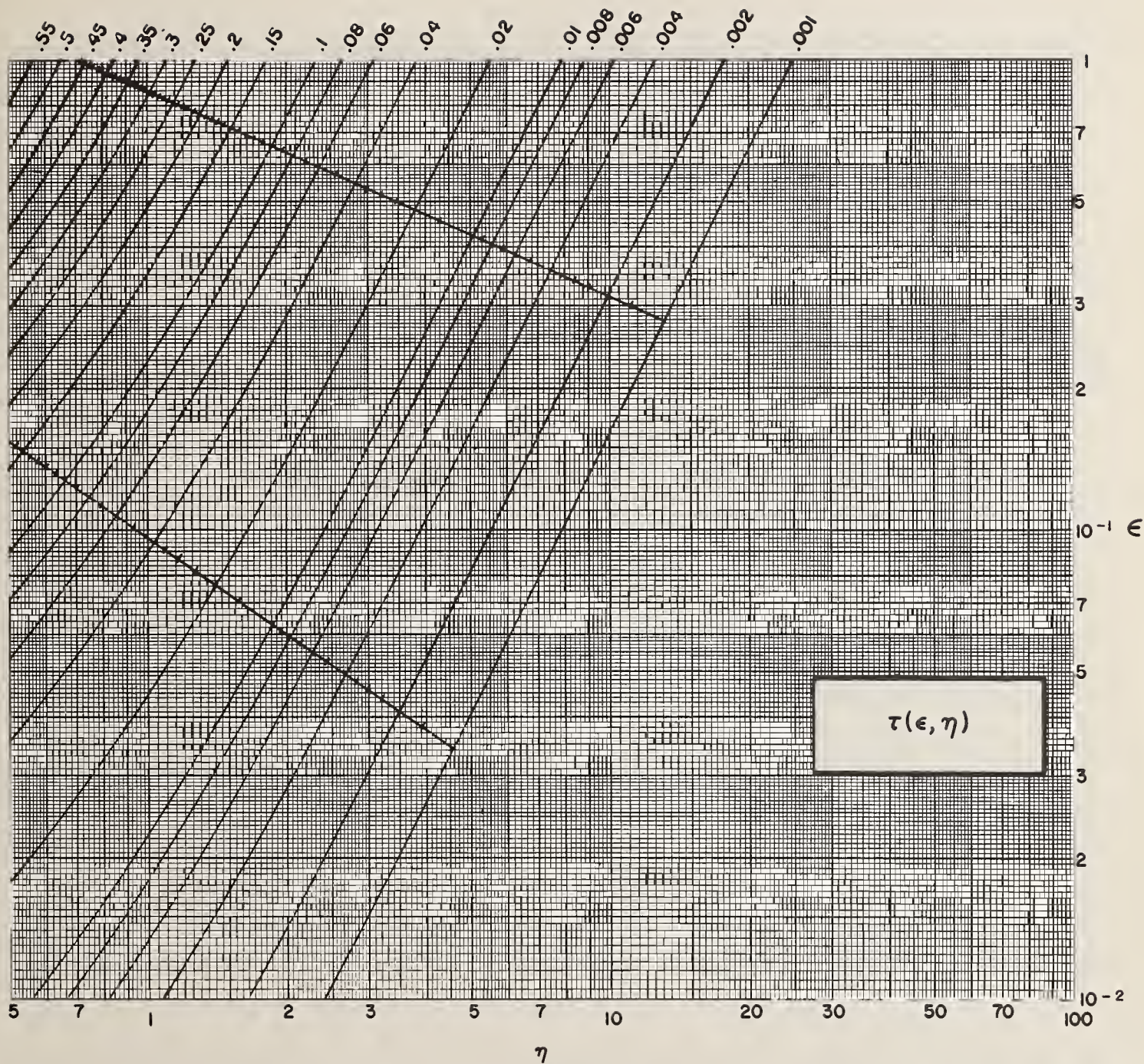
FIGURE 41.2a. *Contours of constant* $\tau(\epsilon,\eta), \epsilon \leq 1$.   *This function is the solid angle fraction subtended by "centered rectangles."*—
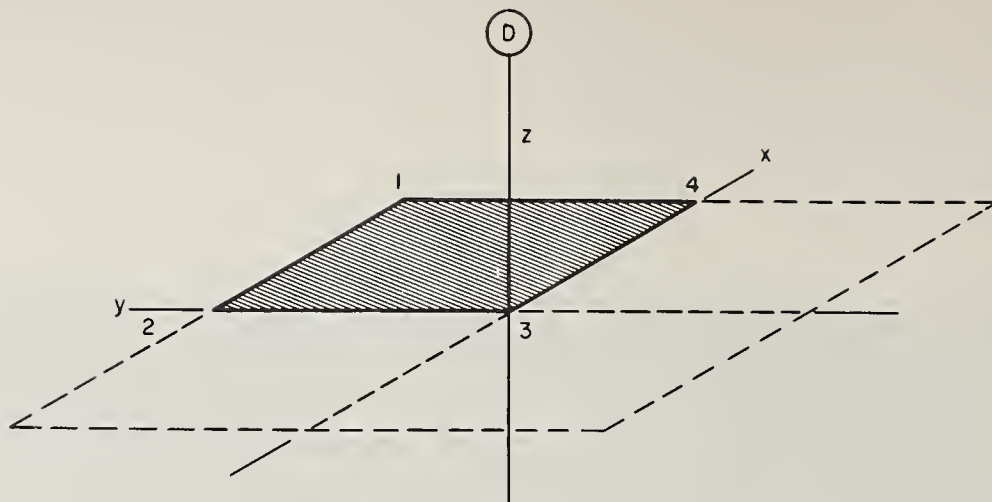Continued.

FIGURE 41.2b. *Contours of constant* $\tau(\epsilon,\eta)\epsilon \geq 1$.   *This function is the solid angle fraction subtended by "centered rectangles."*

72

FIGURE 41.2b. *Contours of constant* $\tau(\epsilon,\eta), \epsilon \geq 1$. *This function is the solid angle fraction subtended by "centered rectangles."*—
Continued

73

FIGURE 41.3. *Reference point (or detector) opposite one corner of a rectangle.*
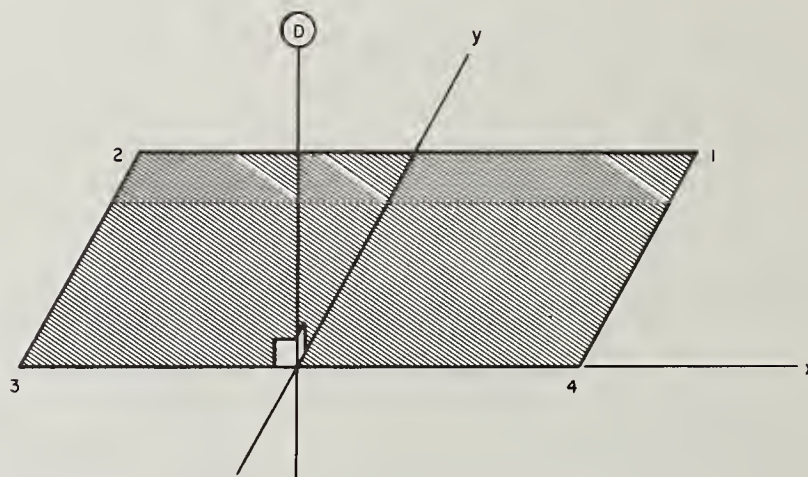
FIGURE 41.4. *Reference point (or detector) opposite the center of one edge of a rectangle.*
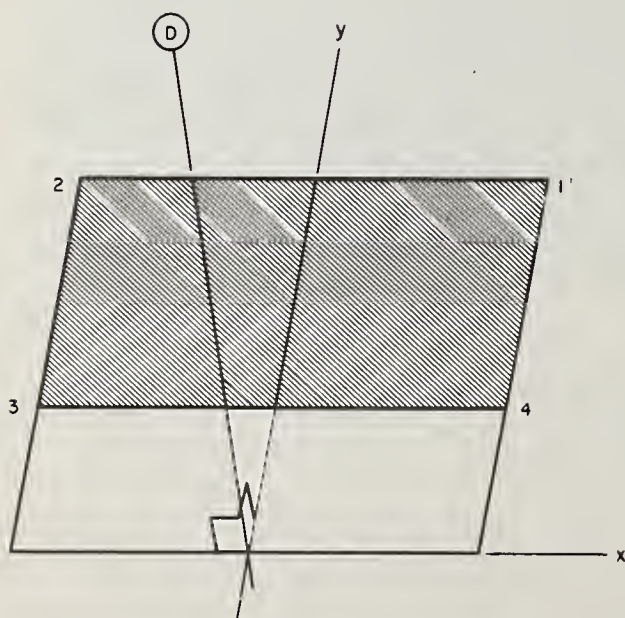
FIGURE 41.5. *Reference point (or detector) on a plane of symmetry of a rectangle.*

To calculate the solid angle fraction for point (d), one first lists

$$\epsilon_1 = 12.5/(35-10) = 0.5$$

$$\epsilon_3 = |(-12.5)/(-10)| = 1.25$$

$$\eta_1 = 24/(35-10) = 0.96; \, q_1 = 1$$

$$\eta_3 = |24/(-10)| = 2.4; \, q_3 = 1.$$

Figure 41.2 then provides the results $\tau(0.5, 0.96) = 0.216$, $\tau(1.25, 2.4) = 0.111$, so that $\omega = 0.5(0.216 + 0.111) = 0.164$. More precise numerical evaluation gives the result $\omega = 0.1659$. *ANSWER.*

Finally, for point (e), one has

$$\epsilon_1 = |(3/4)(25)/(3/4)(-35)| = 0.714$$

$$\epsilon_2 = |(-1/4)(25)/(3/4)(-35)| = 0.238$$

$$\epsilon_3 = |(-1/4)(25)/(1/4)(35)| = 0.714$$

74

$$\epsilon_4 = |(3/4)(25)/(1/4)(35)| = 2.143$$

$$\eta_1 = |24/(3/4)(-35)| = 0.914; \, q_1 = -1$$

$$\eta_2 = \eta_1; \, g_2 = 1$$

$$\eta_3 = |24/(1/4)(35)| = 2.743; \, q_3 = -1$$

$$\eta_4 = \eta_3; \, q_4 = 1$$

Numerical evaluation of the $\tau(\epsilon_i, \eta_i)$, followed by combination as indicated in eq (41.8), yields the result $\omega = 0.1524$. A trial calculation using figure 41.2 as a shortcut gave the less precise value 0.153. *ANSWER.*
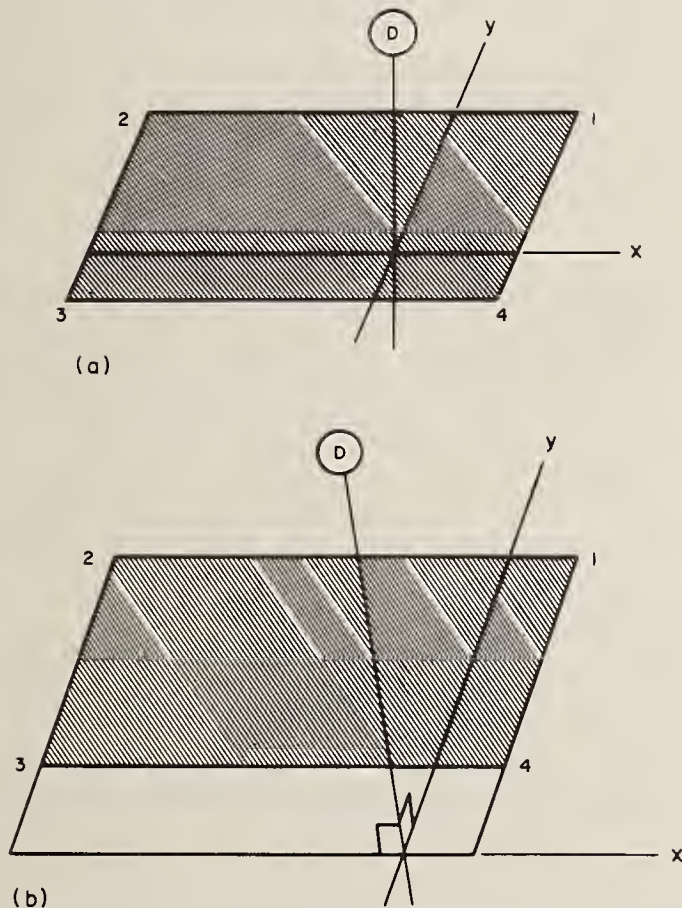
FIGURE 41.6. *Reference point (or detector) opposite arbitrary locations:* (a) *inside and* (b) *outside a rectangle.*
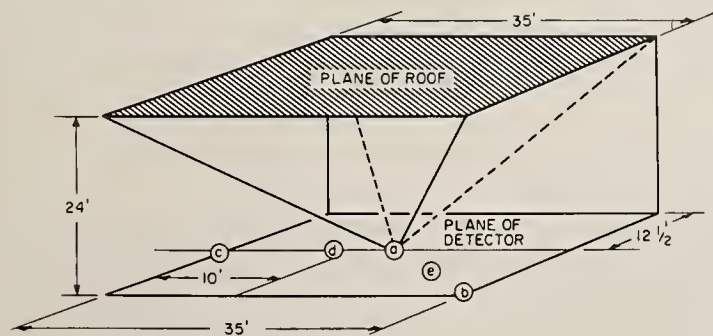
FIGURE 41.7. *Detector positions for the Example, relative to a 25 ft by 35 ft rectangular roof.*

42. Approximation of Rectangles by Circular Sectors

We next consider simple methods for representing rectangles as combinations of annular and circular sectors. If this can be accomplished for "centered rectangles" the extension to the general case is straightforward. Of course, it is in principle possible to make such representations with any accuracy desired, by using many small annular sectors. But this amounts to a form of numerical integration, which we seek to avoid. To be acceptable, a representation must use a minimum number of sectors.

Three methods will be discussed, each illustrated by one of the sketches on the left in figure 42.1. In the first, the elongation of the rectangle is neglected altogether. In the second, the elongation is accounted for by the use of two circular sectors. In the third, mainly for use with rectangles far off center, annular sectors are used.

(1) Approximation by circles: In some cases, eccentricity effects can be shown to be weak, so that two surfaces can be considered equivalent if they subtend the same solid angle fraction. One can then calculate the solid angle fraction $\tau(\epsilon, \eta)$ of a "centered rectangle," and replace the rectangle with a circle subtending $\omega = \tau(\epsilon, \eta)$ (see fig. 42.1a). In the general case of an off-center rectangle, each of the four "centered rectangles" is replaced in this way by a circle, and the corresponding approximation has the form

$$\omega = \frac{1}{4} \left| \sum_{i=1}^{4} (-)^{i+1} q_i \omega_i \right|. \tag{42.1}$$

in analogy with eq (41.8), with the ω_i representing circles. The combination can be viewed as a pair of annular sectors whose combined solid angle fraction is equal to that subtended by the off-center rectangle.

(2) Approximation by two circular sectors: This method attempts to obtain greater accuracy through an attempt to take eccentricity effects into account. In figure 42.1b the rectangle is indicated by a solid line. The dashed lines indicate two squares, one having its sides equal to the length of the rectangle, while the other has its sides equal to the width of the rectangle. The circular arcs represent parts of circles which, if complete, would subtend solid angle fractions equal to values for the squares. The representation consists of the complete smaller circle plus enough of the annular ring between the circles to give the combination a total solid angle fraction equal to that of the rectangle.

If the solid angle fraction of the rectangle is $\tau(\epsilon, \eta)$, the solid angle fractions subtended by the two squares are $\tau(1, \eta)$, and $\tau(1, \eta/\epsilon)$. It is easy to show that the approximation takes the form

$$\omega = a\omega' + (1-a)\omega'', \tag{42.2}$$

75
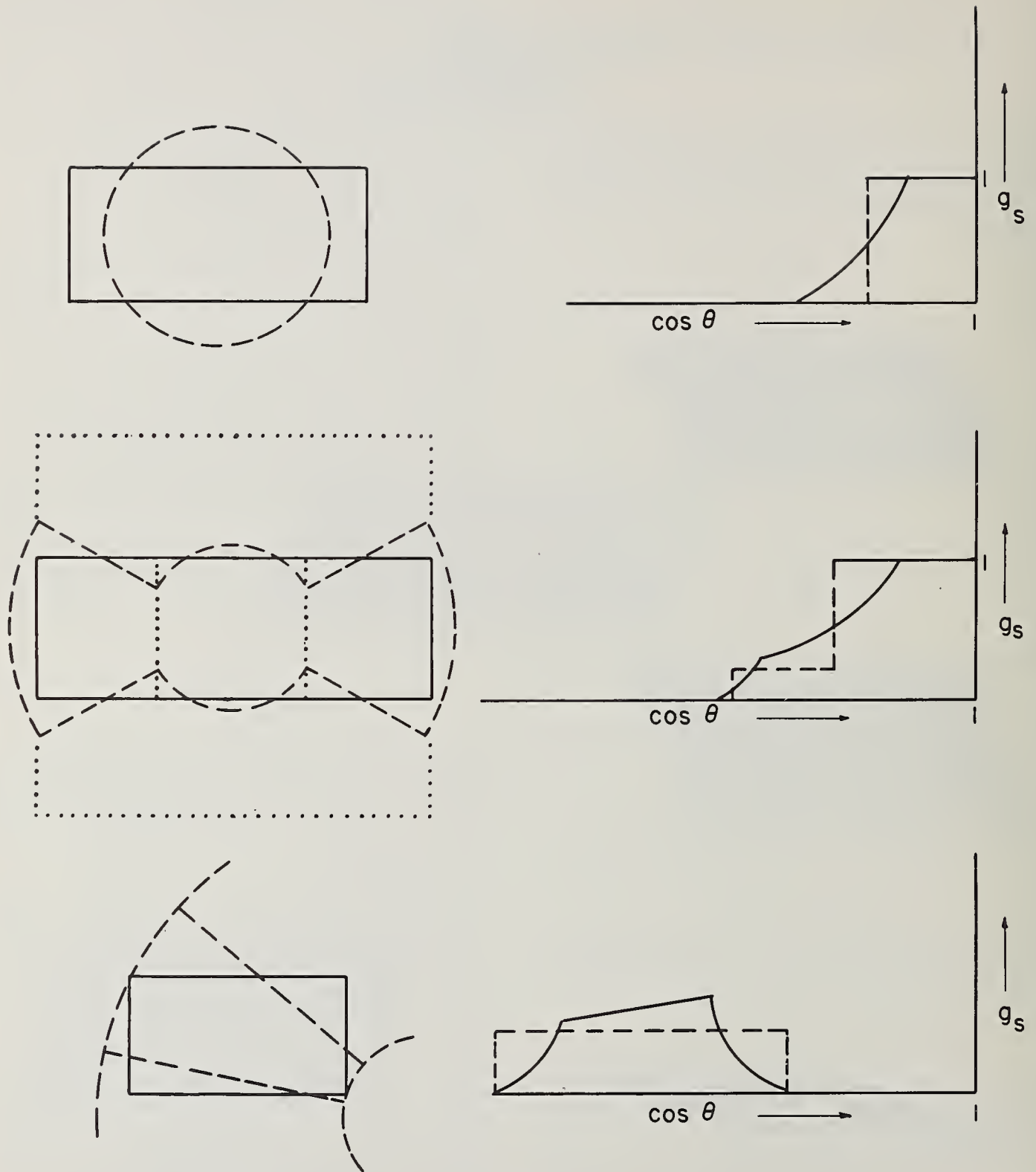
FIGURE 42.1. *Approximation of a "centered rectangle" by circles and annual sectors:*

(a) *Neglecting elongation (Method 1); (b) taking elongation into account in a simple two-term approximation (Method 2); (c) using an annular sector to represent an off-center case (Method 3). The graphs on the right show qualitatively the circular sector approximations (dashed lines) to the $g_r(\theta)$ functions (solid lines) which correspond to the sketches on the left.*

where ω is the solid angle fraction of the ("centered") rectangle, ω' and ω'' represent circles having solid angle fractions $\tau(1,\eta)$ and $\tau(1,\eta/\epsilon)$, respectively, and

$$a=\frac{\tau(\epsilon,\eta)-\tau(1,\eta/\epsilon)}{\tau(1,\eta)-\tau(1,\eta/\epsilon)}. \quad (42.3)$$

Extension to the general case of off-center rectangle is accomplished by the use of eq (42.1), with each of the ω_i referring to a sector-represented "centered rectangle."

(3) Approximation by annular sectors: This method is for use when the four terms in the general case cancel strongly against one another, as when the rectangle is far to one side of the origin of coordinates.

Concentric circles passing through the farthest and nearest corners of the rectangle subtend solid angle fractions $\omega'=\left\{1-\dfrac{\eta_1}{\sqrt{\eta_1^2+\epsilon_1^2+1}}\right\}$ and $\omega''=\left\{1-\dfrac{\eta_3}{\sqrt{\eta_3^2+\epsilon_3^2+1}}\right\}$, respectively. A sector of the annulus between these circles can represent the rectangle if it has the same solid angle fraction. Our representation thus takes the form

$$\omega=m(\omega'-\omega''), \quad (42.4)$$

where ω', ω'' represent the two circles, with solid angle fractions as indicated, and

$$m=\frac{\dfrac{1}{4}\left|\sum_{i=1}^{4}(-)^{i+1}q_i\tau_i\right|}{\left(\dfrac{\eta_3}{\sqrt{\eta_3^2+\epsilon_3^2+1}}-\dfrac{\eta_1}{\sqrt{\eta_1^2+\epsilon_1^2+1}}\right)} \quad (42.5)$$

Since this last method is applied to off-center rectangles primarily, there is no reason to consider combinations of such representations.

43. Calculation of Geometry Factors for Rectangles

As a last step in the calculation of geometry factors for rectangles, we replace ω in the preceding section by $G(X,\omega)$, a geometry factor. We can do this because the G's combine linearly just like the ω's. Thus, (42.1) takes the form

$$G(X,\omega)=\frac{1}{4}\left|\sum_{i=1}^{4}(-)^{i+1}q_iG(X,\omega_i)\right|, \quad (43.1)$$

where the term on the left is the approximate geometry factor for the rectangle, and the terms on the right are geometry factors for circles subtending solid angle fractions ω_i.[37]

[37] Note that eq (43.1) is exact when the $G(X,\omega_i)$ correspond to the centered rectangles determined by the four corners of the off-center rectangle, rather than to circular sector approximations to these centered rectangles.

Similarly, in method (2) utilizing circular sectors, eq (42.2) becomes

$$G(X,\omega)=aG(X,\omega')+(1-a)G(X,\omega''), \quad (43.2)$$

where the value of a is given by eq (42.3). Combination of the four results of the type eq (43.2) into an expression of the form eq (43.1) gives the circular sector approximation for the general case.

Finally, the annular sector approximation (3) for a geometry factor is obtained by translating eq (42.4) into

$$G(X,\omega)=m[G(X,\omega')-G(X,\omega'')], \quad (43.3)$$

where m is given by eq (42.5).

These methods can be applied to any of the geometry factors represented generically by $G(X,\omega)$, with greater accuracy in some cases than in others. No attempt has been made to compare systematically the accuracy of the different approximation methods in different types of calculations.

EXAMPLE 1: A rectangular underground shelter 40 ft x 20 ft is covered with a concrete slab of effective mass thickness $X=150$ psf. Fallout on the slab emits gamma radiation of intensity sufficient to give a response D_0 to a detector 3 ft above an idealized plane similarly contaminated. Calculate the detector response 10 ft below the slab, half-way between the center and one corner, using the circular approximation. Figure 43.1 illustrates the configuration.

To determine the detector response one first calculates the parameters ϵ_i, η_i, and τ_i for each of the corners of the roof slab, using figure 41.2.

i	ϵ_i	η_i	τ_i	q_i
1	30/15	10/15	0.58	1
2	$\lvert 30/(-5)\rvert$	$\lvert 10/(-5)\rvert$	.278	-1
3	$\lvert(-10)/(-5)\rvert$	$\lvert 10/(-5)\rvert$	.205	1
4	$\lvert(-10)/15\rvert$	10/15	.40	-1

Using figure 28.10 we next calculate L_a for circles having the same solid angle fraction:

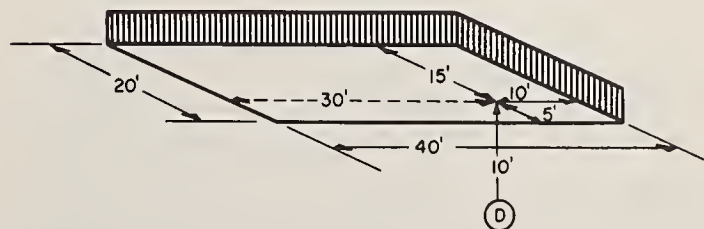| i	ω_i	$L_a(150,\omega_i)$
1	0.58	0.73
2	.278	.49
3	.205	.39
4	.40	.61

FIGURE 43.1. *Detector below the roof slab of an underground shelter, as in Examples 1, 2, and 3.*

77

Finally, we make the combination for the general case:

$$D = D_0 L(150)(1/4)\left| \sum_{i=1}^{4} (-)^{i+1} q_i L_a(150,\omega_i) \right|$$

$$= D_0(.0057)(.555) = 0.0032 D_0. \quad ANSWER.$$

The circular approximation has fairly obvious limitations. It cannot be applied accurately for length/width ratios which differ by more than perhaps a factor of three from unity, unless the directional distribution involved is either nearly isotropic or nearly monodirectional. In the example just worked, the term $L_a(150,\omega_2)$ is expected to be rather inaccurate because ϵ_2 is 6; but this term contributes only about 10 percent of the final result.

Clearly this method can be expected to become more inaccurate when the terms cancel rather than add, i.e., if the detector is to one side of the roof slab. Also, values obtained will represent an overestimate or underestimate depending on whether radiation contributes more at angles near perpendicularity or at angles nearly grazing the source plane. Thus the value obtained in this example is an overestimate because radiation emerges from the roof slab with greater intensity at angles near the perpendicular.

EXAMPLE 2: Re-calculate the detector response for the preceding example, using a circular sector approximation.

Using the ϵ_i, η_i, and τ_i values already determined, the following table is easy to calculate:

i	ω'	ω''	a	$1-a$	$L_a(150,\omega')$	$L_a(150,\omega'')$
1	0.48	0.71	0.569	0.431	0.68	0.78
2	.128	.71	.743	.257	.26	.78
3	.128	.336	.630	.370	.26	.55
4	.336	.48	.556	.444	.55	.68

From these values, using eq (43.2), we obtain

i	ω_i	$L_a(150,\omega_i)$
1	0.58	0.723
2	.278	.394
3	.205	.367
4	.40	.608

The final combination then yields

$$D = D_0 L(150)(1/4)\left| \sum_{i=1}^{4} (-)^{i+1} q_i L_a(150,\omega_i) \right|$$

$$= D_0(0.0057)(0.523) = 0.0030 D_0. \quad ANSWER.$$

The value is to be compared with $0.0032 D_0$, which was obtained by the circular method. The agreement is surprisingly good, considering that the length/width ratio of the roof slab is 2. The largest part of the disagreement appears to come from the term corresponding to the second corner, with its length/width ratio of 6. The ratio of values given by the two approximations for this term is about 0.81.

EXAMPLE 3: Consider the rectangular roof slab of the preceding examples as two adjacent squares, and calculate the contribution to the detector response from the square farthest from the detector. The detector is still considered to be 10 ft below the roof, halfway between center and corner.

The values of the parameters ϵ_i, η_i, and τ_i turn out to have the same magnitudes as before; the only changes are in the q_i, which affect the value of m:

i	ϵ_i	η_i	τ_i	q_i
1	30/15	10/15	0.58	1
2	$|30/(-5)|$	$|10/(-5)|$	.278	-1
3	$|10/(-5)|$	$|10/(-5)|$	.205	-1
4	10/15	10/15	.40	1

The sign changes lead to increased cancellation, so that the resulting solid angle fraction is reduced to 0.063.

The values of ω' and ω'' can now be calculated:

$$\omega' = 1 - \frac{10/15}{\sqrt{\left(\frac{20}{15}\right)^2 + \left(\frac{10}{15}\right)^2 + 1}} = \frac{5}{7};$$

$$\omega'' = 1 - \frac{2}{\sqrt{2^2 + 2^2 + 1}} = \frac{1}{3}$$

Inserting these values into eq (42.5), we obtain $m = .063(21/8) = .165$.

We next obtain the values

$$L_a(150,\omega') = .78, L_a(150,\omega'') = .54,$$

from figure 28.10, and make the final combination indicated by eq (43.3),

$$D = D_0 L(150)(0.165)(0.78 - 0.54) = 0.00023 D_0. \quad ANSWER.$$

This result is much smaller than the value obtained in the preceding examples partly because the solid angle fraction is much smaller and partly because the radiation tends to go downward rather than sideways after emergence from the roof slab.

44. Further Discussion of Geometry Factors

It is possible to calculate geometry factors while avoiding the use of approximations like those described in the preceding Sections. To accomplish this, the circular source data obtained from expressions typified by eq (27.1) must be replaced by calculations using more general integral forms of types eqs (16.2) and (16.3), with $g_s(\theta,\varphi)$ and $g_s(\theta)$ corresponding to rectangles rather than circles.[38]

The "centered rectangle" case is the only one that need be considered in this connection because off-center cases are always obtainable as linear combinations. Because ϵ and η uniquely

---

[38] For an alternative and different approach to the calculation of geometry factors see Section 49 and references 29, 30, and 41.

specify a centered rectangle configuration, it is in principle possible to make extensive tabulations of geometry factors $G(X,\epsilon,\eta)$, using these variables in place of ω. Presumably $G(X,\epsilon,\eta)$ can be presented, for each X, by means of contour diagrams similar to figure 41.2. In the future this may prove to be a desirable way of presenting geometry factor data, particularly for radiation directional distributions which depend on an azimuthal angle φ as well as a polar angle θ, as in the case of radiation emerging from a vertical wall adjacent to a fallout field.

It is instructive to discuss once more the approximations of the preceding Sections, using the functions $g_s(\theta,\varphi)$ and $g_s(\theta)$. In figure 42.1, the points within the rectangle correspond to (θ,φ) combinations for which $g_s(\theta,\varphi)=1$; while the points outside the rectangle correspond to $g_s(\theta,\varphi)=0$. The circles similarly divide the points in the plane into two sets, one giving $g_s(\theta,\varphi)=1$, the other giving $g_s(\theta,\varphi)=0$. But that of sketch (a) leads to a function $g_s(\theta)=\dfrac{1}{2\pi}\displaystyle\int_0^{2\pi} g_s(\theta,\varphi)d\varphi$ which looks like the solid line of figure 42.1, (a), right; while the circular approximation (dashed line) resembles a step function. Note that the area under both curves must be about the same, since it corresponds approximately to the solid angle fraction. The circular sector and annular sector approximations are similarly compared with the functions they represent in the sketches (b) and (c), right, of the same figure. Thus all three approximations are seen to be combinations of step functions.

Presumably greater accuracy is obtainable by use of approximations which involve more terms; but the greater effort is a serious impediment, and other sources of error tend to be large enough to make such refinements have questionable significance.

45. Acknowledgments

Appendix A. Computations

46. Preparation of Data: Use of Digital Computers

To obtain most of the data presented in this manuscript, it was necessary to rely on digital computer programs. A family of these programs was written for the IBM 704 computer at the National Bureau of Standards, using the SAP system of orders. Because so much of the desired data involved angular distributions of a fairly general type, many of these computer programs involved extensive development and experimentation. Figure A1 is a block diagram showing the system in its final form, and indicating by means of arrows the order followed.

The first to be constructed was the general MOMENTS routine, whose output is a large tabulation of values for coefficients $I_{nl}^{l_0}(E_i)$, as well as dose integrals $D_{nl}^{l_0}$, for a given monoenergetic gamma ray source in a given material. Here, E_i is the i'th scattered energy and the indices n, l, l_0 refer to the n'th spatial moment, the l'th Legendre coefficient of the directional distribution, resulting from a plane source emitting gamma rays having initial directional distribution $P_{l_0}(\cos\theta_0)$, where θ_0 is the initial obliquity angle relative to the normal to the source plane [12]. The calculation is carried out using photon wavelength (in Compton units) as a variable. For most calculations the basic integration interval was $\Delta\lambda=0.025$. This interval was doubled at $\lambda\approx\lambda_0+2$, and redoubled at $\lambda\approx\lambda_0+4$, to keep the total down to manageable proportions. For $1\leq l_0\leq 12$, values of n up to 12 were calculated; while for $l_0=0$, the calculation was extended to $n=18$. Output was
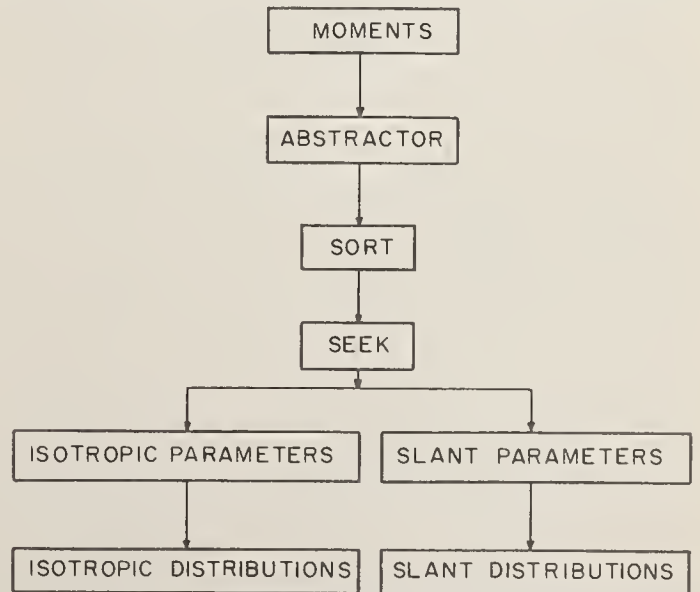
FIGURE A1. *Flow diagram for the computer programs.*

to magnetic tape, and totaled the order of 10^5 numbers. After a number of time-saving modifications of the code, calculations for a single source energy and material took about one half hour of machine time.

The purpose of the ABSTRACTOR code was to make a selection of data from the tape generated by the MOMENTS code. Two types of selection were considered, one essentially linear in the photon wavelength and the other essentially logarithmic and including all the source wavelengths to be used. Both selections included the integral data, treating it as if it corresponded to spectral energies. (Four types of integral data were included: Data for the total dose, the total scattered dose, the once-scattered dose, and the multiply scattered dose.) By selecting about 1/10 of the scattered energies, it was possible to put on a single magnetic tape results for the following source wavelengths:

$$\lambda_0 = 0.05, 0.075, 0.1, 0.125, 0.15, 0.2, 0.25,$$
$$0.3, 0.4, 0.5, 0.6, 0.8, 1.0, 1.2, 1.6, 2.0,$$
$$2.4, 3.0, 4.0, 5.0, 7.0, 9.0, 12.0, 15.0.$$

On another tape was put data for the source wavelengths 0.384, 0.434, and 0.77, corresponding to Co^{60} and Cs^{137}. Initial calculations were for penetration in H_2O. These were followed eventually by calculations for concrete, and still later by calculations for Fe.

Following the abstraction, the SORT code reordered the data from

$$(E_0(l_0(n(l(E_i)))))$$

to

$$(E_0(l_0(l(E_i(n))))),$$

because it was thought that the tape search time would be cut down by having all the spatial moments in a group together. (This was probably an ineffective modification, all things considered.)

From the basic moment-coefficient data it was possible to construct spatial and directional distributions corresponding to many different source configurations. Of these configurations, two types had special importance: (a) those corresponding to isotropic sources ($l_0 = 0$), and (b) those corresponding to plane sources emitting at a fixed obliquity angle θ_0 relative to the normal to the source plane. Accordingly a tape search subroutine called SEEK was written, which, for specified E_0, E_i, l would yield a set of moments describing one or the other type of distribution.

Two codes were then constructed to determine actual distribution parameters. In the first, called ISOTROPIC PARAMETERS, the isotropic distribution moments were used to calculate the coefficients of a power series representation of the *point* isotropic build-up factor. In other words, the (plane source) moments were turned into point source moments, and were used to determine

coefficients A_j in the representation

$$I_i^{PTI}(E_i) = \frac{1}{4\pi r^2} \sum_{j=0}^{i_{max}} A_j (\mu_0 r)^j e^{-(\mu_0 r)}, \qquad (A1)$$

of the l'th Legendre coefficient of the point isotropic source angular distribution. The A_j coefficients, for a specified set of l, E_i, and E_0 values, were punched on an IBM card, together with the descriptive l, E_i, and E_0 values. It may be of interest to note that this calculation involved a matrix inversion, which was accomplished in a very simple way by hand, using the bi-orthogonal polynomial system U_n^m of Ref. 12. Equation (A1) refers also to the integral data, which, in fact, was utilized almost exclusively.

In the second program of this type, called SLANT PARAMETERS, calculations were made of the constants A_j^e, A_j^0, B_j^e, and B_j^0 in a representation

$$I_l^{PLO}(E_i, \cos \theta_0, z) = 1/2 \left(\sum_{j=0}^{i_{max}} A_j^e e^{-B_i^e z} \pm \sum_{j=0}^{i_{max}} A_j^0 e^{-B_i^0 z} \right)$$
$$(A2)$$

of the l'th harmonic coefficient of the angular distribution corresponding to a plane oblique (or slant) source at specified initial obliquity angle θ_0. In this calculation the values of B_0^e, B_0^0 were fixed at the value $(\mu_0/\cos \theta_0)$ and the values of B_1^e, B_1^0 could be assigned arbitrarily. The other constants were all determined so that the moments of the approximate distribution agreed with the known values and with the known value of the source strength. The coefficients for "even" and "odd" component distributions, as indicated by the superscripts, were calculated separately and punched on separate IBM cards, together with identifying data for E_0, E_i, $\cos \theta_0$, and a parity indicator which was zero or one.

The calculation of slant distribution parameters was a fairly tricky business, because the B_i's were determined as the roots of polynomial equations. These roots could always turn out to be imaginary, signifying an oscillatory and therefore nonphysical distribution. The arbitrary B_1 coefficient was sometimes given a variety of values in the search for a reasonable, real set of roots.

Many sets of parameter cards were punched, mostly corresponding to integral (dose) data, with $l = 0$. Sets were prepared for values of l up to $l = 7$ for isotropic sources, dose data, and various E_i spectral energies. Values for l greater than zero were not calculated for oblique sources, nor were calculations made for more than a very few E_i values. This was partly because most relevant shielding data did not require these details, and partly because the slant parameter calculations were expensive as well as tricky, and required careful examination of results.

The final machine programs calculated spatial distributions, and in the case of the isotropic source cases, directional distributions. Specifically, the SLANT DISTRIBUTIONS program

could calculate penetration data for an arbitrary combination of source obliquities, source energies, and scattered energies, so long as these obliquities and energies were represented in the deck of binary parameter cards. In general, dose parameter cards for the source energies already mentioned were available, and the source directions included $\cos \theta_0 = \pm 1, \pm .9, \ldots \pm .1, 0$.

The ISOTROPIC DISTRIBUTIONS program was much more complicated. Initially, this program determined the total intensity or an angular distribution resulting from a Legendre sum, for a point isotropic source or a plane isotropic source. Superposition of different source energies was possible. All the angular distributions for the fission source were obtained with this early form of the code. The resulting angular distributions were mostly not directly usable because of large oscillations; it was a case of too few coefficients to describe a peaked distribution. These angular distributions were smoothed by adding angular functions of the forms

$$\alpha(\cosh \beta - \cos \theta)^{-3/2} - \sum_{l=0}^{7} (l+1/2)a_l P_l(\cos \theta),$$

Point Isotropic Source, (A3)

and

$$\alpha(\cos \theta)^{-1} e^{-\beta z/\cos \theta} - \sum_{l=0}^{7} (l+1/2)b_l P_l(\cos \theta),$$

Plane Isotropic Source. (A4)

where α, β are arbitrary constants, and the $a_l's$ and $b_l's$ are the expansion coefficients of the accompanying function. It will be seen that additions of this type do not affect the values of the first 8, machine-calculated Legendre coefficients.

The resulting, hand-calculated angular distributions are those of figures 26.1 and 26.3. Because of the work involved in obtaining these distributions from the machine output, it appeared highly desirable to include methods for obtaining such distributions in the machine code itself. Accordingly, a series of modifications was incorporated in the code: (1) For the plane, isotropic calculations, the unscattered component was calculated exactly, and the scattered component was represented by a simple Legendre sum. (2) For the point isotropic calculations, the Legendre coefficients were first calculated. Then the $l=3$ and $l=5$ coefficients were used to obtain coefficients α and β for a function $\alpha(\cosh \beta - \cos \theta)^{-3/2}$ so as to make the corresponding coefficients in the Legendre sum of that function equal to the known coefficients. Finally, the angular distribution was calculated using the expression

$$D(\cos \theta) = \alpha (\cosh \beta - \cos \theta)^{-3/2}$$
$$+ \sum_{l=0}^{7} (l+1/2)[D_l - a_l] P_l(\cos \theta). \quad (A5)$$

(3) Provisions were made to extend all calculations to include ring source, circular source, and circular

clearing source types, and another modification was made to provide for the determination of both unscattered and scattered components of the point isotropic source (total dose).

Since this code provided for superposition of different source energies, and for modification of the output angular distribution (Legendre sum only) to correspond to different reference axes, it made possible calculations for different spectra as well as the calculations of angular distributions incident on vertical walls (See eq 27.7). The angular distributions in Appendix B were calculated using this code.

Because of the extensive development work that accompanied the writing of these codes, they included many features which turned out not to be useful or desirable. They have never been put in such a form that general circulation appeared desirable. An effort is presently underway to rewrite the best features of this series, using the Fortran system, for general use.

47. Preparation of Data: Hand Computations

For the most part, the hand computations were perfectly straightforward integrations over the machine-produced data. One exception is to be noted: Integration of expressions eqs (27.11), (27.12), and (27.16) was accomplished in the most obvious way only once, namely for the fission data. Thereafter it was noted that one could obtain the same result in a far easier way by using integral data such as L_a, S_a, and P_a. The advantage is twofold: The azimuthal integration is carried out analytically and the obliquity integration does not involve extremely peaked functions. The trick involves using an identity such as

$$d\cos\theta l(d, \cos\theta) = S(d)dS_a, \cos\theta \leq 0, \quad (A6)$$

to write the expression for W_b in the form

$$W_b(d, 1-\cos \alpha) = \frac{2}{\pi} \int_{S_a(d,1-\sin \alpha)}^{1} dS_a \cos^{-1} \left[\frac{\cos \alpha}{\sqrt{2\omega - \omega^2}} \right],$$

(A7)

where $dS_a = d[S_a(d,\omega)]$.

In future calculations it would be highly desirable to arrange it so that all the integrations are carried out by machine. This will probably involve angular distribution output either in the form of punched cards or on magnetic tape.

48. Comments on Accuracy

In discussing the material of this manuscript in regards to accuracy, it is convenient to distinguish three types of error: (1) errors due to inaccurate input information; (2) errors due to the procedure used to calculate distributions and produce the graphs; and (3) errors due to procedures for using the data, which are traceable to the inadequacies of the schematization.

It is clear that the use of a particular approximate fission spectrum, namely that for 1.12 hour old fission products, to represent all practical situations, is by far the largest error of the first type. The magnitude of such errors can be estimated roughly from data such as that in figure 26.6. For planning purposes the shielding factors may be *defined* relative to a particular spectrum. This doesn't alter the fact that the data may not represent an experimental situation exactly, but it does encourage a shift of attention to other parts of the problem, since then the validity of the spectrum and the accuracy of shielding factor calculations are considered separately.

The other major type of input information is the cross sectional data. We expect small inaccuracies in the differential scattering cross section due, e.g., to atomic binding corrections in the Klein-Nishina expression, to have negligible effect on the accuracy of the calculations. On the other hand, errors in the *total* cross sections which, generally speaking, are expected to be less than 1 percent in magnitude, can result in errors in the barrier factors at the deeper penetrations which are up to 10 times larger, i.e., 5 to 10 percent. A change in air density has the effect of a change in total cross section; and this can be brought about by temperature or altitude variations. Finally, not all data was prepared using precisely the conversion factor of eq 26.1; there were differences of a few tenths of a percent. For this reason, and due also to the use of overlays in preparing the graphs, the data are not expected to be internally consistent to better than about 5 percent.

Generally speaking, the attenuation data represented in the barrier factors can be calculated with much greater accuracy than the angular distributions which are used to obtain geometry factors. Calculations of barrier factors for point and plane isotropic sources, i.e., the $L(X)$ and $P(X)$ curves, are probably accurate to within 5 percent, assuming that the input data is exactly correct. Considering the different sources of error together except for the spectrum assumption, these curves should be correct to within, say 8 percent. On the other hand, the $S(d)$, $S'(X)$, and $W(X,d)$ are appreciably less accurate; and it is difficult to assess quantitatively the accuracy of these curves even though some of the major sources of error are known. Perhaps for guidance purposes it may be useful to give "educated guesses" that excluding the assumption of spectrum, errors in $S(d)$ may be in the range of 10 to 15 percent; errors in $W(X,d)$ for small X are perhaps 10 percent and for large X may be two or three times larger; and errors in $S'(X)$ can be expected to increase roughly linearly with X, from 0 at $S'=1$ to perhaps as much as 100 percent at $S'=10^{-4}$.[39]

Turning to angular distributions and geometry factors, the inherent inaccuracies of the calculations can be seen visually in the Co^{60} and Cs^{137} angular distributions in Appendix B, which have not been smoothed. The distributions of figures. 26.1 and 26.3 originally looked very much the same but were arbitrarily smoothed with french curves. Errors in the range of 20 to 25 percent, perhaps even greater, can be expected at places in these data. However, the integrations which yield geometry factors improve the situation somewhat. Generally speaking, we expect the geometry factors to be quite accurate when they are large and to approach the accuracy of the angular distributions from which they were obtained when they are very small. Thus, from right to left the geometry factor curves vary from no error to errors of perhaps as much as 25 percent, with the L_b and L_c curves being more reliable than this because they were not obtained from angular distributions. Combinations of geometry and barrier factors, such as in figures 28.18, 28.19, and 28.20 have different accuracy in different regions as determined by the separate errors inherent in the two ingredient factors.

Finally, in regards to the utilization of the data, there are several comments which can be made. Use of water data to represent concrete gives results normally within the accuracy of the calculations if the 0.9 factor differences are correctly applied. But it should be remembered that near the source, where the total contribution of scattered photons is a relatively small part of the detector response, the difference between water and concrete is negligible, certainly not as large as 10 percent; and at great penetrations the difference can be larger than 10 percent. Errors due to estimation of boundary effects probably approach the magnitude of the total boundary effect. And errors due to the use of circular source data to represent rectangular source geometry factors will vary greatly with the situation. They can perhaps be estimated by the use of several calculations using different superpositions of data, as was indicated in the problem worked out in Section 43.

49. Alternative Data Types and Procedures

The use of circular source data for computation of geometry factors is only one of several possible procedures involving different data types. For example, in Section 44 it was indicated that geometry factors for rectangular source types could be calculated directly.

An interesting alternative procedure has been explored by Berger, Hubbell, and Lamkin [29, 30, 41]. This consists of using the Legendre coefficients of the directional distributions rather than the directional distributions themselves. If, in eqs (16.2) and (16.3) the dose angular distribution (D) is written in the form of a Legendre series, the detector response D_S takes the form of a sum of products in which one factor is a

[39] Errors in $S(d)$ stem from moderately rough calculations of the angular distribution; errors in $W(X,d)$ come largely from the spectrum and angular distribution assumed as source for the wall penetration; and errors in $S'(X)$ are due to its calculation as a small difference between large numbers.

Legendre coefficient of the series and the other factor is the corresponding coefficient of the Legendre series representation of g_S. Hubbell, Lamkin, and Bach [41] have prepared extensive tables of the g_S Legendre coefficients to make such calculations feasible; but tables of Legendre coefficients for the relevant dose angular distributions have never been prepared.

The Legendre coefficient approach needs more attention. It is easy to apply, and has as its main limitation a tendency for the series of products to converge slowly when the angular distribution has a sharp peak, as it often does (figs. 26.1 and 26.3), and when the solid angle fraction of g_S is at the same time small, as it often is. This limitation may prove more apparent than real.

Appendix B. Data for CO⁶⁰ and CS¹³⁷

50. Introductory Comments

Procedures for the calculation of the data represented in the figures B1 through B50 have already been described. The main differences from the fission source data stem from the use of desk computers in that case for some calculations performed by digital computer in the case of Co^{60} and Cs^{137}, the procedures involved not being entirely identical.

The figures given here are in the same sequence as the corresponding fission source figures in the main text; and data for the two source types have been placed adjacent to one another.

No attempt has been made to analyze the obvious similarities between the figures for the different source types. It is clear that many of the geometry factors are quite insensitive to source spectrum.
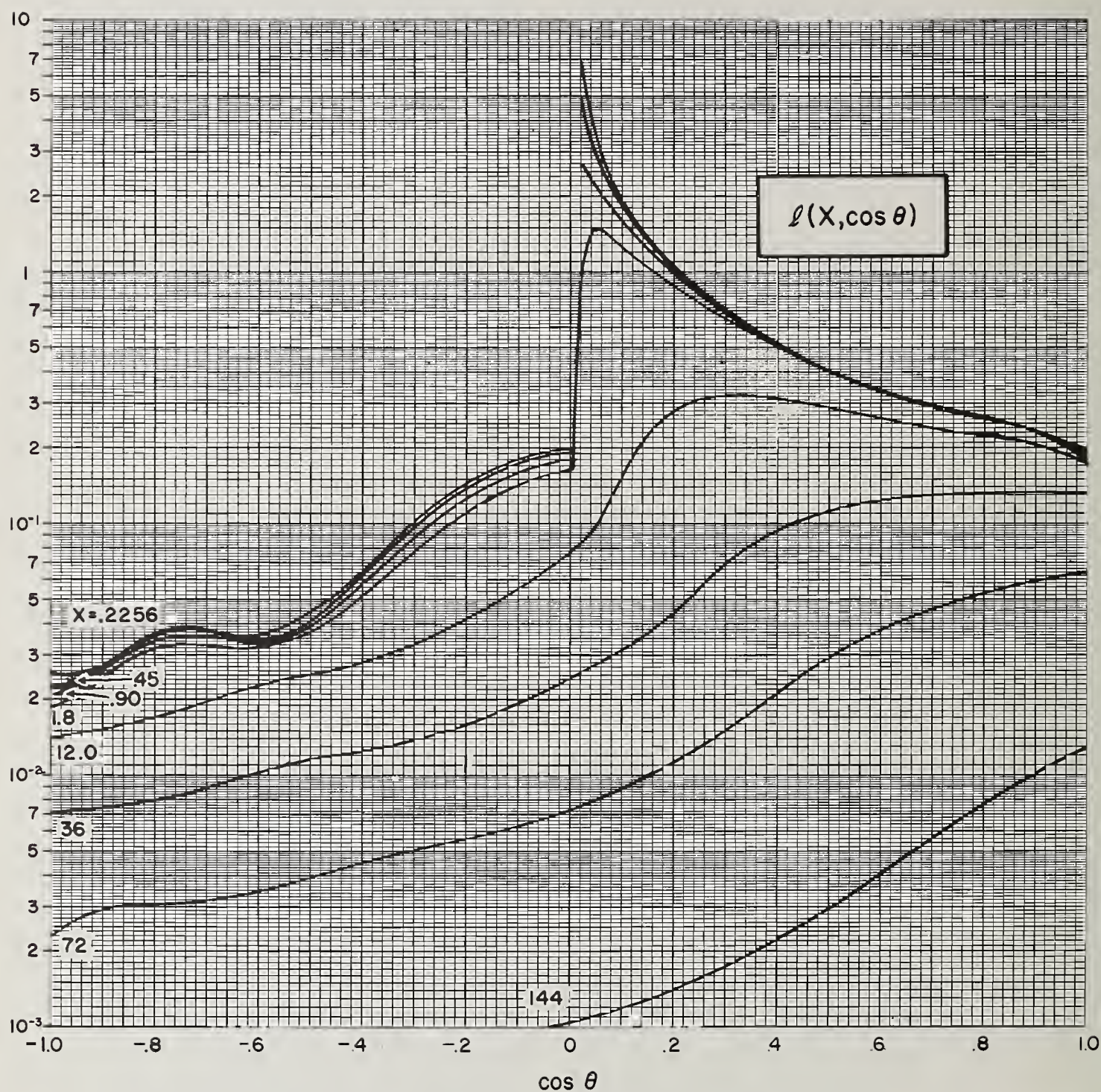
FIGURE B1. *Co–60, concrete.*
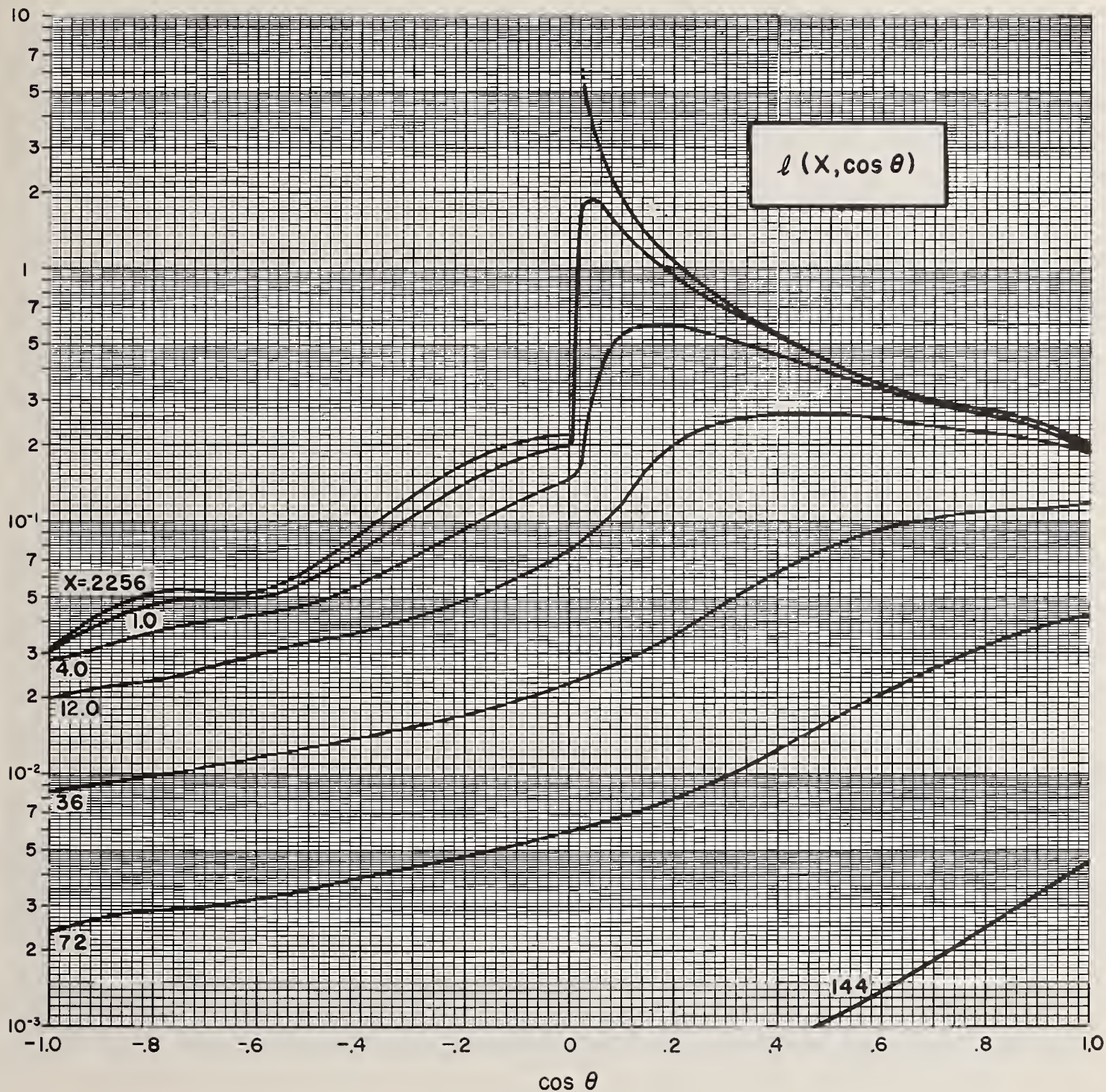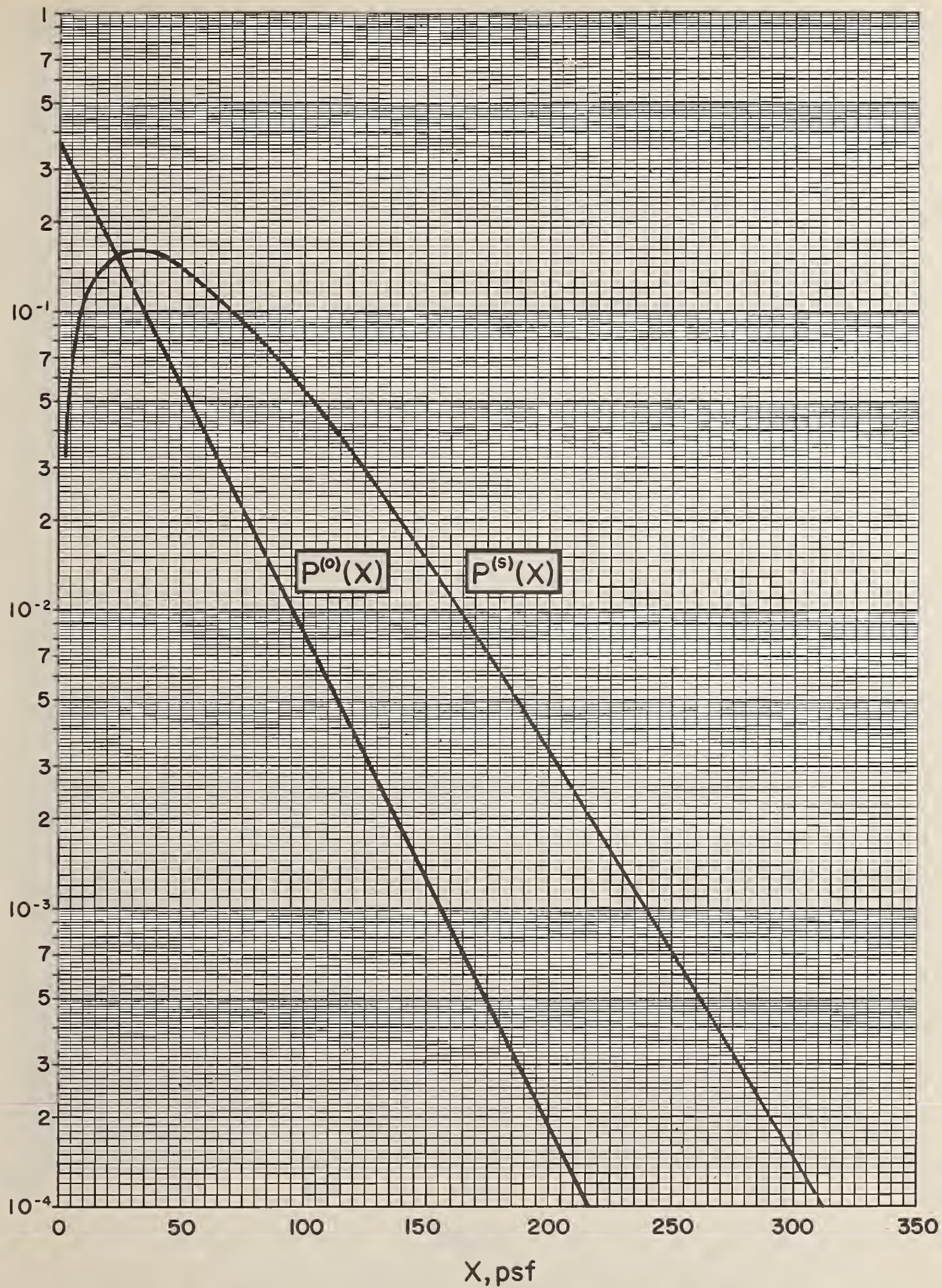
FIGURE B2. Cs–137, concrete.
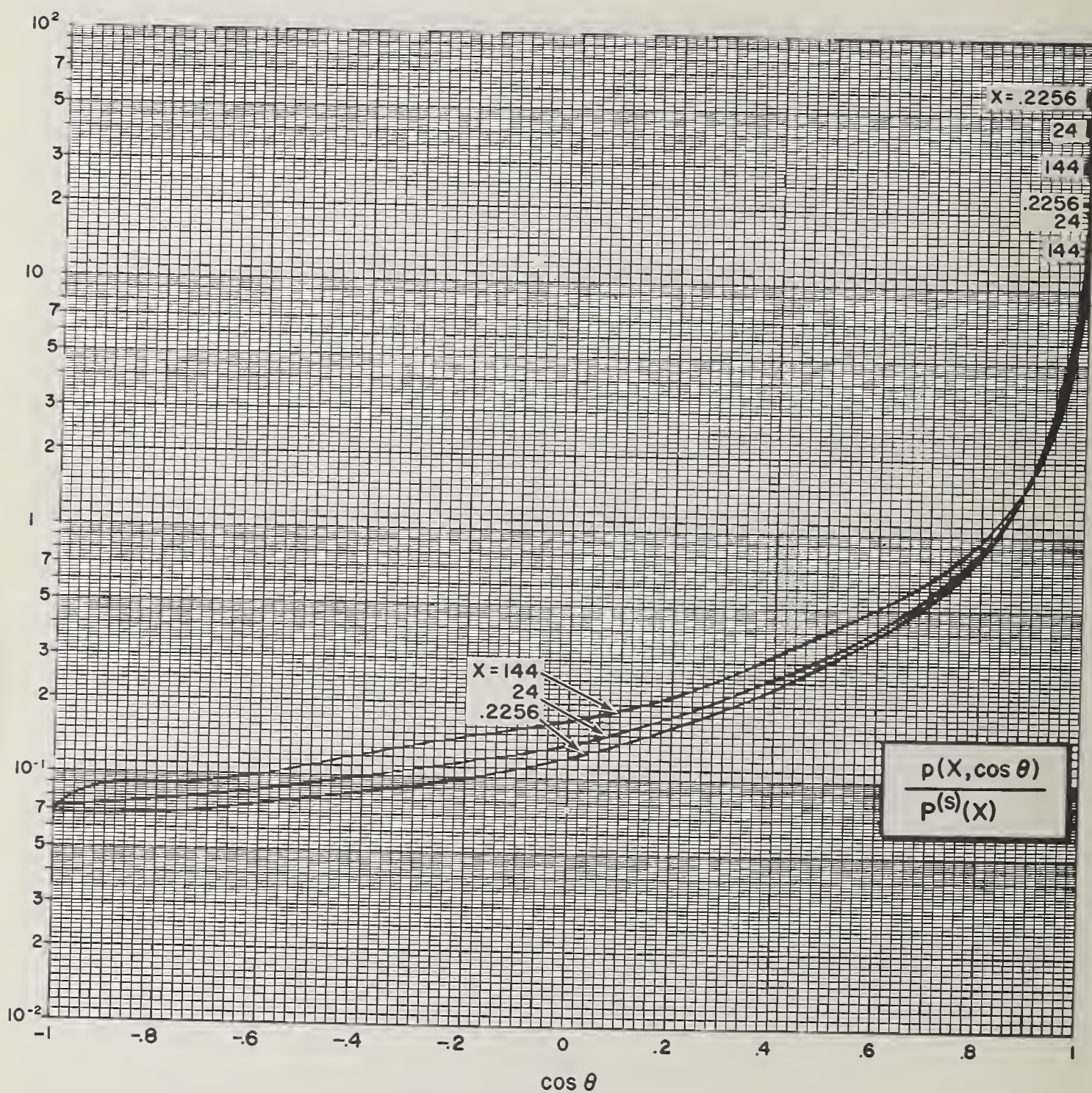
FIGURE B3. *Co–60, concrete.*
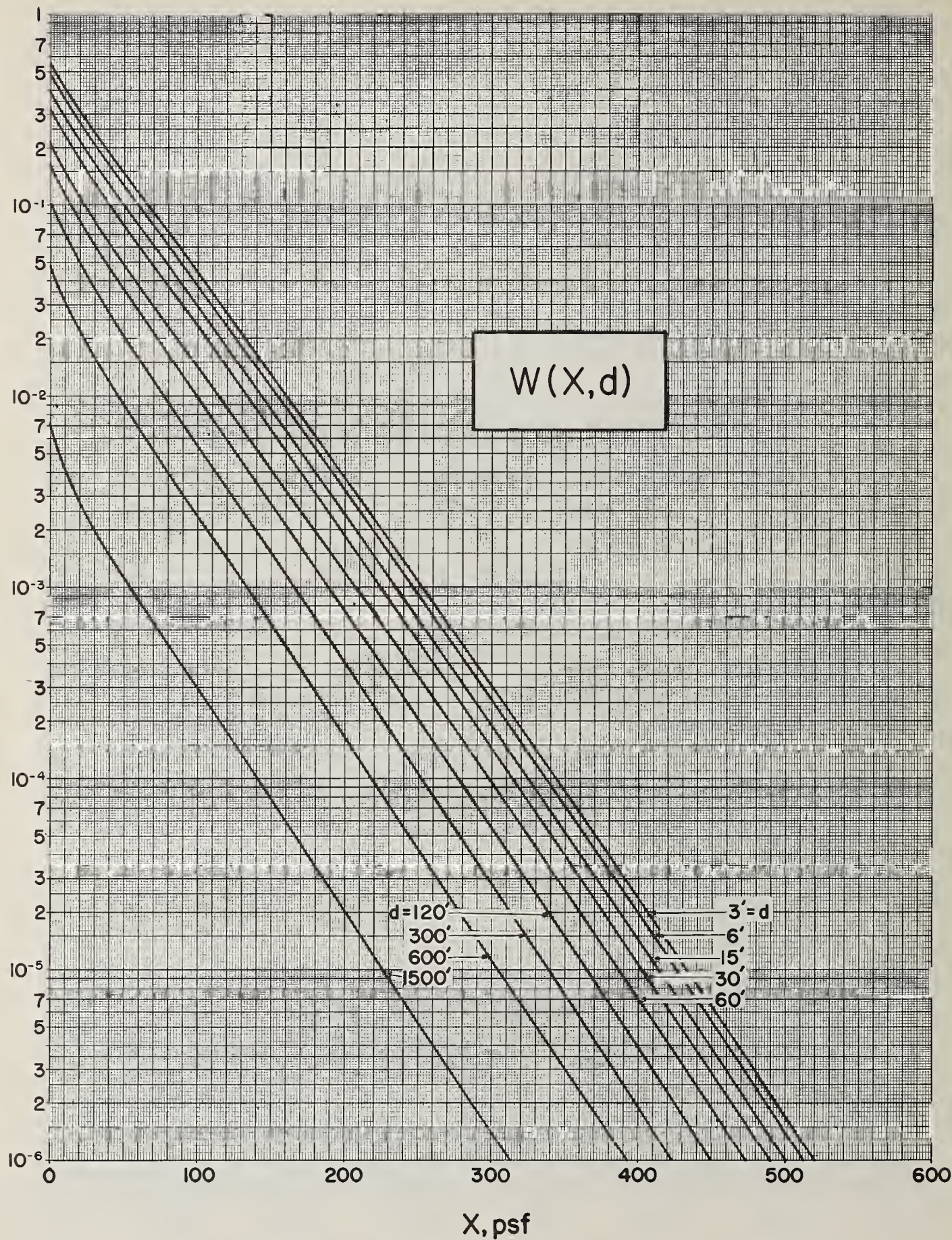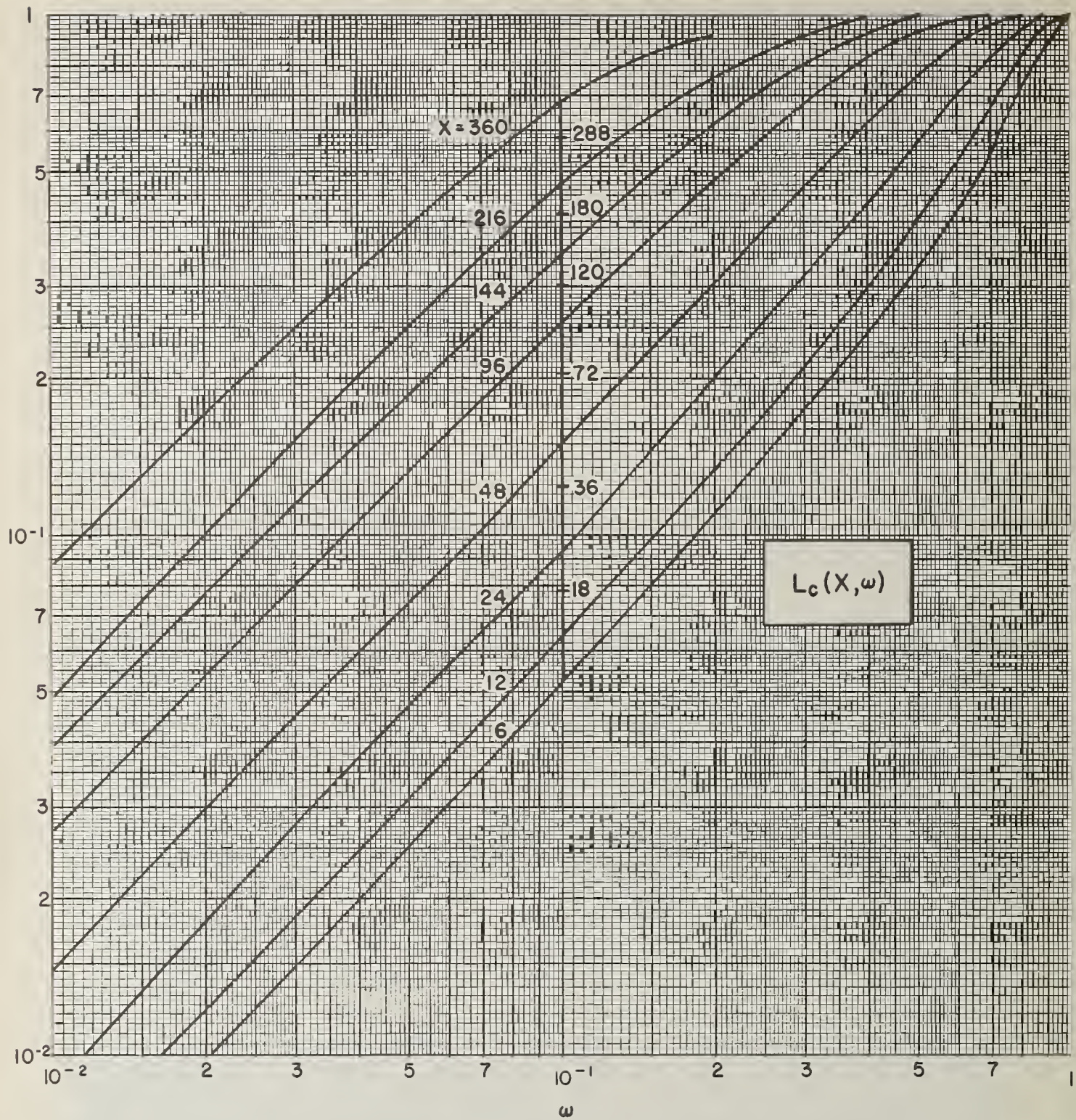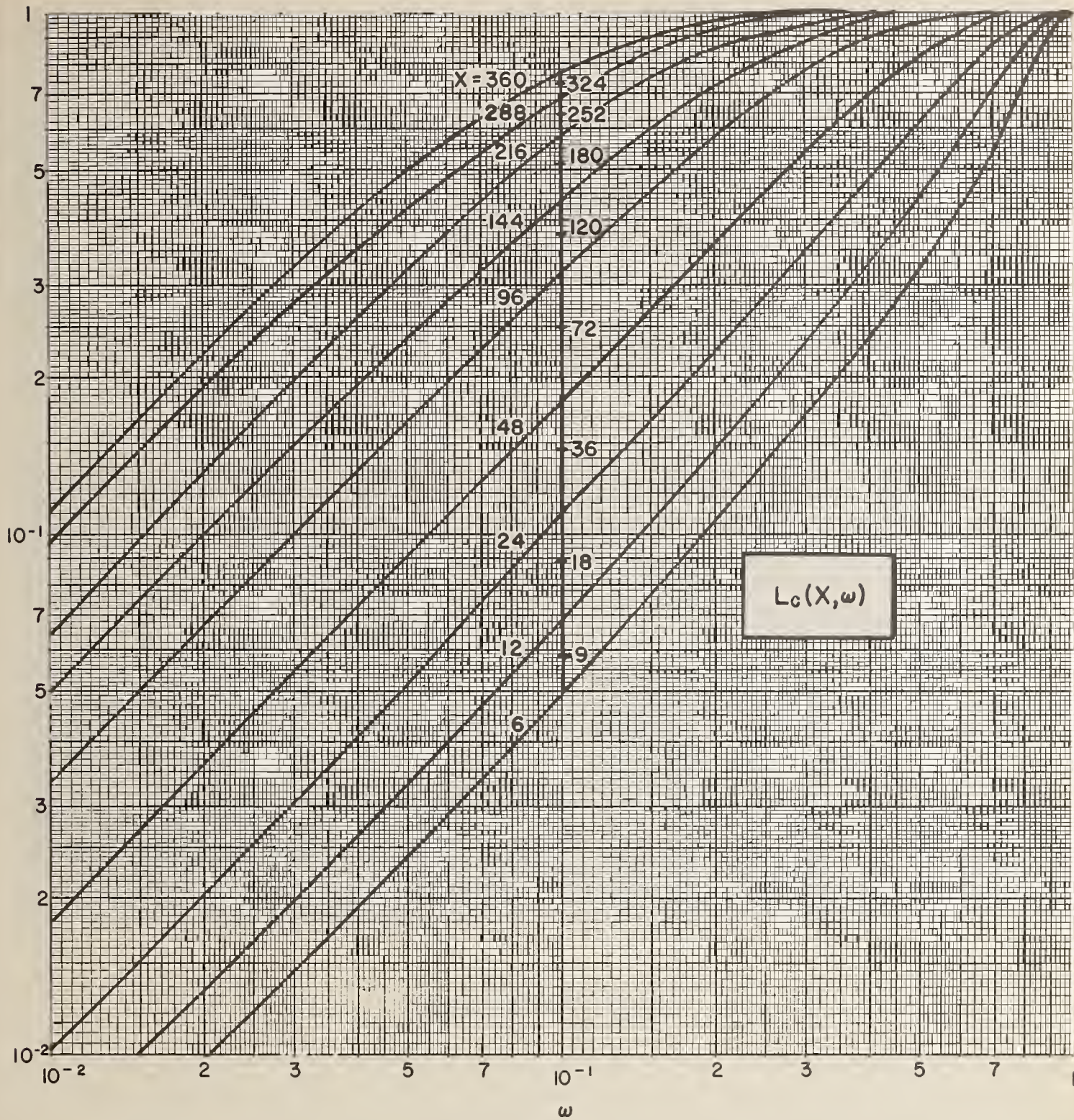
86
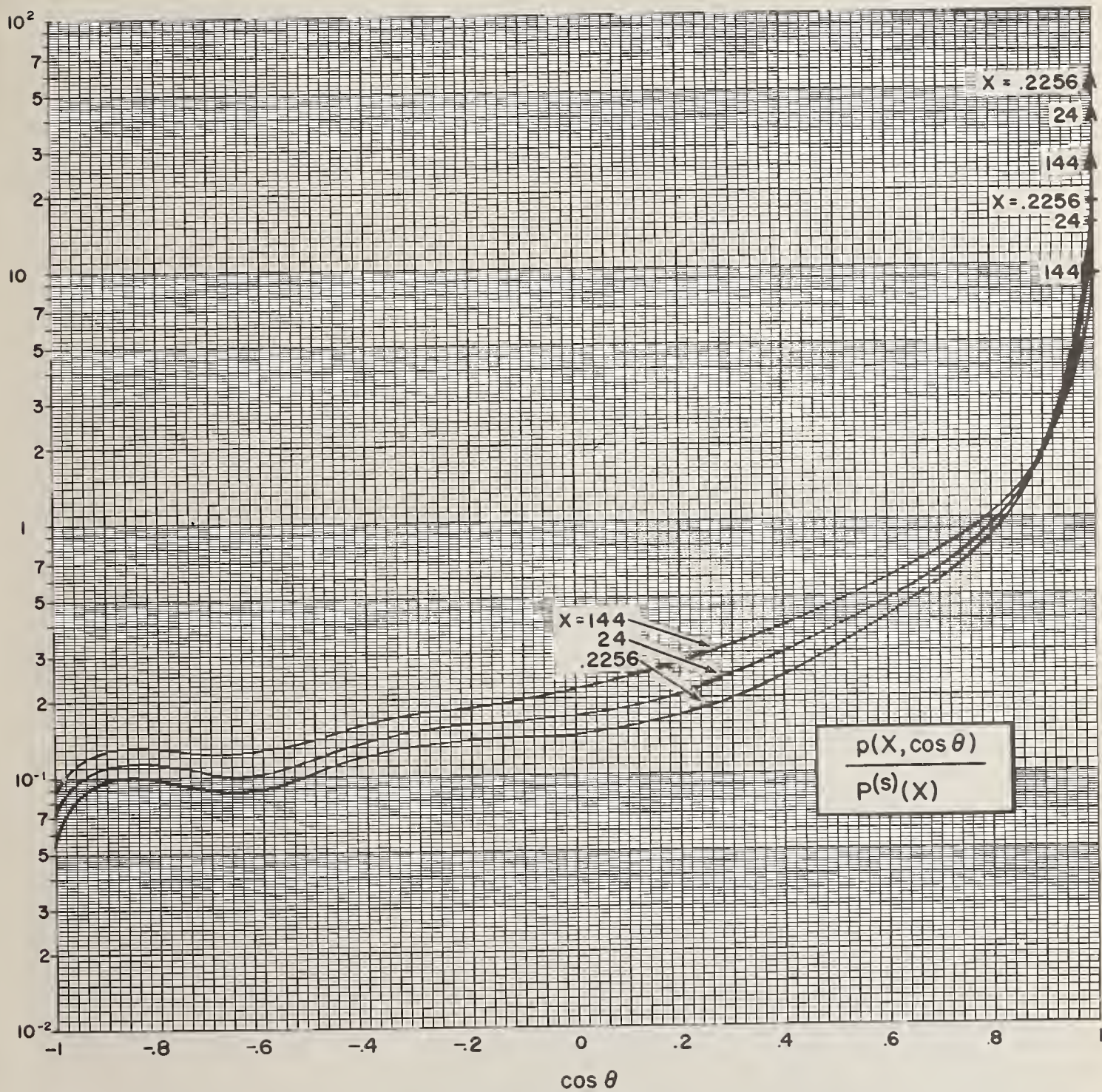
Figure B4. *Cs-137, concrete.*

$$\cos\theta_o s(X, \cos\theta_o)$$
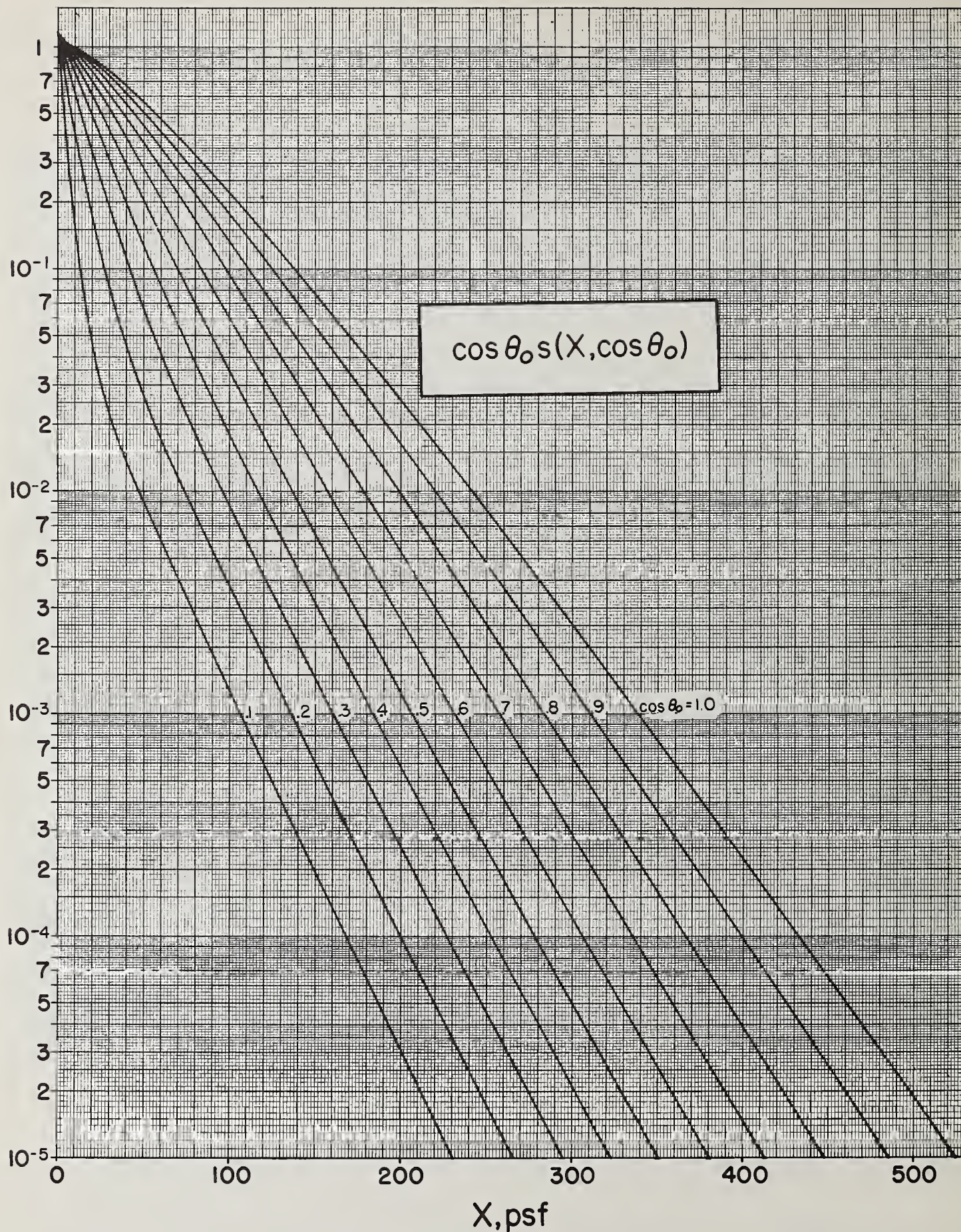
FIGURE B5. *Co–60, concrete.*

88
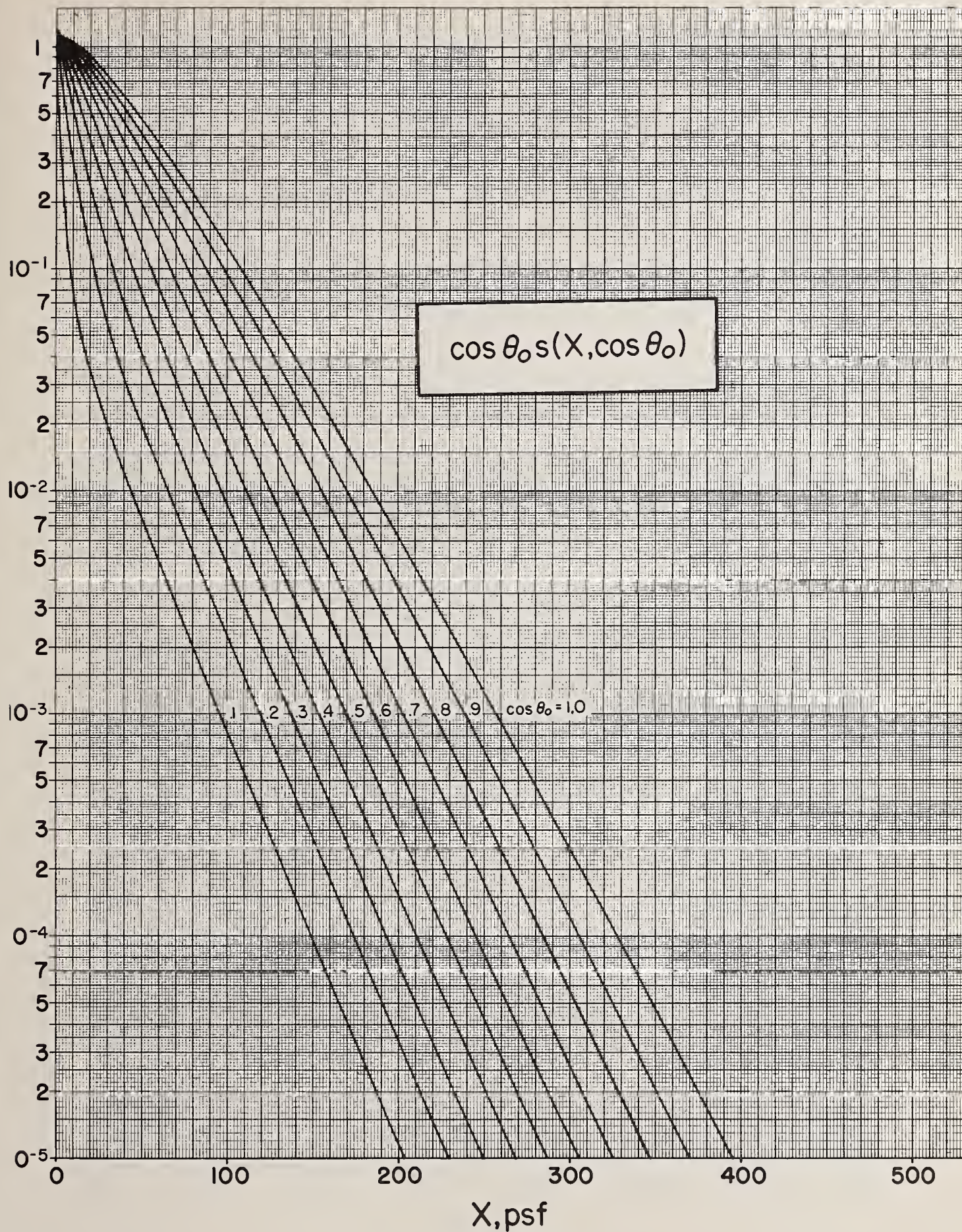
FIGURE B6. *Cs–137, concrete.*
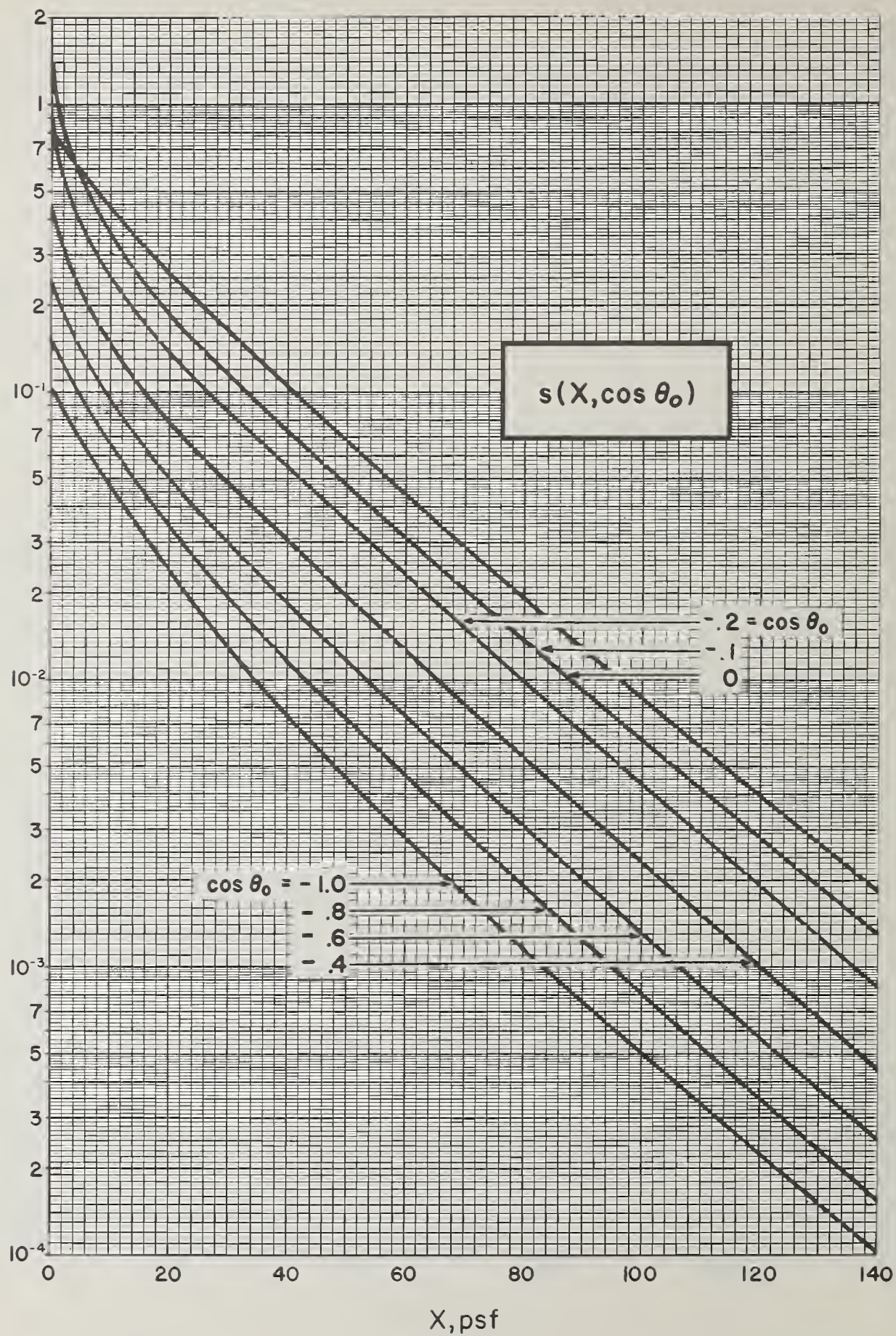
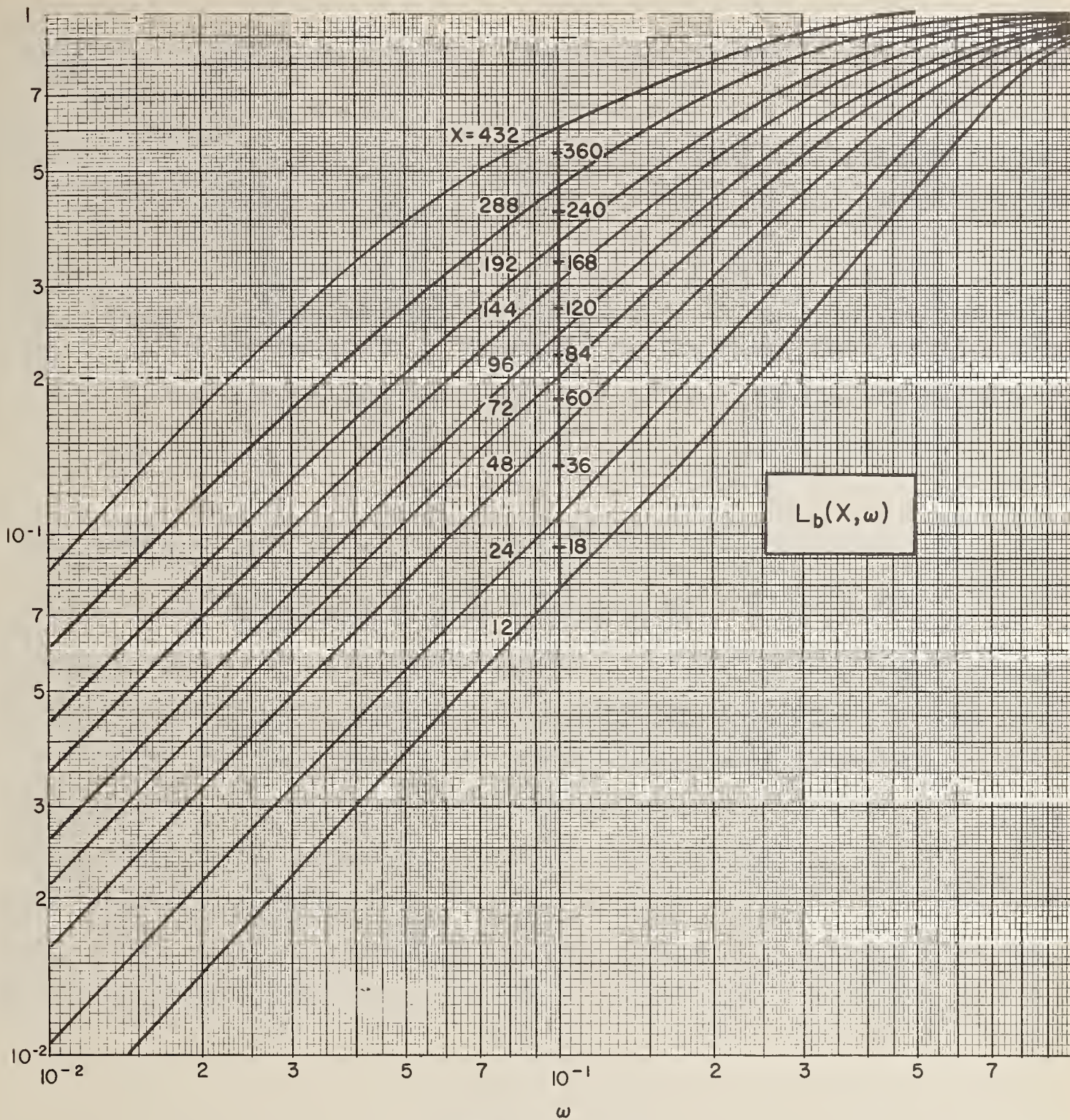FIGURE B7. *Co–60, concrete.*

90
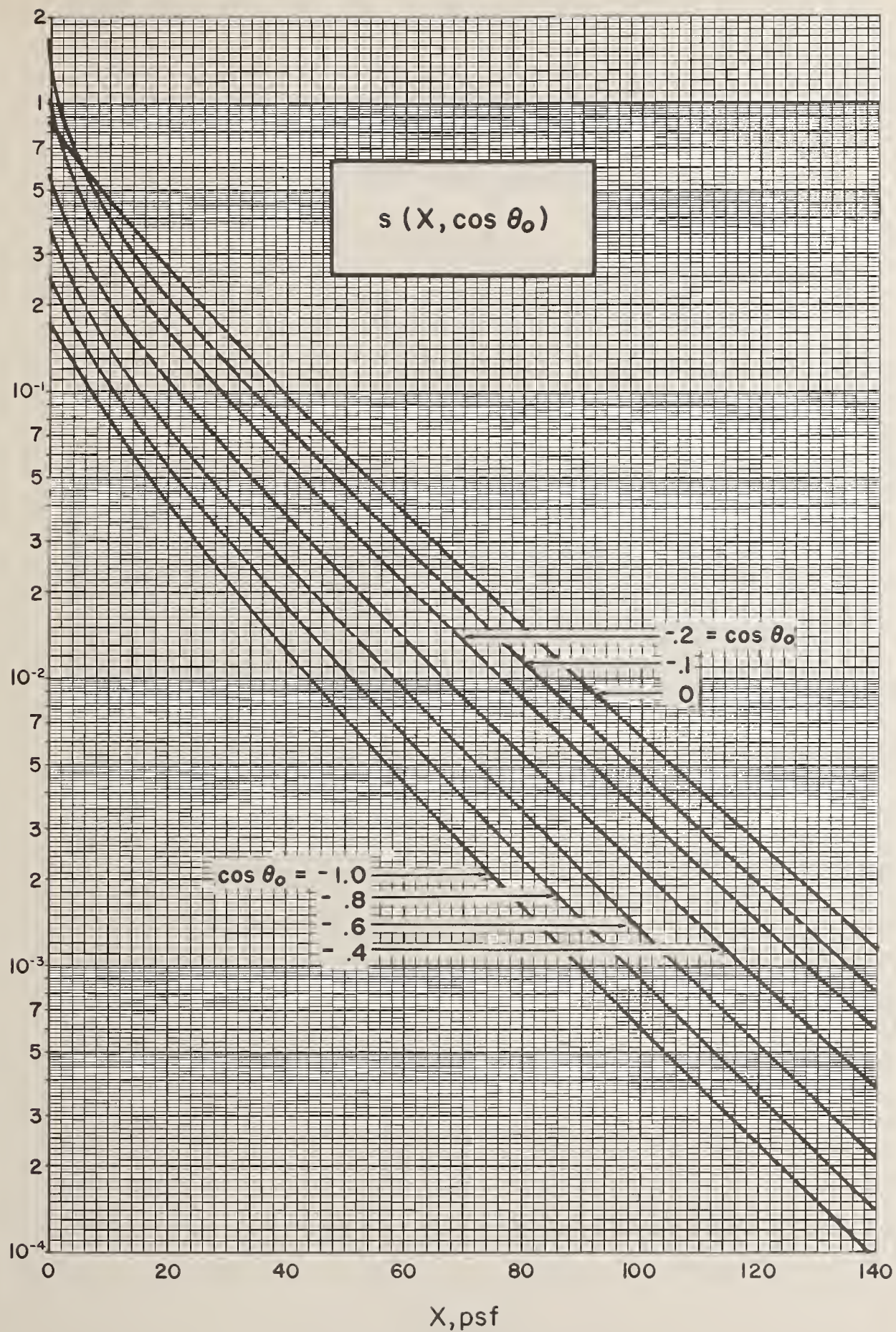
FIGURE B8. *Cs-137, concrete.*
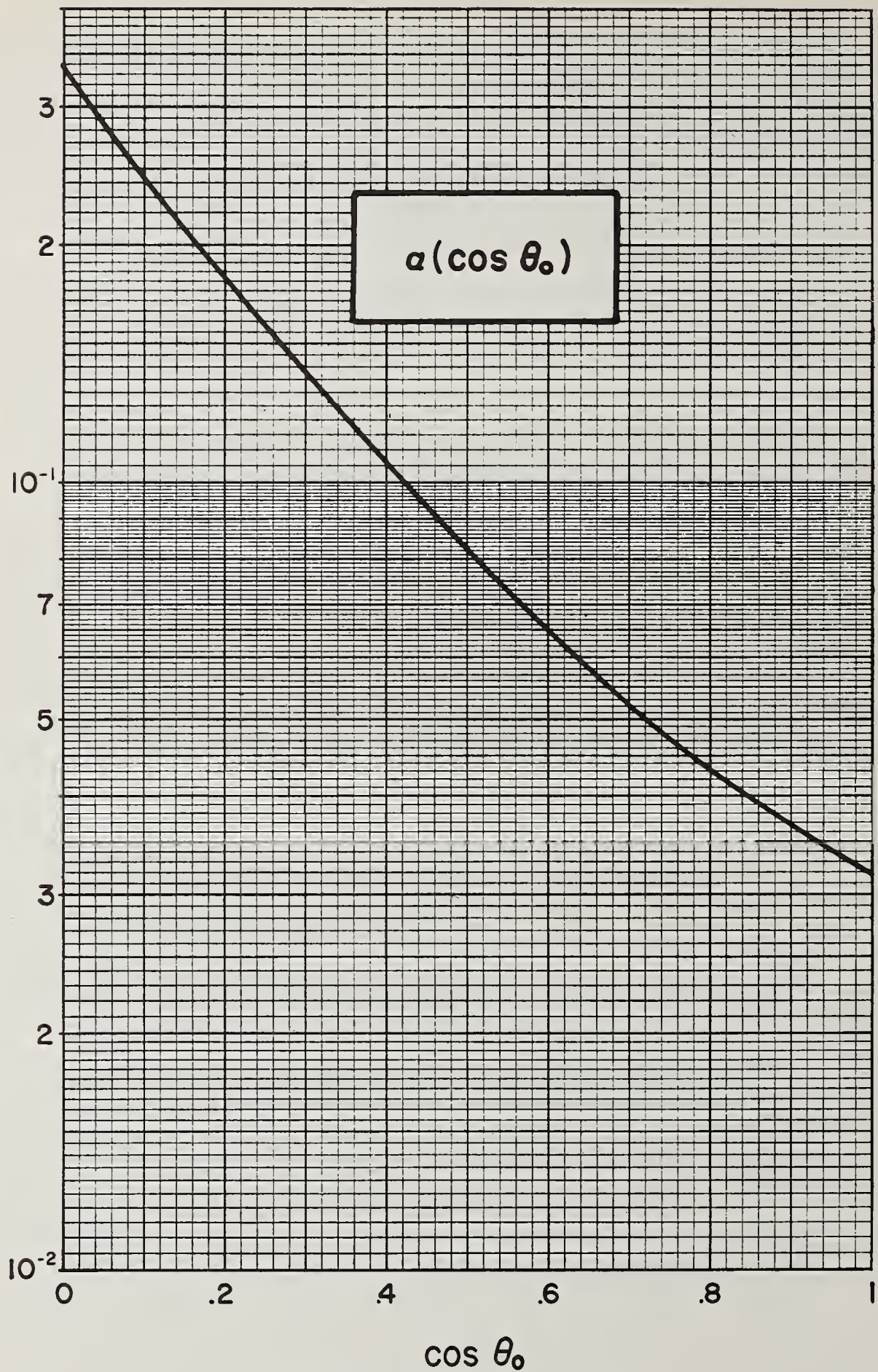
FIGURE B9. *Co–60, backscatter from concrete.*
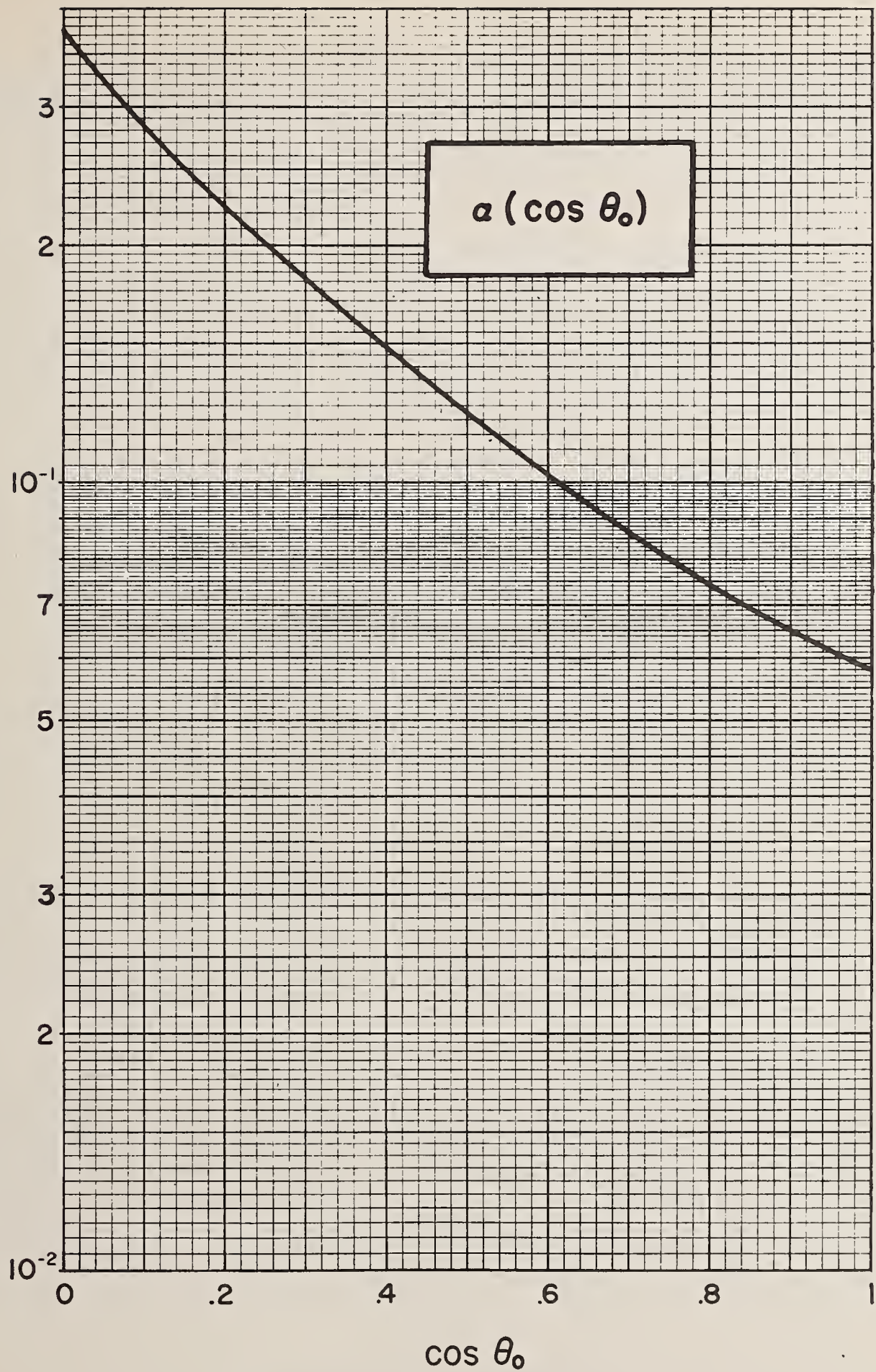
FIGURE B10. *Cs–137, backscatter from concrete.*
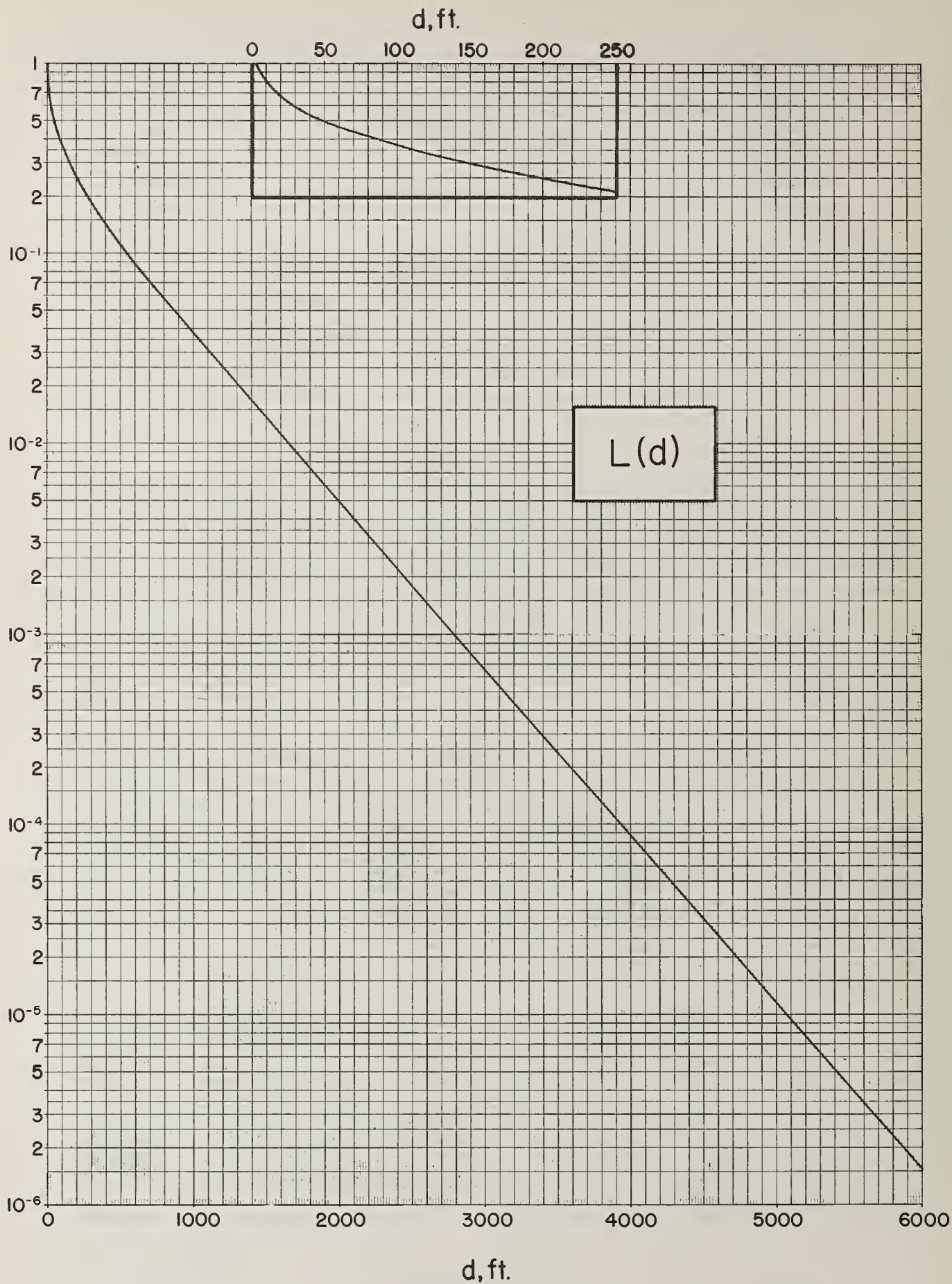
FIGURE B11. *Co-60, H₂O.*

94
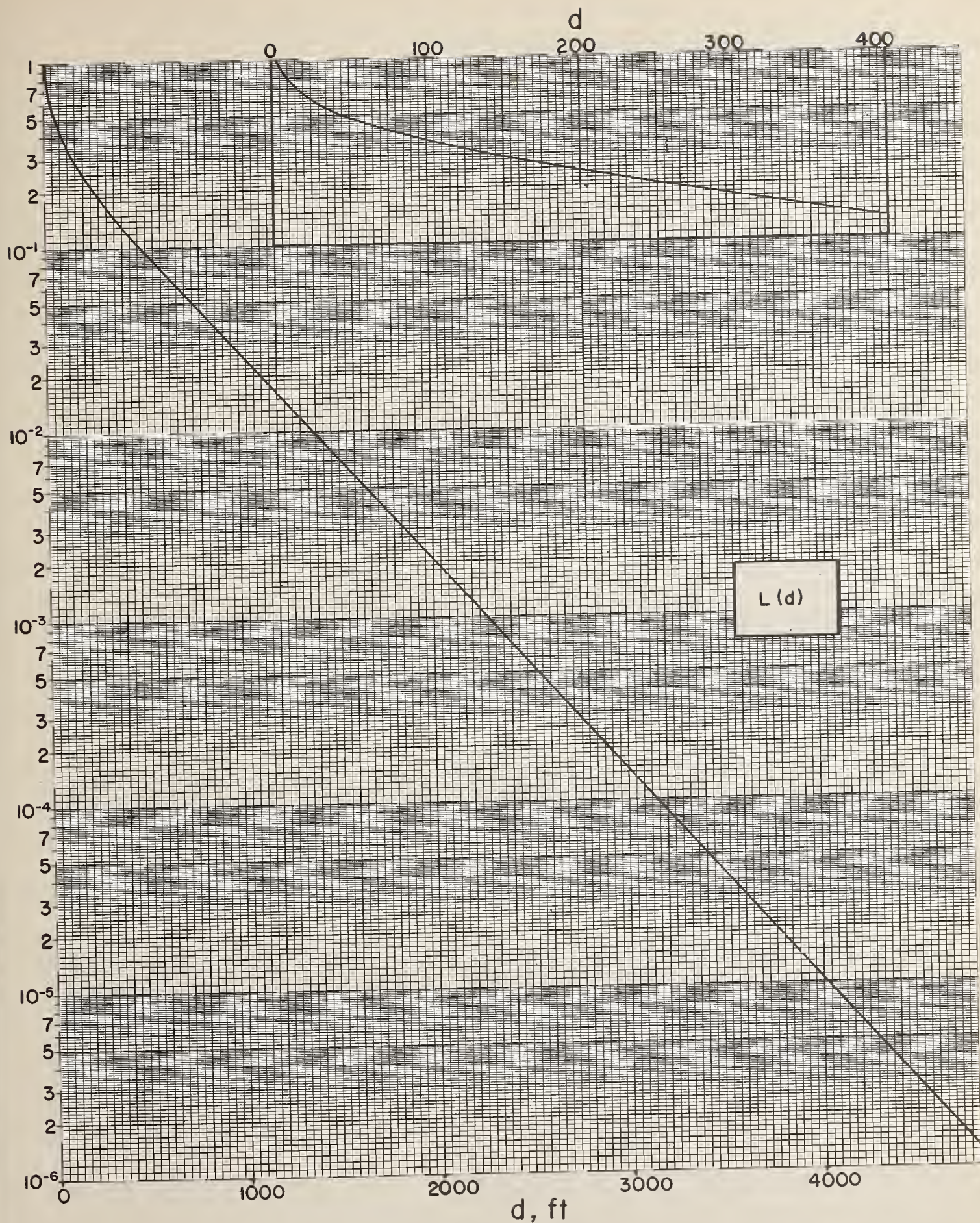
FIGURE B12. Cs–137, H₂O.

95
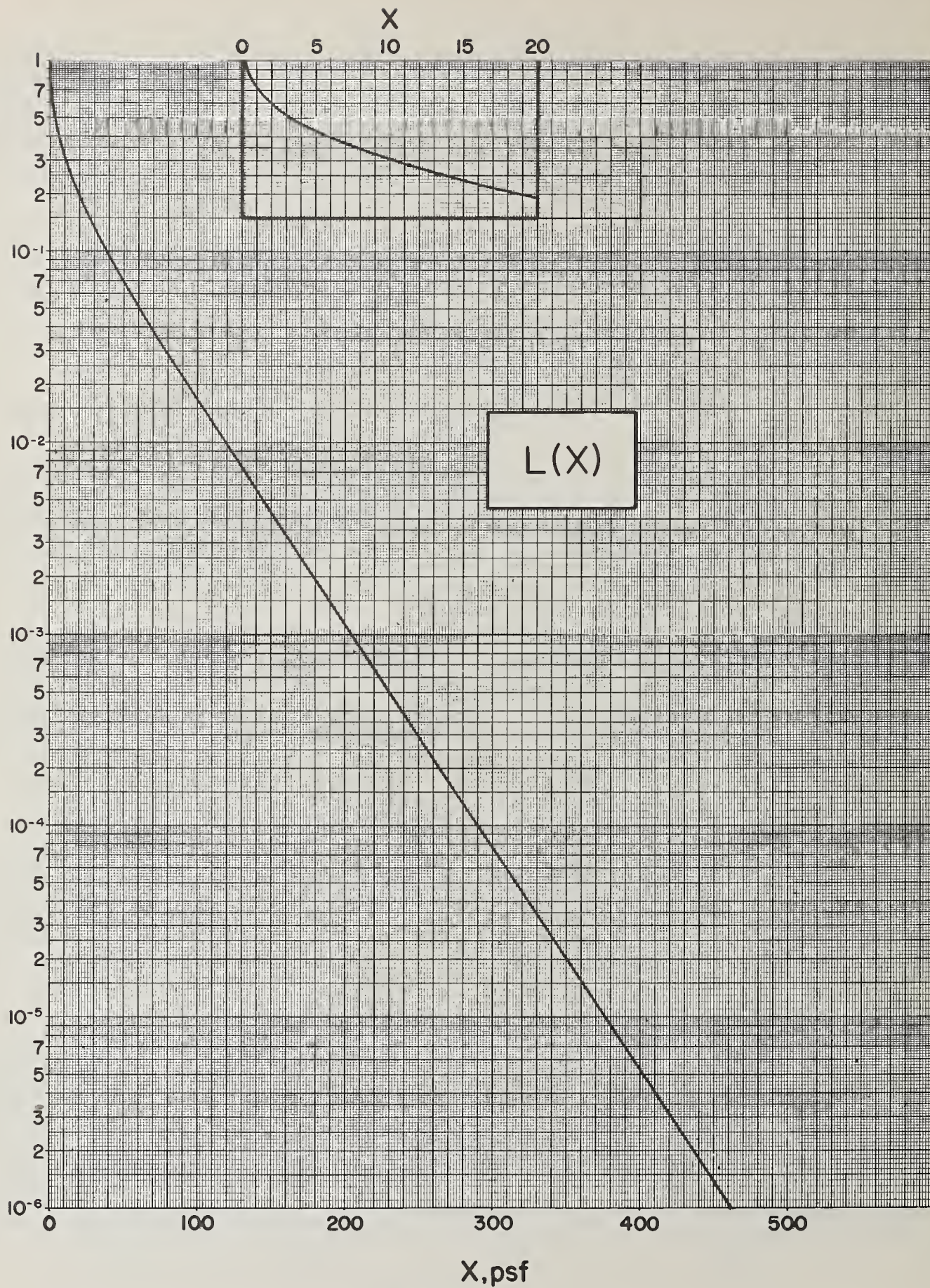
FIGURE B13. *Co–60, concrete.*

96
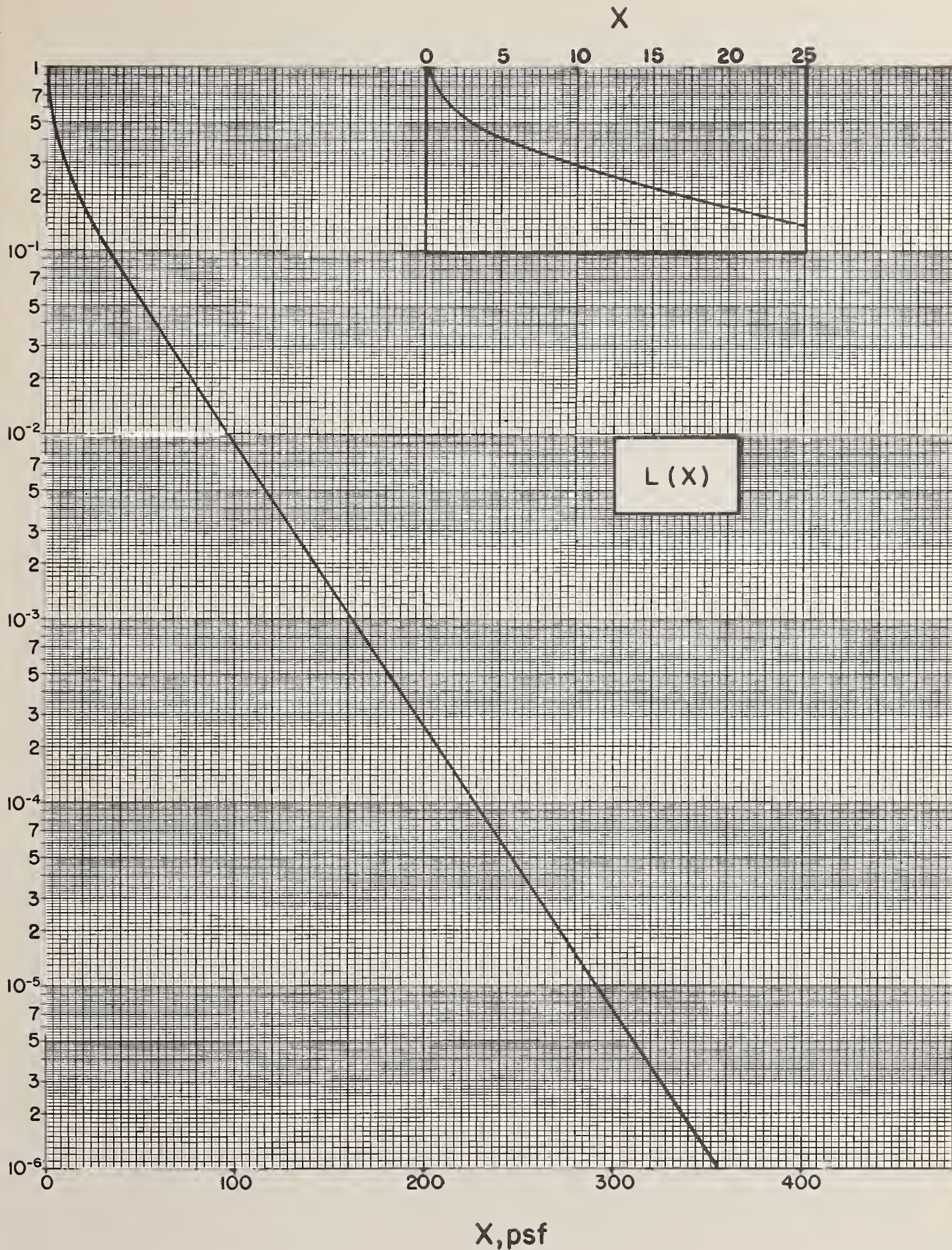
Figure B14. *Cs-137, concrete.*
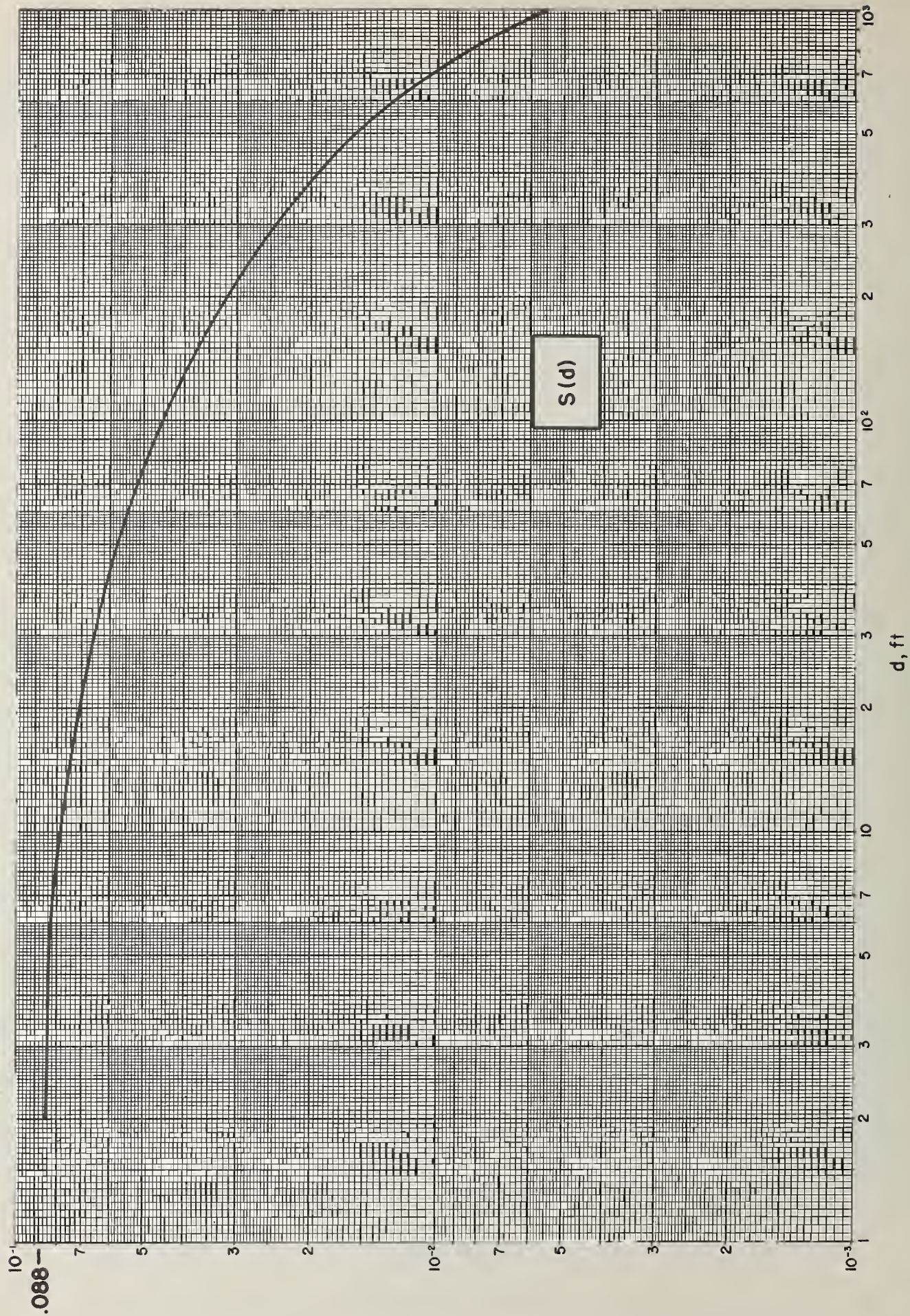
FIGURE B15. *Co–60, H₂O.*

S (d)

d, ft

98

S(d)
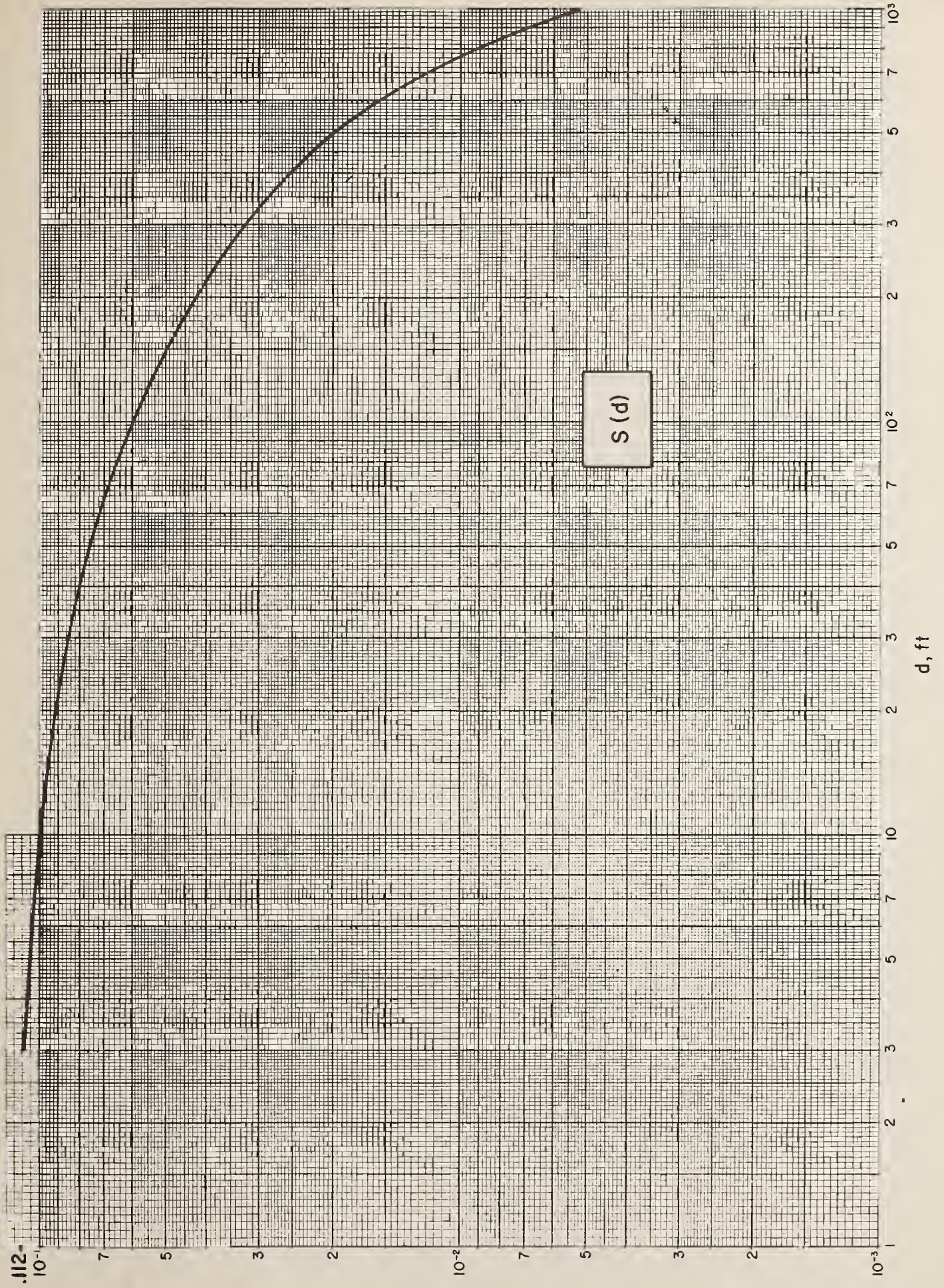
FIGURE B16. *Cs–137*, *H₂O*.

99
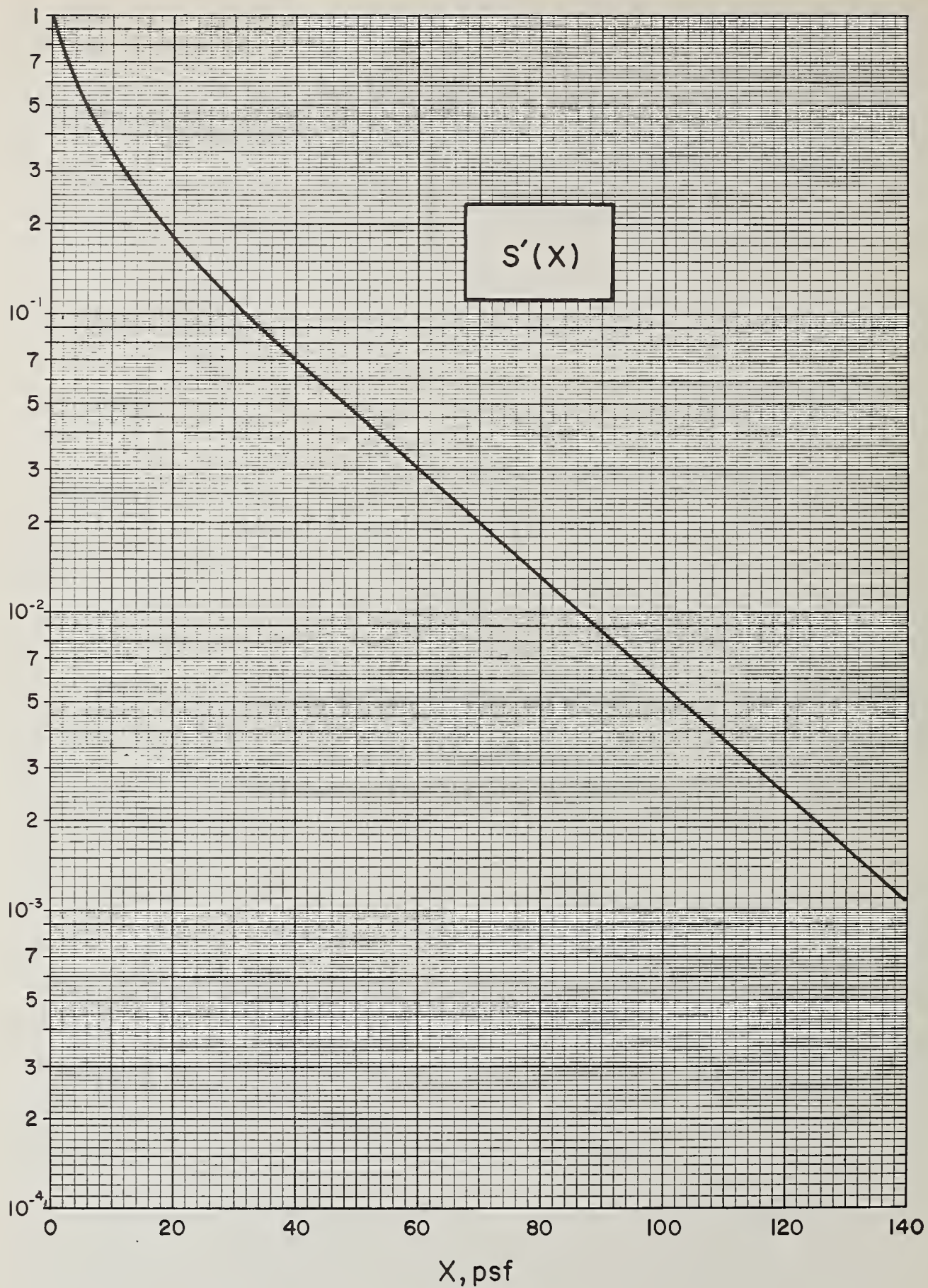
FIGURE B17. *Co–60, concrete.*

100
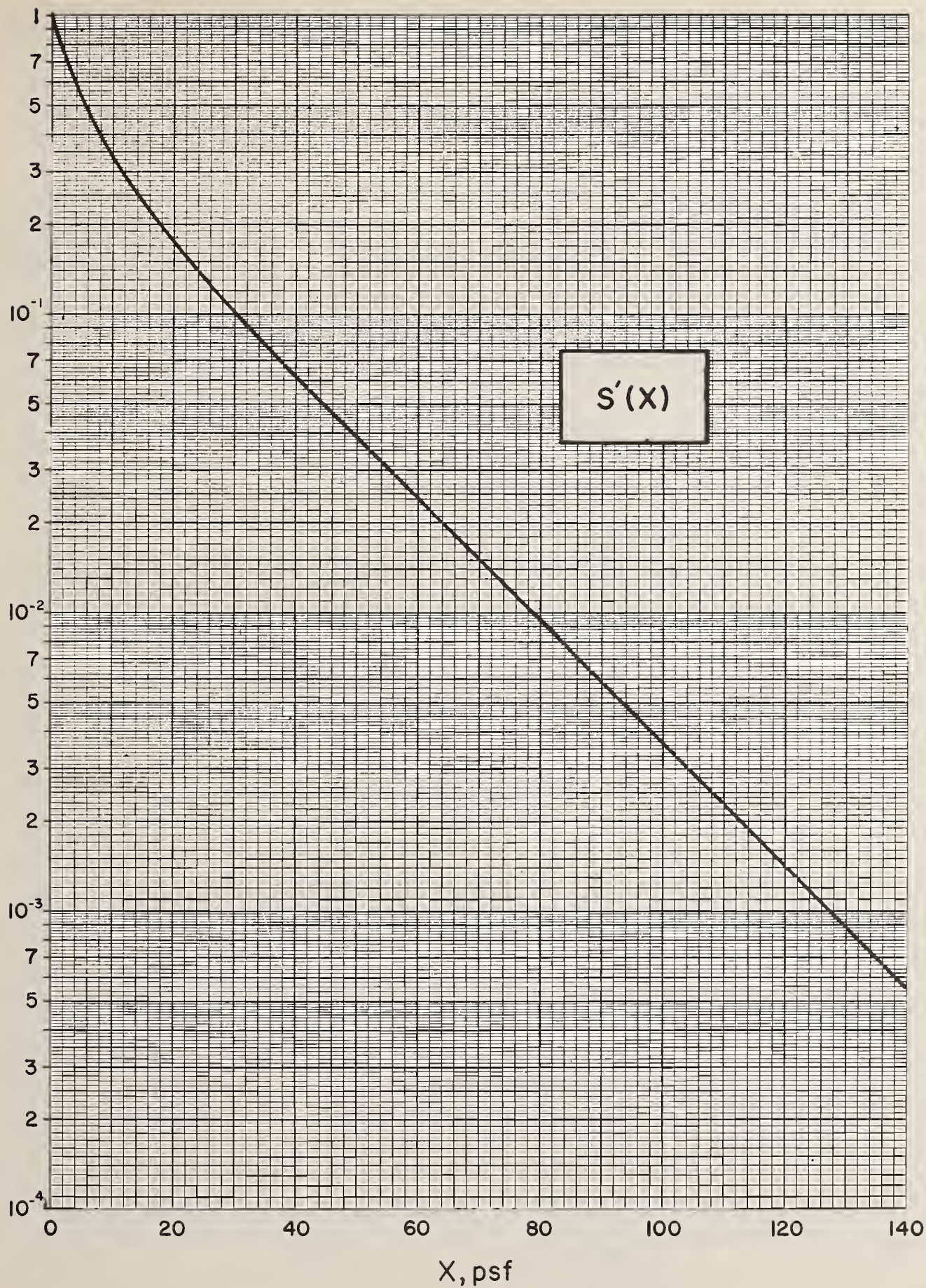
FIGURE B18. *Cs-137, concrete.*
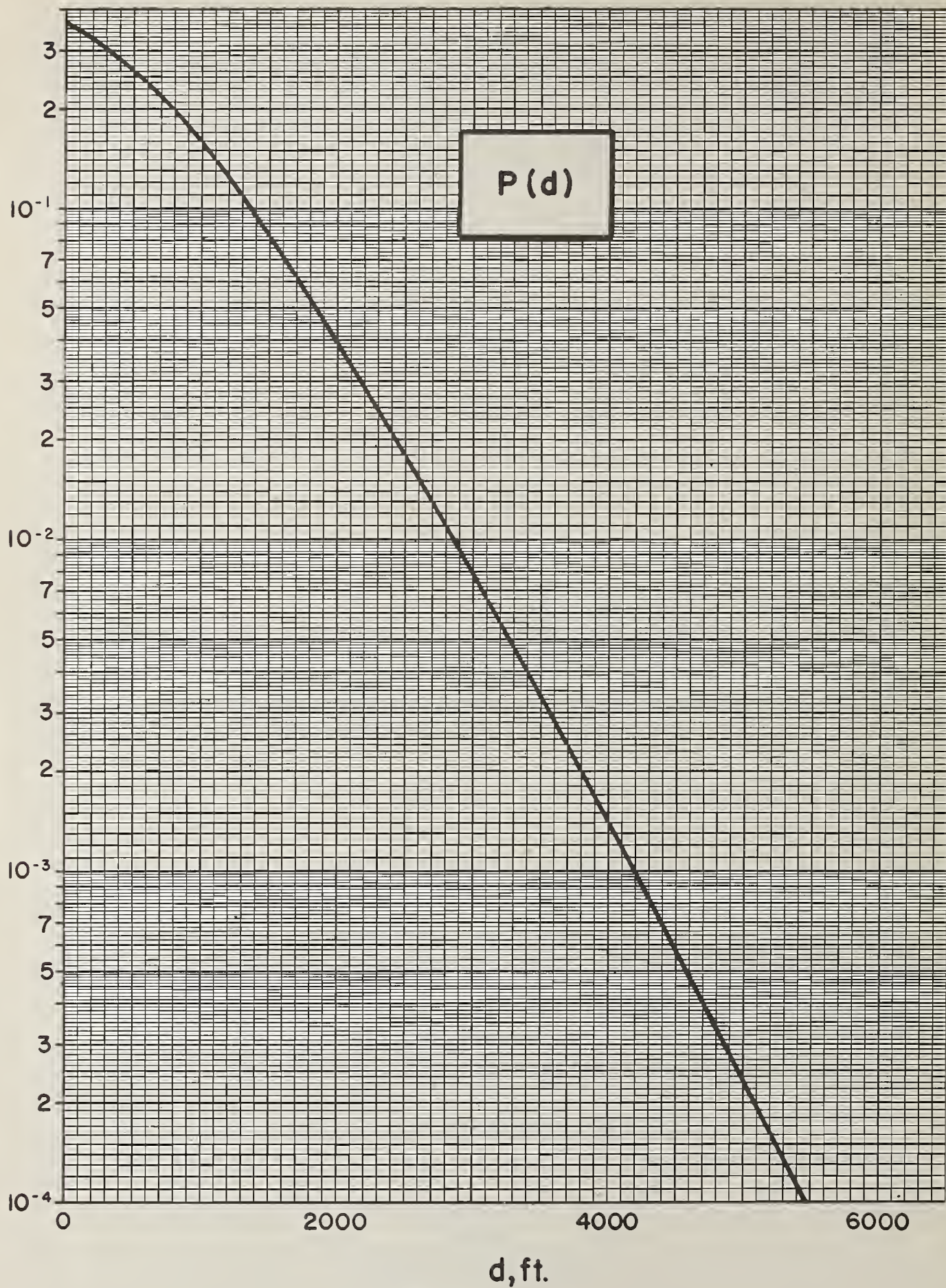
FIGURE B19. *Co–60, H₂O.*
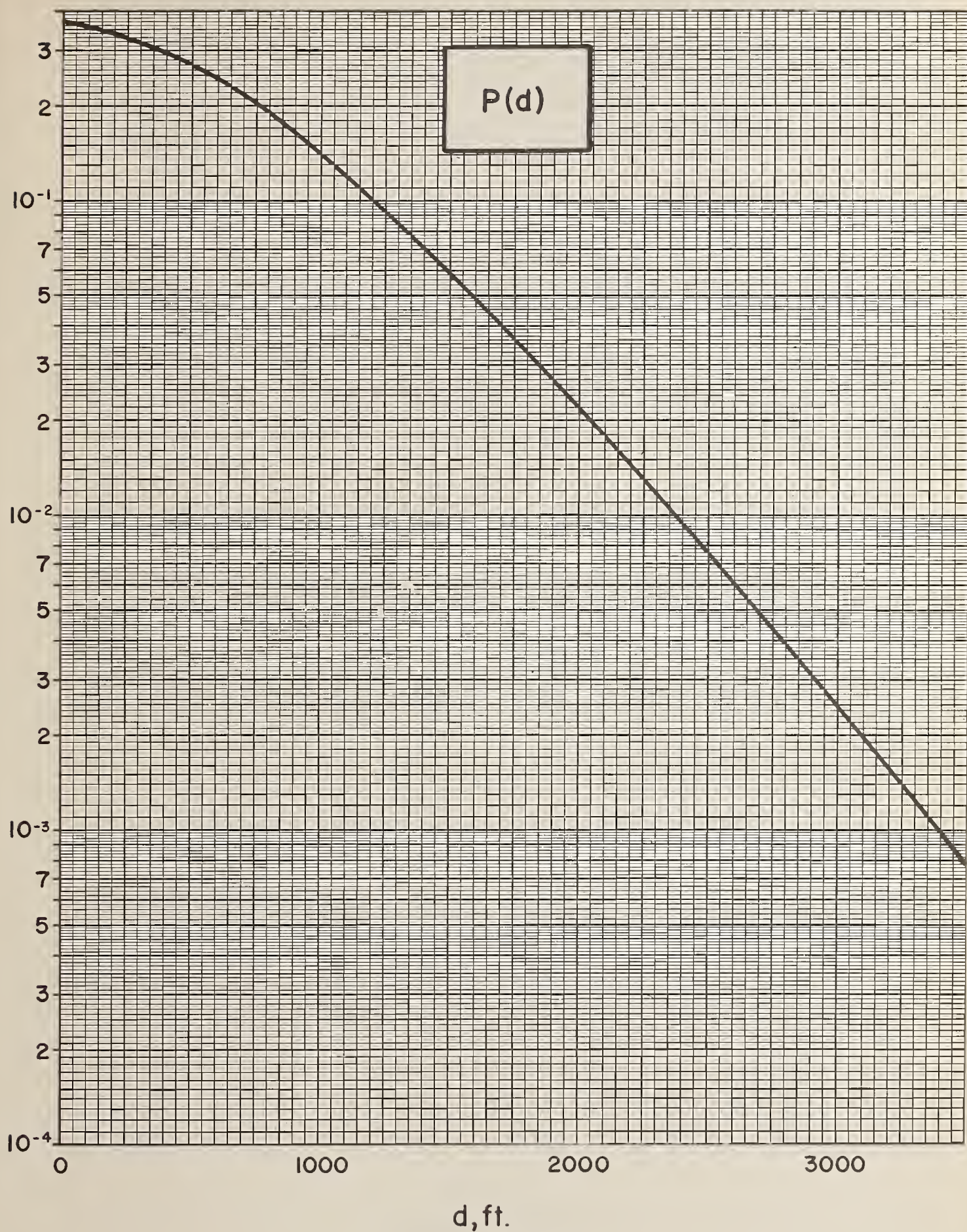
FIGURE B20. *Cs-137, H₂O.*
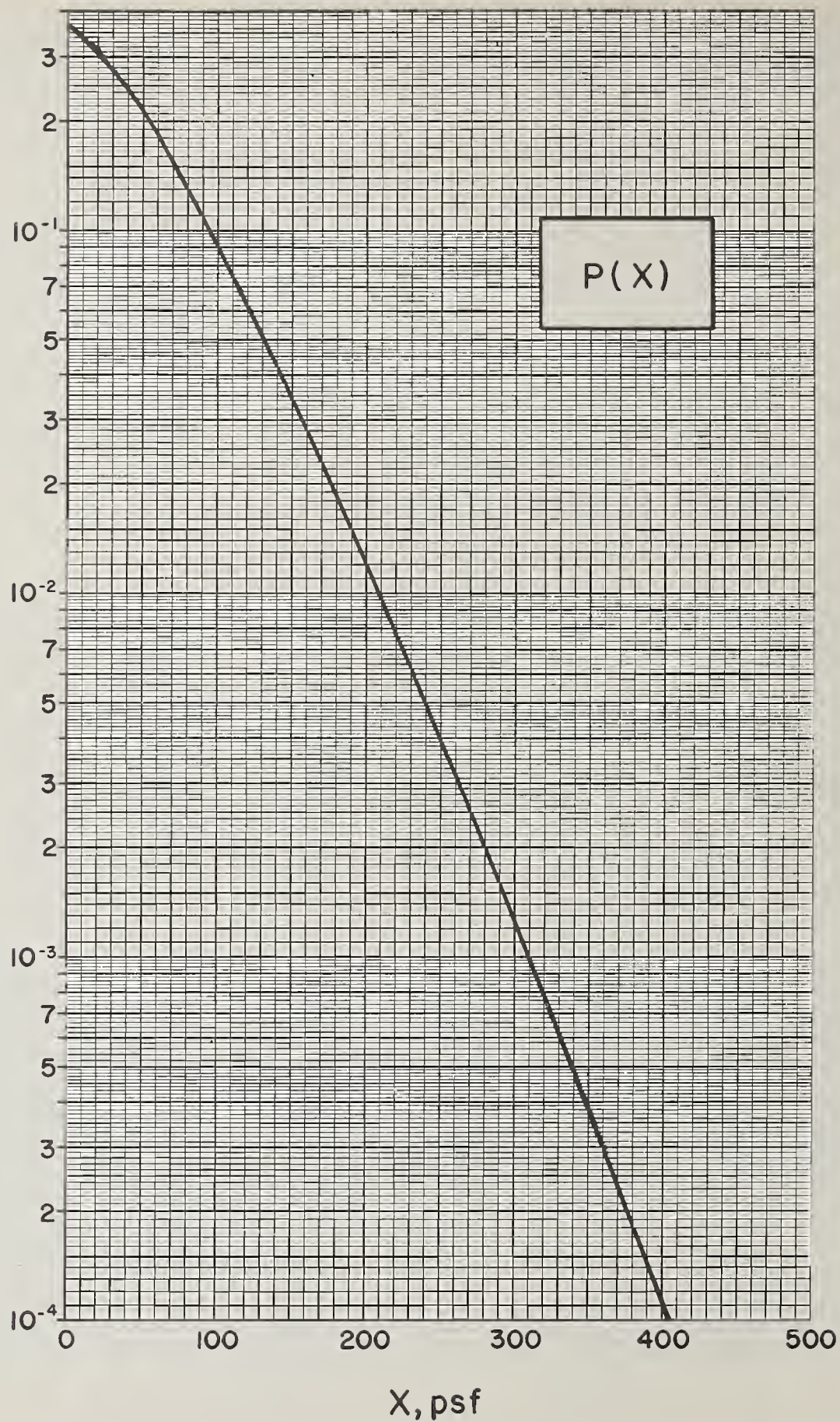
FIGURE B21. *Co-60, concrete.*
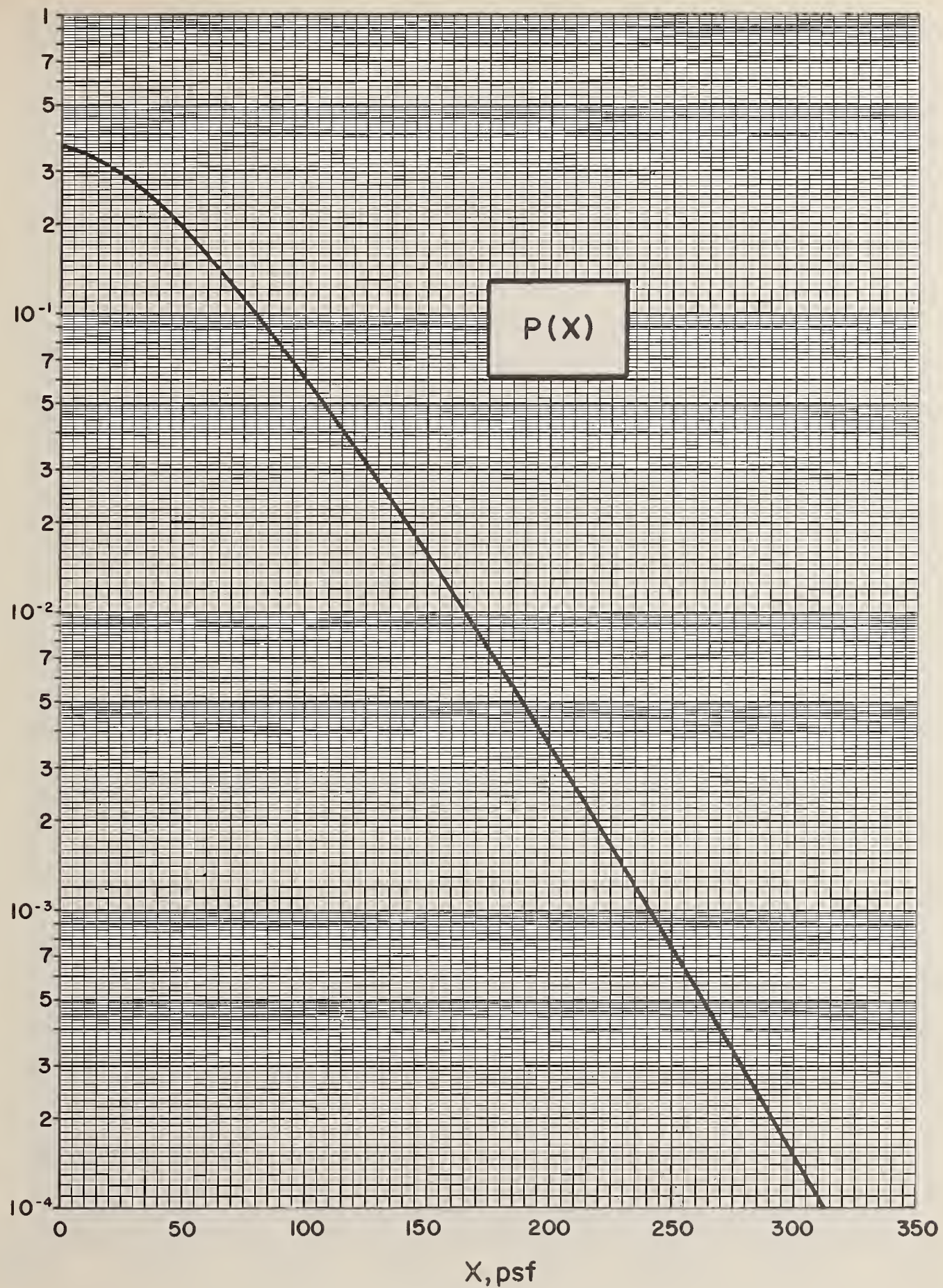
FIGURE B22. *Cs–137, concrete.*
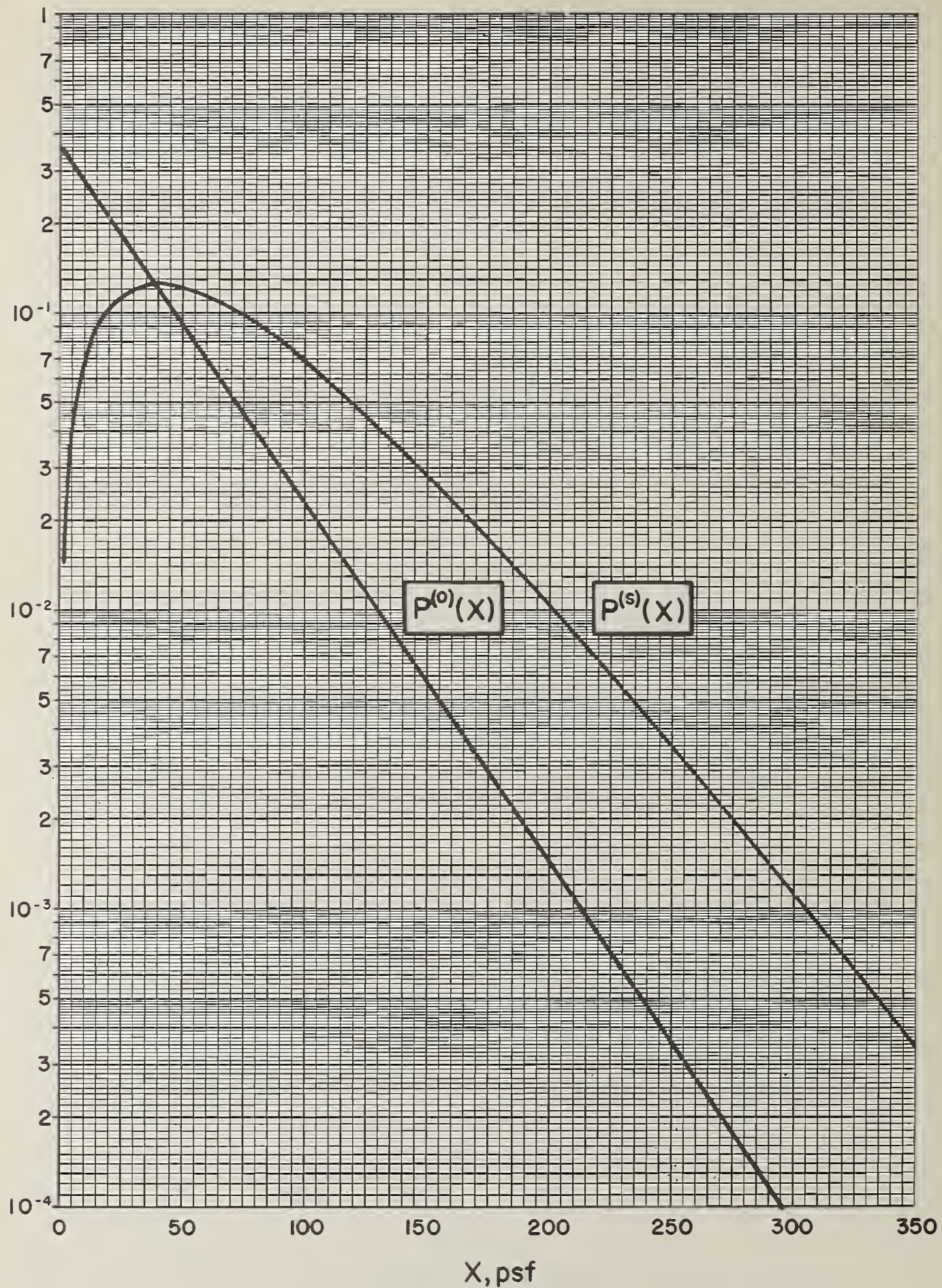
FIGURE B23. Co–60, concrete.

106

FIGURE B24. *Cs-137, concrete.*

107

FIGURE B25. *Co–60, H₂O data for l(d,cosθ), concrete data for s(X,cosθ₀).*

W(X,d)

X,psf

d = 150
300
600
1500

3' = d
6'
15'
30'
60'
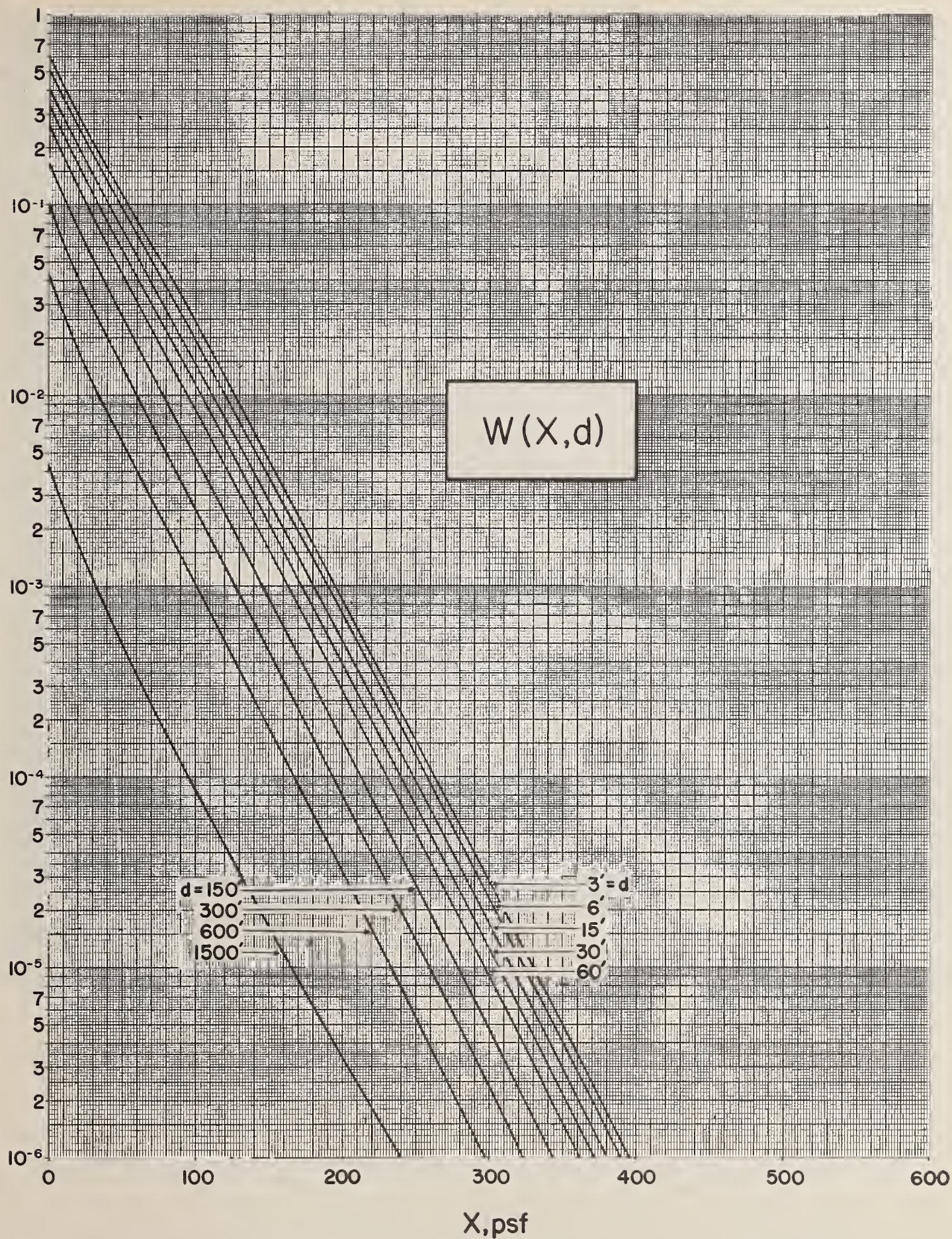
FIGURE B26. *Cs–137, H_2O data for $l(d,cos\theta)$, concrete data for $s(X,cos\theta_0)$.*

FIGURE B27. *Co–60, concrete.*

FIGURE B28. *Cs–137, concrete.*
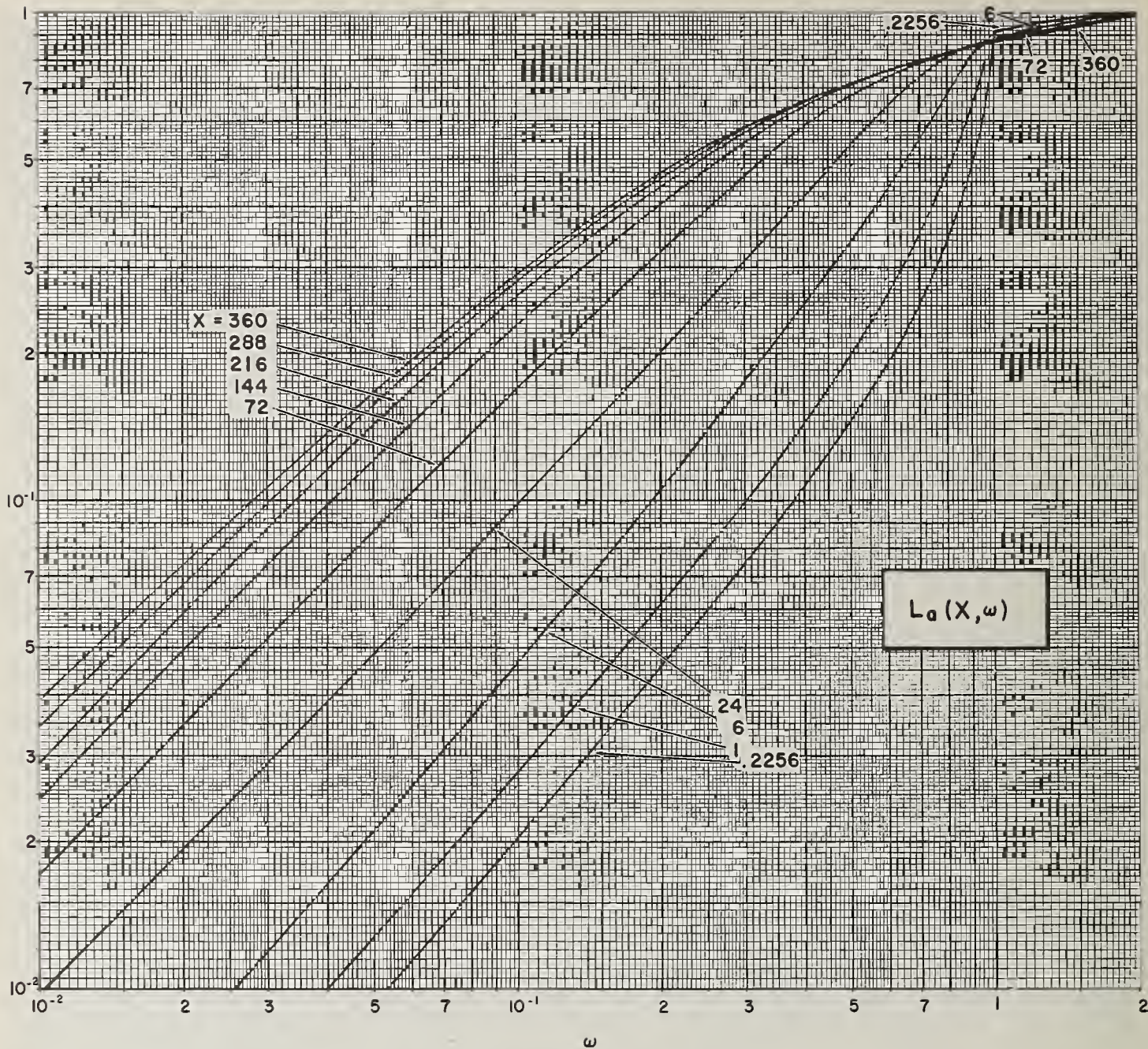
FIGURE B29. *Co–60, concrete.*

112
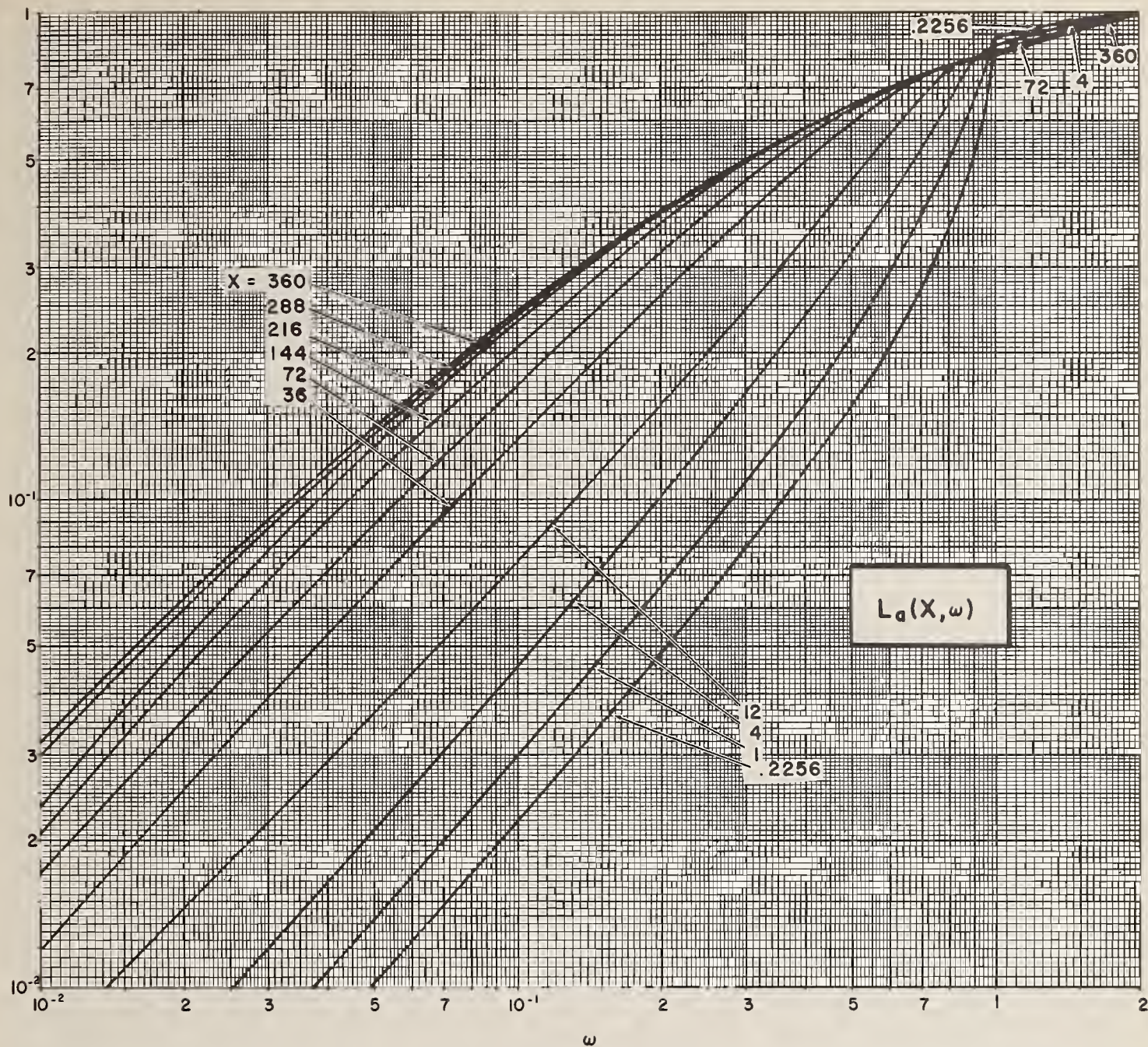
FIGURE B30. *Cs–137, concrete.*

113
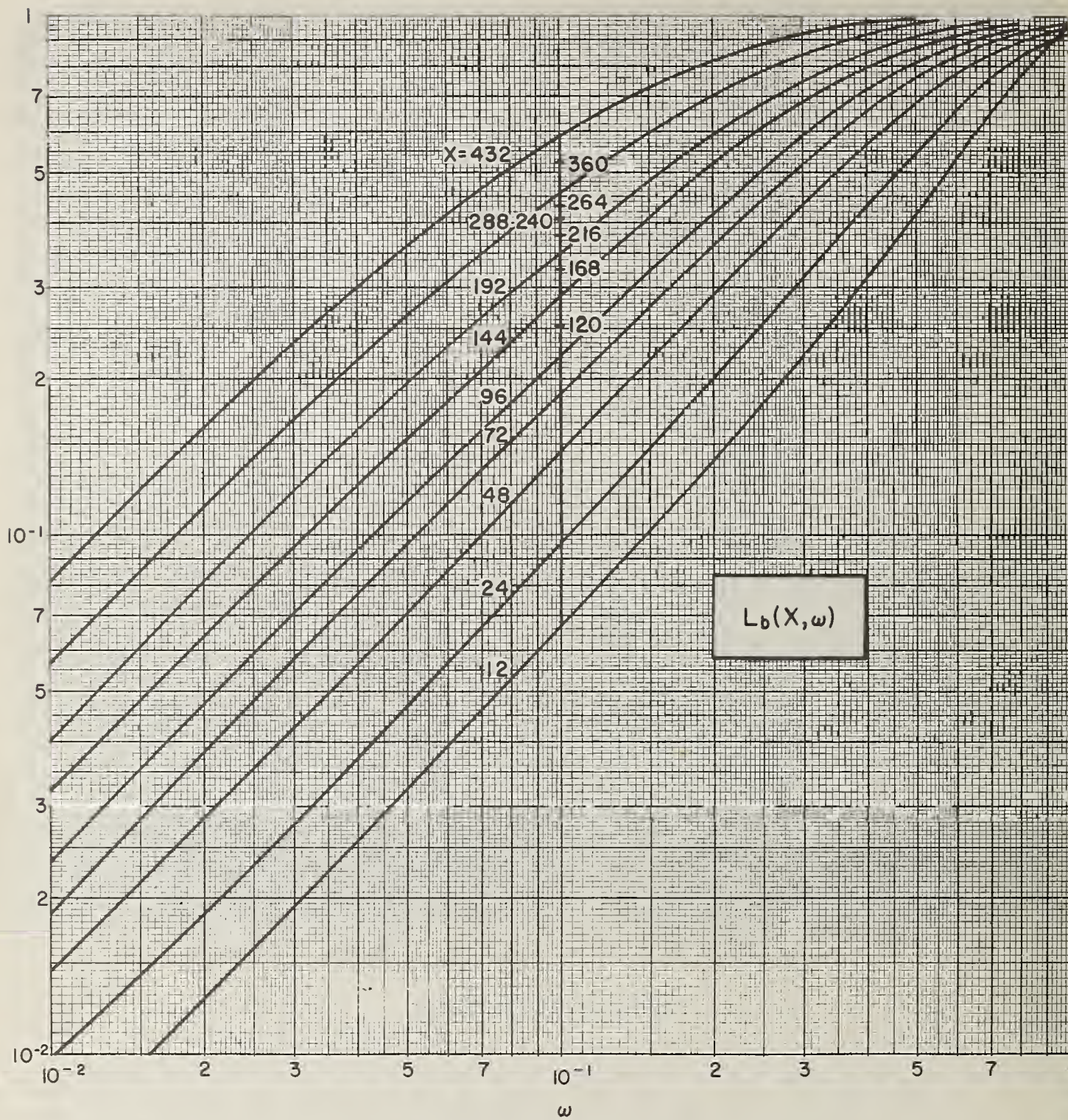
FIGURE B31. *Co–60, concrete.*

114

FIGURE B32. *Cs–137, concrete.*
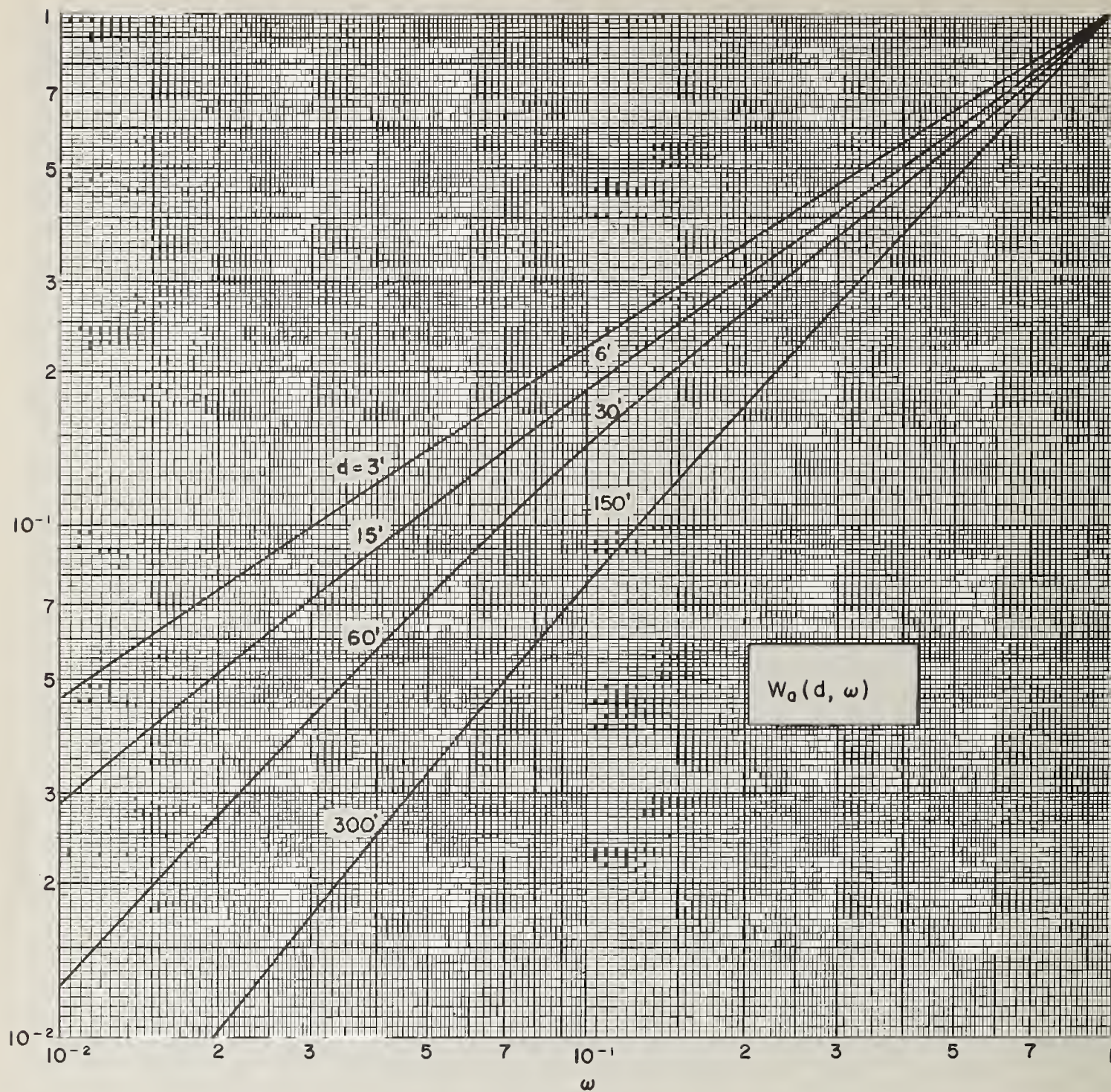
FIGURE B33. *Co-60, H₂O.*

116
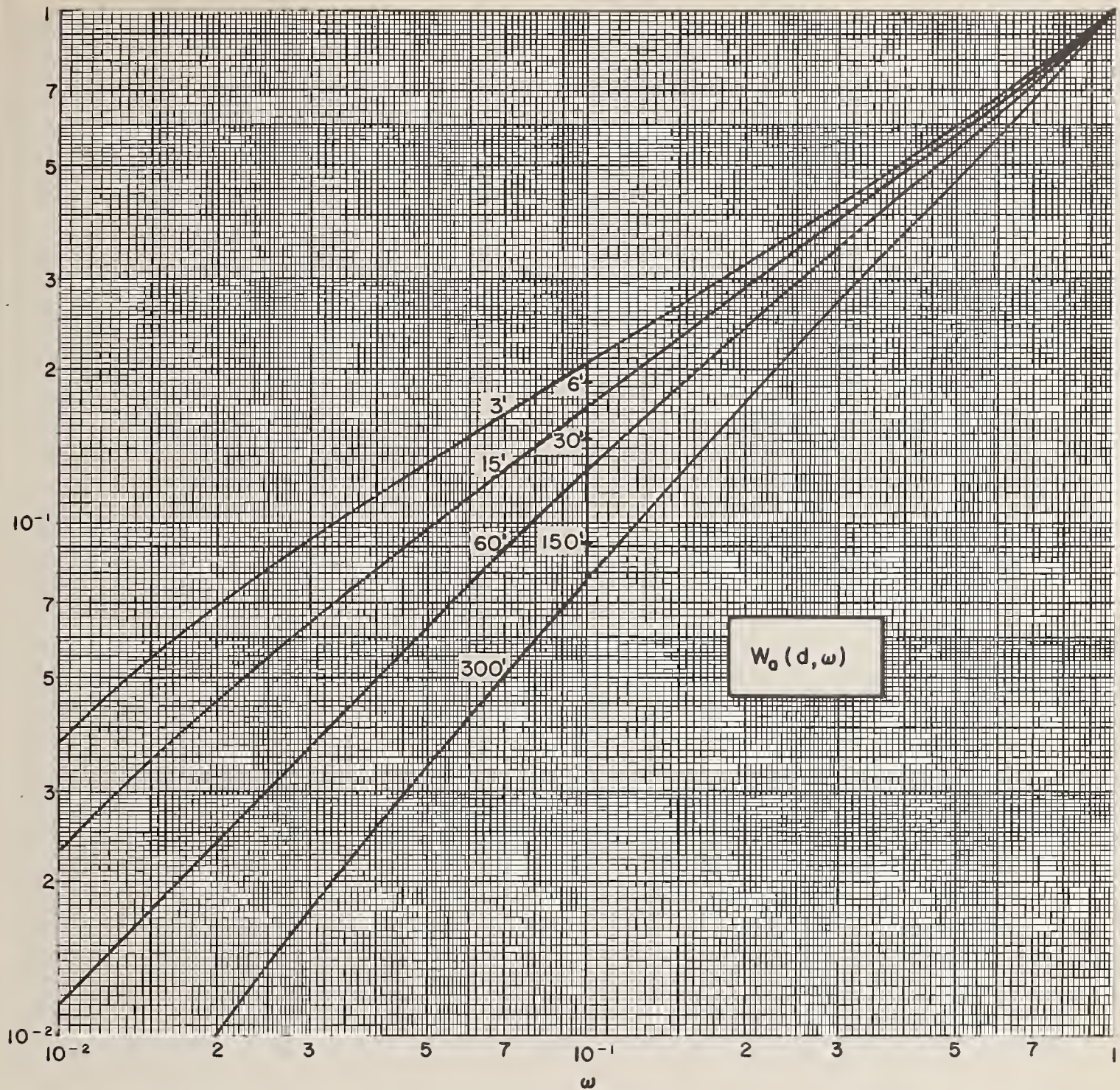
FIGURE B34. *Cs–137, H₂O.*
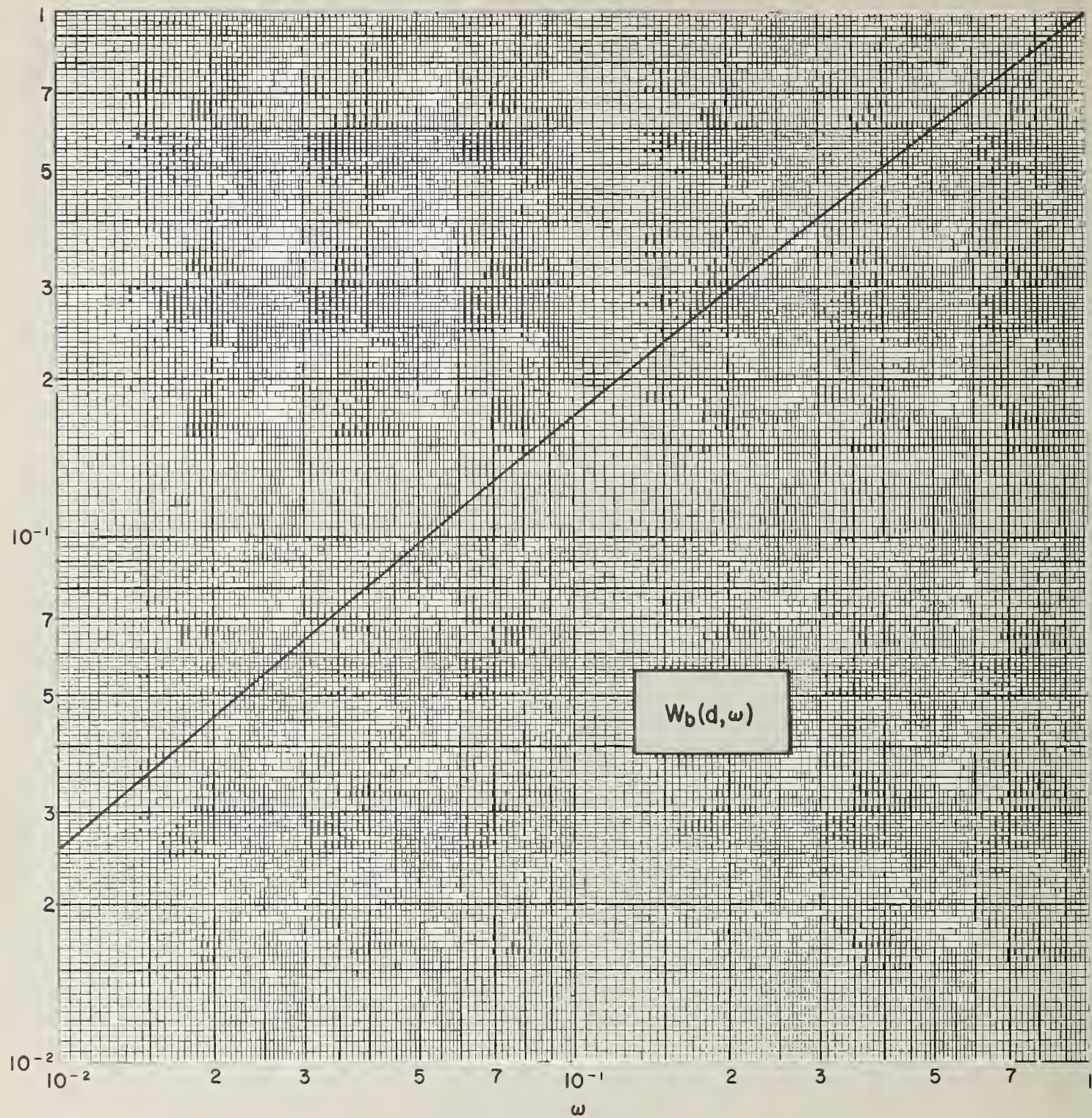
FIGURE B35. *Co–60, H₂O*.

118
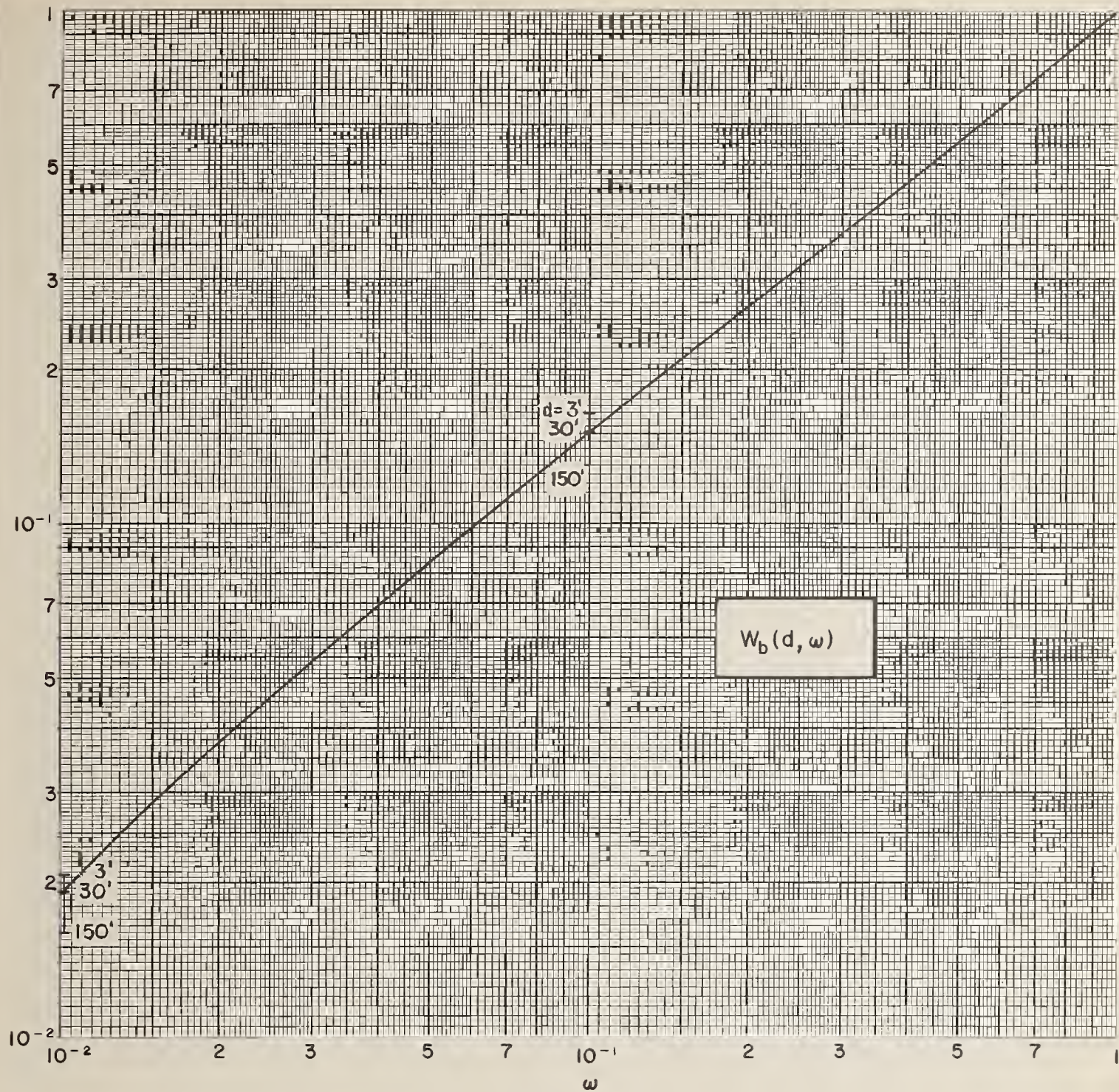
FIGURE B36. *Cs–137, H₂O.*

119
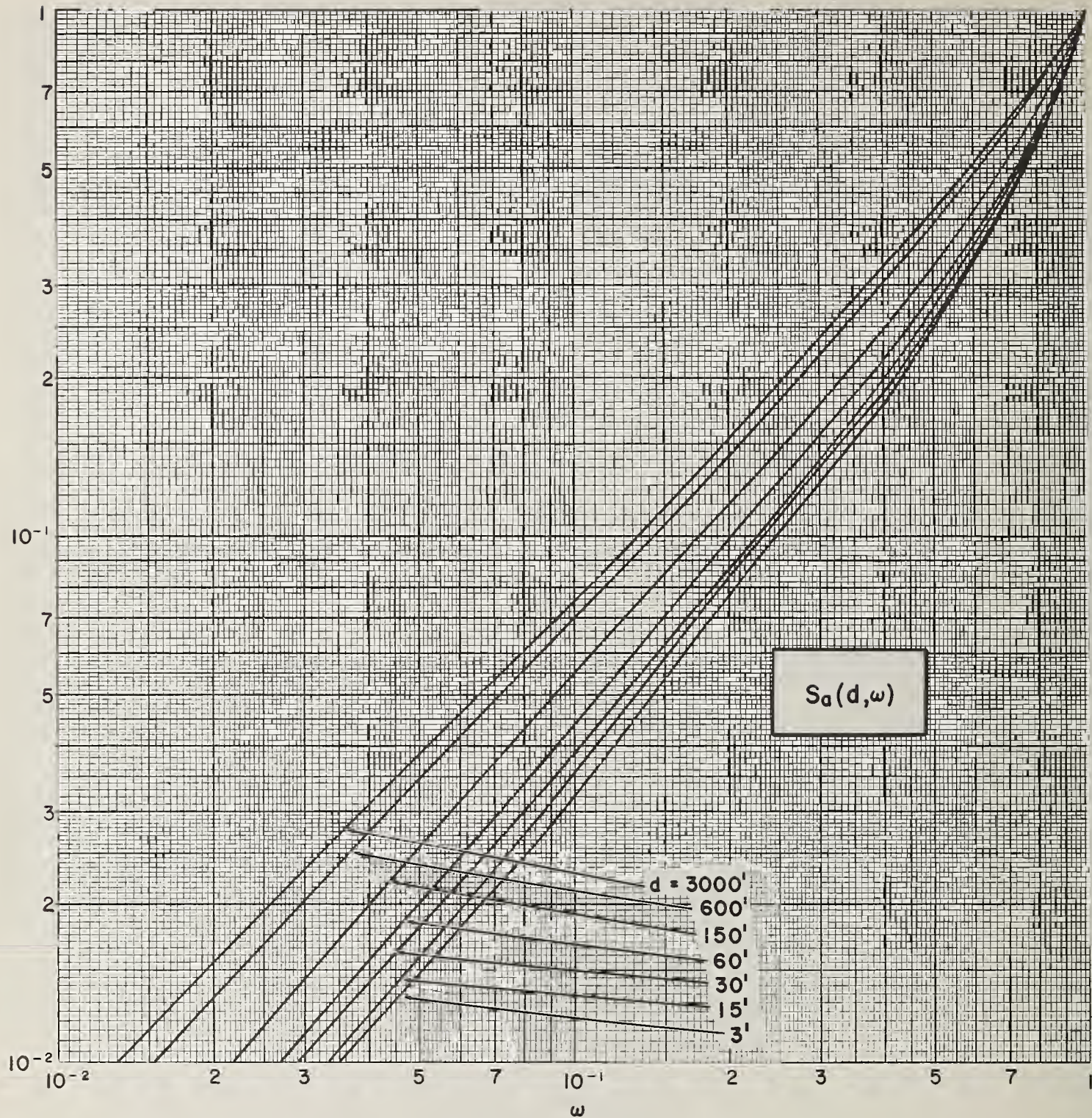
FIGURE B37. *Co–60, H₂O.*

120
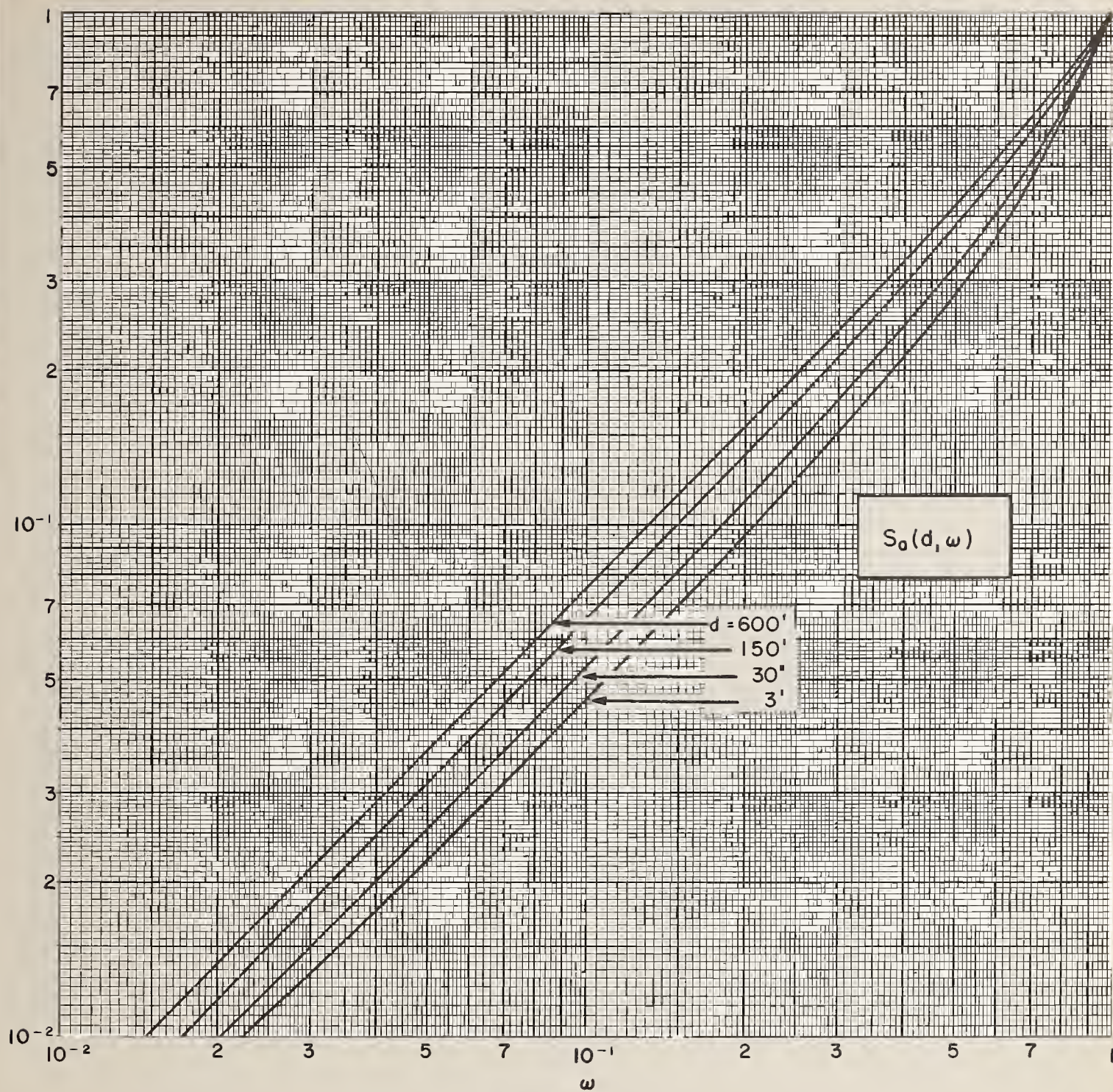
FIGURE B38. *Cs–137, H₂O.*

121
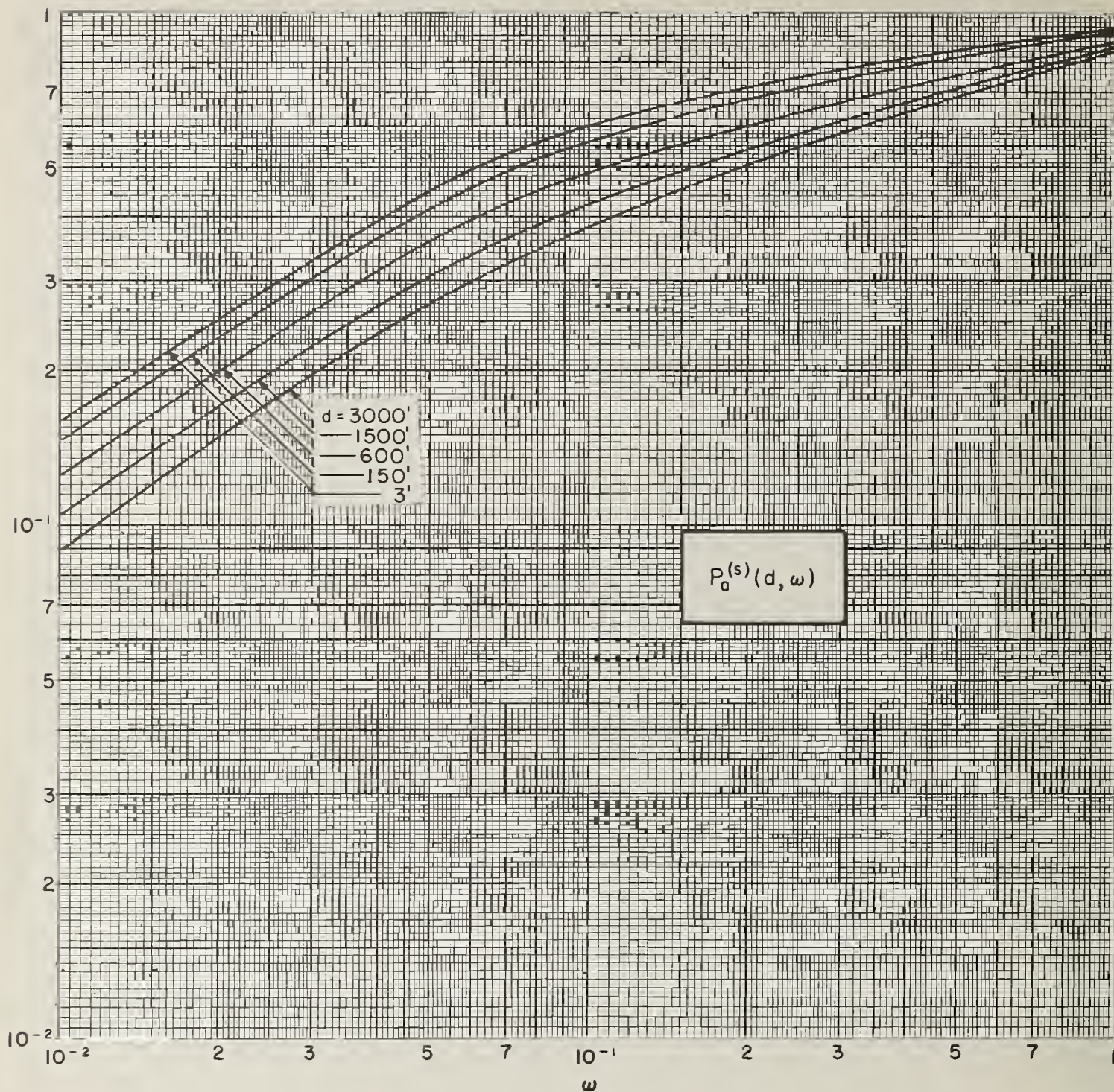
FIGURE B39. *Co-60, H₂O.*
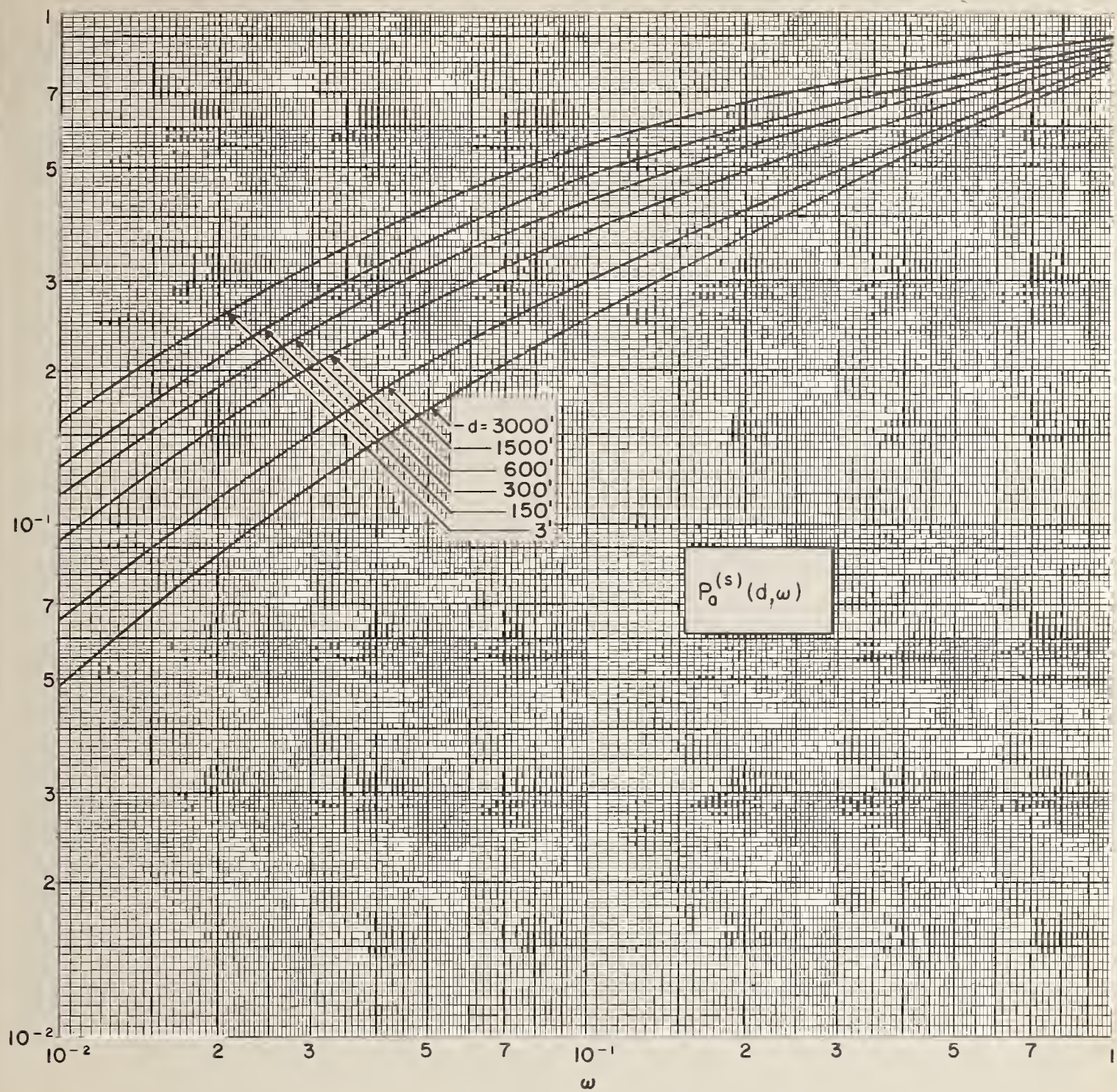
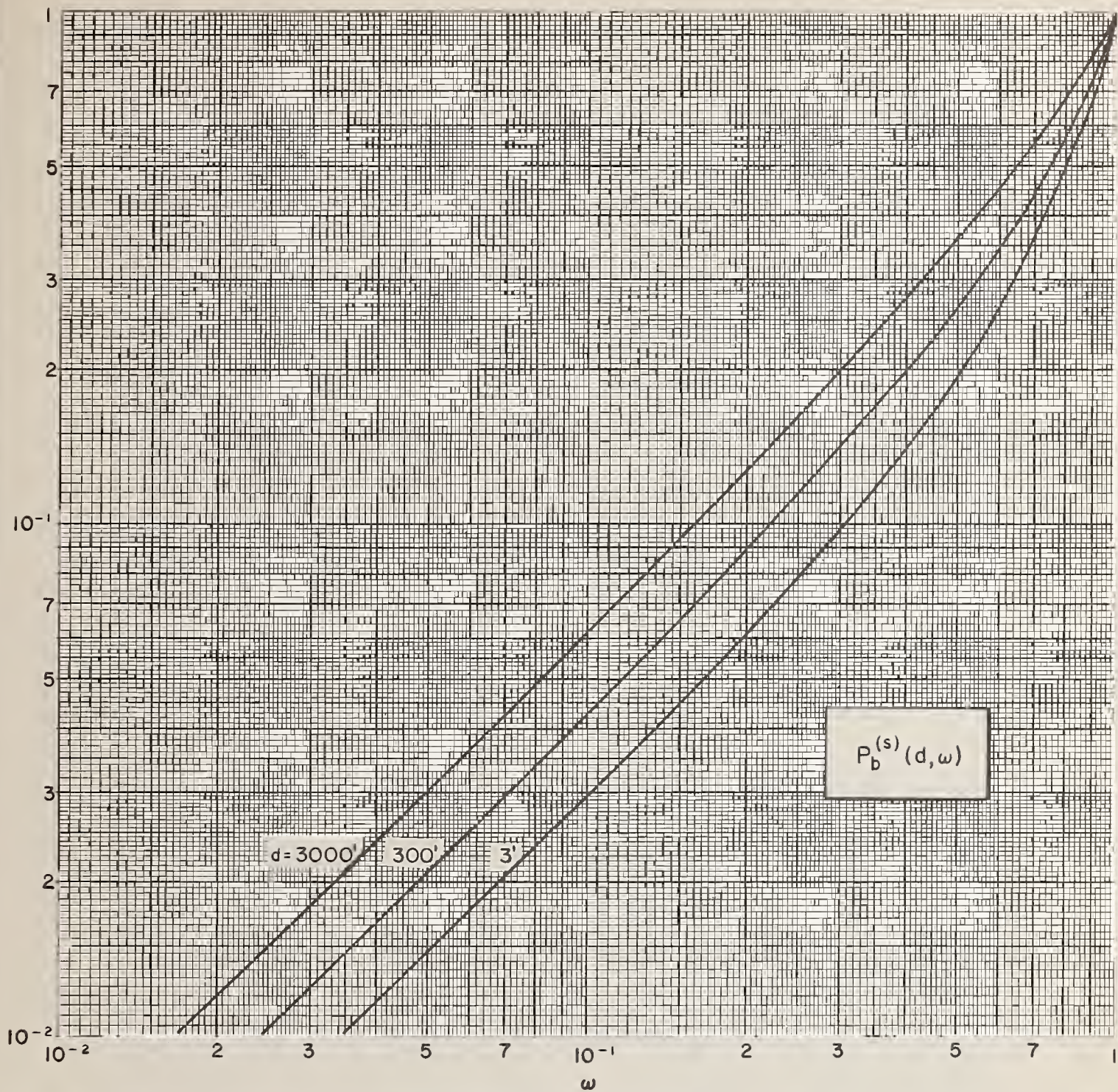FIGURE B40. *Cs–137*, H_2O.

123
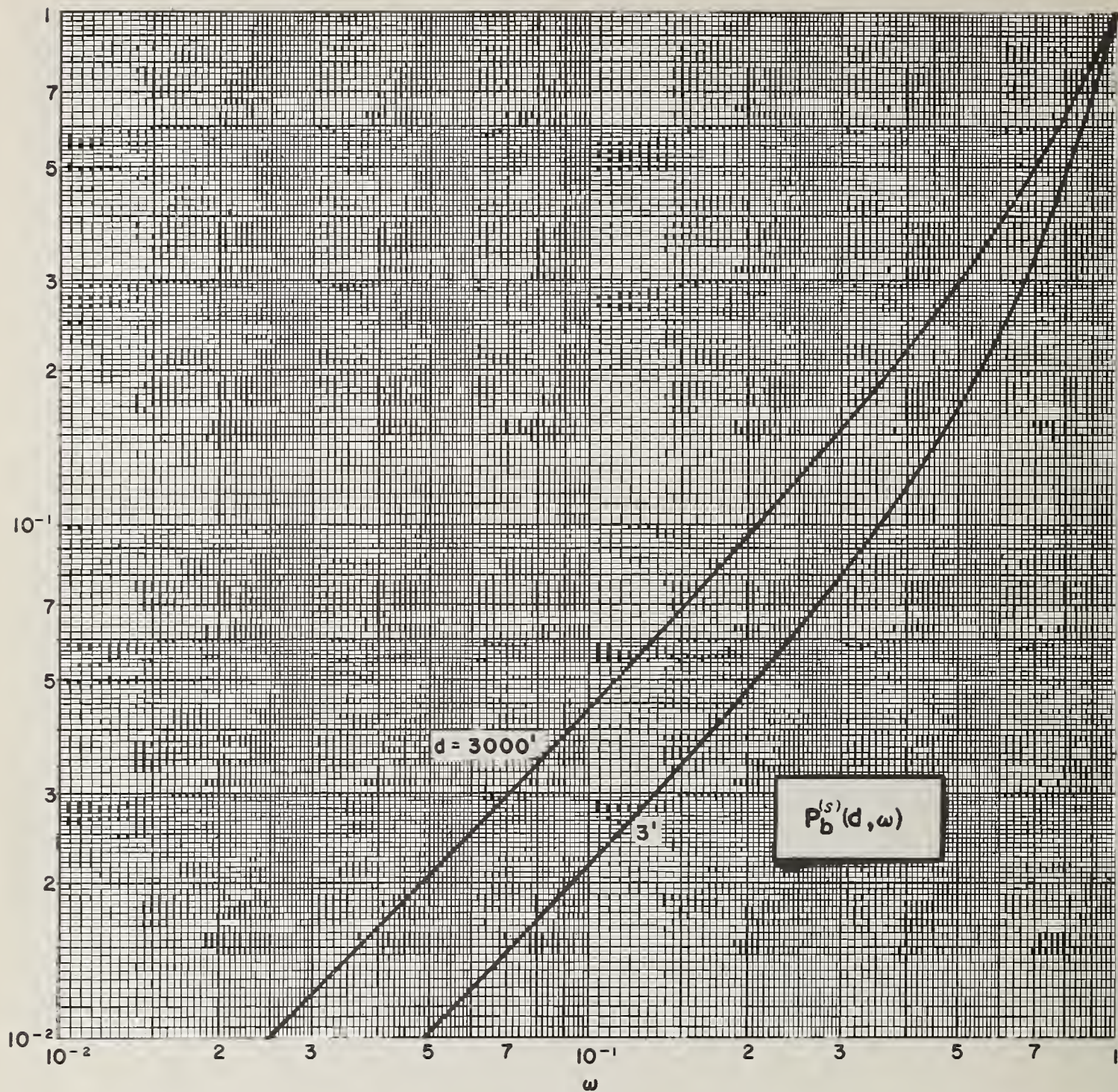
FIGURE B41. *Co–60, H₂O.*

124

FIGURE B42. *Cs–137, H₂O.*
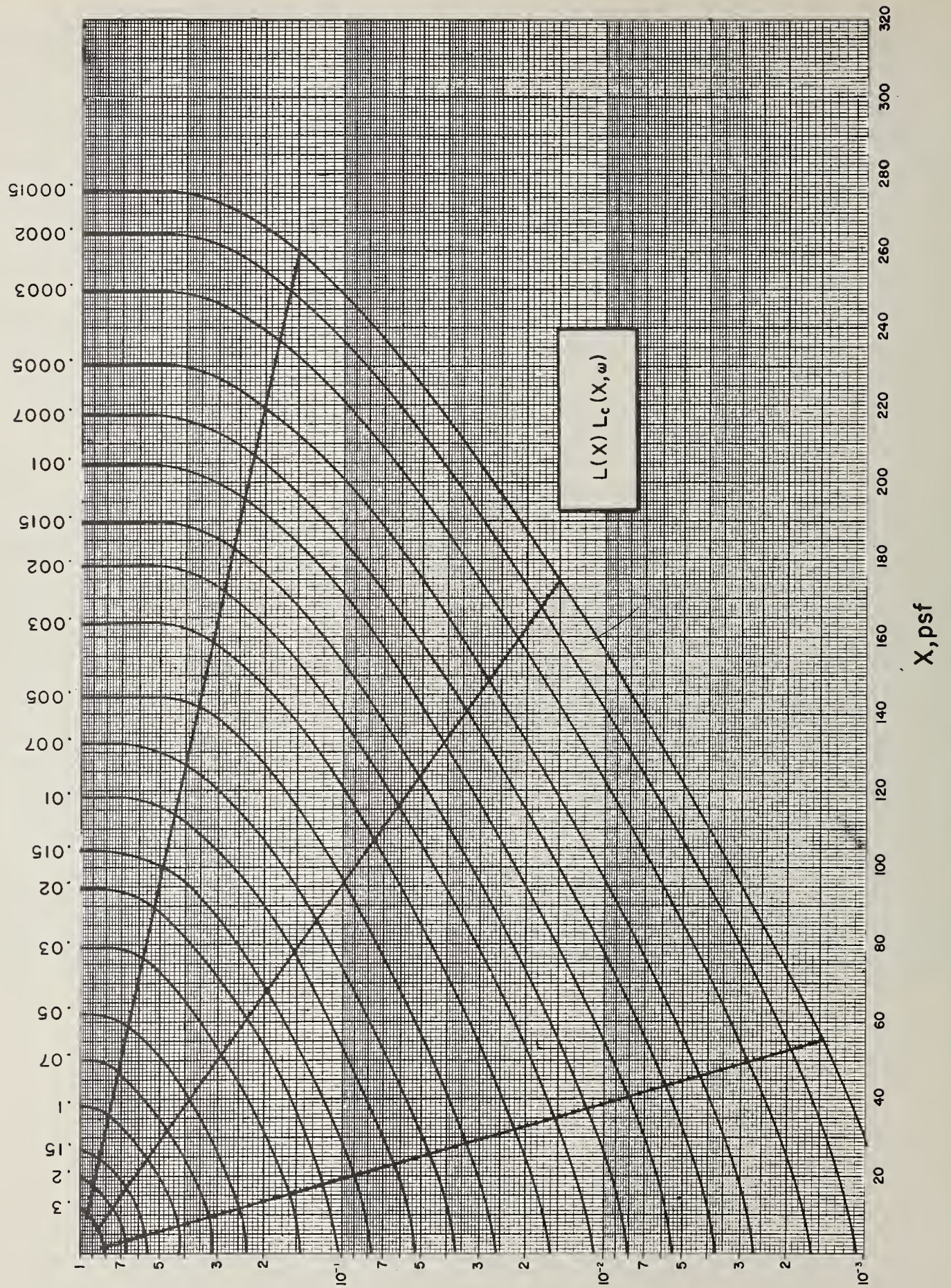
FIGURE B43. *Co-60, concrete.*

126
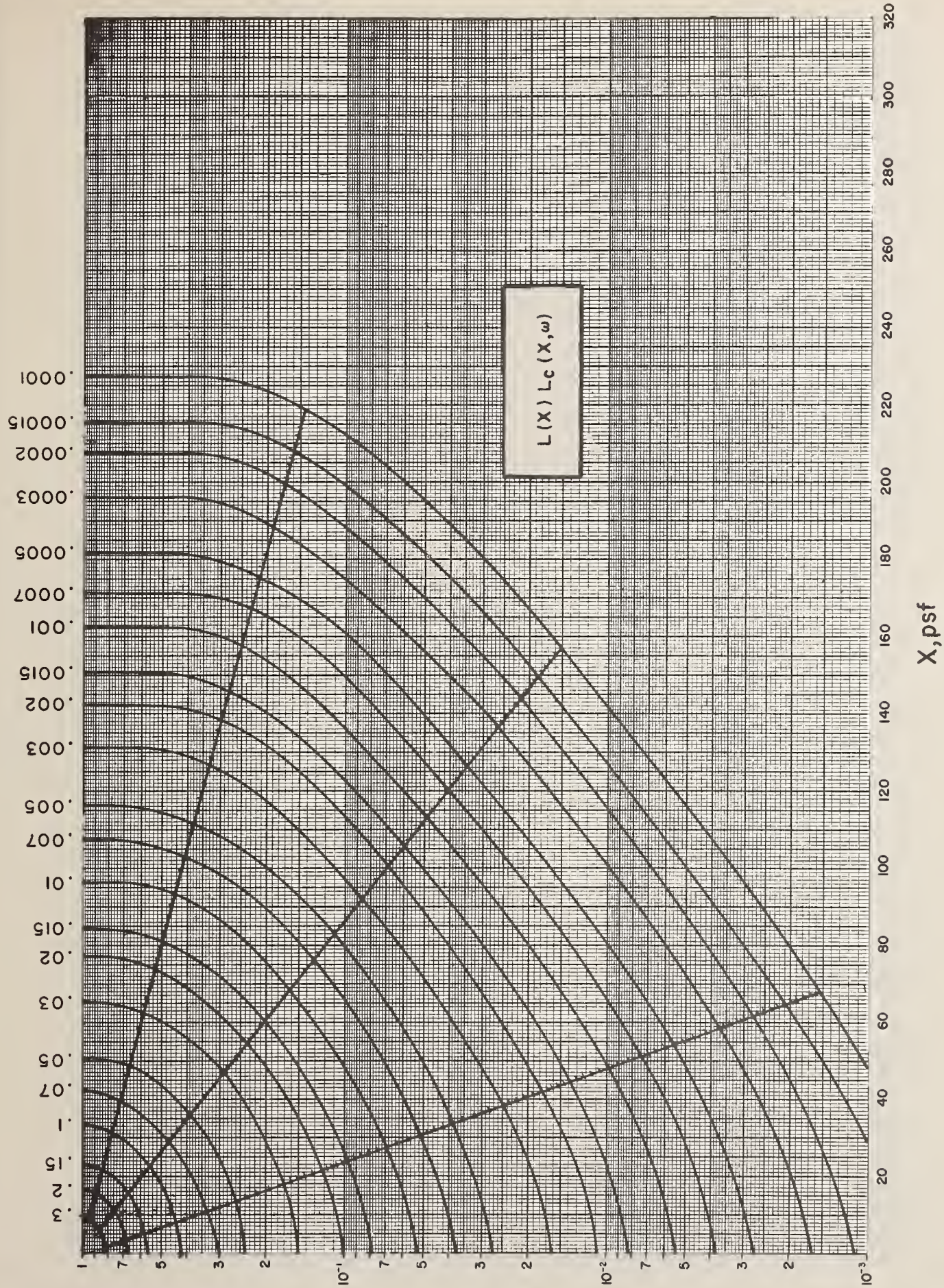
FIGURE B44. *Cs-137, concrete.*

X, psf

L(X) Lc(X,ω)

127
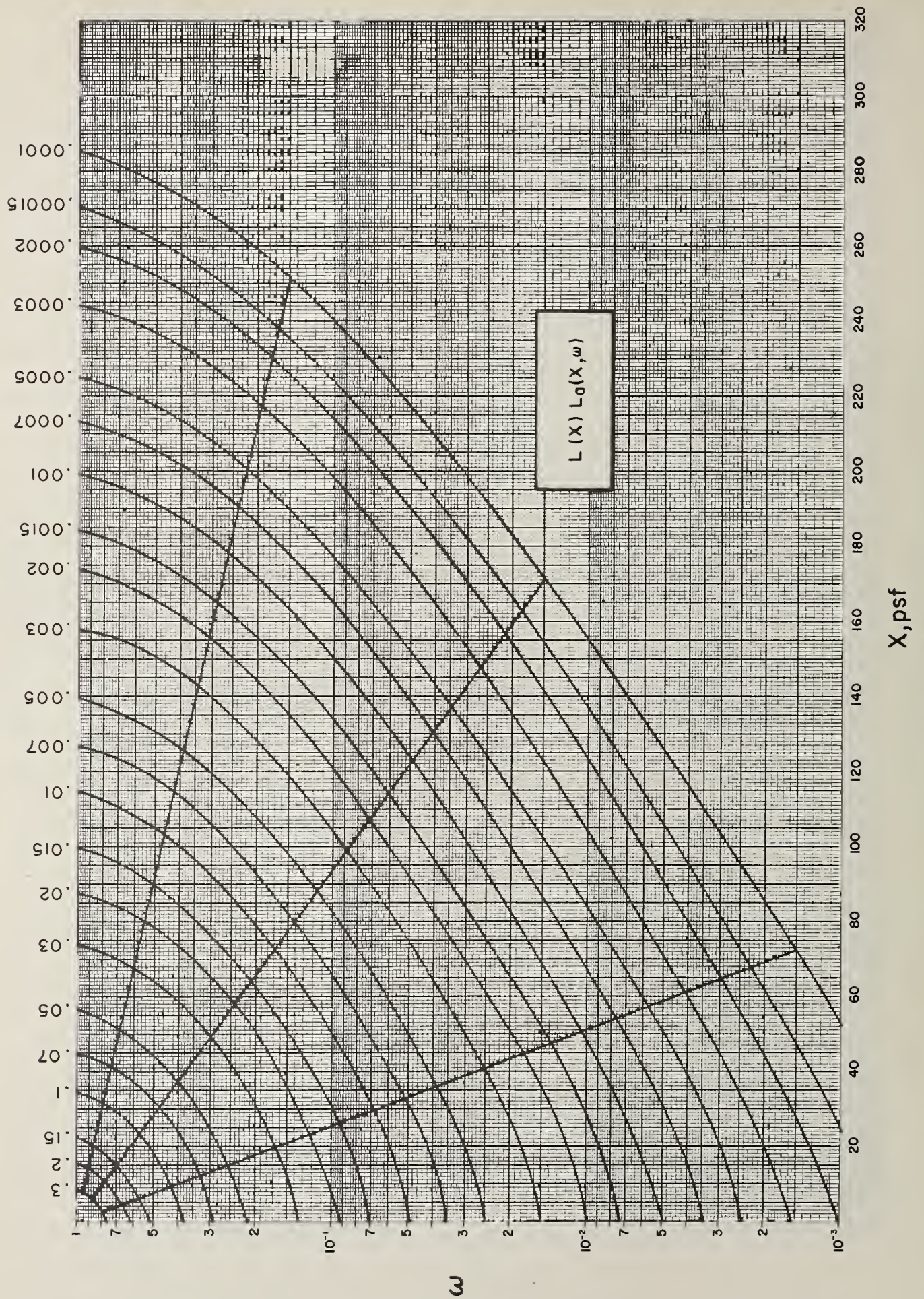
FIGURE B45. *Co–60, concrete.*

128
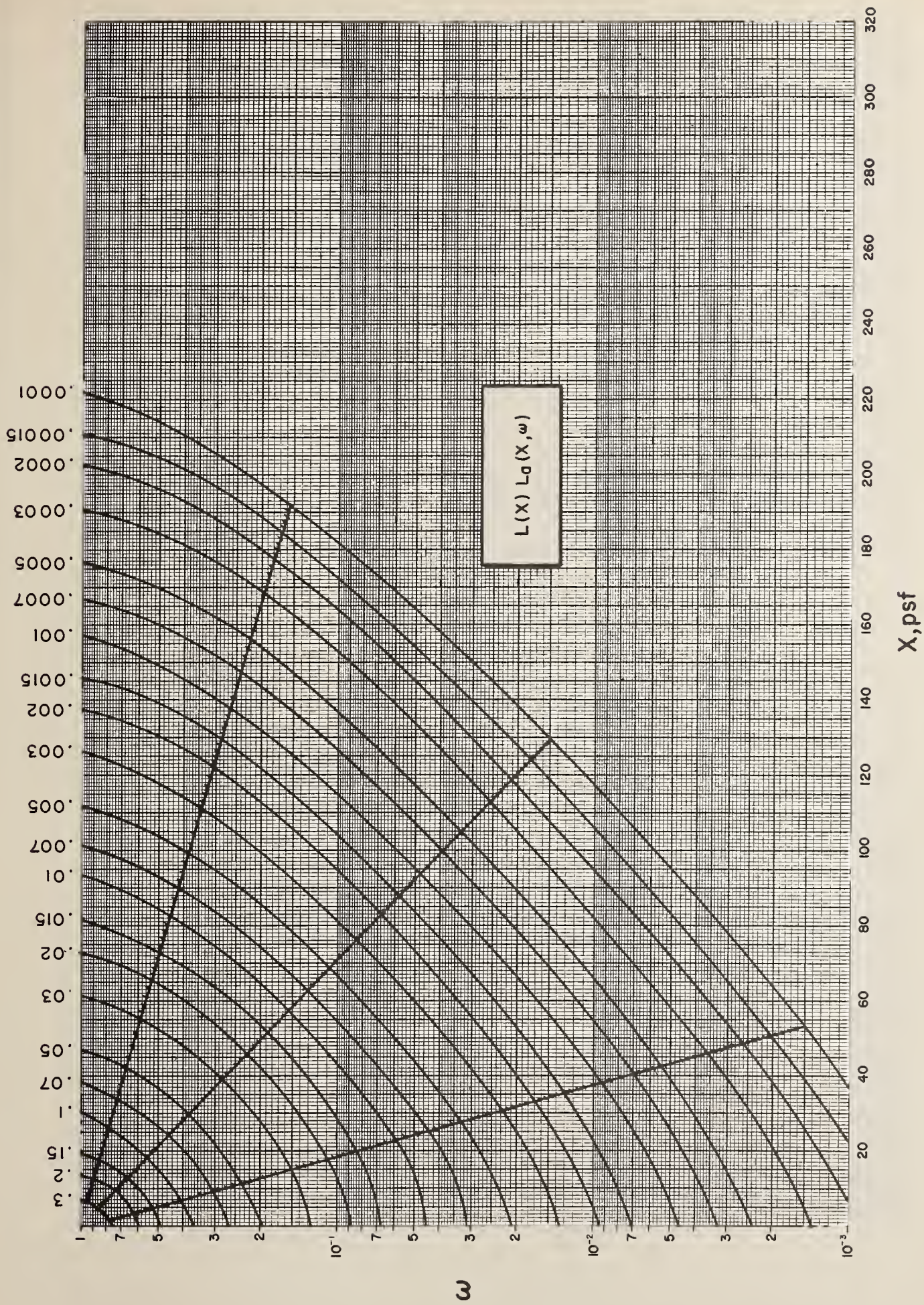
FIGURE B46. *Cs–137, concrete.*

X,psf

129
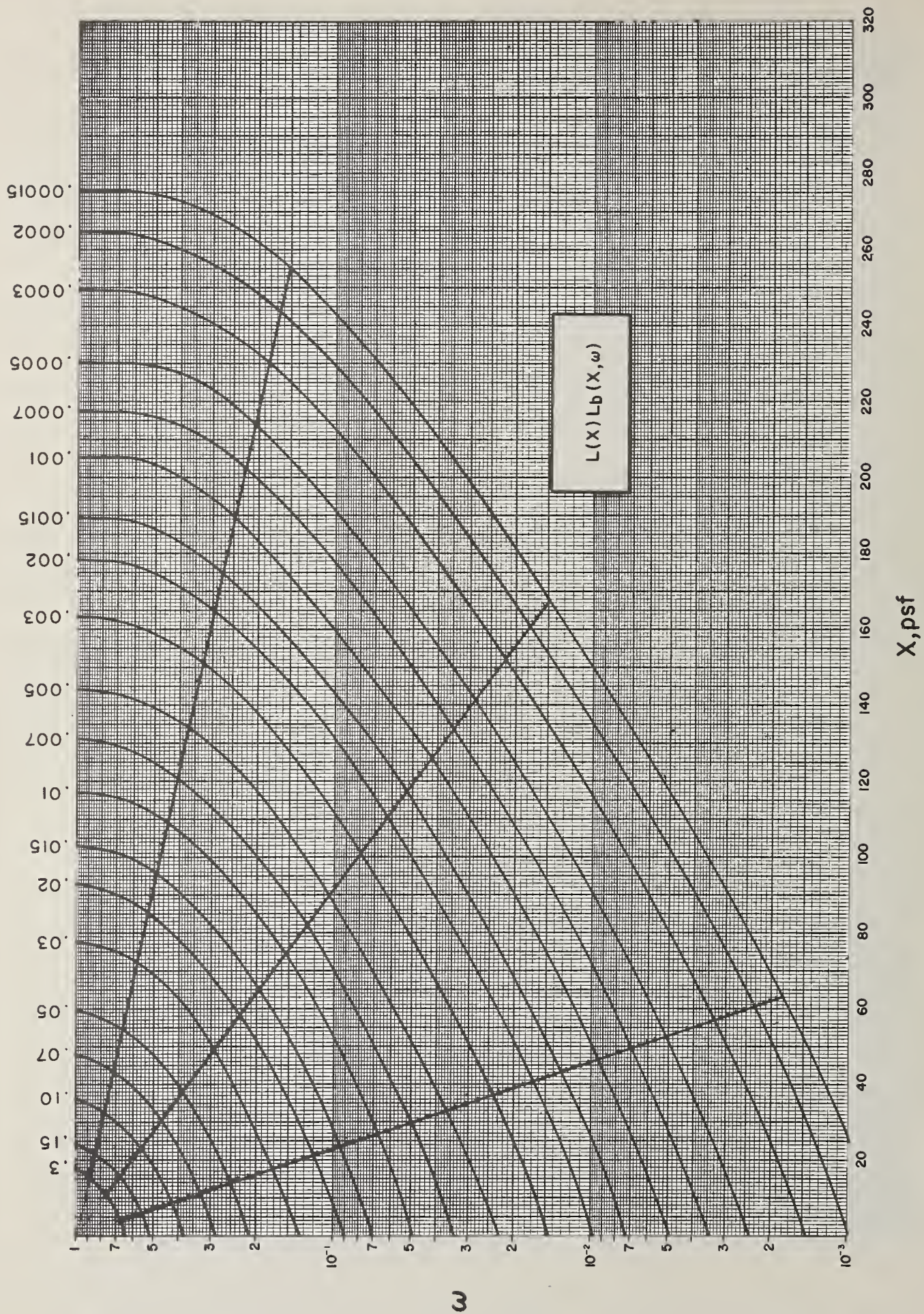
FIGURE B47. *Co–60, concrete.*
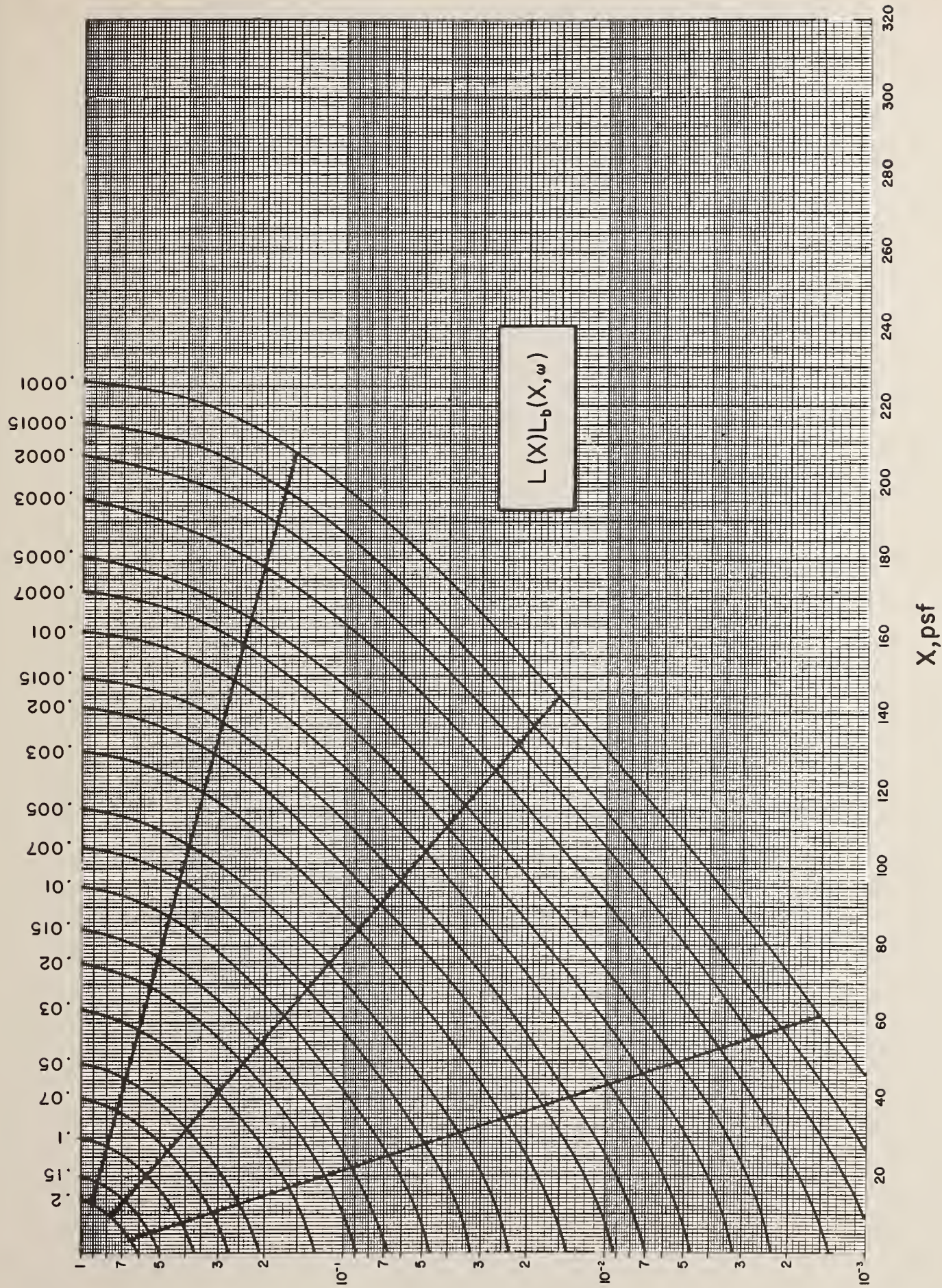
FIGURE B48. *Cs-137, concrete.*

131

$$\frac{\int_{X}^{\infty} dX' \ell(X', \cos\theta)}{\int_{X}^{\infty} dX' \ell(X', 1)}$$

X	$\int_{X}^{\infty} \ell(X', 1) dX'$
0	12.3
9	10.6
36	6.33
72	2.87
144	.495
216	.0875
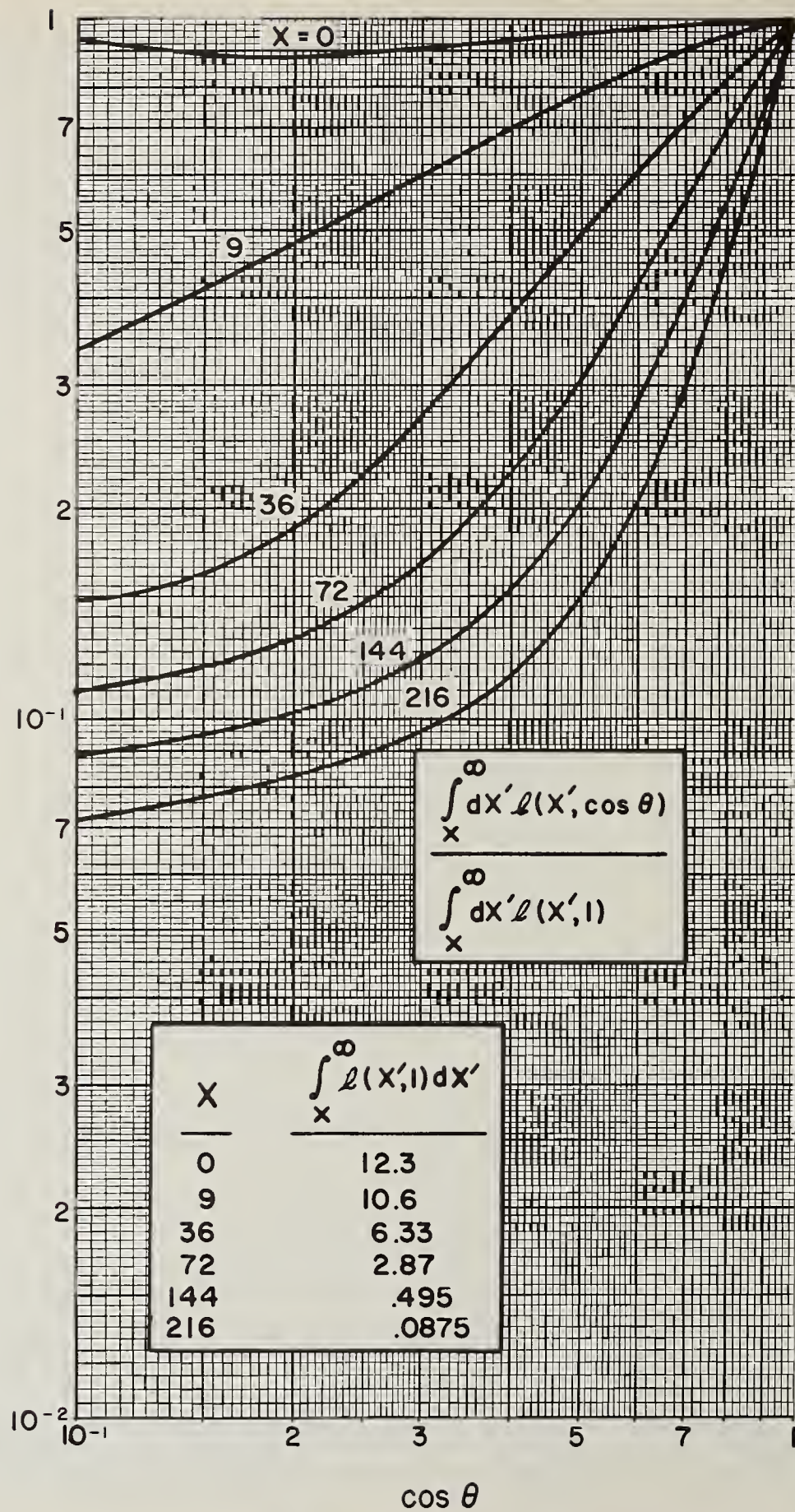
FIGURE B49. *Co–60, concrete.*

132

FIGURE B50. *Cs–137, concrete.*

The figure shows a log-log plot with axes $\cos\theta$ (horizontal, from 10^{-1} to 1) and the vertical axis from 10^{-2} to 1. The plotted quantity is:

$$\frac{\int_{x}^{\infty} \ell(x', \cos\theta)\,dx'}{\int_{x}^{\infty} \ell(x', 1)\,dx'}$$

Curves are labeled X = 0, 9, 36, 72, 144, 216.

X	$\int_{x}^{\infty} dx'\, \ell(x', 1)$
0	9.67
9	7.74
36	3.80
72	1.35
144	.135
216	.0120

133

References

[1] T. Rockwell, III (Editor), Reactor shielding design manual (McGraw-Hill, New York, N.Y., 1957).

[2] Reactor Handbook, **1**, AECD–3645 (USAEC 1955).

[3] H. Goldstein, Fundamental aspects of reactor shielding, (Addison-Wesley Publ. Co., Reading, Mass., 1958).

[4] B. T. Price, C. C. Horton, and K. T. Spinney, Radiation Shielding (Pergamon Press, Inc., New York, N.Y., 1957).
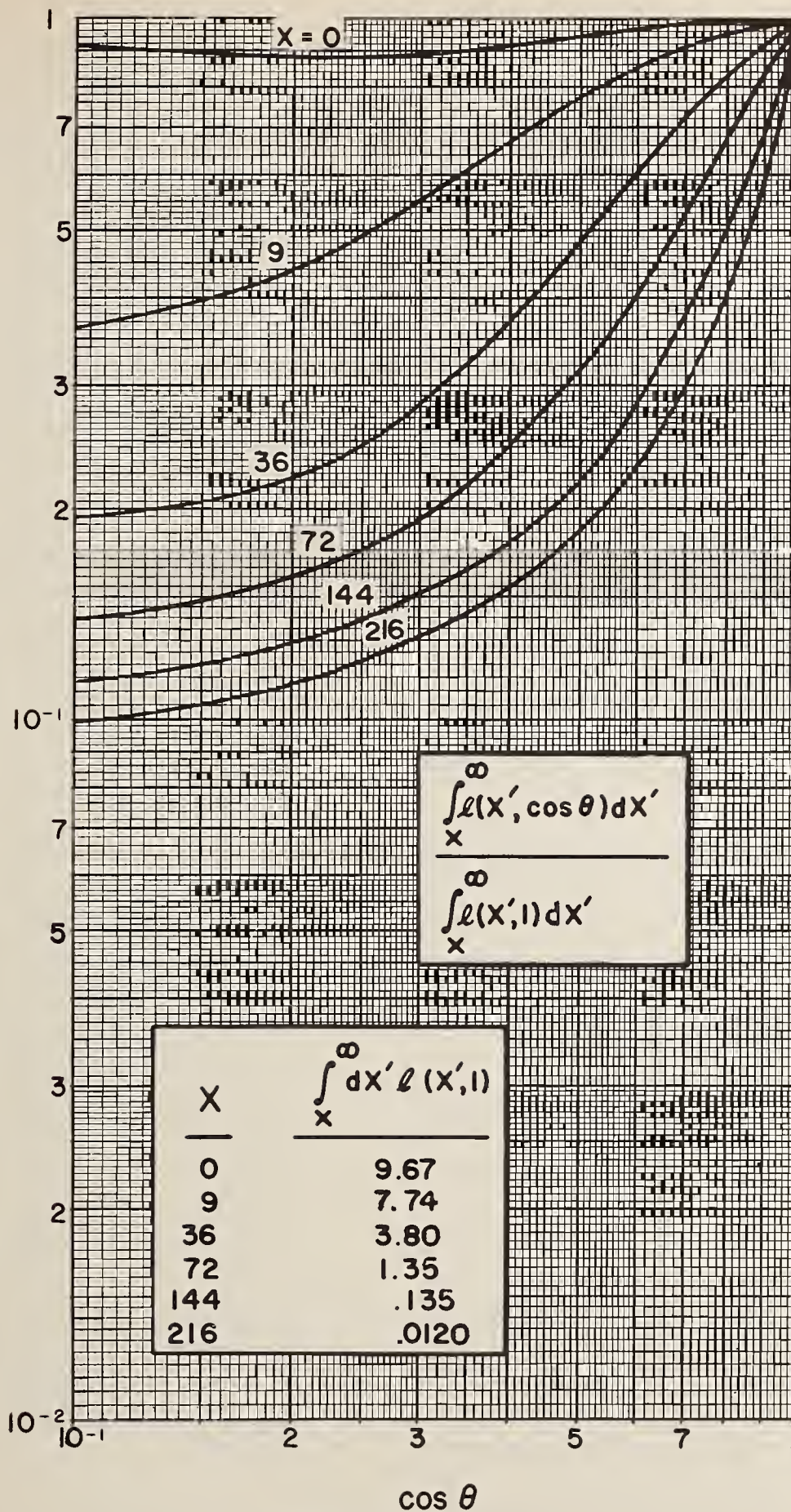
[5] Reactor Physics Constants, ANL–5800 (Office of Technical Services, U.S. Dept. of Commerce, Washington 25, D.C., July 1958).

[6] S. Glasstone (Editor), Effects of Nuclear Weapons, (Pergamon Press, Inc., New York, N.Y., 1957).

[7] A method for Evaluating the Protection Afforded Buildings Against Fallout Radiation (ODM, Washington, D.C., July 1, 1961). Unpublished.

[8] W. Malich and L. A. Beach, Radiation protection afforded by barracks and underground shelters, NRL Rept. 5017 (U.S. Naval Radiological Defense Laboratory, San Francisco, Calif., Sept. 18, 1952).

[9] R. R. Putz and A. Broido, A computation method for gamma radiation intensity in the presence of general shielding and source configurations (Proj. Civil, Univ. of California, Dec. 1957).

[10] F. C. Brooks, et al., Radiological Defense Planning Guide, TOI–58–26 (Tech. Operations, Inc., Burlington, Mass., 1958).

[11] Assessment of the protection afforded by buildings against gamma radiation fallout (Home Office, London, England, 1957).

[12] U. Fano, L. V. Spencer, and M. J. Berger, Penetration and diffusion of X-rays, Handbuch der Physik, **38** II, 660 (Springer-Verlag, Berlin, Germany, 1959).

[13] G. M. Corcos, On the small-scale, nonhomogeneity of fallout deposition (Univ. of California, Oct. 30, 1958).

[14] K. H. Larson, Adherence of fallout to trees and shrubs, USNRDL Letter Report (Unpublished) (U.S. Naval Radiological Defense Laboratory, San Francisco, Calif., Jan. 1959).

[15] H. Nishita and K. H. Larson, Summary of certain trends in soil-plant relationship studies of the biologically availability of fallout debris, Rept. No. UCLA–401 (Univ. of California School of Medicine, Los Angeles, Calif., July 28, 1957).

[16] E. P. Cronkhite, et al., Response of human beings accidentally exposed to fallout radiation, J. Am. Med. Assoc., **159**, 430–4 (Oct. 1, 1955).

[17] R. L. Mather, Brief summary of gamma radiation spectra from residual radiation sources, following a nuclear detonation, U.S. Naval Radiological Defense Laboratory Shielding Symp. **I**, 115 (San Francisco, Calif., Oct. 1956).

[18] A. T. Nelms and J. W. Cooper, U^{235} fission product decay spectra at various times after fission, Health Physics **1**, 427–441 (Sept. 1958).

[19] J. F. Scoles, Fission product gamma ray spectra, Convair Rept. FAM–1042 (San Diego, Calif., Aug. 1958).

[20] C. F. Miller, Gamma decay of fission products from the slow neutron fission of U^{235}, USNRDL–TR–187 (U.S. Naval Radiological Defense Laboratory, San Francisco, Calif., July 11, 1957).

[21] P. J. Dolan, Gamma spectrum of Uranium–238 fission products at various times after fission, DASA 526 (Defense Atomic Support Agency, Wash., D.C., May 1959).

[22] R. Björnerstedt, Gamma radiation from nuclear weapons fallout, Arkiv för Fysik, **16**, 293 (Oct. 28, 1959).

[23] C. S. Cook, Energy spectrum of gamma radiation from fallout, USNRDL–TR–318 (U.S. Naval Radiological Defense Laboratory, San Francisco, Calif., Oct. 26, 1959).

[24] Report of the International Commission on Radiological Units and Measurements (ICRU), NBS Handb. 62 (1956).

[25] R. C. Bolles and N. E. Ballou, Calculated activities and abundances of U^{235} fission products USNRDL–456 (U.S. Naval Radiological Defense Laboratory, San Francisco, Calif., Aug. 30, 1956).

[26] C. F. Miller, Gamma decay of fission products from the slow-neutron fission of U^{235}, USNRDL–TR–187 (U.S. Naval Radiological Defense Laboratory, San Francisco, Calif., July 11, 1957).

[27] J. Moteff, Miscellaneous data for shielding calculations, Rept. No. APEX–134, (USAEC 1953).

[28] G. J. Hine and G. L. Brownell (Editors), Radiation Dosimetry (Academic Press, Inc., New York, N.Y., 1956).

[29] M. J. Berger, The dose received from partially shielded gamma ray detectors. Unpublished report.

[30] M. J. Berger and J. C. Lamkin, Sample calculations of gamma ray penetration into shelters: Contributions of skyshine and roof contamination, J. Research NBS, **60**, 109 (1957) RP 2827.

[31] F. H. Attix and V. H. Ritz, A determination of the gamma ray emission of radium, J. Research NBS, **59**, 293 (1957) RP 2801.

[32] R. T. McGinnies, X-ray attenuation coefficients from 10 kev to 100 Mev, NBS Circ. 583 Suppl. (Oct. 30, 1959).

[33] H. Goldstein and J. E. Wilkins, Jr., Calculations of the penetration of gamma rays (USAEC Rept. NYO–3075) (1954).

[34] M. J. Berger and D. J. Raso, Monte Carlo calculations of gamma ray backscattering, Radiation Research **12**, 20 (1960).

[35] E. W. Cannon, Building materials as commonly used in existing urban buildings in the United States, Project Civil Report (Inst. of Eng. Research, Univ. of Calif., Richmond, Calif., Jan. 1958).

[36] F. Titus, Penetration in concrete of gamma radiation from fallout, AEC Rept. ITR–1477 (Oct. 22, 1957).

37] C. F. Ksanda, A. Moshkin, and E. S. Shapiro, Gamma Radiations from a rough infinite plane, USNRDL–TR–108 (U.S. Naval Radiological Defense Laboratory, San Francisco, Calif., Jan. 18, 1956).

[38] C. E. Clifford, J. A. Carruthers, and J. R. Cunningham, Scattered gamma radiation from a simulated fallout field using Cs–137, DRCL Rept. No. 296 (Defense Research Chemical Labs., Ottawa, Canada, Jan. 1959).

[39] E. T. Clarke, J. F. Batter, and A. L. Kaplan, Measurement of attenuation in existing structures of radiation from simulated fallout, Rept. TO–B 59–4 (Tech. Operations, Inc., Burlington, Mass., Apr. 27, 1959).

[40] W. B. Boast, Illumination Engineering, Chapt. 7, Determination of illumination from surface and line sources, 82–100 (McGraw-Hill Book Co., New York, N.Y., 1953).

[41] J. H. Hubbell, R. L. Bach, and J. C. Lamkin, Radiation field from a rectangular source, J. Research NBS 64C (Eng. and Instr.), No. 2, 121–138 (Apr.–June 1960).

THE NATIONAL BUREAU OF STANDARDS

The scope of activities of the National Bureau of Standards at its major laboratories in Washington, D.C., and Boulder, Colorado, is suggested in the following listing of the divisions and sections engaged in technical work. In general, each section carries out specialized research, development, and engineering in the field indicated by its title. A brief description of the activities, and of the resultant publications, appears on the inside of the front cover.

WASHINGTON, D.C.

Electricity. Resistance and Reactance. Electrochemistry. Electrical Instruments. Magnetic Measurements. Dielectrics. High Voltage.

Metrology. Photometry and Colorimetry. Refractometry. Photographic Research. Length. Engineering Metrology. Mass and Scale. Volumetry and Densimetry.

Heat. Temperature Physics. Heat Measurements. Cryogenic Physics. Equation of State. Statistical Physics.

Radiation Physics. X-ray. Radioactivity. Radiation Theory. High Energy Radiation. Radiological Equipment. Nucleonic Instrumentation. Neutron Physics.

Analytical and Inorganic Chemistry. Pure Substances. Spectrochemistry. Solution Chemistry. Standard Reference Materials. Applied Analytical Research. Crystal Chemistry.

Mechanics. Sound. Pressure and Vacuum. Fluid Mechanics. Engineering Mechanics. Rheology. Combustion Controls.

Polymers. Macromolecules: Synthesis and Structure. Polymer Chemistry. Polymer Physics. Polymer Characterization. Polymer Evaluation and Testing. Applied Polymer Standards and Research. Dental Research.

Metallurgy. Engineering Metallurgy. Microscopy and Diffraction. Metal Reactions. Metal Physics. Electrolysis and Metal Deposition.

Inorganic Solids. Engineering Ceramics. Glass. Solid State Chemistry. Crystal Growth. Physical Properties. Crystallography.

Building Research. Structural Engineering. Fire Research. Mechanical Systems. Organic Building Materials. Codes and Safety Standards. Heat Transfer. Inorganic Building Materials. Metallic Building Materials.

Applied Mathematics. Numerical Analysis. Computation. Statistical Engineering. Mathematical Physics. Operations Research.

Data Processing Systems. Components and Techniques. Computer Technology. Measurements Automation. Engineering Applications. Systems Analysis.

Atomic Physics. Spectroscopy. Infrared Spectroscopy. Solid State Physics. Electron Physics. Atomic Physics.

Instrumentation. Engineering Electronics. Electron Devices. Electronic Instrumentation. Mechanical Instruments. Basic Instrumentation.

Physical Chemistry. Thermochemistry. Surface Chemistry. Organic Chemistry. Molecular Spectroscopy. Molecular Kinetics. Mass Spectrometry.

Office of Weights and Measures.

BOULDER, COLO.

Cryogenic Engineering. Cryogenic Equipment. Cryogenic Processes. Properties of Materials. Cryogenic Technical Services.

CENTRAL RADIO PROPAGATION LABORATORY

Ionosphere Research and Propagation. Low Frequency and Very Low Frequency Research. Ionosphere Research. Prediction Services. Sun-Earth Relationships. Field Engineering. Radio Warning Services.

Radio Propagation Engineering. Data Reduction Instrumentation. Radio Noise. Tropospheric Measurements. Tropospheric Analysis. Propagation-Terrain Effects. Radio-Meteorology. Lower Atmosphere Physics.

Radio Systems. Applied Electromagnetic Theory. High Frequency and Very High Frequency Research. Modulation Research. Antenna Research. Navigation Systems.

Upper Atmosphere and Space Physics. Upper Atmosphere and Plasma Physics. Ionosphere and Exosphere Scatter. Airglow and Aurora. Ionospheric Radio Astronomy.

RADIO STANDARDS LABORATORY

Radio Physics. Radio Broadcast Service. Radio and Microwave Materials. Atomic Frequency and Time-Interval Standards. Millimeter-Wave Research.

Circuit Standards. High Frequency Electrical Standards. Microwave Circuit Standards. Electronic Calibration Center.